PAP-488

TWO PHASE FLOW
IN
HYDRAULIC STRUCTURES

DR. ALAN ERVINE
DEPT. OF CIVIL ENGINEERING
UNIVERSITY OF GLASGOW
SCOTLAND

LECTURE SERIES PRESENTED TO THE BUREAU OF RECLAMATION

JULY 1985

A REVIEW OF BUBBLY AND AIR POCKET FLOWS IN CIVIL ENGINEERING HYDRAULIC STRUCTURES

A series of lectures presented to the

United States Bureau of Reclamation, Denver.

D. A. ERVINE

JULY 1985

CONTENTS

List of Main Symbols used in Bubbly Flow Sections

d	jet thickness or circular jet diameter
D	closed conduit dimension
d_b	air bubble diameter
d_n	circular nozzle diameter
dp	penetration depth of air bubbles into a pool
Fr_1	jet Froude Number at plunge point ($u_1/\sqrt{gd}$)
Fr	general Froude Number
g	gravitational constant
H	height of fall or drop length of a plunging jet
ℓ^*	turbulent eddy length
ℓ^*_{max}	maximum turbulent eddy length
L_r	Length ratio, (prototype/model), reattachment length shear layer
L_d	disintegration length of a plunging jet
L	droplength of a plunging jet (= H)
q_{at}	rate of air entrainment per unit length (into the flow
q_{an}	rate of air transport along a closed conduit
q_w	water discharge rate per unit length
Re	Reynolds Number of flow (ud/ν)
R	radius of curvature of jet surface disturbances
u_1	jet velocity at plunge point (sometimes v or v_1)
u_o	mean outlet water velocity in a closed conduit
u^*	fluctuating turbulent component of velocity
u^*/u_1	turbulence intensity at plunge point (sometimes Tu)
u_i^*	inception jet velocity required to entrain air

u_{1min}	minimum jet velocity required to transport air in a closed conduit
u_{omin}	minimum outlet velocity required to transport air in a closed conduit
U_e	entrainment velocity into a shear layer
U_r	recirculation velocity around a spreading shear layer
U_b	air bubble velocity in a shear layer
U_{br}	air bubble rise velocity in stationary water
U_n	water velocity at circular nozzle exit
We (or Wb)	Weber Number of flow ($\rho u^2 d/\sigma$)
x	streamwise direction
y	normal to streamwise direction
α	void fraction (sometimes given as C_1 concentration)
β	ratio of air flow to water flow (q_a/q_w)
β_{at}	air/water ratio of air entrained into a flow
β_{an}	air/water ratio of net air transport along a closed conduit
δ	magnitude of jet surface disturbance
ϵ	relative turbulence intensity in shear layer (Thomas) jet surface disturbance (Ervine)
μ	absolute viscosity (air or water)
ν	kinematic viscosity
ρ_a, ρ_w, ρ_f	density of air, water, foamy mixture
σ	surface tension coefficient
θ	angle of conduit to horizontal

SECTION 2

Bubbly flows - Theoretical models and analysis.

2.1 Inception conditions for air entrainment

2.2 Quantity of air entrained

2.3 Bubble escape and bubble transport mechanisms

2.1 Inception conditions for air entrainment

Every hydraulic situation involving air entrainment requires certain conditions to be met before air will be entrained. A wide range of inception conditions have been formulated, based on velocity, Froude Number, Reynolds/Weber Number, turbulence intensity, boundary layer thickness, etc. Every case demands that the free water surface is 'broken' (i.e. overcoming surface tension), with the major 'breaking' mechanism being turbulent fluctuations in the flow (u*).

This is certainly the case for wall jets and plunging jets which require surface disturbances, driven by turbulent fluctuations, to form an air bubble and entrain it into the flow at the plunge point (See Fig. 2.1).

It is also the case for natural surface aeration in high velocity open channel flows. In this case, turbulent fluctuations near the free surface must produce enough upward force to overcome surface tension and propel a droplet of water out of the flow. The droplet entrains an air bubble in its wake.

In the case of hydraulic jumps, the free surface is 'broken' by the point of discontinuity at the toe of the jump in the form of a surface roller. A minimum inception condition of $Fr_1 > 1$ is therefore required.

Our discussion on inception will centre, at least in the first instance, on wall jets and plunging jets at steeper conduit slopes than conventional hydraulic jumps.

Formulation of non-dimensional groups for inception velocity for jets

If we assume that the jet on Figure 2.1 is either circular, diameter d, or plane, thickness d, and that inception is dependent on the turbulent fluctuating component u*, the eddy size ℓ^*, and viscous, gravitational, inertial and surface tension forces are also important, then we can write

$$f(u_1, \mu, \sigma, g, \rho, u^*, \ell^*, d) = 0 \quad \ldots\ldots (2.1)$$

Using the method of synthesis by forming groups having length, we have,

$$f\left(\frac{u_1^2}{g}, \frac{\nu}{u_1}, \frac{\sigma}{\rho u_1^2}, \frac{\nu^{2/3}}{g^{1/3}}, \frac{\nu^2\rho}{\sigma}, \left(\frac{\sigma}{\rho g}\right)^{\frac{1}{2}}, \frac{u^{*2}}{g}, \frac{\nu}{u^*}, \frac{\sigma}{u^{*2}\rho}, \ell^*, d\right) = 0 \quad \ldots\ldots (2.2)$$

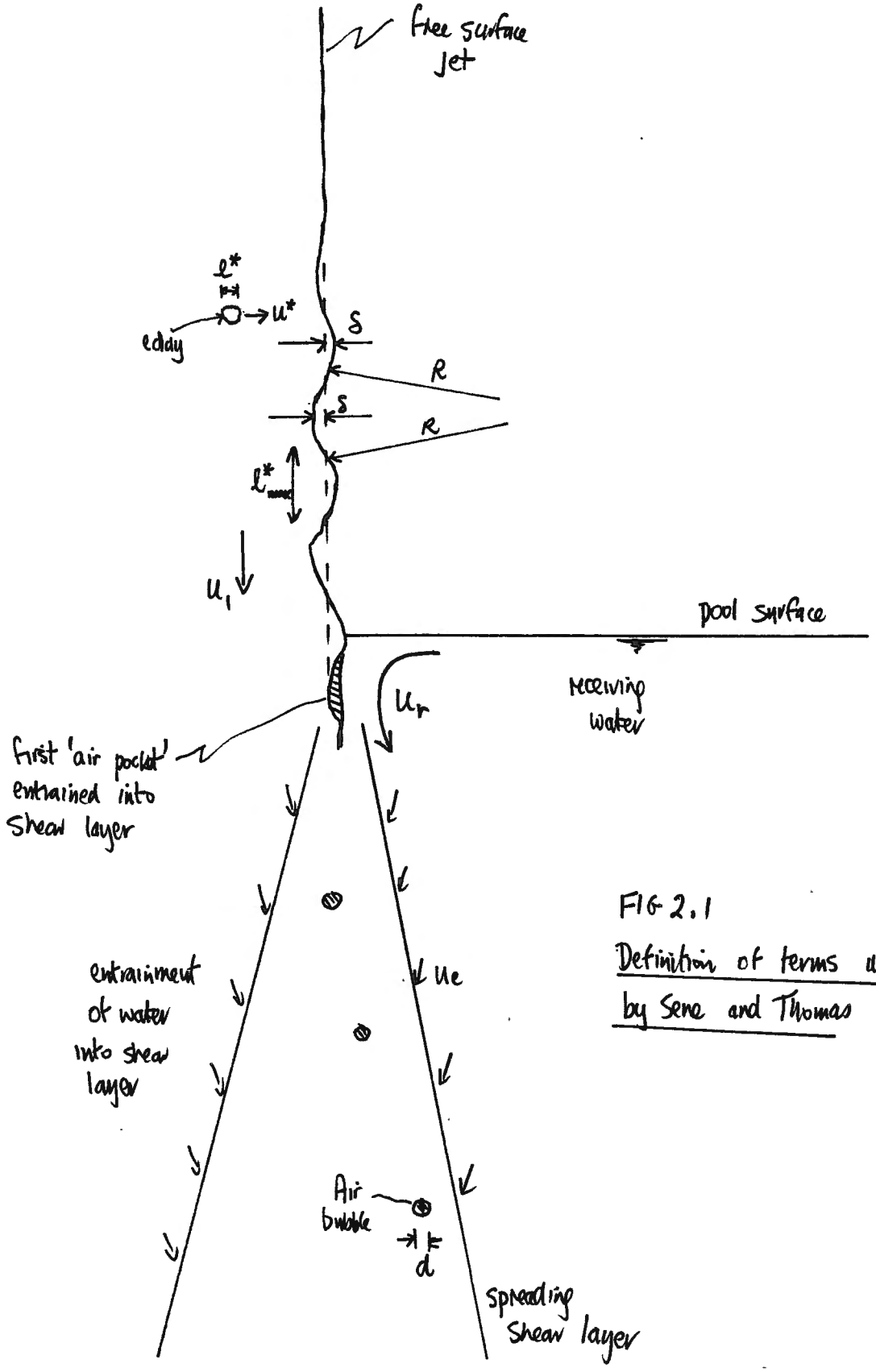

FIG 2.1
Definition of terms used by Sene and Thomas

The number of variables not containing density and relevant lengths in (2.1) is 5, implying that four of the length parameters in (2.2) can be chosen along with ℓ^* and d. The four parameters chosen must contain between them every variable at least once. For instance we can choose,

$$f\left(\frac{u_1^2}{g}, \frac{\nu}{u_1}, \left(\frac{\sigma}{\rho g}\right)^{\frac{1}{2}}, \frac{\nu}{u^*}, \ell^*, d\right) = 0 \qquad \ldots\ldots (2.3)$$

If we now divide through by either ℓ^* or d_j we may obtain

$$f\left(\frac{u_1^2}{g\ell^*}, \frac{\nu}{u_1\ell^*}, \frac{(\sigma/\rho g)^{1/2}}{\ell^*}, \frac{\nu}{u^*\ell^*}, \frac{d}{\ell^*}\right) = 0$$

This may be written in the form,

$$\frac{u_1^2}{g\ell^*} = f\left(\frac{u_1\ell^*}{\nu}, \frac{u^*\ell^*}{\nu}, \frac{(\sigma/\rho g)^{1/2}}{\ell^*}, \frac{\ell^*}{d}\right) \qquad \ldots\ldots (2.4)$$

Several points can be noted from this relationship.

At the point of inception for air entrainment, the jet velocity u_1 is denoted by the inception velocity u_i^*, and the eddy length ℓ^* is given by the maximum eddy length ℓ^*_{max}, which is approximately equal to the bubble diameter d_b (Sene, Ref). Hence from (2.4) we might obtain,

$$\underset{①}{\frac{u_1^2}{g d_b}} = f\left(\underset{②}{\frac{u_1 d_b}{\nu}}, \underset{③}{\frac{u^* d_b}{\nu}}, \underset{④}{\frac{(\sigma/\rho g)^{\frac{1}{2}}}{d_b}}, \underset{⑤}{\frac{d_b}{d}}\right) \qquad \ldots\ldots (2.5)$$

Now for air entrainment we may assume d_b (model) $\simeq$ d_b (prototype) and hence from ② u_1 model $\simeq$ u_1 prototype for inception, or from ② and ③ together $(u_1/u^*)_{model} \simeq (u_1/u^*)$ prototype. u^*/u_1 is the turbulence intensity. From ④, $(\sigma/\rho g)^{1/2}$ is the capillary length and $\simeq d_b$ (if capillary length is 2.7 mm and bubbles of approximately 3 mm diameter are entrained). Hence ④ might reduce to unity as an order of magnitude. Thus,

$$\frac{u_1^2}{g d_b} = f\left(\frac{u^*}{u_1}, \frac{d_b}{d}\right) \qquad \ldots\ldots (2.6)$$

where u^*/u_1 is the turbulence intensity of the flow. It is generally assumed that d_b/d is only significant in jets whose thickness is of the same order as the bubble diameter. That is, for eddies to grow to a maximum size ℓ^*_{max} to be approximately equal to a bubble diameter 1-5 mm, then the jet would require to have at least this order of

magnitude thickness. Hunt (Ref) states that jet surface disturbances are reduced if eddy sizes ℓ^* are smaller than about 4 times capillary length (say 10 mm). Thus for jets, say, >10 mm thickness,

$$u_i^* \simeq \sqrt{g d_b}\ f(u^*/u_i) \qquad \ldots\ldots (2.7)$$

The inception velocity for air entrainment for larger jet thicknesses is a function of the turbulence intensity.

A theoretical model

The most cogent argument to date on the nature of the inception velocity to entrain air was presented by Sene (Ref) based on arguments previously outlined by Thomas (Ref).

Referring to Figure 2.1, a plunging jet with velocity u_i enters a pool where a mixing layer is set up and the receiving water entrained into the mixing layer also forms a larger recirculating flow of velocity U_r, where $U_r \propto u_i$. Sene indicates a value of $U_r/u_i \sim 0.035$. The dynamic pressure in the receiving flow is therefore of the order $\frac{1}{2}\rho u_r^2$.

The plunging jet itself is assumed to carry air bubbles into the mixing layer by the mechanism of surface disturbances on the jet free surface, indicated on Figure 2.1 by δ. Surface disturbances caused by fluctuating components of velocity in the flow, u*, and δ is approximated to $u^{*2}/2g$, the energy head of the turbulent eddies. The length scale of the turbulent eddies in the jet is given by ℓ^* and it is assumed that most of the air is entrained at maximum eddy lengths given by ℓ^*_{max}. It can be seen from Figure 2.1 that surface disturbances are assumed to form a shallow circular arc of radius R on the jet surface. Therefore the pressure set up by surface tension forces the maintain this shape is given by $2\sigma/R$, where σ is the surface tension coefficient.

Sene and Thomas argue that at the point of jet impact, the receiving flow will try to follow the undulations on the jet surface, and that air will only be entrained when the receiving water is unable to follow jet undulations, and a "gap" or pocket is formed which is subsequently transferred into the mixing layer. Thus the criterion for inception of air entrainment is given by

$$2\sigma/R \geq \tfrac{1}{2}\rho u_r^2 \qquad \ldots\ldots (2.8a)$$

In order to obtain an estimate for R, is was assumed that the length of a jet surface undulation could be approximated to ℓ^*_{max}, the maximum

length scale of turbulent eddies causing entrainment. Hence from Figure 2.1

$$R \sim l^{*2}_{max}/8\delta \qquad \left(\text{where } \delta \sim u^{*2}/2g\right) \qquad \ldots\ldots (2.8b)$$

Combining equations (2.8a) and (2.8b) we obtain that the maximum eddy length is given by

$$l^*_{max} \simeq 4\,\frac{(u^*/u_1)}{(u_r/u_1)}\left(\frac{\sigma}{\rho g}\right)^{\frac{1}{2}} \qquad \ldots\ldots (2.9)$$

where $\sqrt{\frac{\sigma}{\rho g}}$ is known as the capillary length and for the formation of air bubbles is approximately equal to the air bubble diameter.

Sene and Thomas argue that the volume of air held in a jet surface undulation is of the order $l^{*2}_{max}\,\delta$, and at inception only single air bubbles are formed, so that

$$l^{*2}_{max}\,\delta \simeq \frac{d_b^3}{2} \simeq \frac{1}{2}\left(\sqrt{\frac{\sigma}{\rho g}}\right)^3 \qquad \ldots\ldots (2.10)$$

where d_b is the air bubble diameter. Also at inception, the jet velocity is the inception jet velocity U_i^*, combining (2.9) and (2.10) we obtain,

$$u_i^* \simeq \frac{1}{4}\frac{(u_r/u_1)}{(u^*/u_1)^2}\left(\sqrt{\frac{\sigma g}{\rho}}\right)^{\frac{1}{2}} \qquad \ldots\ldots (2.11)$$

where u^*/u_1 is the relative turbulence intensity and σ/ρ is constant for air/water. The value of Ur/u_1 is assumed to be approximately equal to 0.035.

The value of equation (2.11) is not in the quantitative prediction of the inception velocity but the implication that the inception velocity ($U_i^* \propto \frac{1}{(Tu)^2}$) is proportional to the inverse turbulence intensity squared.

This may well represent an oversensitivity of the contribution of the relative turbulence intensity, as a very smooth jet may have Tu ≈ 0,01 and a very rough jet Tu ≈ 0,1, which would imply a difference in inception velocity of 100 times in the two types of jet. This has been shown by Ervine, McKeogh and Elsawy not to be the case, as a jet with Tu ~ 0.4% gave U_i^* of 3.6 m/s, whereas a jet with Tu ~ 8% gave U_i^* of 0.8 m/s, which is closer to $U_i^* \propto \frac{1}{(Tu)^{\frac{1}{2}}}$.

Experimental and empirical evaluations of the critical inception velocity

Lin and Donelly (Ref) investigated the air entrainment

characteristics of circular plunging laminar jets and discovered that certain conditions of the jet were required before air bubbles were entrained into the flow. The criterion of inception proposed for their small scale jets ($Re < 10^3$) was

$$Re \simeq 0{,}045\ We^{1.35} \qquad \ldots\ldots (2.12)$$

based on the premise that viscous and surface tension effects dominated the process at least for this scale of jet.

Equation (2.12) can be rewritten in the form

$$U_i^* = \frac{6.22\,\sigma^{0{,}794}}{\rho^{0{,}206}\,\mu^{0{,}587}\,d^{0{,}206}} = \frac{K}{d^{0{,}206}} \qquad \ldots\ldots (2.13)$$

for air-water at constant temperature.

U_i^* is inception velocity to entrain air bubbles

d is jet diameter at impact point.

The implication of decreasing inception velocity for increasing jet diameters proved misleading for all jet diameters as the surface tension forces on the small diameter jets used, dampened surface disturbances in the jet, reducing the scale of eddies possible.

Later work by Van de Sande and Smith (Ref) and Ervine (Ref) indicated that for larger jet dimensions, the inception velocity tended towards a constant value, and the mechanism of entrainment at the point of inception was most influenced by surface disturbances on the jet surface.

This concept was later taken up to McKeogh (Ref) and Ervine, McKeogh and Elsawy (Ref) in testing inception velocities of plunging circular jets at various turbulence levels. A photograph overleaf (Figure 2.2) shows a plunging jet with impact velocity ≈ 3 m/s, $Re \approx 3 \times 10^4$, $Fr \approx 10$ and turbulence level ≈ 0,002, entraining no air bubbles. Previous work had shown that rough turbulent jets had an inception velocity around 1 m/s. A series of tests was carried out revealing that the inception velocity was more or less constant with increasing jet diameter, but varied considerably with increasing jet turbulence level. A plot of inception velocity with relative intensity is shown below, indicating that U_i^* for typical rough turbulent jets is ≈ 0,8 to 1.0 m/s. (See FIG. 2.3)

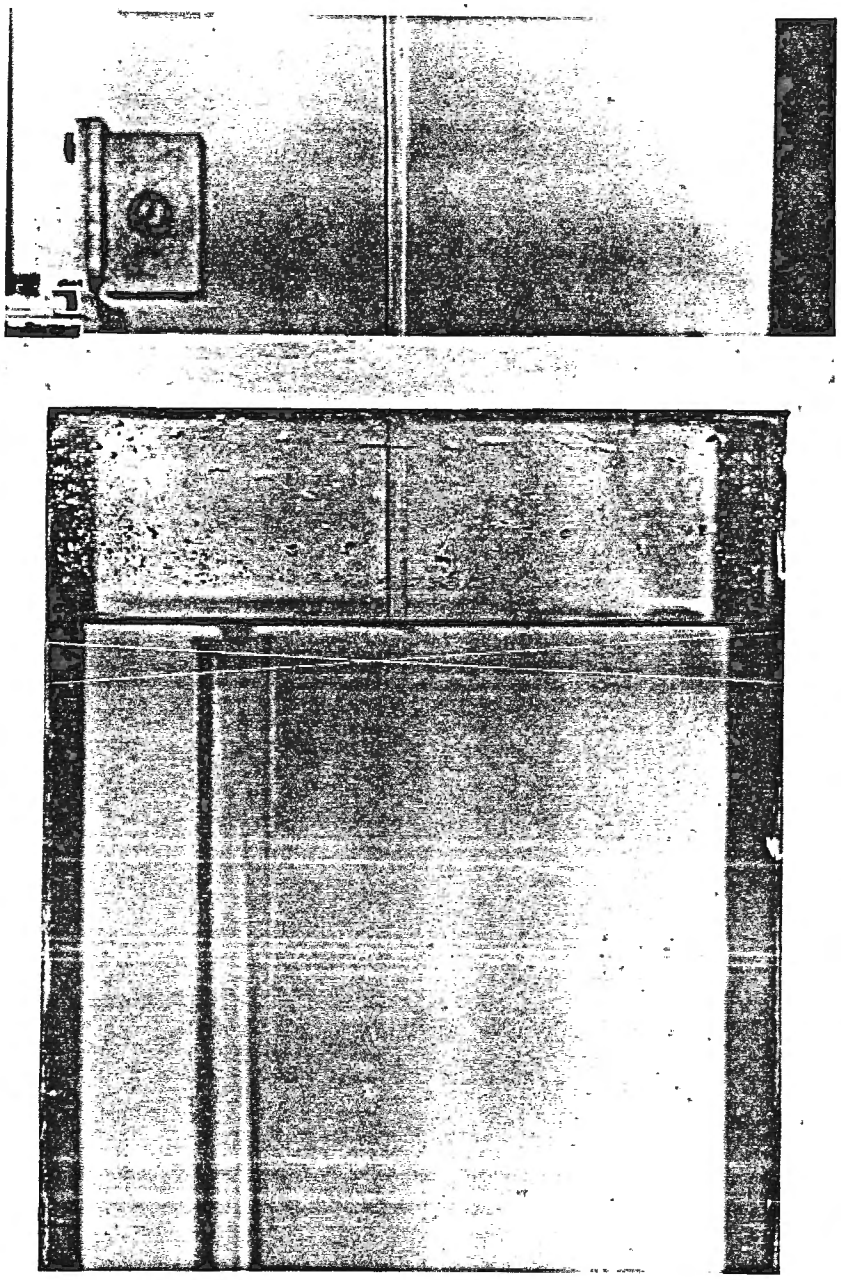

IMPACT OF A VERY SMOOTH 0.2% TURBULENT JET WITH THE POOL AND POSITION OF LASER BEAMS FOR VELOCITY AND TURBULENCE MEASUREMENT. Note the absence of air bubbles. (Mc Keogh)

FIG. 2.2.

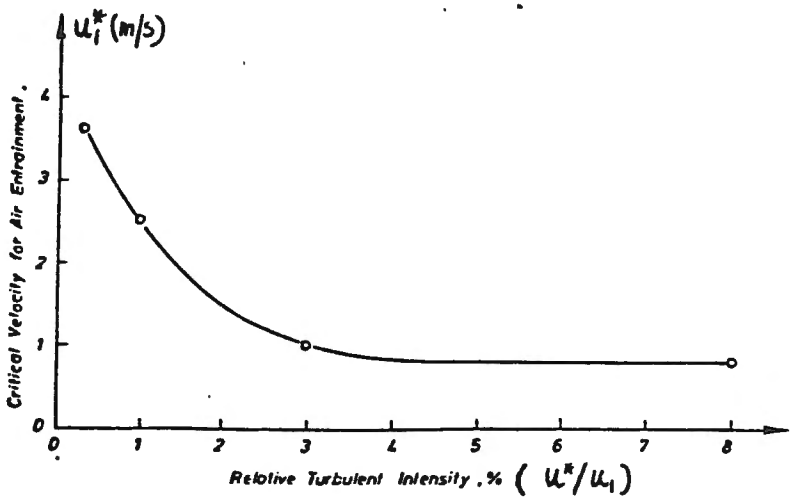

Figure 2.3 : The critical velocity for air entrainment in a plunging circular jet. (Ervine et al)

The implications of this graph are that

(1) Jet surface disturbances are an important factor in determining inception velocities (U_i^*)

(2) Small scale Froude models will entrain relatively less air than prototypes as $(U_i^*/U_1)_{model} > (U_i^*/U_1)_{prototype}$.

(3) A minimum of model scale can be calculated below which entrainment will not occur as U_i^* is constant for all scales.

(4) The model turbulence level U^*/u_1, ideally should be at least equal to that of the prototype structure.

2.2 Theoretical models for quantity of air entrained

In this section we will deal with the rate of air entrainment by a jet plunging through the atmosphere, a wall jet, and a hydraulic jump, but only in the sense of the total air entrained into the shear layer at the plunge point. Section 2.3 will deal with aspects of bubble detrainment (escape) from the shear layer, and bubble transport downstream with the flow and out of the shear layer.

Air entrainment by jets is a complex phenomenon and as yet does not have a definitive theory to describe the phenomenon, nor indeed, a comprehensive empirical correlation to describe the quantity of air entrained. Researchers are agreed that factors which contribute to the quantity of entrainment into a shear layer might be listed as -

- gravitational, inertial, viscous, surface tension forces,

- surface disturbances on the jet surface characterised by turbulent velocity components and turbulent eddy lengths.
- ambient pressure of the atmosphere.
- the angle of impinging jet.
- conditions in the receiving flow such as the velocity in any recirculation eddy, foam layer on the receiving flow, etc.

Analysis is complicated by the fact that at least three fundamental mechanisms for air entrainment have been proposed (shown overleaf on Figure 2.4)

(1) Entrainment due to surface disturbances on the jet. (Van de Sande (Ref), Ervine et al (Ref), Sene (Ref)). This occurs in lower velocity jets (U_1 < 5-10 m/s).

(2) Entrainment due to a continuous layer of air between jet and receiving flows (Van de Sande, Sene, etc.). This occurs in high velocity jets (U_1 > 10 m/s).

(3) Entrainment along a highly agitated free surface with a deep layer of foam (Thomas Ref). This may occur often in hydraulic jump entrainment, where air bubbles are entrained into the shear layer both at the toe of the jump and along the free surface roller.

Entrainment types (1) and (2) will be analysed in this section, with analysis for type (3) in Sections 2.3 and 3.3.

Formulation of non-dimensional groups to describe rate of air entrainment due to jet surface undulations

Consider the jet shown on Figure 2.1 with velocity greater than inception so that air is entrained, and assume that entrainment is achieved in the undulations in the jet surface, caused by U* and ℓ*, the fluctuating component of velocity and eddy length. Other influences on the rate of entrainment are inertial, gravitational, viscous, and surface tension forces, as well as the absolute value of jet velocity u_1. If the jet is plane, the rate of entrainment is given by q_a, and for circular jets $q_a = {}^{Q_A}/_{\pi d}$, where πd is the jet circumference at the point of impact. The droplength L is not included as it influences the velocity at impact already denoted by U_1, the size of the undulations δ, already denoted by U*, and the eddy length denoted

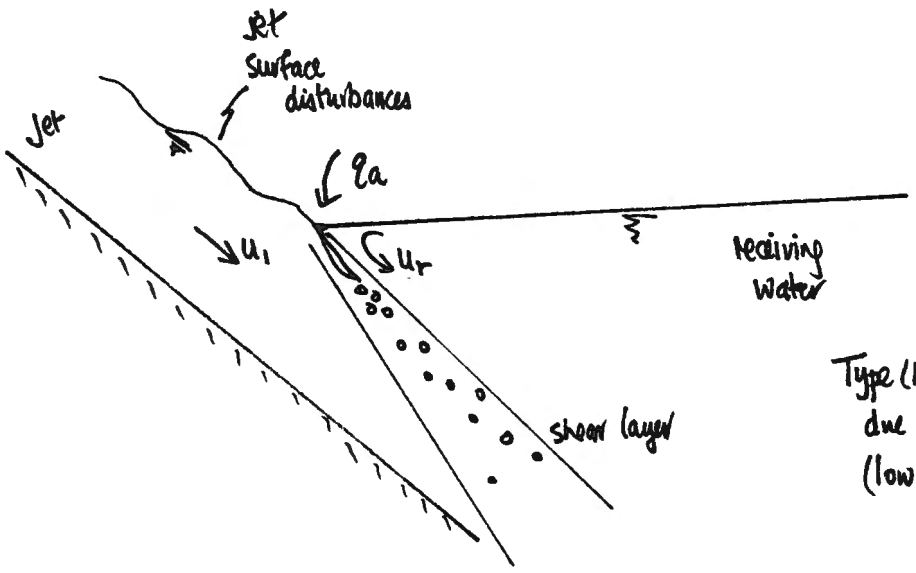

Type (1) Entrainment due to surface disturbances (low velocity)

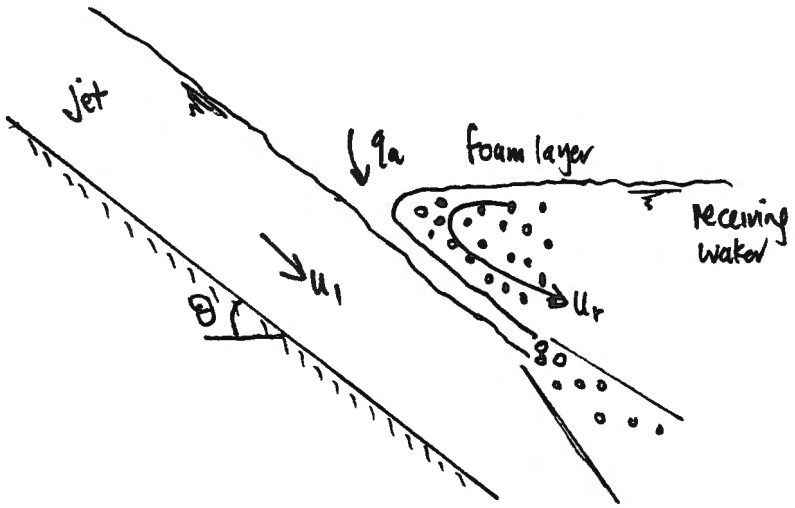

Type (2) Entrainment along thin layer of air (high velocity)

Type (3) Entrainment along foam roller + toe (hydraulic jump)

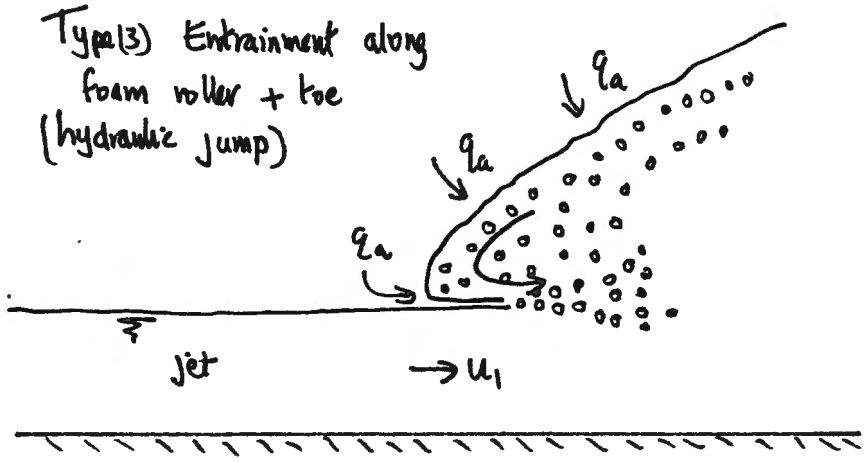

$\theta < 20°-30°$

FIG. 2.4.

by ℓ^*. The exclusion of droplength L, effectively excludes the flow conditions either at the overflow point or exit nozzle which ever is the case. In other words we are assuming that amplification of jet disturbances has not occurred, as in the case of wall jets. We may write

$$q_a = f\left(\rho, g, \sigma, \mu, u_1, u^*, \ell^*, d\right) \qquad \ldots\ldots (2.14)$$

Or by the method of synthesis,

$$f\left(\frac{q_a}{u_1}, \left(\frac{q_a^2\rho}{\sigma}\right)^{\frac{1}{2}}, \frac{q_a^{2/3}}{g^{1/3}}, \frac{\nu^{2/3}}{g^{1/3}}, \left(\frac{\sigma}{\rho g}\right)^{\frac{1}{2}}, \frac{\nu^2\rho}{\sigma}, \frac{u_1^2}{g}, \frac{\nu}{u_1}, \frac{\sigma}{\rho u_1^2}, \frac{u^{*2}}{g}, \frac{\nu}{u^*}, \frac{\sigma}{\rho u^{*2}}, \ell^*, d\right) = 0 \qquad \ldots\ldots (2.15)$$

We may choose for instance,

$$f\left(\frac{q_a}{u_1}, \frac{u_1^2}{g}, \frac{\nu}{u_1}, \frac{u^{*2}}{g}, \frac{\sigma}{\rho u_1^2}, \ell^*, d\right) = 0$$

or

$$\frac{q_a}{u_1 d} = f\left(\frac{u_1^2}{gd}, \frac{u_1 d}{\nu}, \frac{\rho u_1^2 d}{\sigma}, \frac{u^{*2}}{gd}, \frac{\ell^*}{d}\right) \qquad \ldots\ldots (2.16)$$

This becomes, for the ratio of air to water

$$\beta_{at} = f\left(Fr_1, Re_1, We_1, \frac{u^{*2}}{gd}, \frac{\ell^*}{d}\right) \qquad \ldots\ldots (2.17)$$

The term $\frac{U^{*2}}{gd}$ can be rewritten $\left(\frac{U^*}{U_1}\right)^2\frac{U_1^2}{gd}$ and as $\frac{U_1^2}{gd}$ is already included we can denote this as $\left(\frac{U^*}{U_1}\right)^2$, or turbulence intensity squared.

According to Sene and Thomas (Refs), air is entrained by maximum eddy lengths given by, $\ell^*_{max} \propto (Tu)\left(\frac{\sigma}{\rho g}\right)^{\frac{1}{2}}$ or as turbulence intensity is already included we may denote ℓ^*/d as $(\sigma/\rho g)^{1/2}/d$.

Thus we may write

$$\beta_{at} = f\left(Fr_1, Re_1, We_1, \left(\frac{u^*}{u_1}\right)^2, \frac{(\sigma/\rho g)^{\frac{1}{2}}}{d}\right) \qquad \ldots\ldots (2.18)$$

Hunt (Ref) has shown that het thickness d is no longer significant when $d > 4\left(\frac{\sigma}{\rho g}\right)^{\frac{1}{2}}$ or 4 times capillary length, or approximately 11 mm. Thus for jets with d > 11 mm,

$$\beta_{at} = f\left(Fr_1, Re_1, We_1, (Tu)^2\right) \qquad \ldots\ldots (2.19)$$

According to Kobus (Ref) Reynolds number is not significant if $> 10^5$ and we may write,

$$\beta_{at} = f\left(Fr_1, (Tu)^2\right) \quad \text{for } Re > 10^5 \text{ and } d > 11\,mm \qquad \ldots\ldots (2.20)$$

$Re > 10^5$ is an onerous condition for jets entraining air just past the inception velocity, as $U_1 \simeq$ 1 m/s, then d ≃ 0.1m (100 mm) which is substantial for a model.

If the jet thickness criterion is satisfied in the model, say d > 10 mm, then to satisfy $Re > 10^5$, we need $U_1 \geq$ 10 m/s.

It should be pointed out that three important parameters have been omitted from this analysis, the angle of the jet θ, the pressure of the ambient atmosphere $\Delta p/\rho u_1^2$, and the droplength of a plunging jet L, which effectively denotes the initial jet conditions, if the impact jet conditions are already established.

Thus a more complete similitude analysis would be of the form,

$$\beta_{at} = f\left(Fr_1, Re_1, We_1, Eu_1, (Tu)^2, \frac{(\sigma/\rho g)^{1/2}}{d}, \theta, L/D\right) \quad \ldots\ldots (2.21)$$

which in fact is almost intractable for comparing model/prototype plunging jet behaviour.

Most of the plunging jet and wall jet tests to be described have been carried out at atmospheric pressure, and hence Euler Number may be discarded.

A range of θ values has been used, but this may be corrected approximately to the vertical case, say.

Unfortunately in many cases $Re < 10^5$ and d < 11 mm and the best we can hope for in any correlation of existing data of plunging jets would be,

$$\beta_{at} = f\left(Fr_1, Re_1, We_1, (Tu)^2, \frac{(\sigma/\rho g)^{1/2}}{d}, L/d\right) \quad \ldots\ldots (2.22)$$

If we could arrange all jets > 10 mm and identical model/prototype turbulence intensity then $\beta = f(Fr, Re, L/d)$.

This of course may only apply in the context of low velocity jets with entrainment due to surface undulations, and will not necessarily apply with high velocity jets, say $U_1 >$ 10 m/s.

Quantity of air entrained due to jet surface undulations (Type (1))

It will be noted in the foregoing dimensional analysis, that a simple theoretical model for entrainment by jets is unlikely. The simplest models for jets not plunging over long lengths should include Froude number terms either Fr^2 or Fr -1, Reynolds Number Re, turbulence intensity (Tu) and if possible, an allowance for the inception velocity

U_1^* to entrain air. In some cases the Reynolds number is omitted (Kobus for Re > 10^5) where viscous effects do not have a significant influence.

Consider the model of Sene (Ref) and Thomas as already discussed in Section 2.1 and shown on Figure 2.1. Sene argues that air is entrained when the circulating eddy in the receiving flow can no longer follow the surface of the jet undulations, giving the criterion, $2\sigma/R \geq \frac{1}{2}\rho u_r^2$

Most of the air is assumed to be entrained by maximum eddy sizes ℓ^*_{max} given by $\ell^*_{max} \sim 4 (u^*/u_1)/(u_r/u_1) \sqrt{\sigma/\rho g}$

as already discussed on Page .

The magnitude of surface disturbance δ is given by $u^{*2}/2g$, where U* is the turbulent velocity component.

Thus for a <u>plane</u> plunging jet, Thomas argues that the volume of air held in a single jet surface undulation is given approximately by $\ell^{*2}_{max}\ \delta$, and hence the rate of air entrainment by

$$q_a \simeq \ell^{*2}_{max}\ \delta\ u_1 \qquad \ldots\ldots (2.23)$$

or

$$q_a \simeq 8\ \frac{(u^*/u_1)^2}{(u_r/u_1)^2}\ \frac{u^{*2}}{g}\ u_1 \sqrt{\sigma/\rho g} \qquad \ldots\ldots (2.24)$$

For $u^{*2} = u_1^2 \left(\frac{u^*}{u_1}\right)^2$ and $\sigma/\rho g$ = constant we have,

$$q_a = K/g\ (u^*/u_1)^4/(u_r/u_1)^2\ u_1^3 \qquad \ldots\ldots (2.25)$$

where U^*/U_1 is the turbulence intensity

U_r/U_1 is the velocity ratio at entrance to shear layer to which Sene assigns a constant value ($\simeq$ 0.035).

Dividing by the water velocity U_1 d (for a plane jet).

$$\beta_{at} = K\ Fr_1^2\ (Tu)^4 \qquad \ldots\ldots (2.26)$$

indicating an overly strong dependence on turbulence intensity. For a given turbulence intensity $\beta \propto Fr^2$ as already advocated by other authors.

Sene's analysis as applied to plunging circular jets contains two qualifications:-

(a) the droplength of the jet is much shorter than the jet disintegration length, so that amplification of surface disturbances does not occur (see Section 3.1),

(b) the circular jet diameter is sufficiently large so that surface tension forces do not dampen jet disturbances

The relationship proposed for short circular plunging jets is

$$\beta_{at} = \frac{Q_a}{Q_w} = K \frac{(u^*/u_1)^4}{(u_r/u_1)^2} \; u_1^2/gd \qquad \ldots\ldots (2.27)$$

which is of similar form to that of plane jets again implying

$$\frac{Q_a}{\pi d} = q_a \propto u_1^3 \qquad \ldots\ldots (2.28)$$

For low velocity circular jets.

This result $q_a \propto u_1^3$, has been put forward for low velocity plunging jets by previous authors

Renner (1975)	$\beta = K\ Fr^2$	$K \simeq 0.0015$ to 0.00275
Kobus & Rao (1975)	$\beta = K\ Fr^2$	(general principle)
Casteleyn, Van Groen & Kolkman (1977)	$\beta \propto K\ Fr^2 (1-\frac{0.8}{U_1})^3$	$K \simeq 0.006$ to 0.01
Goldring (1979)	$\beta = K\ Fr^2 (1-\frac{0.8}{U_1})^3$	$K \simeq 0.0025$
Ervine & Ahmed (1984)	$\beta = K\ Fr^2 (1-\frac{0.8}{U_1})^3$	$K = 0.00275$ to 0.012
Sene (1984)	$\beta = K\ Fr^2$	$K = 0.0004$ to 0.004

This illustrates a concensus for plane jets that $q_a \propto U^3$, or $\beta \propto Fr^2$, with the latter three authors attempting to incorporate the inception velocity U_i^* ($\simeq 0.8$ m/s) discussed in Section 2.1. None has specifically included turbulence intensity (Tu) as in Sene's theoretical formulation.

Kobus (1984, Ref) states for the general case of plunging jet entrainment $\beta = K\ (Re, Tu)\ Fr^2$, where Re is significant for $Re < 10^5$. Kobus (1984) has put forward a tentative framework in Figure 2.5 below, illustrating the effect of viscosity for $Re < 10^5$, incorporating the inception velocity, and showing $\beta = K\ Fr^2$ for $Re > 10^5$. This diagram

requires to be tested against existing data, (a) for each mechanism of air entrainment $q_a \propto U_1^3$, $q_a \propto U_1^{3}/_2$, (b) for partially disintegrated plunging jets, and also (c) to test the Kobus thesis that Turbulence intensity (Tu) has no significance when $R > 10^5$.

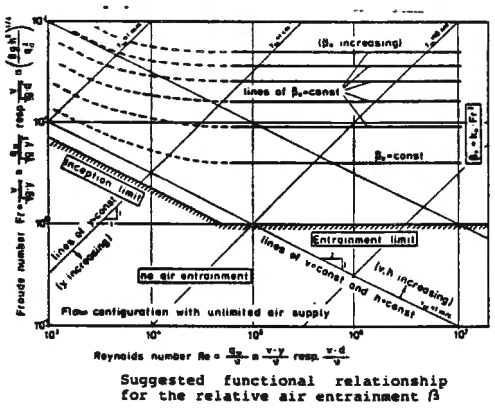

Figure 2.5 Kobus framework for load self aeration

Quantity of air entrained due to continuous layer of air above jet surface (Type (2))

There is some evidence, Van de Sande and Smith (Ref), Sene (Ref) that high velocity jets exhibit a different mechanism of entraining air into receiving water. The model proposed by Sene is sketched below.

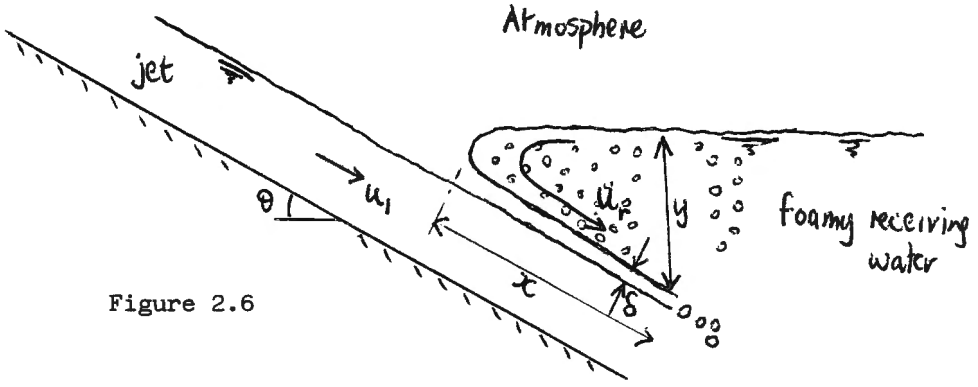

Figure 2.6

The receiving water is already foamy with reduced density $\rho_f = \rho_w (1 - C_f)$.

For the layer of air to penetrate receiving water

$$\tfrac{1}{2} \rho_{air} u_1^2 > \tfrac{1}{2} \rho_f u_r^2 \qquad \ldots\ldots (2.20)$$

and as $U_r/U_1 \simeq 0.035$, then air can penetrate receiving water almost with no foam in receiving water $\rho_f/\rho_w \simeq 1$.

It can be seen from the sketch above, the pressure difference along the thin layer of air, thickness δ, from inlet to point of air bubble formation is

$$\Delta p = \rho_f g y \simeq \rho_f g x \sin\theta$$

and hence net force $$\Delta p\, \delta = \rho_f g x \sin\theta\, \delta \qquad \ldots\ldots (2.30)$$

This force is balanced by the shear stress imparted to the air layer by the flow jet below, at speed U_1, assuming the contribution from the recirculating foamy layer is small, $Ur \lll U_1$.

Sene approximated this force to τx, and assuming a laminar air layer

$$\tau x \simeq \mu_a \frac{u_1}{\delta} x \qquad \ldots\ldots (2.31)$$

Equating forces and calculating the rate of air flow as $U_1\, \delta = q_a$ we have

$$q_a \simeq \sqrt{\frac{\mu_a u_1^3}{\rho_f g \sin\theta}} \qquad \ldots\ldots (2.32)$$

Sene modifies the relationship above to account for air velocity profile in the thin layer to give a revised estimate

$$q_a \simeq \frac{1}{3}\sqrt{\frac{2\mu_a u_1^3}{\rho_f g \sin\theta}} \qquad \ldots\ldots (2.33)$$

The same relationship applies for circular jets, except $q_a = Q_a/\pi d$.

The application of (2.33) above appears to be for jets of $U_1 > 7$–10 m/s when the jet surface undulation type of entrainment is less significant possibly due to the fact that surface undulations have reached a maximum value, or that pre-entrainment of the jet has occurred.

Sene also used this type of analysis to predict (speculatively) the rate of entrainment at the toe of the hydraulic jump as shown below.

Figure 2.7
(Hydraulic jump)

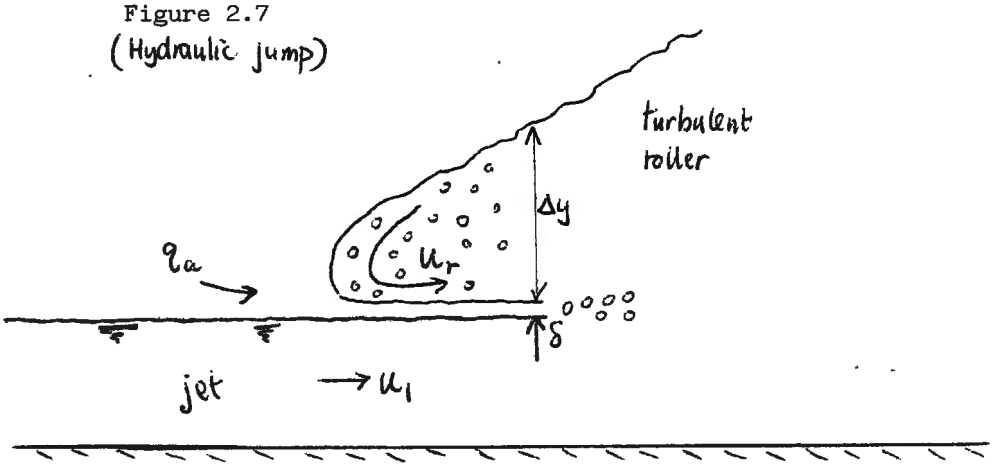

The pressure difference along the gap $\Delta p \simeq \rho_f g \ \Delta y$, (where $\rho_f < \rho_w$) is again balanced by the shear imparted to the air by the jet below $\mu_a u_1/\delta$. Hence $\delta \sim \left(\frac{\mu_a}{\rho_f g}\frac{\Delta x}{\Delta y} u_1\right)^{1/2}$ and the air flow q_a is given by

$$q_a \simeq \frac{1}{3}\sqrt{\frac{2\mu_a}{\rho_f g}}\sqrt{\frac{\Delta x}{\Delta y}}\ u_1^{3/2} \qquad \ldots\ldots (2.34)$$

$\Delta x/\Delta y$ may be approximated for jumps to the jump length, $L_r/y_2 - y_1$. Equation (2.34) implies non-similitude between the ratio of air to water β, and the jet Froude Number (Fr_1), but only incorporates entrainment at the toe of the jump, whereas air is also entrained into the free surface roller. (Thomas Ref).

It is interesting to speculate on the quantity of air predicted from (2.34). For a jump we may assume $\Delta x/\Delta y \simeq 5$, and $q_a \simeq \left(\frac{\mu_a u_1^3}{\rho_f g}\right)^{1/2}$ If we now assume $\rho_f \simeq \rho_w$, and substitute for μ_{air}, i.e. μ_{water} 1×10^{-3} and $\mu_{air} \simeq 1.8 \times 10^{-5}$ then $\mu_{air} \simeq \mu_{water}/55$. Hence we obtain

$$q_a \simeq 0.13\left(\frac{\mu_w u_1^3}{\rho_w g}\right)^{1/2} \quad \text{or} \quad \beta \simeq 0.13\left(\frac{\mu_w u_1}{\rho_w g d^2}\right)^{1/2}$$

This becomes

$$\beta \simeq 0.13\left(\frac{\mu_w}{\rho_w u_1 d}\cdot\frac{u_1^2}{gd}\right)^{1/2} = 0.13\ Fr/(Re)^{1/2}$$

Even for the highest foam air concentration $C_f \simeq 0.5$ and $\rho_f \simeq \rho_{w/2}$ we obtain

$$\beta \simeq \frac{0.18\ Fr_1}{(Re)^{1/2}}$$

At Re = 10^3, $\beta \simeq 0.005\ Fr_1$)
Re = 10^4, $\beta \simeq 0.0015\ Fr_1$) These are shown below compared with Kalinske and Robertson etc., giving very low estimates for β.
Re = 10^5, $\beta \simeq 0.0005\ Fr_1$)

We can only conclude here, that either the analysis is inadequate or a large proportion of air entrainment into hydraulic jumps comes from the turbulent surface roller as postulated by Thomas. It is more likely that the above analysis of Sene is applicable to high velocity jumps $U_1 \simeq 10$ m/s, in which case pre-entrainment of the jump has been ignored.

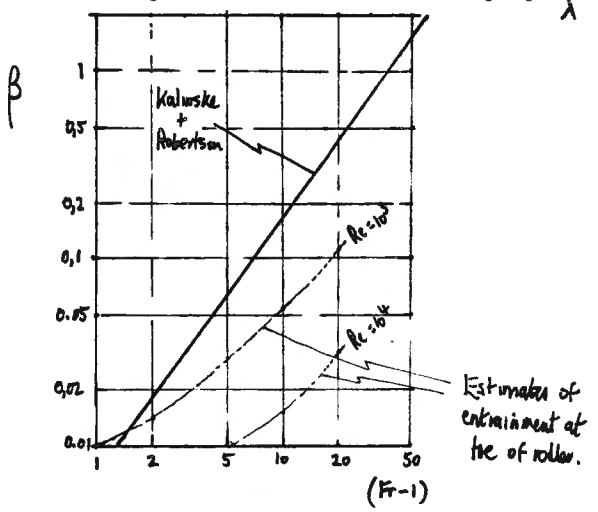

Figure 2.8

Summary of Section 2.2

An estimation of the quantity of air entrained by a plunging wall jet is complicated by the fact that Froude and Reynolds Number similarity is required at the same time (or Re > 10^5), up to three separate mechanisms are possible Type (1), (2) and (3), and the process is sensitive to the turbulence intensity of the jet (U^*/U_1). Some of three points are illustrated in Figure 2.9 overleaf.

(1) Van de Sande and Smith covered a wide velocity range of circular jets showing that at low velocities $q_a \simeq U_1^3$, and at higher velocities > 10 m/s, $q_a \simeq U_1^{1.5 \rightarrow 2}$. This has important implications for model/prototype comparisons. If the same is true for plane jets, then correlations based on $q_a \simeq U_1^3$ or $\beta \simeq Fr_1^2$ may overestimate prototype entrainment if U_1 (prototype) is greater than 10 m/s. It is still not absolutely clear if the regime $q_a \simeq U_1^3$ ceases for U_1 > 5 m/s as experimental data beyond this range is very limited. More tests are required.

(2) The effect of turbulence intensity is illustrated clearly on the two low velocity plots by Sene. The upper curve gives the maximum entrainment possible (upper surface of plane jet) in an artificially rough jet, while the lower curve (artifically smoothed jet) gives a prediction of the minimum possible entrainment.

$$\left.\begin{aligned} q_{a(max)} &\simeq 0.0004\ U_1^3 \\ q_{a(min)} &\simeq 0.00004\ U_1^3 \end{aligned}\right\} \text{ Sene, for low velocity jets.}$$

It is interesting that other low velocity plunging jet data fit between these two limits.

A jet entraining air on both surfaces would give values of q_a twice as high as predicted by Sene (up to $.0008\ U_1^3$).

(3) At this stage we have an unresolved problem. Renner and Kobus state that the ratio of air to water, $\beta = K\ Fr^2$, at least for Froude Numbers less than 10. Therefore for this condition $q_a \propto U_1^3$ irrespective of the velocity acting. By implication, entrainment is always by surface undulation mechanisms. That is, $q_a \propto U_1^3$, or $q_a \propto (U_1^2)\ U_1$, or for a given turbulence level U^*/U_1, $q_a \propto U^{*2}\ U_1 \propto \delta\ U_1$. Thus surface disturbances continue to increase with increasing jet velocity and δ is always proportional to U^{*2}. This also implies that a model operating at say 2 m/s will give $q_a \propto (2)^3 = 8$, and a

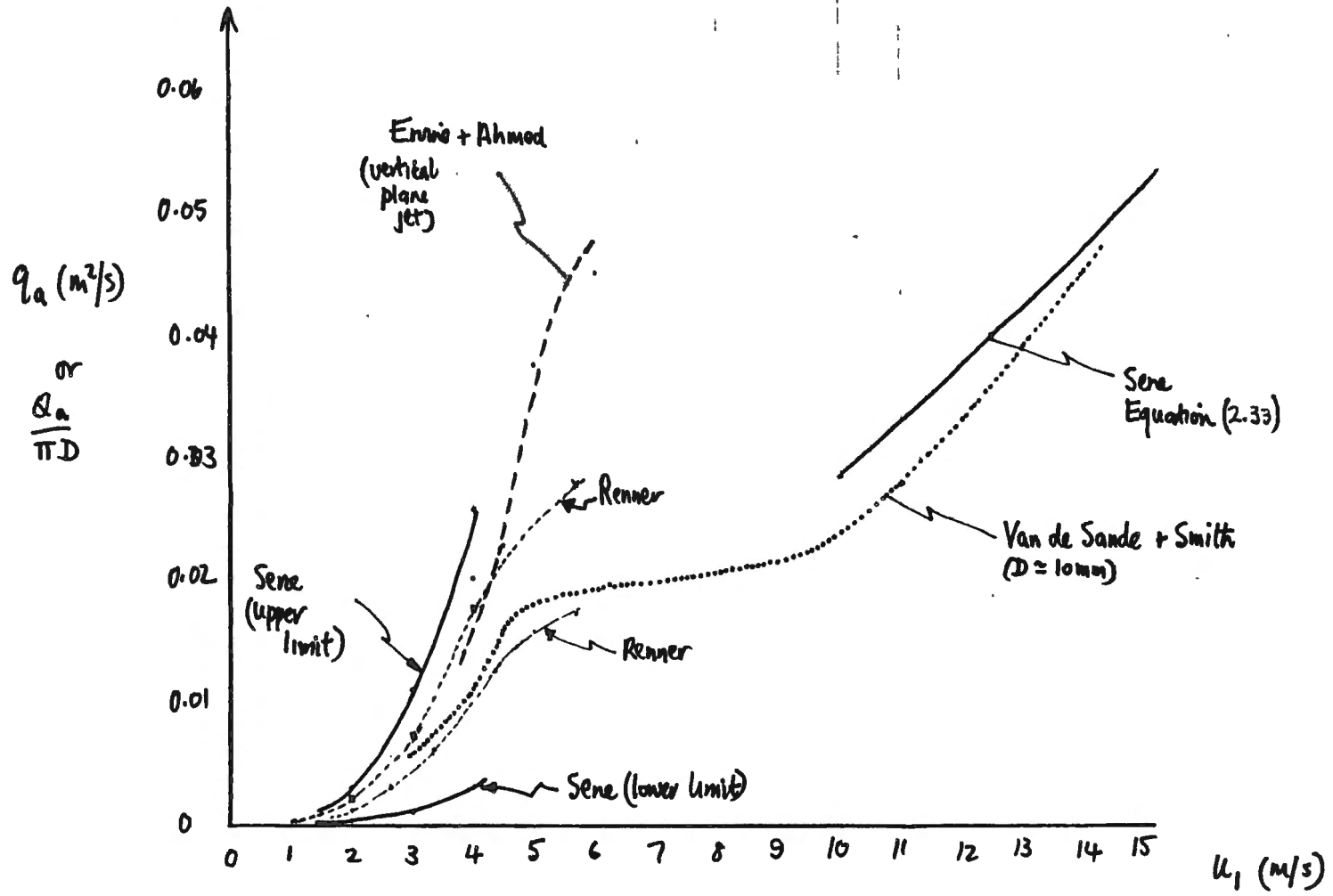

FIG 2.9 Rate of air entrainment into shear layer by plunging jets.

prototype say at 10 m/s will give $q_a \propto 10^3 = 1000$. In order for this to occur the ratio of the prototype to model surface disturbances would have to be $(10/2)^2 = 25$ times.

The counter evidence from Sene and Van de Sande and Smith is that surface disturbances do not continue to grow indefinitely. From the limited data it appears that surface disturbances reach a maximum around 5-7 m/s. Therefore just beyond 5 m/s, $q_a \propto \delta U_1 = KU_1$, as δ becomes constant (See Figure 2.9). We might enter then a regime of linear increases in air entrainment with velocity. Around this stage the intermittent entrainment by surface disturbances becomes a continuous layer of air between jet and roller, or $q_a \propto U_1^{3}/_{2}$. This is equivalent to saying that surface disturbances are no longer significant and entrainment is comparable to air from the boundary layer of a laminar jet.

It is more likely that air entrainment generally, (ignoring contributions from pre-entrainment) would be made up of a combination of surface disturbances and air boundary layer entrainment in the form

$$q_a = K_1 u_1^3 + K_2 u_1^{3/2} \qquad \ldots\ldots (2.34b)$$

In this sense K_2 may be insignificant at low jet velocities, and

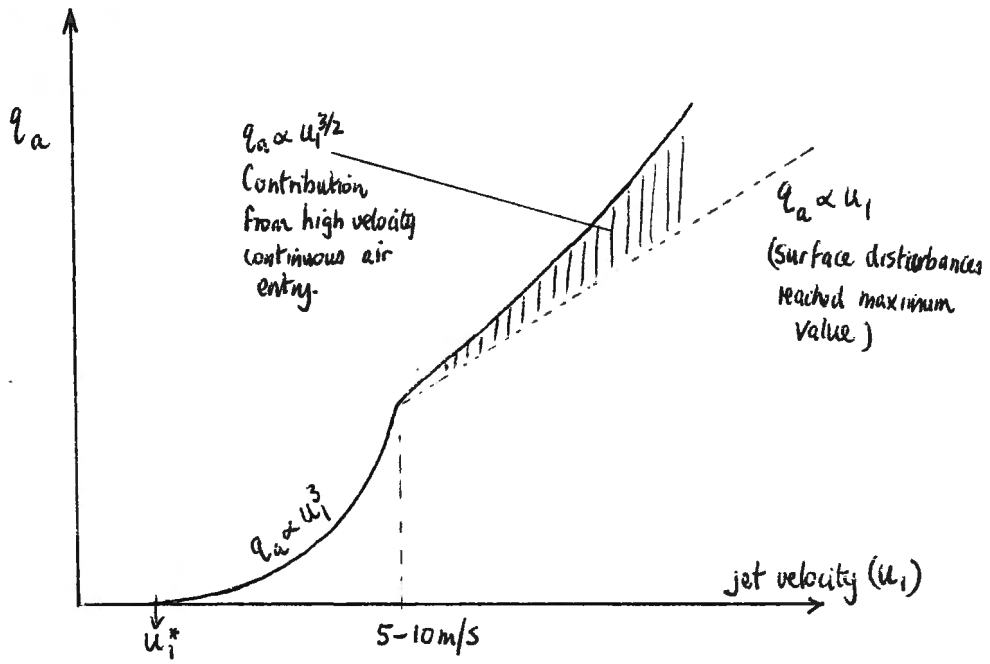

Figure 2.10

K_1 may be small at very high velocities. The value of K_1 is obviously influenced by Reynolds Number (Kobus), turbulence intensity (Sene and Thomas), and the value of jet thickness but only for jet thickness less than say 30 mm.

One obvious weakness in the high velocity entrainment argument is that pre-entrainment possibility is ignored, and as a first order approximation may scale on Fr_1^2.

Section 2.3 Bubble escape and bubble transport mechanisms

In Section 2.2 we considered the quantity of air entrained into a flow for plunging jets, wall jets and to a limited extent, hydraulic jumps. In this section we will consider air bubble behaviour after the point of entrainment (in the shear layer, etc.), with the discussion initially limited to plane wall jets and hydraulic jumps.

Consider first a plane wall jet impinging on a conduit full condition as shown on Figure 2.11. Assuming the jet velocity u_1 is greater than the inception velocity to entrain air U_1^*, then air bubbles are carried into the shear layer and are subjected to a range of forces including buoyancy, drag, inertia, vorticity etc. A recirculating vortex is usually set up with velocity $U_r << U_1$. Water is entrained into the shear layer from either side, causing a spreading of the shear layer and eventual reattachment on the other side of the conduit as shown. In some cases, when D/d is very large, and the conduit angle is shallow, it may be possible for the shear layer to return to the water surface before reaching the opposite conduit wall.

For a low jet velocity, say just greater than U_1^*, the entrained air bubbles are carried into the flow, but are quickly detrained from the shear layer, (because of bubble buoyancy) and are recirculated to the water surface. In this case, no air bubble transport occurs downstream of the shear layer. This is shown on Figure 2.12 (taken from Ph.D. thesis of A. A. Ahmed).

At slightly higher velocities the mixing region extends in length along the conduit, and tiny air bubbles (diameter ≈ 1 mm) extend some distance beyond the shear layer but net air transport along the conduit is still not occurring. In this case $U_1^* < u_1 < U_{1\,min}$, the jet velocity is still smaller than the minimum jet velocity to transport air, $U_{1\,min}$. This is illustrated on Figure 2.13, again with total air

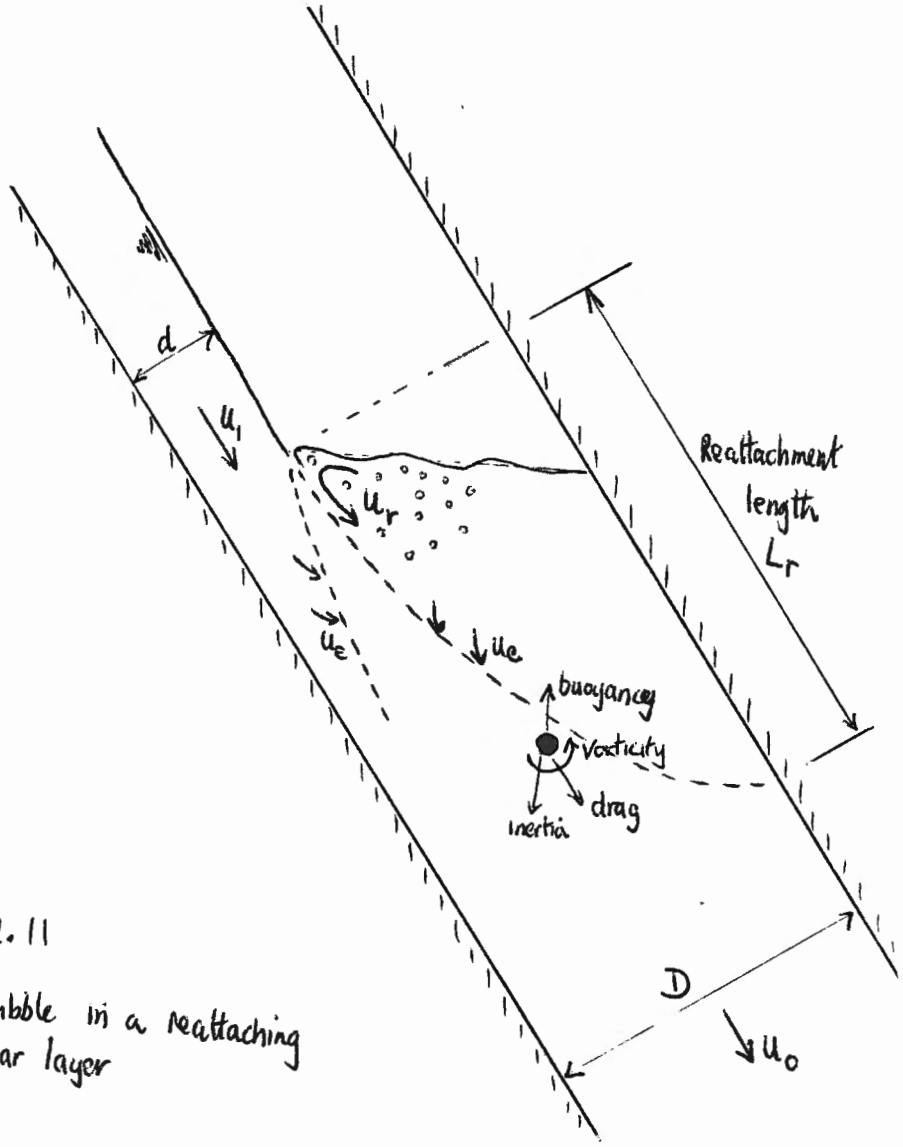

FIG. 2.11

Air bubble in a reattaching shear layer

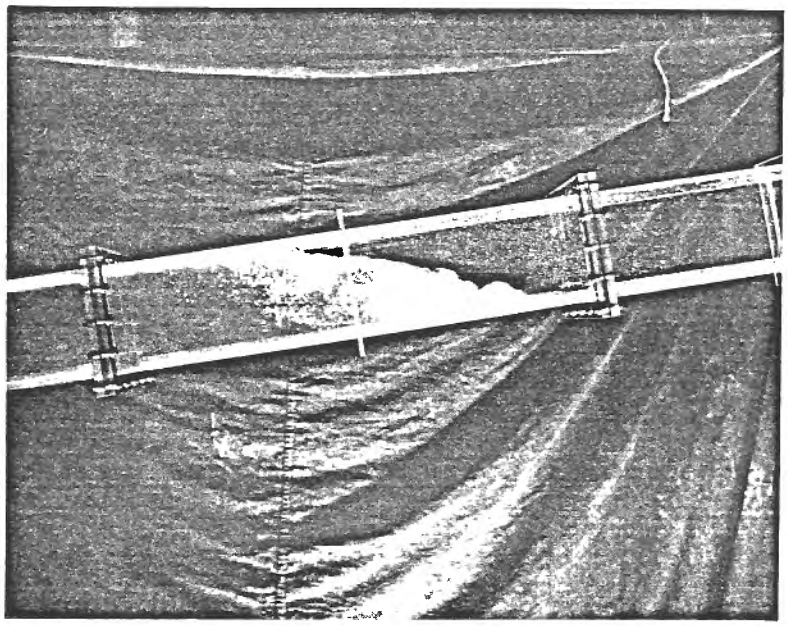

FIG (2.12). Early stage of air entrainment starts in the jet surface.

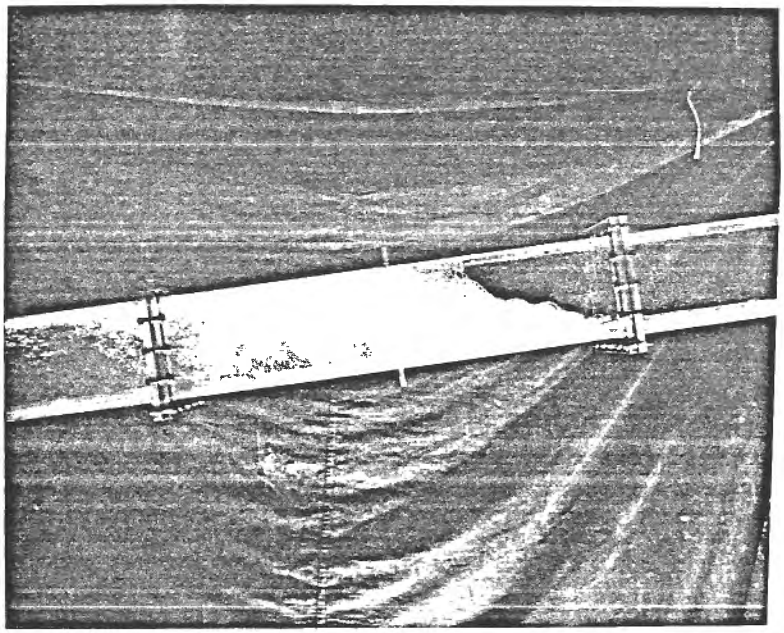

FIG (2.12). Mixing region.

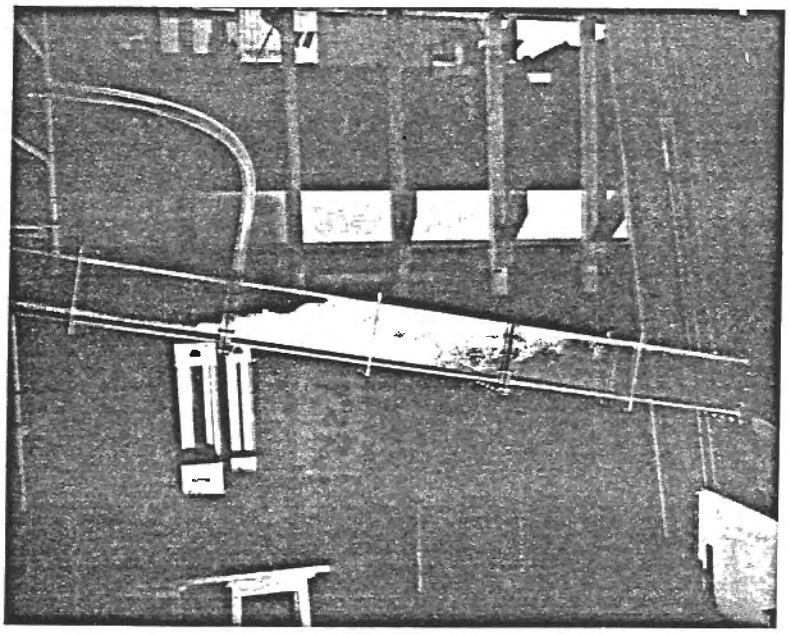

FIG. (2.13). Air bubbles move downstream, but with total recirculation.

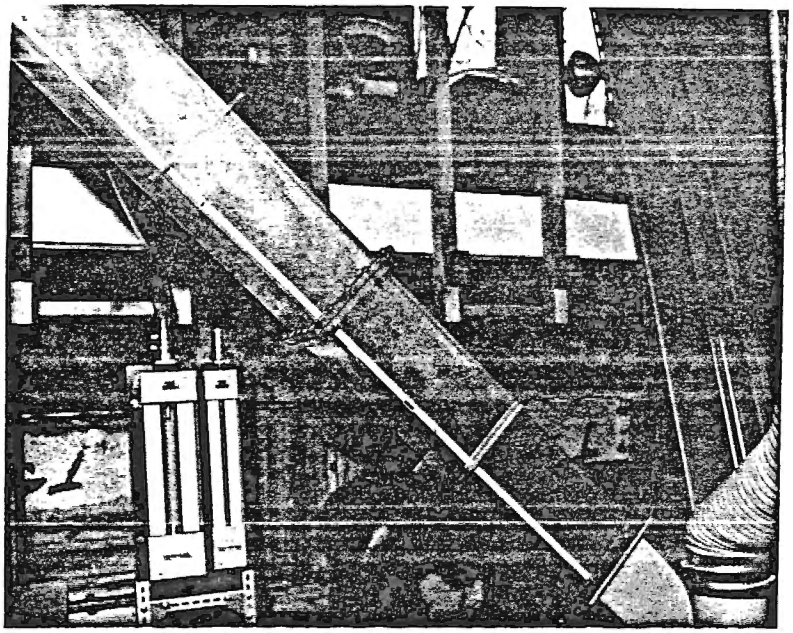

FIG. (2.13). Air bubbles start to move further downstream in form of tiny bubbles.

detrainment, or total deaeration.

At higher jet velocities, $U_1 = U_{1min}$, a point is reached when air bubbles are transported continuously along the length of the conduit. This jet velocity is the minimum velocity to transport air. Initially only small bubble diameters are transported, but at higher velocities, larger bubble sizes are transported (5 mm). This transition region is sometimes characterised by a coalescence of air bubbles on the conduit roof, forming small air pockets, which often "blow-back". This is illustrated on Figure 2.14, overleaf.

At higher jet velocities, $U_1 > U_{1min}$, a larger proportion of the total air entrained into the shear layer, is transported along the conduit. We generally define the total rate of air entrainment into the shear layer as q_{at}, the amount transported downstream as the net air transport q_{an}, and the remainder is detrained and recirculated back to the atmosphere q_{ar}. In this case the entrainment capacity of the flow can be said to exceed the transport capacity.

At much higher velocities $U_1 >> U_{1min}$, a stable condition is reached where most of the entrained air is transported along the conduit. It should be noted here, that in terms of bubbly flows the upper limit of transport generally corresponds to a void fraction of $\alpha = 0.42$, or an air/water ratio $\beta \simeq 0.72$. If the jet is entraining more air than this upper limit for transport then recirculation to the atmosphere is likely to occur again. As an alternative, the bubbly flow can change to slug or air pocket flows, when β values greater than 0.72 can be transported, especially at shallow angles.

The factors which influence how much air is detrained and how much is transported are complex, and will be dealt with in some detail in this section. In broad terms however, the problem can be defined by the forces action on a bubble both in the shear layer and downstream of the shear layer. That is, in the shear layer a bubble is acted upon by inertial, buoyancy, drag and lift (vorticity) forces, and bubble progress along a shear layer will depend on the relative magnitudes of these forces. This will be discussed in the light of recent work by Auton, Sene, Thomas and Hunt (below), recent experiments by Ervine and Ahmed, and in the light of a detrainment analysis by Neale Thomas, applied to Type 3 entrainment, where air is entrained along the length of a shear layer (such as hydraulic jumps) by a foamy surface

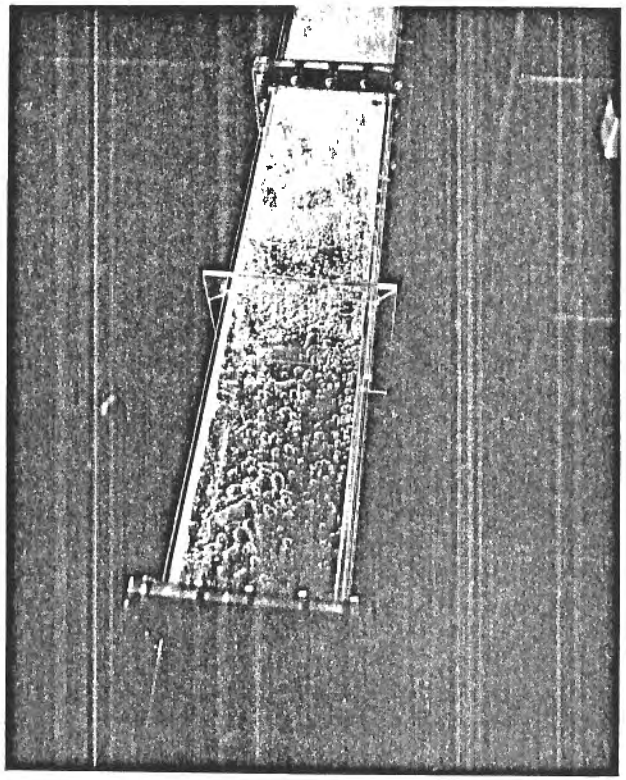

FIG (2.14). Air bubbles coalesce to form large air bubbles.

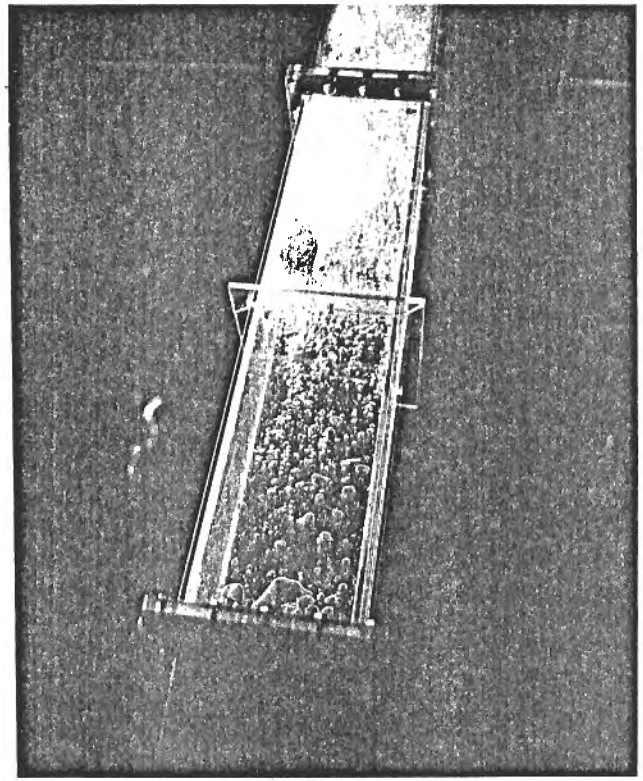

FIG (2.14). Large air bubbles start to move upwards.

roller. Downstream of the shear layer, vorticity and inertial forces may be considered small compared to drag and buoyancy, and simpler analyses may be possible.

Let us consider first the most complex section of the analysis, the behaviour of an air bubble in a turbulent shear field caused by an impinging jet. The work of Thomas et al is the most relevant.

Simulation of bubble trajectories in vortices in a shear layer

The most recent work on the behaviour of air bubbles in shearing vortices has been carried out by Thomas, Auton, Sene and Hunt (Ref) at Cambridge, England. Their work originated from research into plunging wall jet air entrainment and the influence of shearing vortices downstream of the plunge point entrapping air bubbles in the cores of vortices as shown on the sketch below.

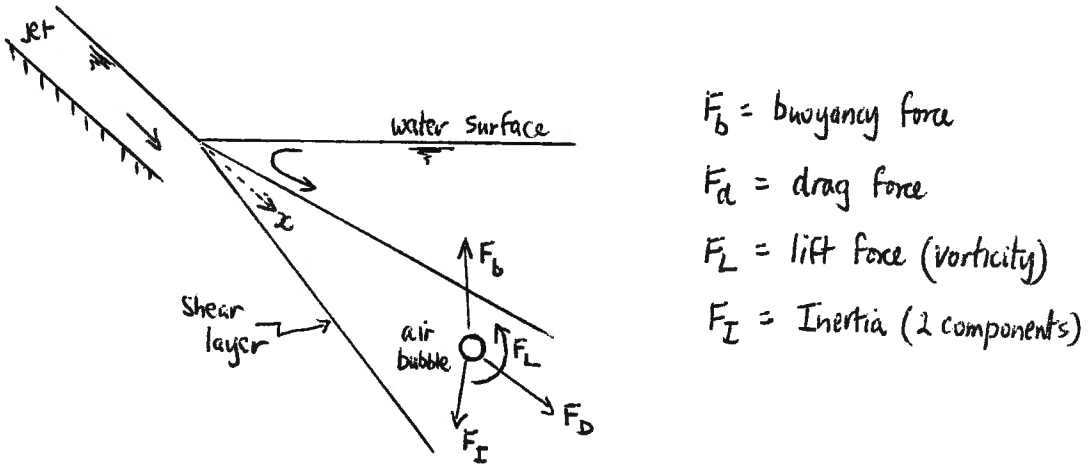

Figure 2.15

Forces on spherical bubble

Ignoring the density of air ρ_a << ρ_w, Auton has written an expression for the resultant force on a bubble.

$$F = -\rho_w \bar{V} g + \rho_w \bar{V} \frac{du}{dt} - \rho_w \bar{V} C_{VM} \left(\frac{\partial u_b}{\partial t} - \frac{du}{dt} \right)$$

buoyancy; particle acceleration; Virtual mass force

$$- \rho_w \bar{V} C_L (u_b - u) \wedge \omega - \rho_w \bar{V} g \left(\frac{u_b - u}{u_{br}} \right) \left| \frac{u_b - u}{u_{br}} \right|$$

lift force due to Vorticity; drag force on bubble

..... (2.35)

where F is the resultant force on the bubble

$\bar{v}$ is bubble volume

U is local water velocity vector

U_b is bubble velocity vector

U_{br} is bubble rise velocity in fluid at rest

$\frac{d}{dt} = \frac{\partial}{\partial t} + U.\nabla$

C_{vm} is virtual mass coefficient (= 0.5)

C_L is lift coefficient (= 0.53)

ω is the vorticity vector ($\nabla \Lambda U$)

For the simplified case of $^{\partial U_b}/_{\partial t} = 0$ in the virtual mass force, Sene (Ref) has written Equation (2.35) in terms of the acceleration (total derivative) of the bubble.

$$\frac{du_b}{dt} = -g + \frac{du}{dt} + C_{VM}\frac{du}{dt} - C_L(u_b - u)\Lambda\omega - g\left(\frac{u_b - u}{u_{br}}\right)\left|\frac{u_b - u}{u_{br}}\right|$$

which becomes

$$\frac{du}{dt} = 3\frac{du}{dt} - 2g - 2C_L(u_b - u)\Lambda\omega - 2g\left(\frac{u_b - u}{u_{br}}\right)\left|\frac{u_b - u}{u_{br}}\right| \quad \text{..... (2.36)}$$

(↑ inertia; ↑ buoyancy; ↑ lift (vorticity); ↑ drag)

Sene has used ΔU (the velocity difference between shear layer and recirculating flow) and x (the streamwise direction) to compare the orders of magnitude of the forces above, giving

$$\left[\text{inertia} \sim \frac{\Delta u^2}{x}\right], \left[\text{buoyancy} \sim g\right], \left[\text{lift (vorticity)} \sim \frac{C_L u_{br}\Delta u}{x}\right], \left[\text{drag} \sim g\right]$$

Thus if $U_{br} << \Delta U$, the lift forces can be neglected compared to inertia; inertia can be neglected compared to drag and buoyancy if $\frac{\Delta U^2}{x} << g$, and so forth.

Thomas, Auton, Sene and Hunt used a form of Equation (2.36) above to investigate the behaviour of bubbles rising under buoyancy from a point below a vortex core (shown overleaf). The resulting trajectories are shown on Figure 2.16 indicating a certain width w, whereby bubbles entering within the region are trapped in the vortex core. This was verified experimentally.

Dimensional analysis showed that this width could be correlated by

$$\frac{w g}{u_{br}^2} = f\left(\Gamma g/u_{br}^3\right) \quad \text{..... (2.37)}$$

where Γ is the ciruclation in the vortex. The trapping width increased with ciruclation in the vortex (Ref).

Thomas et al went on to simulate bubble injection into a shear layer using a technique of discrete vortex modelling. Early simulations revealed a large proportion (80% in their case) of bubbles were entrapped by vortex cores, but a wider range of tests requires to be carried out before definite statistics can be presented on the proportions of bubbles trapped by vortices trapped in a free shear layer.

Ultimately this type of analysis by Thomas et al will lead to more accurate predictions of bubble behaviour in shear layers, including detrainment, (bubble escape) and bubble transport. The analysis however requires extensive computer modelling and is not yet at a stage of development to become common place in the Civil Engineering context. In the meantime we can use more approximate methods, especially with regard to closed conduit hydraulic structures.

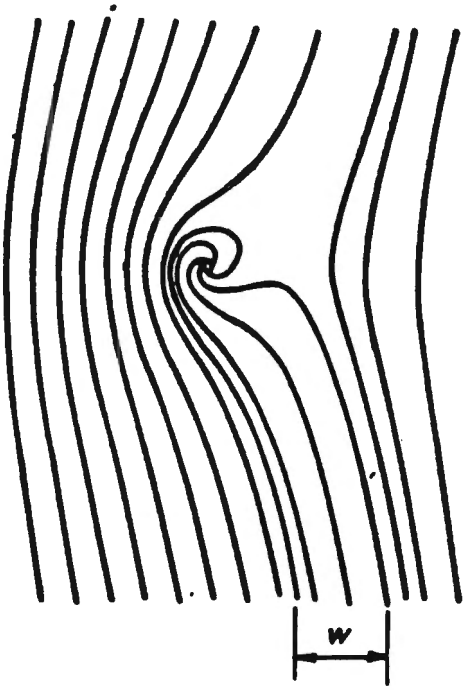

Figure 2.16 : Paths of bubble with a rise velocity near two-dimensional vortex. Note that bubbles rising from the region W are trapped in the vortex core.

Figure 2.16

A significant finding of Sene's work on bubble escape and bubble behaviour in a shear layer is that the slip velocity of bubbles is close to the bubble rise velocity U_{br}. That is, if U is the local water velocity in the shear layer, and U_b the local bubble velocity then $U - U_b \simeq U_{br}$. Thus for a bubble in a shear layer at an angle θ to the horizontal as shown in the sketch overleaf.

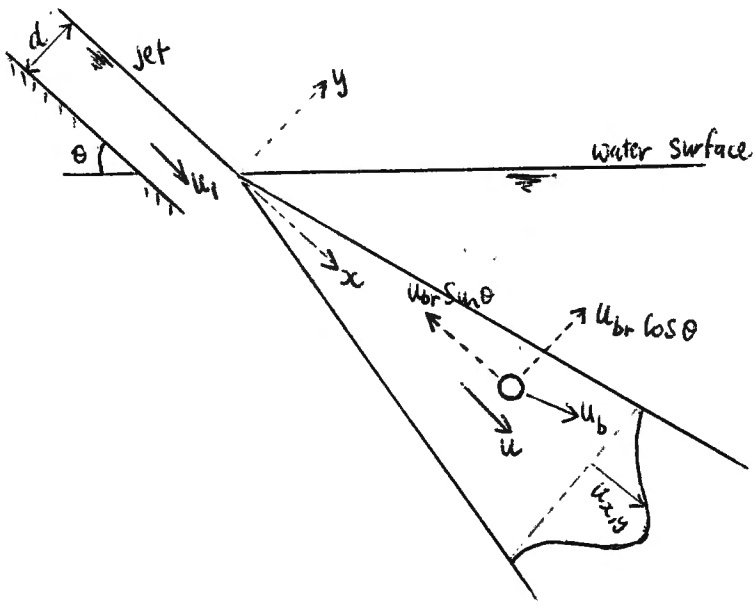

$$\begin{cases} \dfrac{dx_b}{dt} = u - u_{br}\sin\theta \\ \dfrac{dy_b}{dt} = u_{br}\cos\theta \end{cases}$$

Figure 2.17

If the velocity in the shear layer U $\gg U_{br}$, and the velocity profile in the shear layer is given by $U_{(x,y}$, then the average bubble velocity at any section is

$$\bar{u}_b(x) = \frac{\int_{-\infty}^{\infty} u_{(x,y)}\, dy}{\delta(x)} \qquad \ldots\ldots (2.38)$$

where $\delta_{(x)}$ is the width of the shear layer at any value of x.

The half angle of spread of the shear layer is approximately tan 14° and we may approximate δ to, $\delta = 2(X)\tan 14°$. Furthermore Reichardt showed $\int_{-\infty}^{\infty} u_{(x,y)}\, dy = 0{,}58\, u_1 \sqrt{xd}$

$$\text{Hence, } \bar{u}_b(x) \sim \frac{0.58\, u_1 \sqrt{xd}}{2x \tan 14°} \sim 1.17\, u_1 \Big/ \sqrt{x/d} \qquad \ldots\ldots (2.39)$$

Therefore the time taken by the bubble to reach a distance X in the streamwise direction

$$T = X/u_b(x) = X\sqrt{X/d}\,/\,1.17\, u_1$$

Assume bubbles originate at the plunge point, then during the time period T, bubbles will rise a certain distance towards the edge of the shear layer. For bubbles to escape the shear layer, then the distance in the y direction is $\delta/2$ and the time $T = \delta/2 \,/\, u_{br}\cos\theta$

Thus we have an expression for the average distance (streamwise) travelled by the bubbles before leaving the shear layer is

$$\bar{X}/d \simeq 0.19 \left(u_1/u_{br}\cos\theta\right)^2 \qquad \ldots\ldots (2.40)$$

Actually the constant 0.19 quoted by Sene, would seem from the arithmetic to be 0.085, but meanwhile assume $\bar{X}/d = K_1\left(u_1/u_{br}\cos\theta\right)^2$

The question now becomes, can Equation (2.40) be used to gain some insights into closed conduit behaviour in the context of minimum velocities to transport air downstream of a shear layer. Sene (Ref) has conducted some measurements which reveal that the reattachment length of a spreading shear layer in a closed conduit is given approximately by

$$L_r/d \simeq 4(D/d - 1) \quad \ldots\ldots (2.41)$$

as indicated on the sketch, and this estimate appears almost independent of conduit angle.

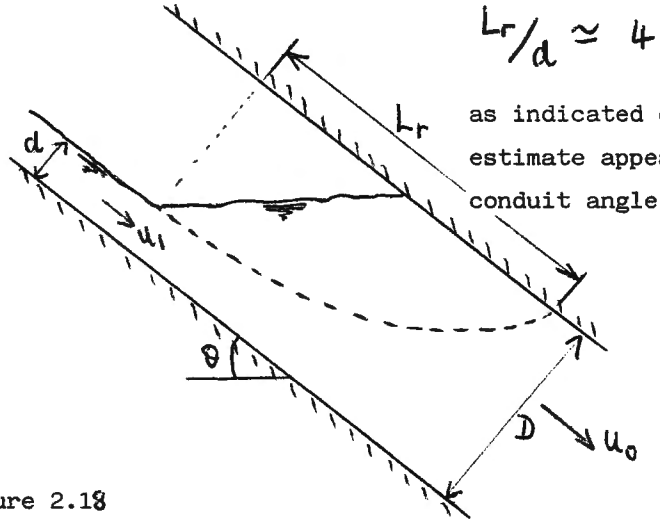

Figure 2.18

Thus we can say as a speculation that the first requirement to transport entrained air bubbles downstream of the shear layer is that the average distance travelled by bubbles given by Equation (2.40) should be at least equal to the value of L_r given in Equation (2.41). Thus our first criterion becomes

$$K_1\left(u_1/u_{br}\cos\theta\right)^2 \simeq 4\left(D/d - 1\right)$$

or alternatively

$$\frac{u_{1\,min}}{u_{br}} \simeq \frac{2\cos\theta}{K}\left(\frac{D}{d} - 1\right)^{1/2} \quad \ldots\ldots (2.42)$$

where K might be or order 0.1 to 0.2 (after Sene), and $U_{1\,min}$ is the jet velocity required to transport air bubbles downstream. (Not to be confused with U_1^*, the jet velocity required to entrain bubbles <u>into</u> the shear layer).

In the event of air bubbles being transported downstream out of the shear layer, the criterion for air bubble transport (ignoring turbulence effects is simply $U_o \geq U_{br} \sin\theta$, where U_o is the conduit

full mean velocity. For a 2-dimensional case, this gives

$$\frac{U_{1\,min}}{U_{br}} = \frac{D}{d} \sin\theta \qquad \ldots\ldots (2.43)$$

which becomes our second criterion for air bubble transport. Actually a third criterion exists, in cases where air pockets form on the roof of the contuit downstream of the shear layer. These often blowback as slugs, even if bubbles can be transported. This is considered in Sections 4 and 5.

A rider requires to be placed on Equations (2.42) and 2.43) in that, air bubbles are not transported until they are entrained in the first place. For steep conduits (say > 30°) this criterion is $U_1^* \simeq 0.8 - 1.0$ m/s or $U_{1min}/U_{br} > 4$. Thus we might say without great justification that Equation (2.42) becomes

$$\frac{U_{1\,min}}{U_{br}} \sim K_1 \cos\theta \left(D/d - 1\right)^{1/2} + 4 \qquad \ldots\ldots (2.44)$$

and Equation (2.43) might become

$$\frac{U_{1\,min}}{U_{br}} = K_2 \, D/d \sin\theta + 4 \qquad \ldots\ldots (2.45)$$

The second criterion for air bubble transport is much more likely to apply to vertical shafts, where $\cos\theta = 0$, and in any case is generally the lesser of the two criteria.

At this stage it may be of interest to compare theory with some limited experimental data. A 60° . SQUARE SHAFT (Ervine & Ahmed) give minimum velocities to transport air as shown on Figure 2.19. This data is compared with $U_{1min}/U_{br} = K_1 \cos\theta \, (D/d - 1)^{1/2} + 4$, giving $K_1 \simeq 8$. This form of relationship in fact appears to be satisfactory for $20° < \theta < 90°$.

For $\theta = 90°$, Equation (2.45) may be applicable as evidenced by Figure 2.20 for Ervine and Ahmed's data. In this case

$$U_{1\,min}/U_{br} \sim 0{,}6 \, D/d \sin\theta + 4$$

For the case of $\theta < 20°$ shallow conduits, the mode of entrainment is by hydraulic jump surface roller. For inception of air entrainment a breaking roller must form, say $Fr_1 \simeq 1.3$, and according to Thomas (Ref) the minimum jet velocity for air transport to occur in a closed consuit downstream of the shear layer is given by

$$U_{1\,min}/U_{br} = \frac{\cos\theta}{\varepsilon} \qquad \ldots\ldots (2.46)$$

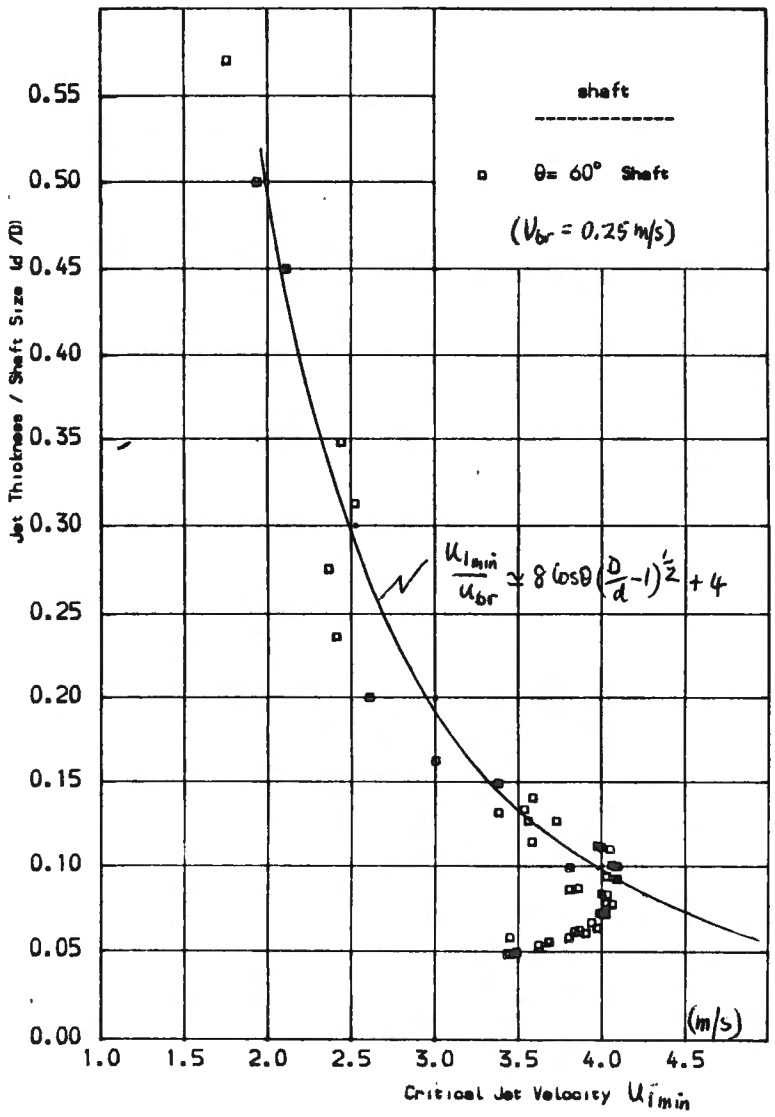

Fig (2.19) The Influence of the Upstream Jet Thickness on the Threshold Jet Velocity to transport Air Bubbles Along Shaft

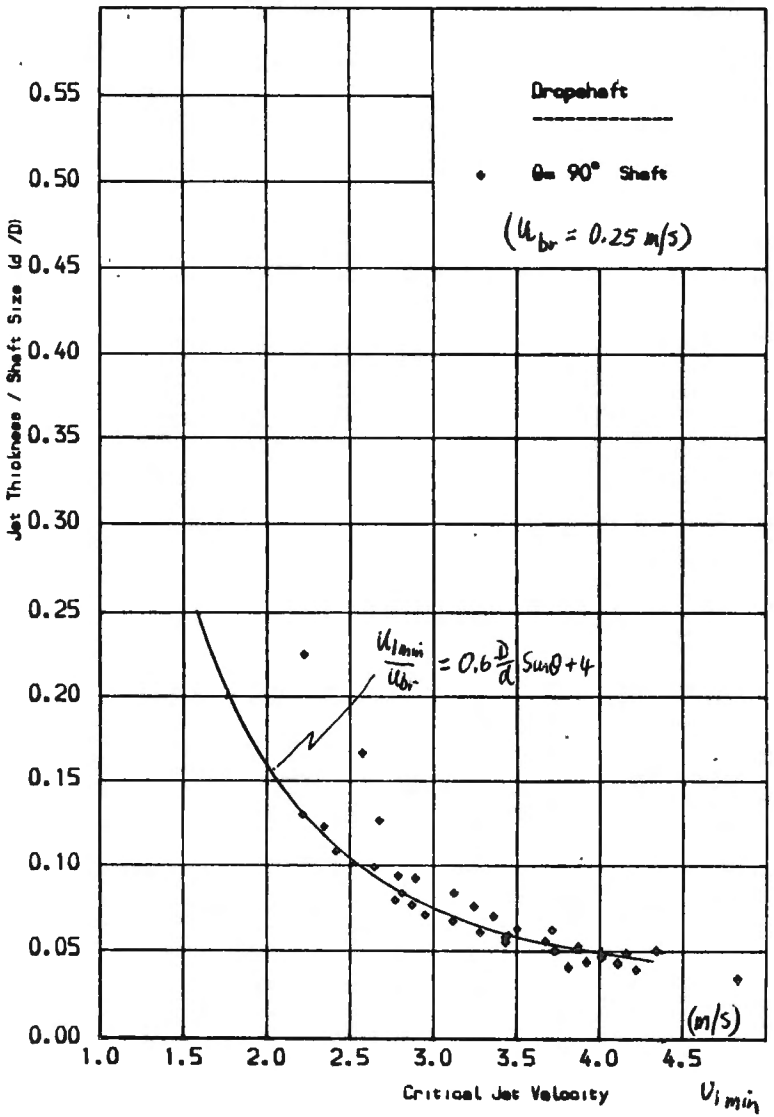

Fig (2.20) The Influence of the Upstream Jet Thickness on the Threshold Jet Velocity to transport Air Bubbles Along Shaft

where ε is the turbulence intensity in the shear layer, usually of order 0.1 to 0.2, and for shallow conduit angles $\cos\theta \rightarrow 1$, $U_{1min}/U_{br} \simeq 5 - 10$ or $U_{1min} \simeq 1.5$ to 2.5 m/s. The value of $U_{1\,min}$ remains constant for all D/d values. This is at least partially borne out in Ervine and Ahmed's data for 10° shaft shown in Figure 2.21. Equation (2.46) is applicable only to surface roller entrainment (Type (3)) usually found in hydraulic jumps at shallow conduit angle (see Thomas analysis). Thus, by way of summary, we can state that the proportion of entrained air which is transported or detrained in a closed conduit, will depend primarily on the value of the jet velocity compared to the minimum jet velocity to tranpsort air $U_{1\,min}$. The value of $U_{1\,min}$ as can be seen in the foregoing discussion is dependent on the angle (or slope) of the conduit, the bubble rise velocity in a shear layer, the ratio d/D, jet thickness to conduit depth, the turbulence intensity generated in the shear layer, etc. As a first estimate the jet velocities required to transport air can be given by

$$U_{1min}/U_{br} \simeq K_1 \cos\theta \,(D/d - 1)^{1/2} + 4 \qquad \text{for } 20° < \theta < 90° \quad (K_1 \sim 5\text{-}10)$$

$$U_{1min}/U_{br} \simeq K_2 \sin\theta \; D/d + 4 \qquad \text{for } \theta = 90° \quad (K_2 \sim 0{,}6)$$

$$\frac{U_{1min}}{U_{br}} = \frac{\cos\theta}{\varepsilon} \qquad \text{for } \theta < 20° \quad (\varepsilon \sim 1/20 \text{ to } 1/4)$$

Jet velocities less than $U_{1\,min}$ will not transport air, and greater than $U_{1\,min}$ will transport air. These estimates of course apply only to conditions where the mixing region is well short of the exit of the conduit.

The proportion of air transported and detrained when $U_1 > U_{1min}$

Once air transport begins in a conduit downstream of the mixing region, $U_1 > U_{1\,min}$, a proportion of the air is detrained back to atmosphere and the remainder transported. Thomas (Ref) carried out a detrainment analysis for the case of surface roller entrainment (as in a hydraulic jump) when the majority of air is entrained into the shear layer from a deep layer of foam above the shear layer. As we shall see below, the most important parameter is the effective bubble rise velocity over the entrainment velocity into the shear layer.

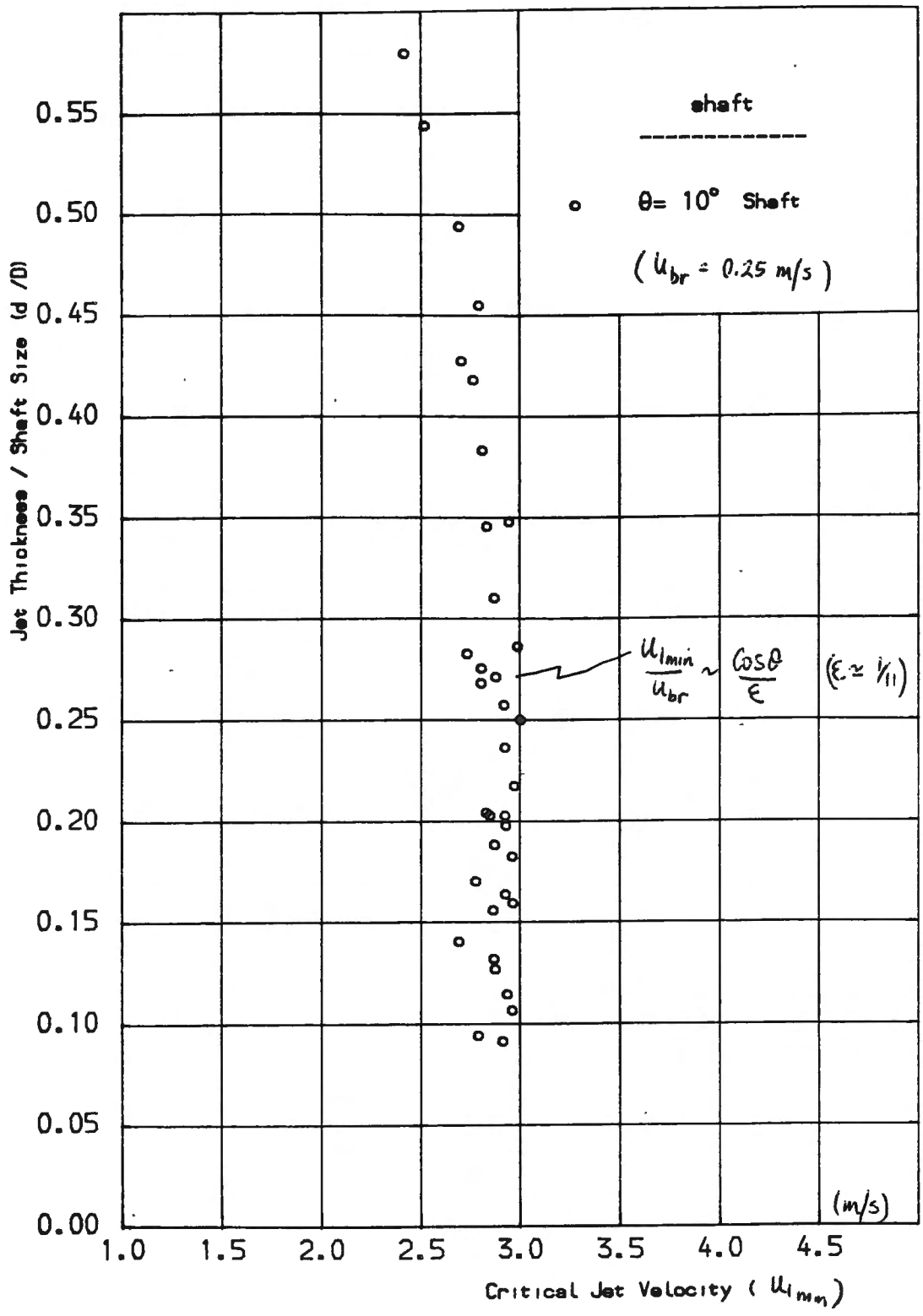

Fig (2.21) The Influence of the Upstream Jet Thickness on the Threshold Jet Velocity to transport Air Bubbles Along Shaft

Thomas air bubble detrainment analysis

Thomas (Ref) postulated a detrainment analysis for air bubbles in a spreading turbulent shear layer. The model is shown overleaf and contains several assumptions.

(1) The free surface plunging jet penetrates the receiving water, generating a surface roller and entraining air bubbles into the shear layer. A thick layer of foam is generated on the surface of the receiving water and air bubbles are entrained into the shear layer from the foam above.

(2) For single phase flows the spreading half angles would be δ_ε^1 as indicated on the sketch. Due to the presence of air bubbles in the shear layer, the free streamline (s) is deflected upwards by an angle δ_1^1. The lower boundary of the shear layer is also deflected upwards so as to make a new half angle δ_B^1, where $\delta_B^1 < \delta_E^1$.

(3) Air bubbles above the streamline S are detrained back to the foam layer and air bubbles below δ are entrained into the flow. Thus net air entrainment into the flow occurs over a spreading angle $\delta_B^1 + \delta_1^1$.

(4) The plunging jet is assumed to have a uniform velocity of V_1 with this velocity considered to act on an air bubble in the mixing layer as shown. The air bubble is also considered buoyant as indicated by the 2 components of bubble rise velocity. The bubble spreads through the shear layer by means of the entrainment velocity V_e, where $V_e/V_1 \approx \delta_e^1 = \varepsilon$. the entrainment coefficient. For single phase flows, Thomas estimates V_e/V_1 to be $\frac{1}{20}$ to $\frac{1}{5}$.

(5) Thomas assumed plane penetrating shear layers as can be seen in Figure 2.22, and as such may not apply directly to hydraulic jumps with strongly curved shear layers.

Referring to Thomas's model, the net quantity of air entrained into the shear layer is given by

$$q_a = C_m \left(V_1 - V_{br} \sin\theta\right)\left(\delta_1 + \delta_B\right) \qquad \ldots\ldots (2.47)$$

where q_a is the air flow rate per unit width

c_m is the air void fraction (or concentration) in the shear layer

$\delta_1 = \delta_1^1 L$ and $\delta_B = \delta_B^1 L$ as indicated on the sketch.

Expression (2.47) can be made meaningful for realistic estimates of C_m and $\delta_1 + \delta_B$.

Conduit angle θ
Bubble rise velocity V_b
Length of shear layer L

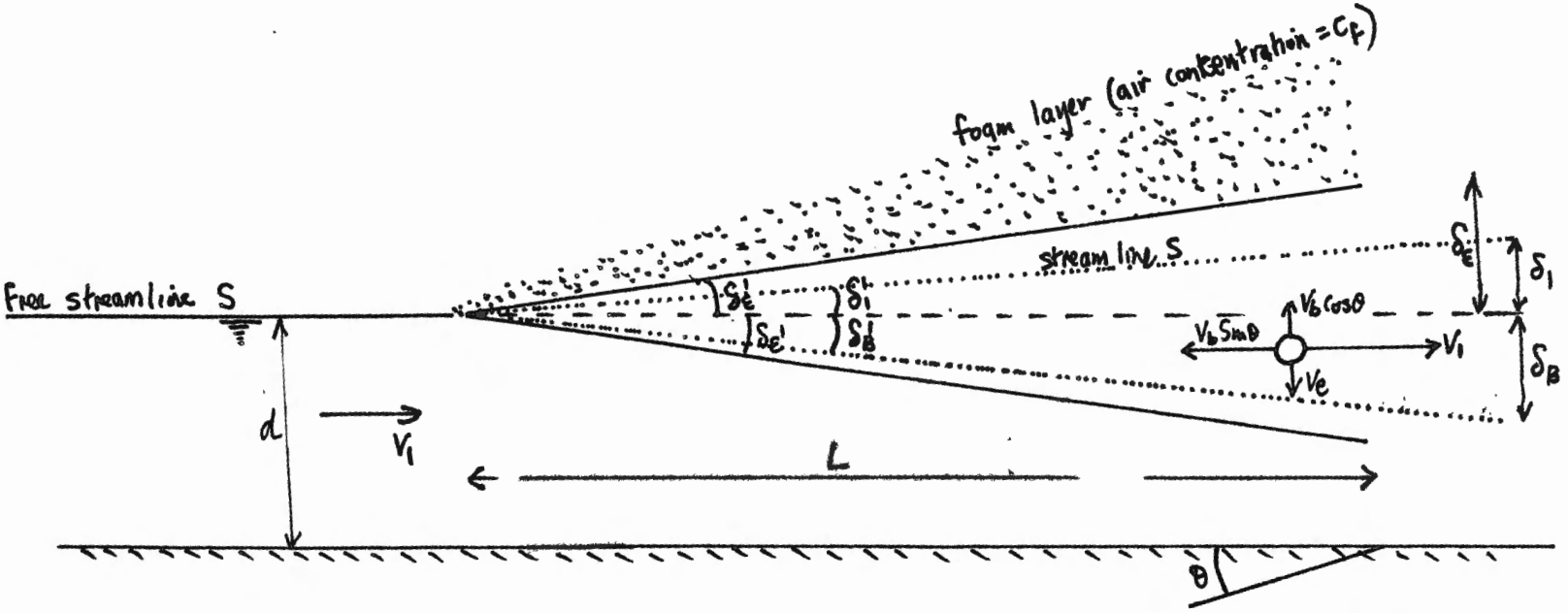

FIG. 2.22

An estimate for C_m the air bubble concentration in the shear layer can be obtained from a continuity expression for the air bubbles from the foam layer being entrained into the mixing layer along length L being equal to the transport of air across the entire shear layer. Namely,

$$C_f(V_e - V_{br}\cos\theta)\,L = \text{entrainment of air bubbles from foam layer} \quad \ldots\ldots (2.48)$$

$$C_M(V_1 - V_{br}\sin\theta)(\delta_B + \delta_\varepsilon) = \text{entrainment and detrainment out of shear layer} \quad \ldots\ldots (2.49)$$

Now $\frac{\delta_\varepsilon}{L} = \delta_\varepsilon' = \frac{V_e}{V_1}$ as already assumed

Thomas postulated that $\frac{\delta_B}{L} = \delta_B' = \frac{V_e - V_{br}\cos\theta}{V_1}$ ..... (2.50)

Hence we obtain an expression for C_m in the form,

$$C_m = \frac{C_f\left(1 - \frac{V_{br}\cos\theta}{V_e}\right)}{\left(2 - \frac{V_{br}\cos\theta}{V_e}\right)\left(1 - \frac{V_{br}\sin\theta}{V_1}\right)} \quad \ldots\ldots (2.51)$$

The limit of equation (5) where buoyancy effects are negligible gives $C_m = \frac{1}{2} C_f$, or the air void fraction in the mixing layer is half layer is half that of the foam layer. If the foam layer concentration is typically 0.5, then $C_m \approx 0.25$. This will be discussed later in the context of plunging free jet entrainment where values of C_m over 0.4 have been measured.

An expression for $(\delta_1 + \delta_B)$ in Equation can be obtained by continuity of the water flows entrained into the shear layer from below (see sketch) and that moving out of the shear layer below the streamline S.

$$V_e L = V_1(\delta_\varepsilon - \delta_B) + (1 - C_m)V_1(\delta_1 + \delta_B) \quad \ldots\ldots (2.52)$$

Using the same argument as before, we obtain

$$\delta_1 + \delta_B = \left(1 - \frac{V_{br}\cos\theta}{V_e}\right)\delta_\varepsilon / (1 - C_m) \quad \ldots\ldots (2.53)$$

Equations (2.51) and (2.53) can be substituted into Equation (2.47) to obtain an expression for the net air flow rate. This can be divided by the water discharge ($U_1 d$) to derive an expression for the ratio of air to water. The resulting air/water ratio splits into a non-buoyant scale independent section and a buoyant scale dependent section, the latter being given by,

$$\left(1 - \frac{V_{br}\,Sin\theta}{V_1}\right)\left(1 - \frac{V_{br}\,Cos\theta}{Ve}\right)\left(\frac{C_m}{C_f/2}\right)\left(\frac{1 - C_f/2}{1 - C_m}\right) \qquad \ldots\ldots (2.54)$$

For the case of $C_f = 0.5$ and $\frac{V_{br}\,Sin\theta}{V_1} \ll 1$, equation (2.54) reduces to

$$\left(1 - \frac{V_{br}\,Cos\theta}{Ve}\right)^2 \Big/ \left(1 - \frac{V_{br}\,Cos\theta}{3\,Ve}\right) \qquad \ldots\ldots (2.55)$$

which effectively is a detrainment scale factor.

It is further argued by Thomas (see Notes of Inception speeds for Air Entrainment) that as $V_e = \epsilon V_1$, where ϵ is the entrainment coefficient or the half angle of spreading shear layers, that at the balance point for inception of air bubbles into the shear layer, $V_e = V_{br}\,Cos\theta = \epsilon\, U_1^*$ (U_1^* is the critical inception speed). Then Equation 2.55 becomes

$$\left(1 - \frac{U_1^*}{U_1}\right)^2 \Big/ \left(1 - \frac{U_1^*}{3U_1}\right) \qquad \ldots\ldots (2.56)$$

The final relationship for air/water ratio of net entrainment proposed by Thomas is,

$$\beta = K(Fr_1 - 1)\left[\left(1 - U_1^*/U_1\right)^2 \Big/ \left(1 - \frac{U_1^*}{3U_1}\right)\right] \qquad \ldots\ldots (2.57)$$

which is applicable mainly to low Froude Number situations ($F_1 < 10$), shallow conduit angles θ, situations with a thick layer of foam at the plunge point, and cases where the transport capacity of the flow downstream of the shear layer in a closed conduit is adequate to carry the net rate of air entrainment. Having stated that Thomas's analysis may be applicable to hydraulic jumps at shallow conduit angles, it should be noted that Equation (2.57) above gave an excellent representation of the entrainment in model siphons where $\theta = 45°$ and a thick layer of foam did not exist (Casteleyn et al) and the shear layers were of the penetrating type.

Also it ignores entrainment at the toe of the jump.

Thomas does not state his reasoning for the ratio of air to water scaling on Fr - 1, but by implication and using the example of a hydraulic jump, if the rate of entrainment is dependent on the length of the jump, then for low Froude Numbers $L = K(y_2 - y_1) = Ky_1(y_2/y_1 - 1)$. The value of y_2/y_1, scales approximately on the Froude Number $\left(y_2/y_1 \propto Fr\right)$, hence $L \propto y_1(Fr_1 - 1)$ where $y_1 = d$. Thus the air flow rate $q_a \propto U_r L$, where U_r is the velocity of the recirculating roller, and $q_a \propto (U_r/U_1)U_1 L$, where U_r/U_1 according to Sene is 0.035. Hence $q_a \propto 0.035 U_1 d\,(Fr - 1)$ or $\beta \propto .035\,(Fr - 1)$. The value of K given by Thomas in Equation (2.57) is approximately $1/40 \rightarrow 1/30$.

If is interest to note that the relationship proposed by Thomas is in a similar form to hydraulic jump entrainment by Kalinske and Robertson (Ref) $\beta = 0.0066\ (Fr_1 - 1)^{1.4}$. Kalinske and Robertson were probably correct in assuming that β scaled on Fr-1 as shown above, but failed to recognise that bubble dynamics in the shear layer would probably not be scaled in Froude Models $\lambda^{as} U_{br} \cos\theta$ remains approximately constant in model and prototype, whereas water velocity terms U_1 or U_e scale with $L_r^{1/2}$. The other point highlighted by Goldring (Ref) is that Thomas assumed plane penetrating shear layers, whereas hydraulic jumps have curved attaching shear layers. A lot of research still requires to be carried out into hydraulic jump entrainment and detrainment, this being one area which has not received extensive analytical treatment. It is discussed in Section 3.3 in more detail.

SECTION 3

BUBBLY FLOWS - EXPERIMENTAL EVIDENCE AND EMPIRICAL CORRELATIONS

3.1 Jets plunging through the atmosphere. Entrainment and dispersion.

3.2 Wall jets in hydraulic structures including siphons and dropshafts. Entrainment, detrainment and bubble transport.

3.3 Hydraulic Jumps. Entrainment and bubble transport.

3.1 Air entrainment by circular jets plunging through the atmosphere

Air entrainment by circular jets issuing from a cylindrical nozzle at low intensity is a great deal more complex phenomenon then entrainment by wall jets or hydraulic jumps. The reasons for this are outlined as follows.

(1) If the jet is initiated by a nozzle, then the Reynolds Number of the nozzle flow and the development of turbulent boundary layers in the nozzle (∝ length) have a strong influence on initial surface disturbances of the issuing jet.

(a) A short slightly converging smooth nozzle, taking flow from a large undisturbed source of water will produce a very smooth jet with a laminar core even at relatively high Reynolds Numbers. This has been shown to have a strong influence not only on the rate of air entrainment at the plunge point but also the inception velocity to cause air entrainment (see Section), and the disintegration length of the plunging jet. Evidence for this is given on Figure 3.2.

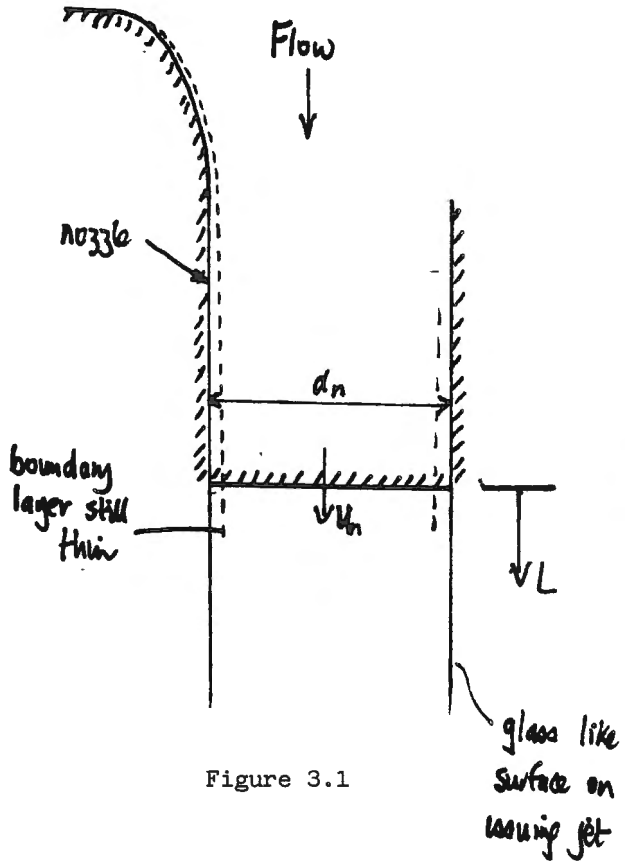

Figure 3.1

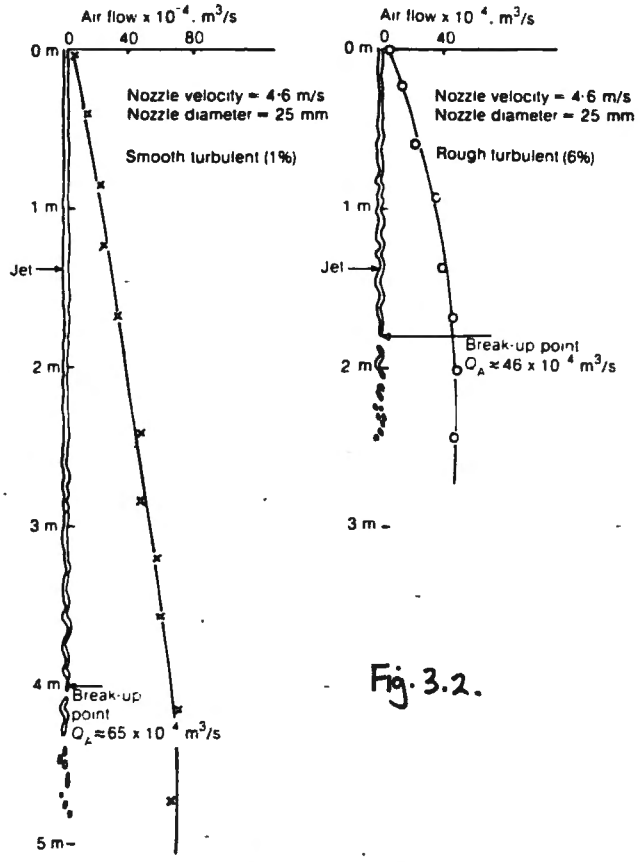

Fig. 3.2.

Typical comparisons between the air flows of two jets of identical nozzle diameters and velocities but differing turbulence levels

(b) A long nozzle or inlet pipe allows the development of boundary layers and can produce fully developed turbulent flow as the jet issues into the atmosphere. The lateral velocity fluctutating components U* (say ≈ V* in the axial direction) induce surface disturbances which become amplified during the plunge.

(2) The surrounding air becomes dragged along by the plunging jet, setting up an air boundary layer. The relative movement of air and water generates a shear stress at the interference (as shown) which may further disturb jet surface undulations. (This may be a similar mechanism to the generation of sea waves by wind). Further acceleration of the jet and amplification of jet surface disturbances may eventually cause the jet to disintegrate into a train of droplets. This combination of hydrodynamic and aerodynamic forces is much more in evidence in plunging jets than wall jets and hydraulic jumps. This is also evidence that the air resistance effect may only be significant for Wb > 10 or $\rho_a u_i^2 d/\sigma$ > 10, which corresponds generally to a high velocity range.

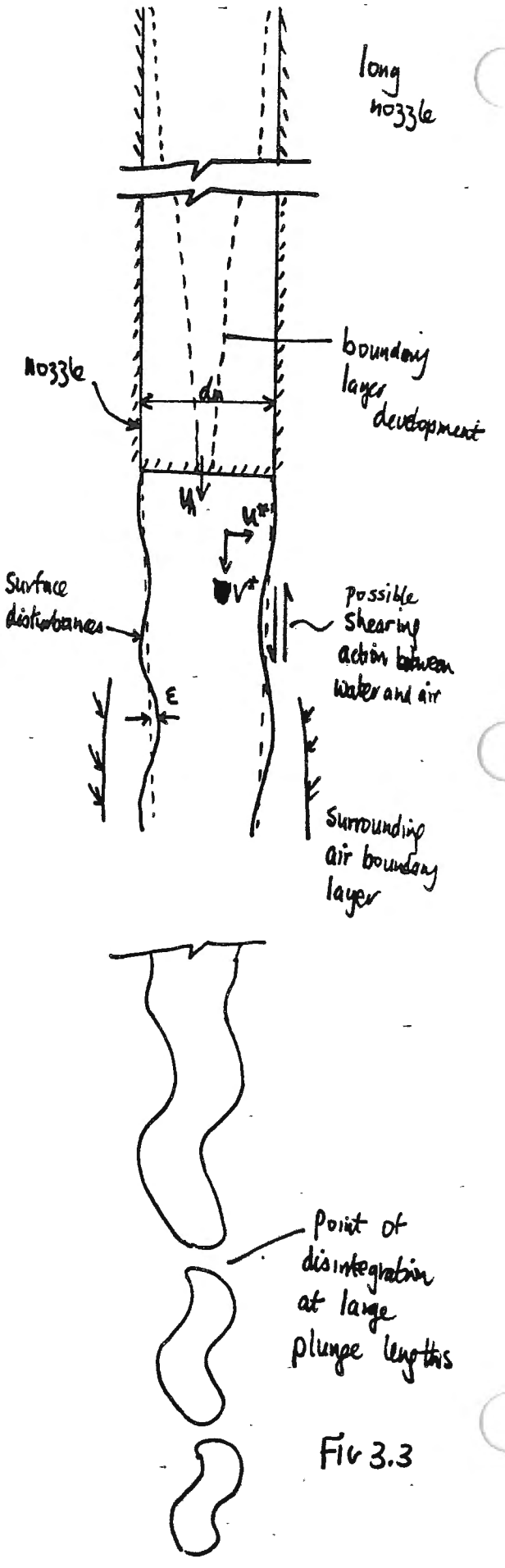

Fig 3.3

(3) The problem is further complicated at the plunge point. Consider the sketch opposite where air is entrained into the receiving water by a jet with surface disturbance ϵ, and surrounding boundary layer. Air enters the pool, assume at the same velocity as jet impact U_1, then air may enter either from the jet surface undulations and/or the surrounding boundary layer. The exact proportion of each is still an open question and in fact makes an analytical solution extremely difficult. Even empirical correlations show wide divergence. On entering the pool, the high shearing stresses produce air bubbles of diameters generally 1 - 10 mm which are then transported downwards in the shear layer. The transport capacity of the shear layer may in fact be just as important in determining the maximum rate of air entrainment as the jet characteristics. It could be argued for instance that the maximum air concentration in the shear layer may be approximately 40 - 50%, then the maximum quantity of air transported might be, $Q_{a(max)} \sim 0.5\, U_1 \left(\frac{\pi d_*^2}{4}\right)$

Conditions at plunge point

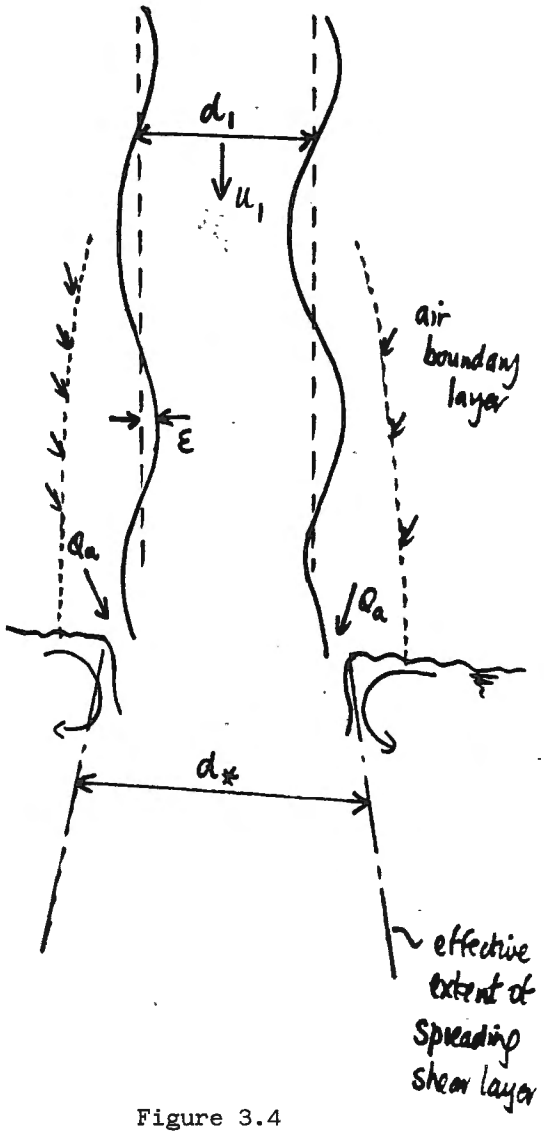

Figure 3.4

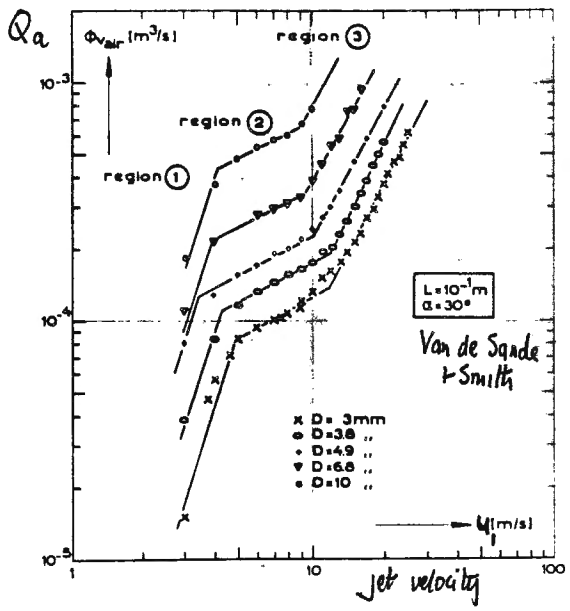

Figure 3.5

(4) The discussion has centred so far on low velocity plunging jets accelerating due to gravity. A different category of jet results for high velocity of exit from the nozzle. A classical study by Van de Sande and Smith (Ref) shows three distinct phases of entrainment with increasing jet velocity. At low velocity $q_{air} \propto U_1^{2 \to 3}$ and intermittent entrainment occurs, a transition stage $q_{air} \propto U_1$, and finally for high velocity jets $q_a \propto U_1^{1.5 \to 2}$. This phenomenon has important implications for for hydraulic structures especially in comparing model/ prototype entrainment. Van de Sande and Smith postulated that air resistance was of importance only in the high velocity region (say > 10 m/s above) but given generally by Wb > 10 where Wb = $\rho_a U_1^2 d/\sigma$. Beyond this point air entry is continuous and surface disturbances, important in low velocity jets, become less important.

Empirical rleationships for air entrainment by circular jets plunging through the atmosphere

Early work on air entrainment by plunging circular jets by Oyama et al (Ref) contained a complex relationship using a range of non-dimensional numbers each related to conditions at the nozzle.

$$\beta = \frac{Q_a}{Q_w} = 0{,}75 \left(Re_n\right)^{1.33} \left(\frac{\sqrt{Wb}}{Re}\right)_n^{2.18} \left(\frac{V_n^2}{gL}\right)^{-0.447} \left(\frac{L}{d_n}\right)^{0.281} \quad \ldots\ldots \text{(3.1)}$$

This work did not incorporate the initial relative turbulence intensity of the jet which has been found by the author to have considerable influence on subsequent jet surface roughness and eventual jet disintegration. However all the jets in this study were of small scale with the turbulence intensity reflected in the Reynolds Number term. The terms Re, Wb and L/d both reflect the surface roughness of the jet and its eventual break-up, with V_n^2/gL, as Froude Number, reflecting the effect of gravity of the jet behaviour. It is of interest to note here that Froude scaling for the air/water ratio is not possible as the non-scaled portion reduces to $\beta_{(prot.)}/\beta_{(model)} = \beta_r \propto L_r^{0{,}905}$

In other words, the air/water ratio increases almost linearly with Froude model scale. This may not be strictly accurate, as already seen under inception velocities, that a velocity (or model scale) exists below which there is zero entrainment of air.

Bin (Ref) has correlated experimental data for circular jet air entrainment from Van de Sande (Ref) Cumming (Ref), Ervine et al (Ref), Henderson et al (Ref), Kumagai and Imai (Ref) and Van de Donk (Ref). His correlation, which has been corrected for jet angles other than vertical, is of the form, $Q_a/Q_w \sim 0.05\ Fr^{0.56} (L/d_n)^{0.4}$

where $Fr = u_1/\sqrt{gd_n}$ (In fact, Bin used $Fr^{0.28}$ where $Fr = u_1^2/gd_n$) ..... (3.2)

The data correlations are shown on Figure 3.6. d_n is the nozzle diameter. Of interest here is the observation that the Reynolds and Weber number of flow are absent, ignoring viscous or surface tension influence. Most of the jets in the data correlations are of relatively small scale, and thus viscous and surface tension forces must influence not only the nature of the surface of the plunging jet but also the inception condition for entrainment, and viscous influence in the shear layer eddies after the point of impingement. Presumably it can be argued that the parameter L/d_n reflects growing jet surface roughness and break up. Initial turbulence intensity is also omitted, but Bin indicates the sensitivity of the data correlations to the length of the jet nozzle which in turn reflects the development of turbulent boundary layers within the jet at the point of entering the atmosphere. Relationship (3.2) implies Froude scaling for air bubble entrainment. From the data correlations in Figure 3.6 it can be seen that ratios of air to water as high as 10 have been recorded, which is around two orders of magnitude larger than typical hydraulic jump entrainment.

Several authors have employed more physical approaches to the quantity of air entrained by circular jets. The most common assumes the rate of air entrainment to vary with the flux of jet energy. ($\rho d^2 v^3$) Van de Sande (Ref) employed this approach for low velocity jets Using the nozzle diameter and jet velocity as a reference point, he incorporated the jet length L, to derive an empirical expression

$$Q_a = 0.015\, X^{3/4} \quad (\text{where } X = d_o^2 u_1^3 L^{1/2} S_w^{-1.5} \alpha) \quad (d_o = d_n) \quad \ldots\ldots (3.3)$$

Again this was correlated by Bin (Ref) for other data sets with the result shown on Figure 3.7. α is the jet angle to the horizontal.

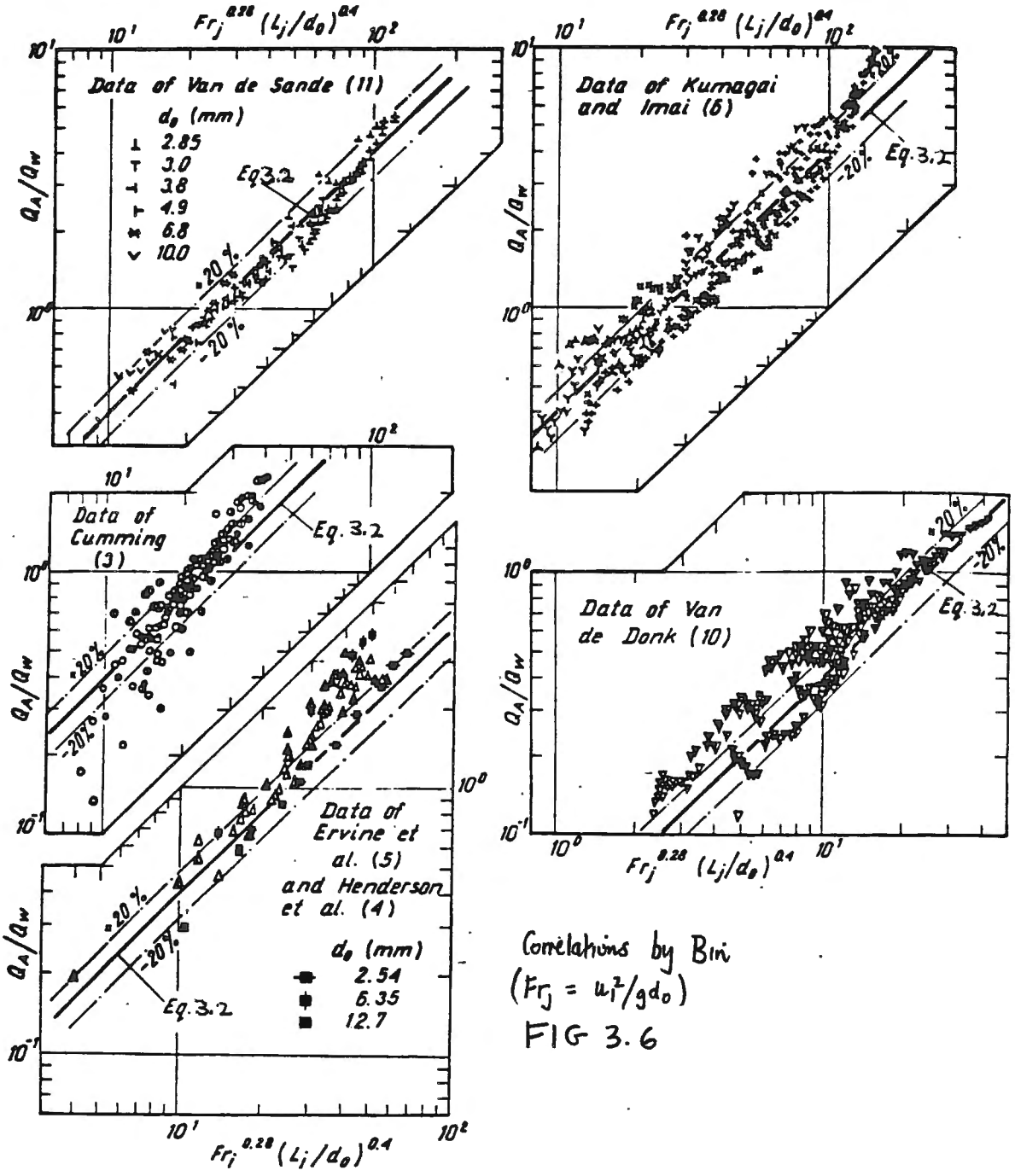

Correlations by Bin
($Fr_j = u_1^2/gd_0$)
FIG 3.6

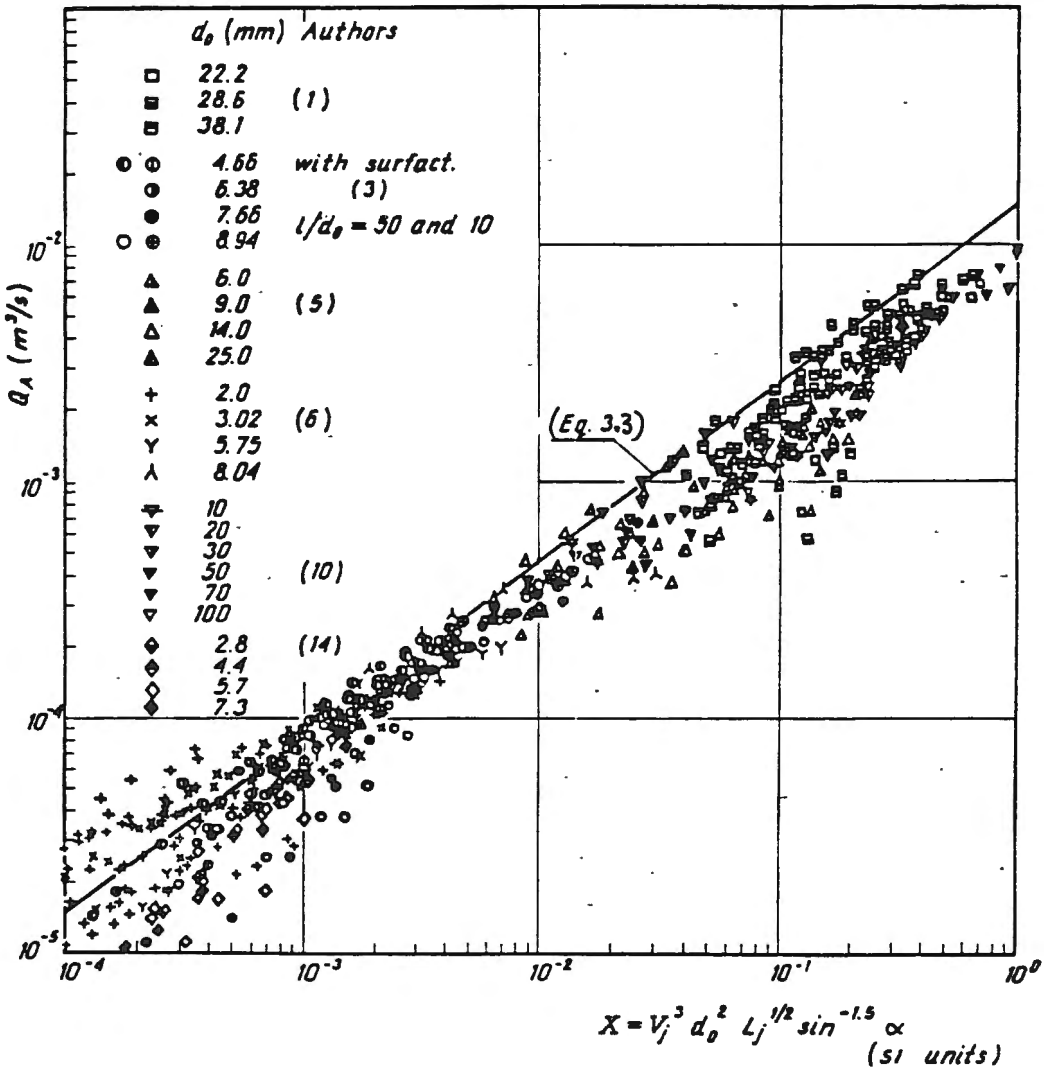

FIG 3.7.
Correlation by Bin compared with Equation (3.3)

From equation (3.3) is can be seen that the air/water ratio for entrainment scales on the length scale (or model scale) $L_r^{1/2}$ for Froude models. McKeogh (Ref) produced an empirical correlation for the rate of air entrainment for high turbulence intensity low velocity jets. The total rate of air entrainment given by,

$$Q_a/Q_w \sim 0.3 \left(H/L_d\right)^{0.7} U_1 + Q_{ao}/Q_w \qquad \ldots\ldots (3.4)$$

where H is the plunge length (= L)

L_d is the jet disintegration plunge length

and Q_{ao} the rate of air entrainment for zero plunge length.

McKeogh found the value of L_d experimentally to be $4.6\ Q_w^{0.2}$. Equation (3.4) implies a strong dependence of the quantity of air entrained to the surface roughness of the jet and the jet velocity. Ignoring the entrained air quantity at zero length of plunge it can be seen from (3.4) that the upper bound value of air/water ratio at the point of jet disintegration is $\beta \simeq 0.3\, U_1$ where U_1 is the jet impact velocity. This value must be suspect for higher velocity flows (prototypes) as β rarely exceeds 3 for highly turbulent jets.

The most interesting facet of McKeogh's relationship (3.4) is that for $H/L_d = 1$, $Q_{ao} \ll Q_a$, then $Q_a = 0.3\, U_1\ Q_w \propto U_1^2\ d_1^2$, or the quantity of air entrained is a function of the momentum of the jet. This is in contrast to the relationship by Van de Sande and Smith (Ref) who found for jet plunge lengths greater than 90% of the jet disintegration length that $Q_a = K + 0.0825\ U_1^3\ d_n^2$ which is proportional to the flux of energy of the jet.

A further physical interpretation of air entrained by low velocity plunging circular jets was attempted by Ervine and McKeogh (Ref). This was based on a simplified model as shown on the sketch below. The falling jet is supposed to increase in effective diameter by virtue of the fact of surface undulations (idealised here as a sinuous wave form of amplitude ϵ). The air held within the surface undulations is assumed to have the same speed as the plunging jet and to contribute to the total rate of air entrainment. A tentative expression is also derived for the total rate of air entrainment possible from the surrounding boundary layer.

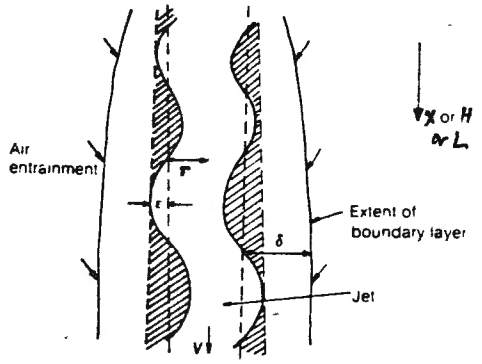

Sinuous wave form of jet showing extent of boundary layer and air entrainment within surface undulations

Figure 3.8

The discharge of entrained air therefore is given by,

$$Q_a = u_1 f\left(\pi(\varepsilon^2 + 2\varepsilon r + r^2) - \pi r^2\right)$$

$$\text{or } Q_a/Q_w = f\left[(\varepsilon/r)^2 + 2(\varepsilon/r)\right] \qquad \ldots\ldots (3.5)$$

or the ratio of air to water is a function of the surface roughness at any point during the plunge. The value of ε/r, local surface roughness/local jet radius could not be predicted analytically and hence resort was made to high speed photographic measurements. Typical measurements of ε/r are shown below, and correlated with the ratio L/L_d, plunge length/disintegration plunge length, and the jet velocity at nozzle exit, V_n.

FIG. 3.9

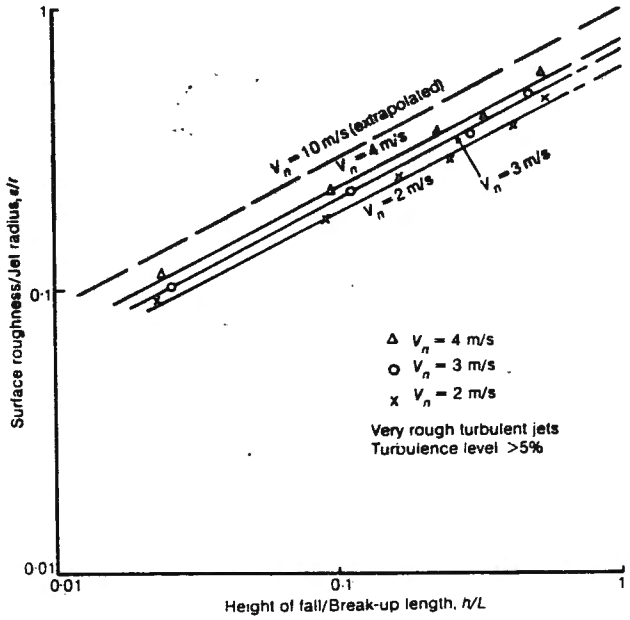

Non-dimensional plot of increase in jet surface roughness falling through the atmosphere for various values of nozzle velocity V_n

The value of this work was not in a quantitative or empirical estimate of the ratio of air/water by plunging circular jets, but as evidenced in the correlation below, an indication that the value of β is highly dependent on the jet surface roughness at the point of impact (or the local jet diameter accounting for the surface undulations). It can also be seen in the Figure below that a substantial contribution to air entrainment comes from the surrounding boundary layer, sometimes as high as 50% of the total air entrained. The maximum air/water ratio is around 3, which is an order of magnitude higher than that of typical hydraulic jumps.

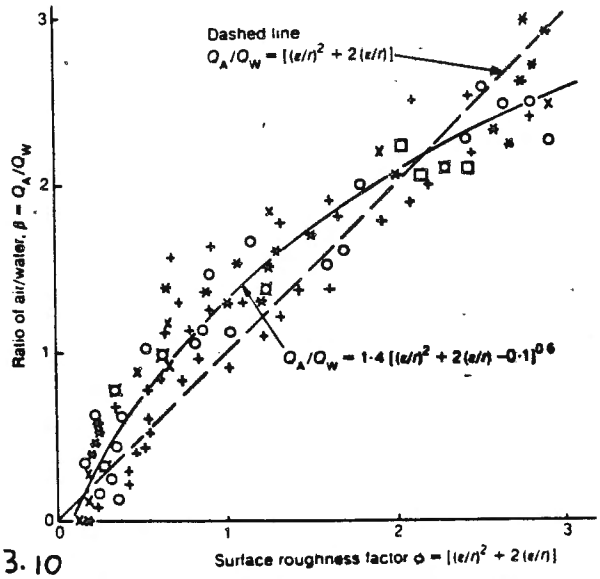

FIG 3.10 Relationship between air entrainment and surface roughness of jet for all turbulence levels

The analysis used by Ervine and McKeogh above was roughly based on a technique developed by Van de Sande and Smith (Ref) for predicting air entrainment by high velocity circular jets. They proposed

$$Q_{a(\text{total})} = Q_{a(\text{undulations})} + Q_{a(\text{boundary layer})} \quad \ldots\ldots (3.6)$$

To determine the amount of air entrained in jet undualtions, Van de Sande et al used photographic technique to show $\frac{D^*}{D} = 0{,}085\,(We\ Re_L)^{1/6}$ where D* is jet diameter at any point, D is initial jet diameter.

$$We = \rho_a u_1^2 D/\sigma \quad \text{and} \quad Re_L = \rho_a u_1 L/\mu_a$$

$$\beta_{(\text{undulations})} \sim 72\times10^{-4}\,(We\ Re_L)^{1/3} - 1 \quad \ldots\ldots (3.7)$$

For a calculation of air carried by the laminar boundary, Van de Sande assumed an air velocity distribution around the jet (Ref) such that

$$Q_{a\ b.l.} = \int_{R^*}^{\infty} V_{air}\, 2\pi r\, dr \qquad \ldots\ldots (3.8)$$

Var de Sande and Smith achieved good correlation between their theory and experimental data at least in the case of the air boundary layer still laminar.

An important finding from their high velocity data, revealed that $q_a = Q_a/\pi d \propto U_1^{1.5 \to 2}$, compared with $U_1^{2 \to 3}$ for low velocity data.

Empirical correlations for rectangular jets plunging through the atmosphere

A rectangular plunging jet falling freely through the atmosphere will not retain its rectangular shape. Surface tension , will encourage the jet to eventually assume a circular shape. A range of shapes may evolve during the transition from a rectangular to circular. There is also some evidence for diverging growth development (Ref) of the rectangular jet.

Ervine (Ref) investigated the rate of air entrainment by a rectangular jet issuing from a rectangular nozzle. Droplengths were limited so that the jet essentially retained its original shape.

The major parameters controlling air entrainment rates were droplength, velocity and jet thickness. ver the range of parameters tested it was found

$$q_a \propto (u_n - u_i^*)\, d_n^{1/2}\, L^{1/2}$$

$$\text{or } \beta = q_a/q_w \propto (1 - u_i^*/u_n)(L/d_n)^{1/2}$$

A final correlation was obtained in the form,

$$\beta_{at} = 0{,}26\,(b/p)\,(L/d_n)^{0.446}\,(1 - u_i^*/u_1) \qquad \ldots\ldots (3.9)$$

where U_i^* is inception velocity to entrain air ($\simeq$ 1.1 m/s).

For wide rectangular jets $b/p \to \frac{1}{2}$ and the total entrainment from both jet surfaces

$$\beta_{at} \sim 0{,}13\,(L/d_n)^{0.446}\,(1 - u_i^*/u_1). \qquad \ldots\ldots (3.10)$$

This correlation is suspect in the sense that none of the plunging jets approached disintegration length, and over the range tested q_a varied with $L^{1/2}$. This is not the case for greater values of L. Also

the rate of entrainment would also become independent of d at higher values of d, hence the correlation on $d^{1/2}$ is applicable only over smaller values of d. The correlation did serve to highlight the concept of inception velocities for air entrainment.

Rogala (Ref) investigated the rate of entrainment by a wide rectangular plunging nappe as shown on the sketch below.

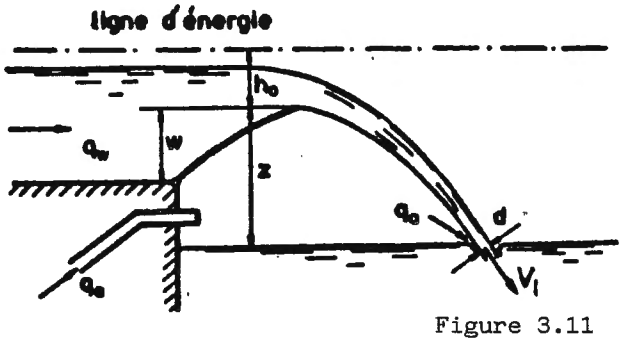

Figure 3.11

Three scale models were tested, giving a correlation for air entrainment from the underside of the nappe in the form,

$$\beta = K\ Fr^{1.51}\ Re^{1.1} \qquad \ldots\ldots (3.11)$$

where Fr is given by $V_1/\sqrt{gd}$ at the impact point.

Re is given by $V_1 h_o/\nu$, and $K = 0{,}784 \times 10^{-9}$

This relationship scales on $L_r^{1.65}$ which is likely to give an overestimate of prototype values of β. A possible explanation is that for higher Reynolds Numbers ($>5 \times 10^4$ or 10^5) and greater values of d, the entrainment rate should become independent of R_e (see Kobus (Ref)). Turbulent dampening in the jet is no longer significant and jet surface roughness will be fully developed compared with small models. This same argument applies to the initial turbulence level at the crest overflow and also the shearing vortices at the point of impact.

Thus $R_e^{1.1}$ may be applicable in the range of models tested, but when $R_e > 10^5$, β is likely to depend only on Fr_1, hence a new relationship might be formed $\beta = K_2\ Fr^{1.51}$ (for $R_e > 10^5$). Kobus and Westrich (Ref) investigated the reoxygenation of cooling water by plunging rectangular jets entraining air into a receiving pool below. Maximisation of air entrainment into the pool can be achieved by cooling water issuing from a a number of slots in parallel rather than say just a single slot. This has the effect of greatly increasing the surface area in contact with the air at the point of jet impact. The Figure below shows the air/water ratio as a function of the plunge length of the jets, for 4 jets and 6 jets in parallel.

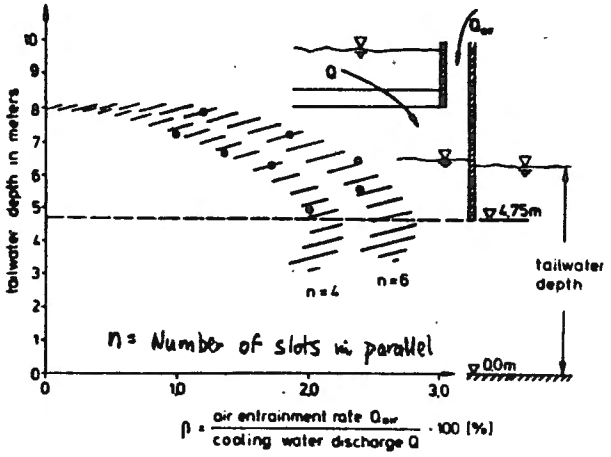

Figure 3.12

The advantage of this system is obvious. If the rate of entrainment by a jet is given by $Q_a = q_a B \simeq U_1^3 B$ (as an order of magnitude, then the same velocity U_1 will exist at the impact point no matter how many jets are used (approx) and the total air entrained will increase by the term B, the total jet width for all n jets, 4, 6, etc.

It is of interest to note that β varies approx with $H^{1/2}$ above, Ervine's correlation for a wide rectangular jet gives $\beta \simeq 0.13\ (H/d_n)^{0.45}$. From the diagram above at the maximum point H ≃ 3.25 m from the slot exit and $d_n \simeq 0.16$ m (Ref). This gives β ≃ 0.49 for one single slot. Assuming a pro-rata increase for 4 and 6 jets we have β (4 jets) ≃ 1.99 and β (6 jets) ≃ 3 which is in close agreement with Kobus and Westrich.

Other research into plunging jet entrainment has centred on oxygen uptake studies at overflow weirs. Avery and Novak (Ref) produced a relationship for the oxygen deficit ratio in the form

$$r - 1 = K\ Fr_1^{1.78}\ Re^{0.53} \qquad \ldots\ldots (3.12)$$

where K ≃ 0.627 x 10^{-4} for tap water

$Fr_1 = V_1/\sqrt{gd}$ and $Re = q_w/\nu$

r is the oxygen deficit ratio given as $\frac{\text{deficit upstream of weir}}{\text{deficit downstream of weir}}$

and is clearly always ⩾ 1.

Although influenced by water quality, salt content, depth of plunge pool, temperature, etc., the value of r - 1 is heavily dependent on air/water ratio (β) from the plunging jet, and Novak's relationship can be compared

in its form to that of Rogola (Equation 3.11). The same comment can be made that for $Re > 10^5$ approx., Equation 3.12 above may overestimate β and hence r_{1s} -1.

Kobus (Ref) makes an interesting comment that previous studies on the value of $r - 1$ may underestimate prototype $r - 1$ values if correlated with the droplength alone, i.e. $r - 1 = f(H)$. That is, if H is held constant for both model and prototype, then model air entrainment β will be much higher than prototype. This can be seen clearly in Ervine's relationship $\beta \propto (H/d)^{0.45}$, when $H_{model} = H_{prototype}$, and $d_{model} << d_{prototype}$ then $\beta_m > \beta_{prototype}$.

Author's comments on plunging jet entrainment

It is apparent that a wide range of empirical correlations are available for air entrainment due to jets plunging through the atmosphere. A unified correlation procedure may be more difficult for plunging jets than wall jets or hydraulic jumps etc. There are a range of reasons why models may underestimate prototype entrainment. These are summarised as follows:

(1) A minimum velocity is required to initially entrain air. This is of the order of 1 m/s but is dependent on turbulence intensity of the flow. Models operating at this range of velocity will entrain relatively small amounts of air.

(2) Viscous effects are important in air entrainment for $R_e < 10^5$ (Kobus). The turbulent eddies are suppressed by viscosity for lower Reynolds Numbers, which in turn influences the intensity of jet surface roughness and the shearing vortices at impingement point. Both these factors contribute to air entrainment.

(3) The absolute value of jet thickness at impact may be significant in the entrainment process (i.e. not just a function of R_e). The scale of eddies causing jet surface roughness is likely to be proportional to the jet thickness (d). If this is or order of magnitude size the same entrained air bubbles then entrainment may be suppressed. Some of the circular jet tests have jet diameter < 5 mm, and jet thickness may suppress entrainment for $d < 10$ to 20 mm.

(4) Plunging jets undergo a gradual process of increasing surface roughness and disintegration. According to limited research carried out to date, this process is not Froude scaled but much more dependent on the initial Reynolds Number of the flow. This phenomenon

requires to be taken into account much more in plunging jets than hydraulic jumps for instance.

(5) There is some evidence that high velocity jets (say $U_1 > 6$ m/s) behave differently from low velocity jets. This is characterised by correlations for entrainment scaled on $U_1^{2 \to 3}$ for lower velocity jets and $U_1^{1.5}$ for higher velocity jets. Care must be exercised for model extrapolations based on $q_a \propto U_1^3$ which may in fact not apply at higher velocities.

Before we discuss some of these points in more detail, it may be useful to investigate scaling factors (model/prototype) for existing correlations.

Scaling for air/water ratios for air entrainment by plunging jets

Froude models of prototype air entrainment situations invariably underestimate air/water ratios. Models at low Reynolds Numbers cause dampening in turbulent fluctuations in the falling jet, reducing entrainment. Apparently plunging jets do not disintegrate according to Froude scaling. Inception velocities are required to initiate entrainment, and also do not conform the Froude scaling. This author has outlined approximate scalings for air/water ratio (prototype/model) based on some empirical relationships postulated to date for jets plunging through the atmosphere.

	Scaling $\beta_p/\beta_m = \beta_r$
Van de Sande ( )) Circular jets Reported by Bin ( )) $\beta \propto F_T^{0.56} (L/d_n)^{0.4}$ (high velocity)	L_r^o
Van de Sande ( ) Circular jets $Q_a \propto V^{3/4} d^{3/2} L^{3/8}$ (low velocity	$L_r^{0,5}$
McKeogh ( ) Circular jets $\beta \propto (L/L_d)^{0.8}$ (smooth turbulent) $(L_d \propto Q_w^{0.35})$	$L_r^{0.1}$
McKeogh ( ) Circular jets $\beta \propto (L/L_d)^{0.7} u_1$ (rough turbulent) $(L_d \propto Q_w^{0.2})$	$L_r^{0.25}$
Ervine ( ) Narrow rectangular jet $\beta \propto (H/D)^{1/2} (1 - \frac{1}{u_1})$	Scales on absolute velocity rather than model scale. High velocities $= L_r^o$
Rogala ( ) wide rectangular jet $\beta \propto F_T^{1.5} Re^{1.1}$	$L_r^{1.65}$

Figure 3.13

Previous correlations for air entrainment by plunging jets have generally ignored (a) the effect of increasing jet thickness with droplength and velocity held constant (b) the effect of increasing droplength with initial jet thickness and velocity held constant and (c) the effect of increasing jet velocity over a wide range when jet thickness and jet droplength are held constant. These can be explained as follows:-

(a) Variation in rate of air entrainment per unit surface length, with velocity (u_1) and droplength (L) constant

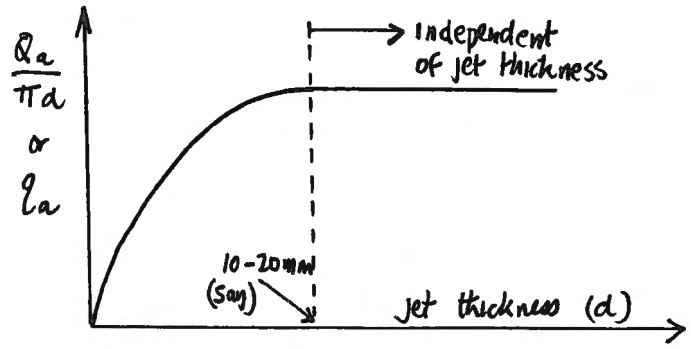

Figure 3.14

For higher jet thickness q_a is independent of d for wide rectangular jets and $\frac{Q_a}{\pi d}$ is independent of d for circular jets, i.e. Turbulent suppression no longer important for higher d values. The independence of d appears to happen for d > 10-20 mm and Reynolds Numbers >5 x 10^4, depending on initial turbulence levels in the jet and air bubble sizes. Most experimenters have used values of d < 20 mm, especially in circular jet research, and hence not generally in independent region.

(b) Jet droplength

A typical sketch of variation of entrainment with droplength is below.

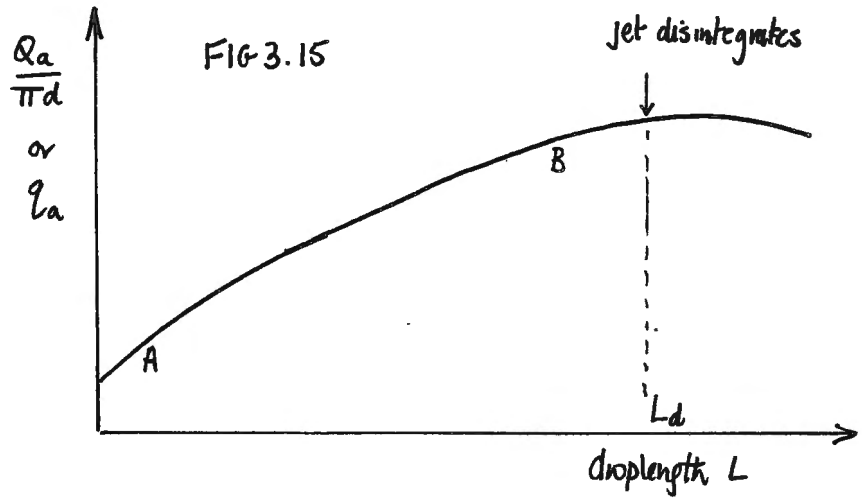

Most correlations are taken from the region AB when $q_a \propto L^{1/2}$ approx. This is not the case for greater droplengths and hence cannot be extrapolated past the jet disintegration length L_d.

(c) The effect of increasing velocity with L and d held constant.

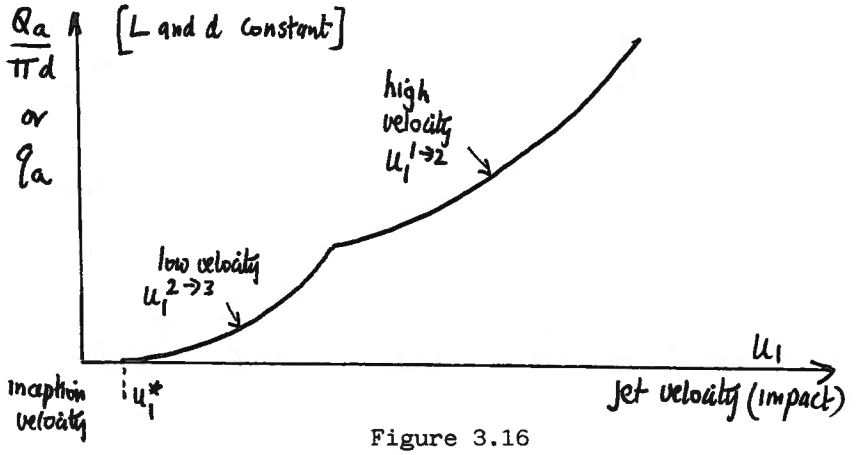

Figure 3.16

For low velocity jets McKeogh (Ref) found the entrainment rate to vary with U_1^2, Van de Sande, $U_1^{2\rightarrow 2.5}$, Renner (Ref) U_1^3, Ervine et al (Ref) $(U_1 - 0.8)^3$, Sene (Ref) U_1^3, while for high velocity jets Van de Sande (Ref) $U_1^{1\rightarrow 2}$, Sene (Ref) $U_1^{1.5}$, illustrating the divergence in the power of the impact velocity, U_1^n.

Thus for plunging circular jets, L and d constant,

$$Q_a/\pi d = K_1 u_1^n$$

where $\begin{cases} n \simeq 2 \rightarrow 3 \text{ at low velocity} \\ n \simeq 1 \rightarrow 2 \text{ at high velocity} \end{cases}$

and rectangular jets

$$q_a = K_2 u_1^n$$

where $n \simeq 3$ for low velocity jets

Incorporating the parameter d, we obtain for circular jets,

$$\frac{Q_a}{K_1 u_1^n d} = f_1(d)$$

$$\frac{q_a}{K_2 u_1^n} = f_2(d)$$

where $f_1(d)$ might be like

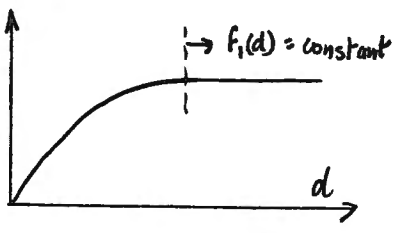

We can assume that $f_1(d)$ = constant when d > 20mm or $R_e > 5 \times 10^4$ or 10^5.

Finally to incorporate, the effect of jet break-up with increasing plunge length, we obtain,

Circular jets

$$Q_a = K_1 d u_1^n f_1(d) \left(L/L_d\right)^{0.7 \to 0.8} \quad \ldots\ldots (3.13)$$

Rectangular jets,

$$q_a = K_2 u_1^n f_2(d) \left(L/L_d\right)^{0.7 \to 0.8} \quad \ldots\ldots (3.14)$$

where L is droplength and L_d disintegration droplength.

Translating these into air/water ratio terms,

(Circular) $$\beta = K_1 u_1^{n-1} \frac{f_1(d)}{d} \left(L/L_d\right)^{0.7 \to 0.8} \quad \ldots\ldots (3.15)$$

(rectangular) $$\beta = K_2 u_1^{n-1} \frac{f_2(d)}{d} \left(L/L_d\right)^{0.7 \to 0.8} \quad \ldots\ldots (3.16)$$

For the case of a plunging rectangular jet n = 3, and for the case of d > 20 mm should give from (3.16) $\beta = K\, Fr_i^2\, (L/L_d)^{0.7 \to 0.8}$, which is similar to wall jets, except for the term (L/L_d) describing jet break-up. A lot more research is required on plunging jets especially at larger scales and velocities.

Bubble dispersion for jets plunging into unconfined pools

There appears to be a minimal amount of research carried out on the nature of the two phase conical diffusion region in the plunge pool. A good deal of work has been carried out on submerged jets but very little on plunging jets entraining large quantities of air bubbles.

If we consider first a jet entraining no air bubbles (single phase) then a system of spreading shear layers will develop as shown overleaf:

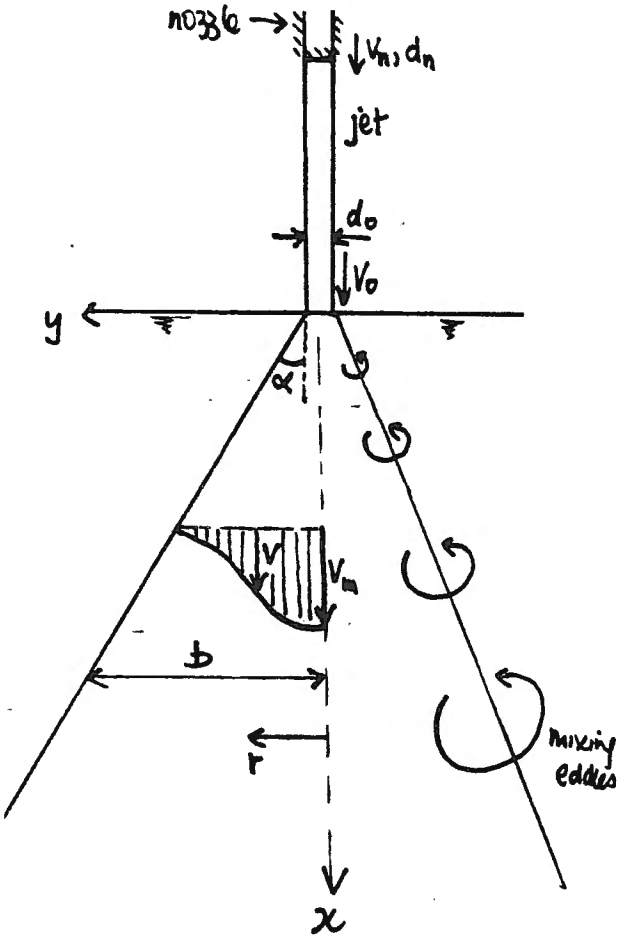

Figure 3.17

The sharp discontinuity between jet velocity and ambient fluid immediately sets up high turbulence intensity shearing eddies which transfer energy and momentum to the ambient fluid. The jet is rapidly decelerated and counterbalancing this, ambient fluid is accelerated and entrained into the spreading core.

Jet analysis is carried out on the assumption of constant momentum flux at any cross section in the core, the mixing eddy length is proportional to b, and $b/_x$ the angle of spread is approximately constant.

The velocity profile at any section shows similarity in the form

$$V/V_m = e^{(-r^2/2\sigma^2)} \quad \ldots\ldots (3.17)$$

where σ is the standard deviation and equal to the value of r where $v = 0.605V_m$.

That is, at any value of r/σ, $\frac{v}{V_m}$ = constant.

If we assume momentum flux is constant for all cross sections then

$$\rho V_o^2 \pi/4 d_o^2 = \rho \int_o^b v^2 2\pi r\, dr \quad \ldots\ldots (3.18)$$

Thus with $V \propto V_m$ at any value of r/σ

$$\int_c^b v^2 2\pi r\, dr \propto V_m^2 \int_o^b 2\pi r\, dr \propto V_m^2 b^2 \quad \ldots\ldots (3.19)$$

We obtain $V_o \; d_o \propto V_m b$

Now if spreading angle approximately constant, $b/_x$ = const, or $b \propto x$.

Thus $V_o \; d_o \propto V_m x$ = constant.

This indicates that the centre line velocity V_m decays linearly with x. ($V_m \propto 1/_x$) the distance from the plunge point.

Albertson (Ref) showed from experimental data that

$$V_m/V_o \sim 6\,(d_o/_x) \quad \ldots\ldots (3.20)$$

The question now presents as to how the turbulent core behaves with the introduction of large quantities of air bubbles. If behaviour was identical to that in Equation (3.20) then we could calculate approximate penetration depths for air bubbles.

$$x/d_o \simeq 6(V_o/V_m) \quad \ldots\ldots (3.21)$$

Assuming air bubbles descend with the flow until a point when V_m is equal to the bubble rise velocity ($\simeq$ 0.25 m/s), then x the penetration depth = $d_p \simeq 24\ V_o\ d_o$. This of course is not possible as the air bubble concentration affects the angle of spreading cone and turbulence intensity in the shear layer.

With substantial quantities of air now entering the spreading cone the characteristics of the cone will change considerably. We can postulate initially that the spreading shear layer will have a greater angle of spread due to the presence of air bubbles, and hence the centre line velocity will decay more rapidly than the case with no air bubbles present. Also the penetration depth of air bubbles will be considerably reduced due to the more rapid decay of jet velocity. Evidence for this is given overleaf in two photographs (McKeogh) of plunging jets with identical velocity and diameter at the point of impact but one jet with a low turbulence intensity and the other high. (Figures 3.18 and 3.19.) It can be seen that the low intensity turbulent jet entrains small quantities of air and has a deep penetration depth, whereas the higher turbulence jet entrains large amounts of air, has a smaller penetration depth and hence a greater spreading angle of shear layer. Further verification of this phenomenon is given on Figure 3.20 (from McKeogh's Ph.D. Thesis, Ref) comparing a jet with no air entrainment to the case of the jet with flow turbulence intensity and small air concentrations (<2%). For no air entrainment $V_m/V_o \simeq 6(d_o/x)$ as in the case of Albertson, whereas with a small amount of air entrainment $V_m/V_o \simeq 3(d_o/x)$. Thus for this particular case, the centre line velocity decay is twice as great with modest amounts of air entrainment. This is also reflected in the angle of spreading shear layer α, which is approximately $1/6$ for a jet with no entrainment, but ¼ for the case of air entrainment with air concentration $\simeq$ 2%.

One would expect therefore, that if air bubbles penetrate to $V_m \simeq 0.25$ m/s then for McKeogh's cases of small air concentration that $x = dp \simeq 12\ V_o\ d_o$ which is half the value of that postulated from Albertsons non air entraining case.

McKeogh did not measure the penetration depth for smooth turbulent jets, but instead measured this value for rough turbulent jets of the type commonly found in civil Engineering structures. He correlated experimental results to give

$$d_p = 2.6(V_n\ d_n)^{0.7} \quad \ldots\ldots (3.22)$$

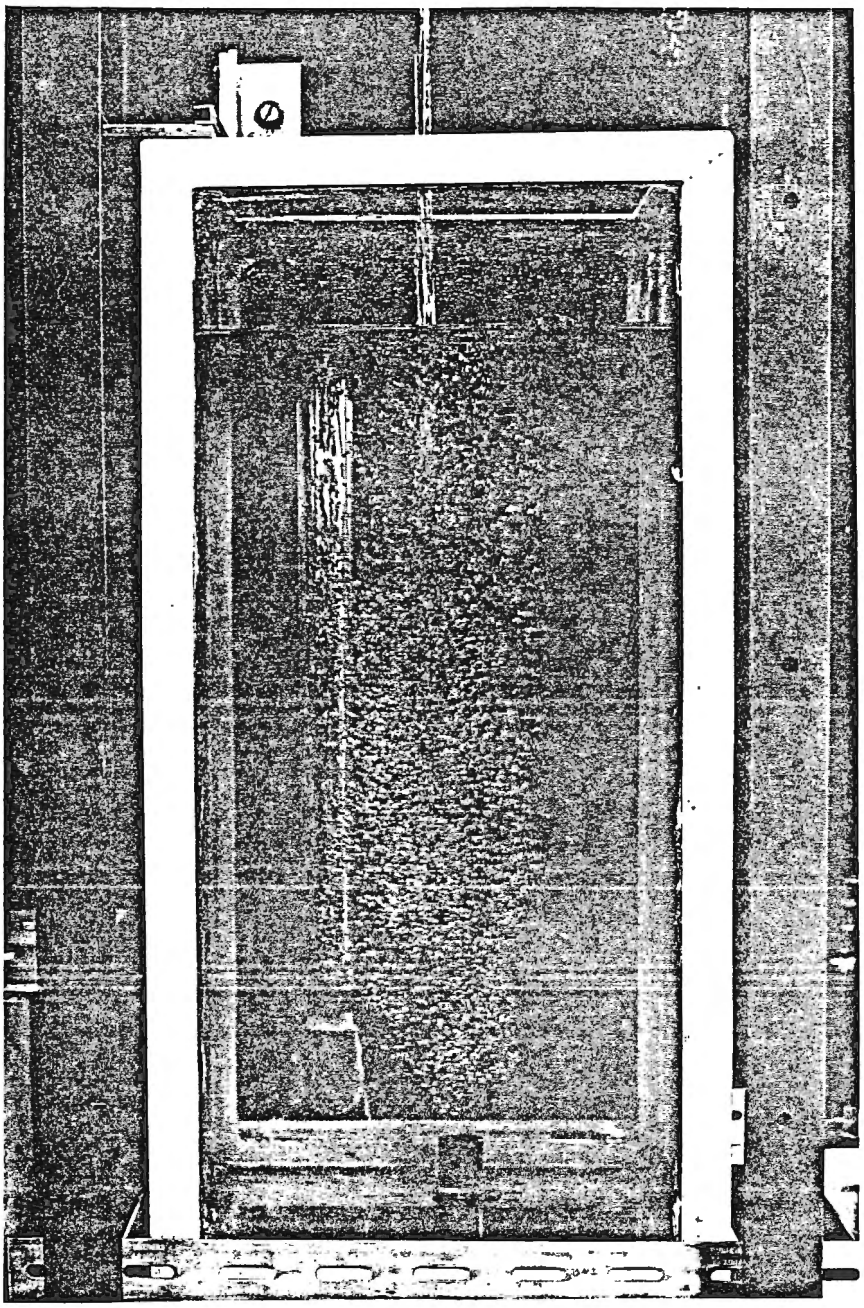

FIG 3.18

2. ENTRAINMENT PATTERN PRODUCED BY A JET OF IMPACT TURBULENCE INTENSITY LESS THAN 1.3%. Note the depth of penetration and low bubble intensity.

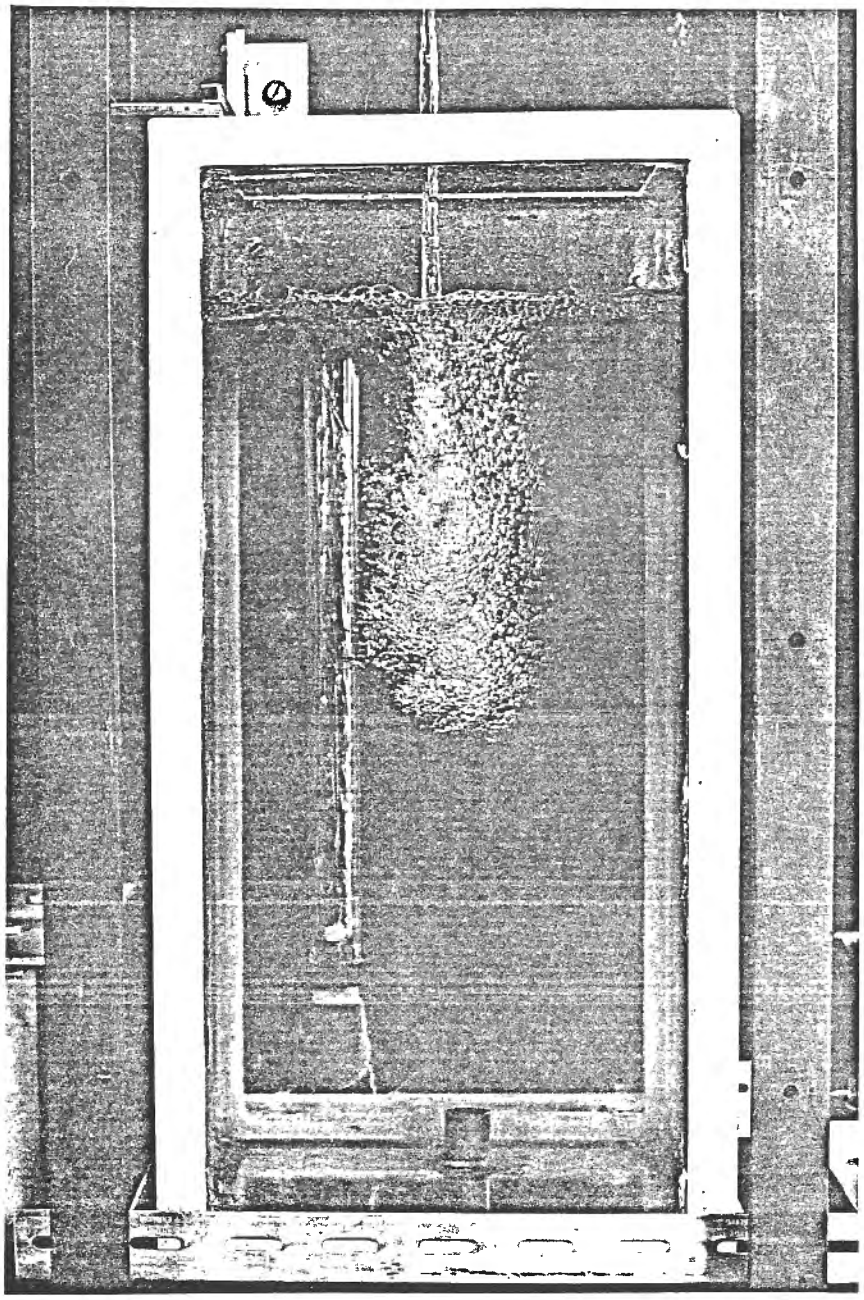

FIG 3.19

ENTRAINMENT PATTERN PRODUCED BY A JET OF IMPACT TURBULENCE INTENSITY OF APPROXIMATELY 5%. Note the depth of penetration reduced from that of Fig. 7.32. and the high bubble intensity.

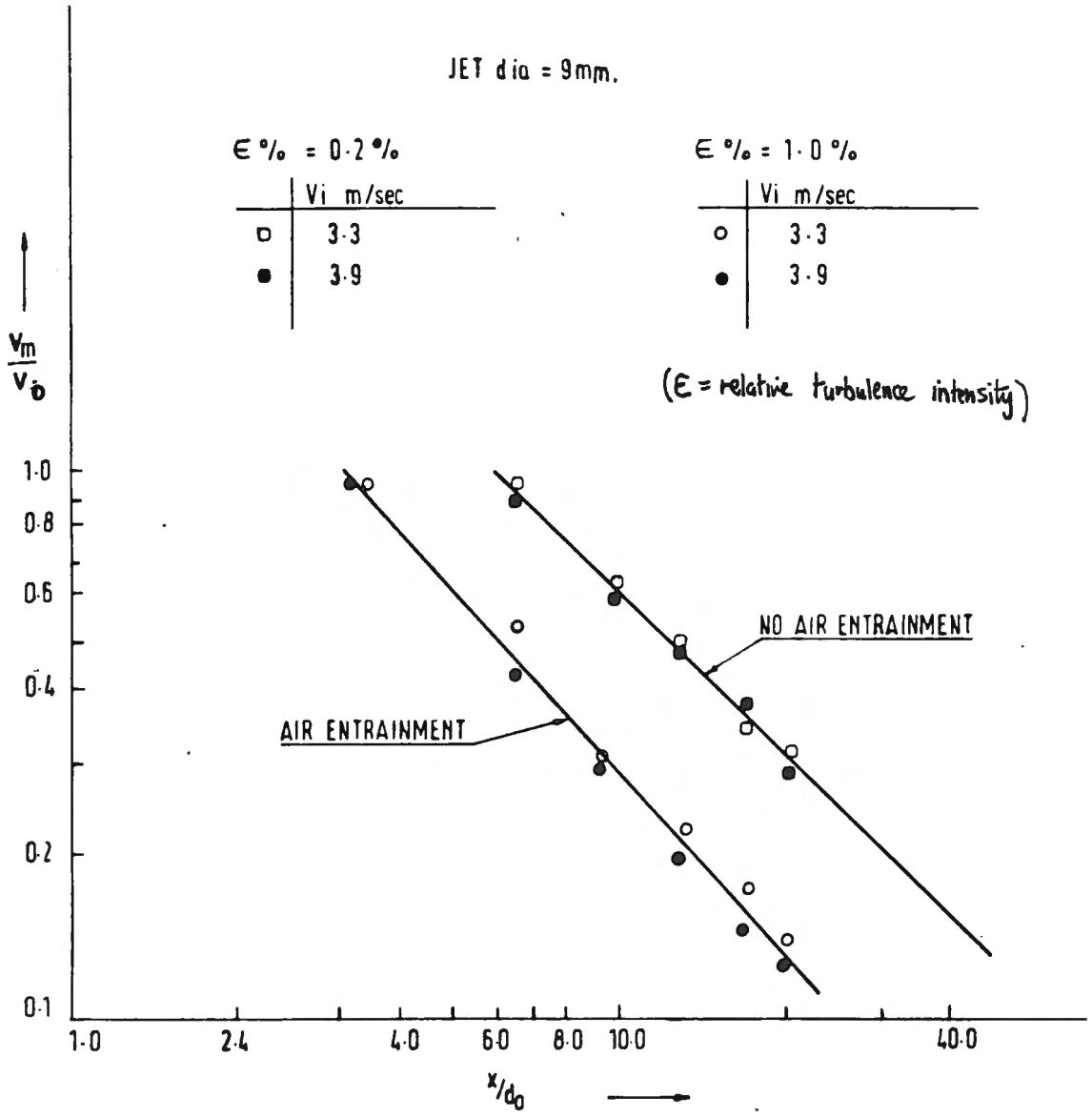

Fig. 3.20 CENTRE LINE VELOCITY DECAY WITH DISTANCE, x, FROM PLUNGE POINT (Mc Keogh)

where V_n and d_n are the velocity and diameter at the nozzle. (For long jet plunge lengths it is difficult to measure V and d at the point of impact).

Vigander (Ref) also measured the penetration depth for rough turbulent high velocity jets varying in diameter from 6 mm to 38 mm. The result is shown below, giving

$$d_p/d_n \sim 1.5\ V_n/V_{br} \quad \ldots\ldots (3.23)$$

Assuming V_{br} the bubble rise speed is ≈ 0.25 m/s, we obtain $d_p \approx 6\ V_n d_n$. Both results are plotted on Figure 3.22 for comparison. It is noted that penetration depths for rough turbulent, high air entrainment jets ($\approx 6V_n d_n$) are approximately 50% of that postulated for smooth turbulent, low air entrainment jets, and approximately 25% of that postulated for jets with zero air entrainment.

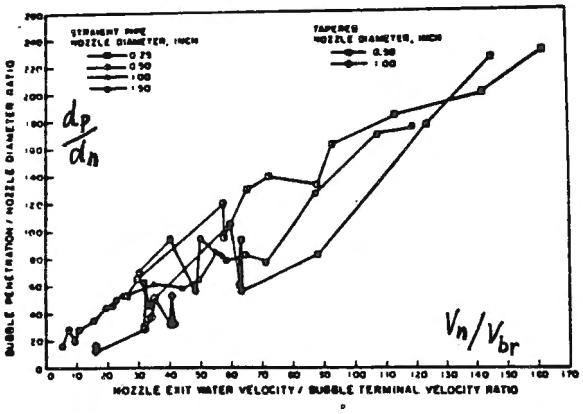

Figure 3.21
Bubble penetration depth correlation (Vigander)

The obvious conclusion from this work is that for the case of unconfined hydraulic structures, rough turbulent jets may entrain more air, but the air and the spreading jet penetrate to smaller depths and hence exhibit much greater energy loss efficiency. Figure 3.23 shows a typical plot of variation of penetration depth with increasing turbulence intensity.

Section 3.2

Experimental and empirical evidence for wall jet air entrainment, detrainment and air transport in siphons and dropshafts

In Section 3.1 the rate of air entrainment by jets plunging through the atmosphere was discussed, with the conclusion that the total rate of entrainment q_{at}, was influenced not only by jet velocity and turbulence level, but also the degree of 'break-up' in the jet. The same break-up phenomenon is not as evident in the wall jet entrainment and hence simpler correlations may be possible. Also in Section 3.1, the emphasis was placed on the total rate of air entrainment into a large pool area at the point of impingement, whereas the thrust of Section 3.2 will be the

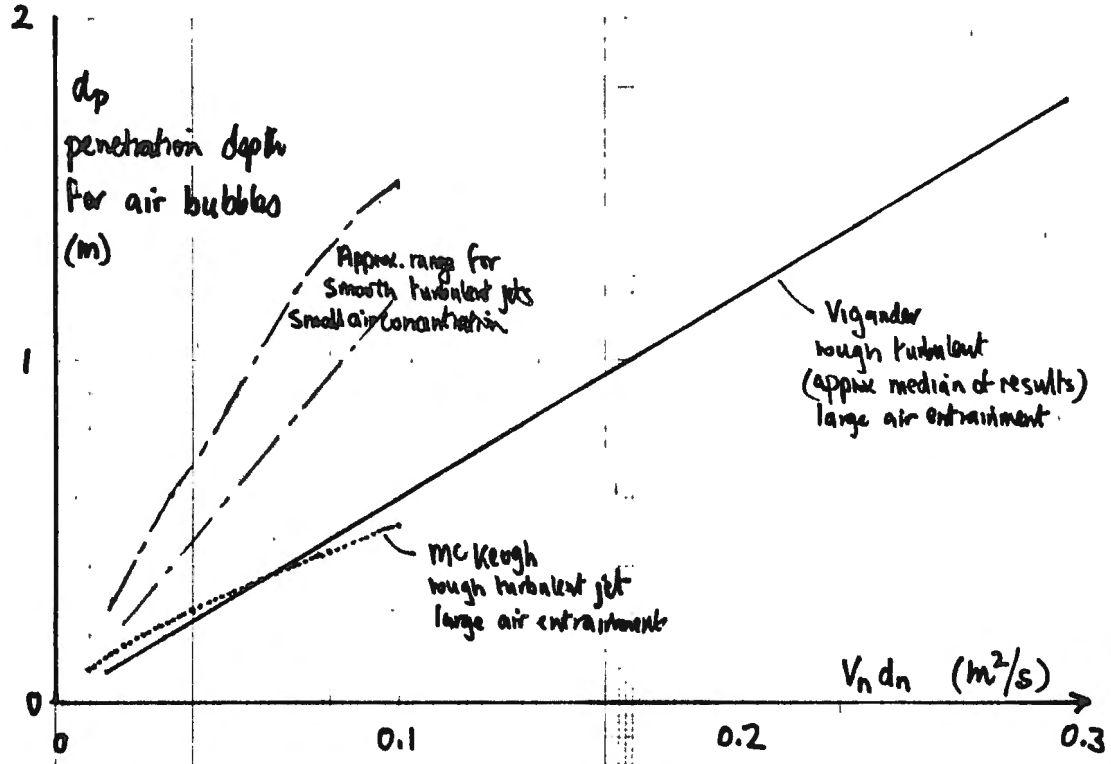

FIG 3.22 Variation of penetration depth with $(V_n d_n)$

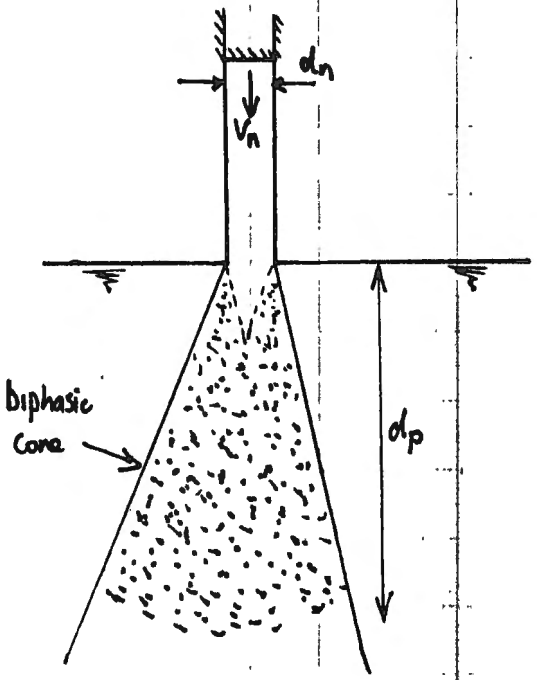

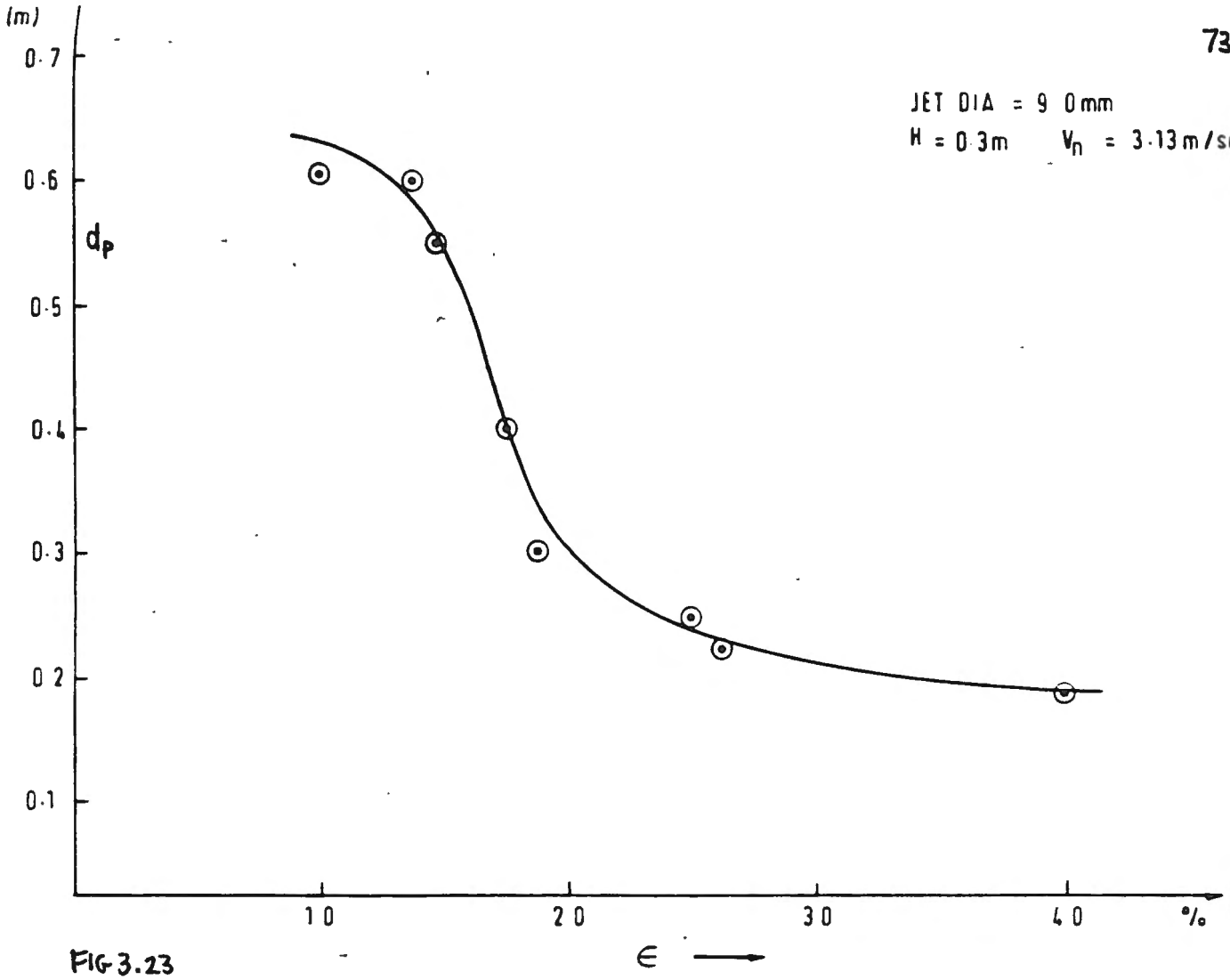

FIG 3.23

VARIATION OF PENETRATION DEPTH, a_p, WITH JET TURBULENCE INTENSITY, ϵ. (Mc Keogh)

net rate of air transport, q_{an}, along the conduit downstream of the point of impingement. Hydraulic jump entrainment and transport will be investigated in Section 3.3.

It is important in this section that the reader is aware of the distinction between the total rate of air entrainment (q_{at}) by a supercritical wall jet into the shear layer, detrainment of air bubbles out of the shear layer recirculating back to atmosphere (q_{ar}), and the net air transport out of the shear layer downstream along the conduit (q_{an}). The latter is the parameter of most practical interest, certainly in the case of siphons and dropshafts. These separate process have already been discussed in Section 2.2 and 2.3, and the reader is referred to these sections for a background of physical conjectures and more analytical treatment of air entrainment.

The behaviour of siphons with regard to air entrainment and transport

A siphon is essentially a closed conduit inverted U-tube, which transfers water from a higher to lower water level with a portion of the siphon length above the hydraulic gradient line. The upper part of the siphon is therefore at sub-atmospheric pressure, with the upper limit of sub-atmospheric pressure around - 10m head of water, at which point cavitation is likely to occur. Most siphon designers use an upper limit of negative pressure around -7.5m head of water so that cavitation problems might be avoided.

A siphon can be short in length, such as 'saddle' siphons over the crest of a dam, or low-head water level control siphons as in river engineering works. Siphons are often of considerable length, such as the high points (above hydraulic grade line) in long pipelines, or a component in the cooling water system of a power station (Goldring, Ref). In most cases the siphon will only run-full when the air trapped in the upper portion of the pipe is removed, usually either by air entrainment and transport, or by air vacuum pump. Siphons which remove air by jet entrainment and transport are said to be "self-priming".

Once the process of jet air entrainment and transport had been set up, it may proceed uncontrolled until the siphon runs full. This is a blackwater siphon and commonly found in storm-water systems. Reservoir and river siphons are nowadays generally designed to have controlled air entrainment and transport. That is, air allowed to enter the siphon at the upper end, so as to replace transported air at the siphon exist. This type of siphon behaves as a smooth valve in the sense that it is capable of remaining stable at any value of water

inflow to the siphon, and the exiting air flow is exactly balanced by the incoming air flow. This is an air-regulated siphon, and exhibits a fine control of the upstream water level which is of particular value in river engineering works. A typical stage-discharge relationship for an air regulated siphon is shown below (Figure 3.24) for the case of a short siphon where the inlet lip is a short distance above the siphon crest level. Four separate stages of flow ensue.

(I) Weir flow - when $Q = C_1 L h^{3/2}$, (h is head above crest level.)

(II) Sub-atmospheric weir flow, $Q \approx C_1 L (\frac{3}{2} y_{cr})^{3/2}$, where the siphon has begun to entrain and transport air, the upper air pocket is under partial vacuum, and we might assume hydraulic criticality at the crest (y_{cr}), giving an upstream apparent head of $\approx \frac{3}{2} y_{cr}$ in the reservoir.

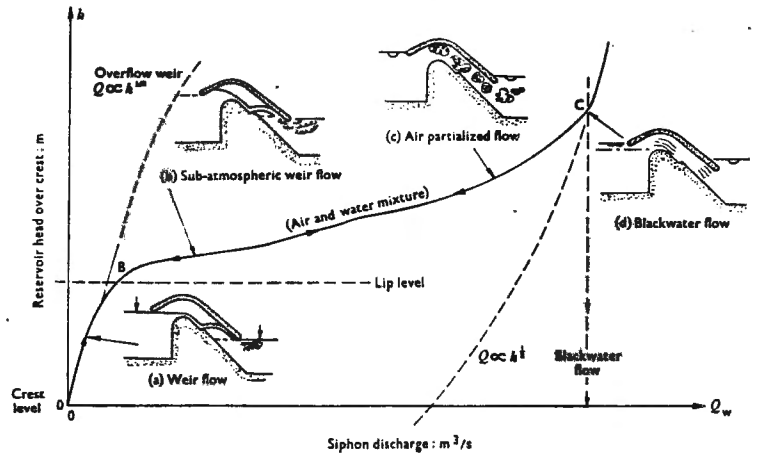

FIG. 3.24

FIG. 3.24 Typical priming characteristic for a siphon spillway

(III) Partialised flow, which is a well mixed two-phase flow. In this case the air pockets are essentially removed and regulating air from the inlet disperses through the water flow. In this case $Q \propto \sqrt{2gH}$ where H is the head across the siphon from upstream to downstream water levels.

(IV) Blackwater or siphon full flow, when all air is removed, no further air enters from the inlet and $Q = C_d A_o \sqrt{2gH}$, where A_o is the cross-sectional area of the siphon barrel and C_d is generally 0.7 to 0.9 depending on siphon design.

This process is illustrated by a series of photographs Figure 3.25(a) to (f) for a low head siphon where the means of air entrainment is by a plunging jet, and a further series of photographs Figure 3.26(a) to (h) for a high head reservoir siphon where the means of air entrainment is by a jet impinging on a wall, causing a surface roller in a manner similar to a hydraulic jump. A third common type of entrainment is simply a wall jet remaining in contact with the lower siphon wall and entraining air at the plunge point entry into the siphon full condition. This has been discussed in detail in sections 2.2 and 2.3.

Air entrainment theories for siphons (1975–85)

In the interests of brevity, only a selection of air entrainment theories over the last 10 years will be considered. These are limited to Ervine (1975), Renner (1975), (Kobus and Rao 1975), Casteleyn, Van Groen and Kokman (1977), Thomas (1978)(1982), Goldring (1979, 1980, 1984), Ervine and Ahmed (1984), and Sene (1984).

A good deal more research than above has been carried out on siphons in the last 10 years, but the intention is to concentrate on research quantifying rates of air entrainment. For instance, Professor Markland (University College, Cardiff) has been engaged in the most innovative aspects of siphon design. Further references on siphons can be obtained from, B.H.R.A. Conf. on Design of Siphons and Siphon Spillways, London, England, May 1975.

Ervine (Ref) measured the rate of air entrainment in three siphon models of a reservoir siphon scales 1:7, 1:10 and 1:20, and the rate of entrainmemt for three low head river siphons also at scales 1:7, 1:10 and 1:20. The measured rates of entrainment are in fact the rates of air transport through the siphon (β_{an}) and are indicated in Figure 3.27. (The design on the reservoir siphons are as shown on the photographs, Figure 3.26 and the low head siphons as shown on Figure 3.25).

It can be seen from Figure 3.27 that the low head siphons in particular revealed large scale effects in the rate of transported air. The value of β_{an} increased almost linearly with model scale (L_r),

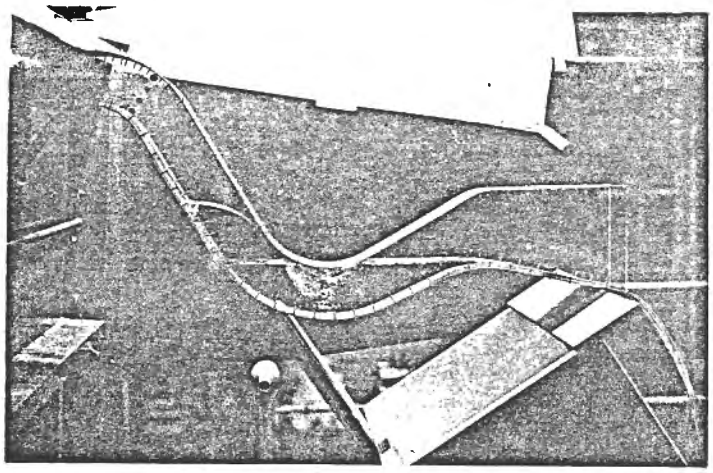

(a) Weir flow

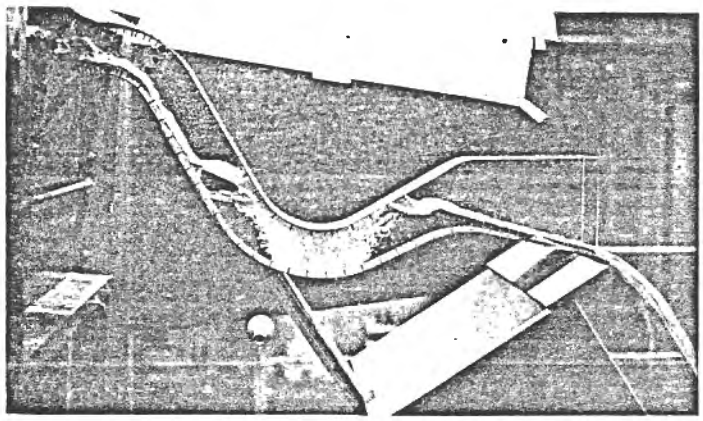

(b) Sub-atmospheric weir flow (deflected nappe)

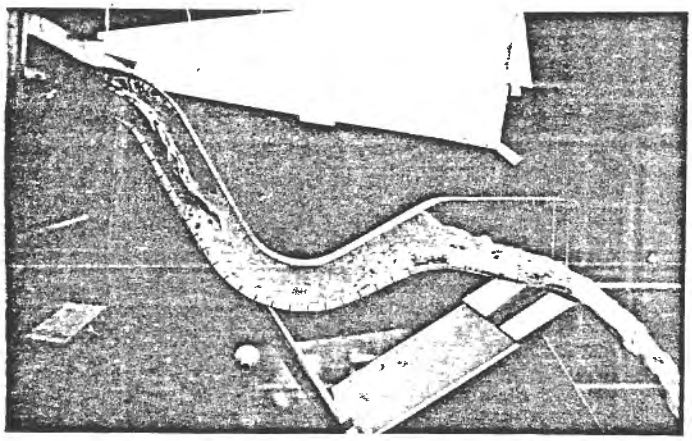

(c) Depressed nappe

FIG.3.25

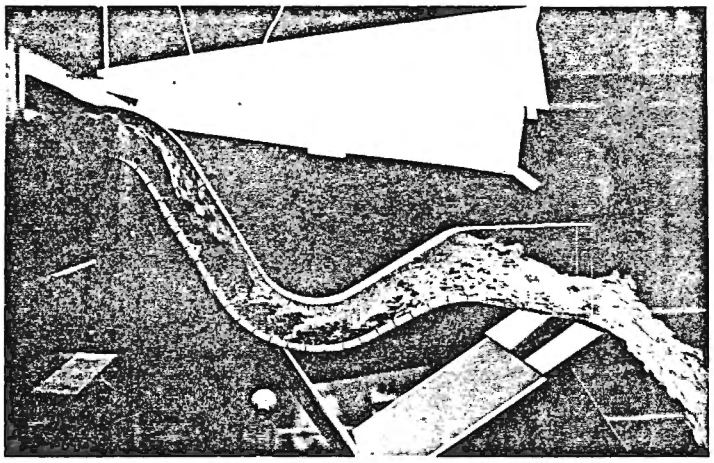

(d) Air pocket nearly disappears

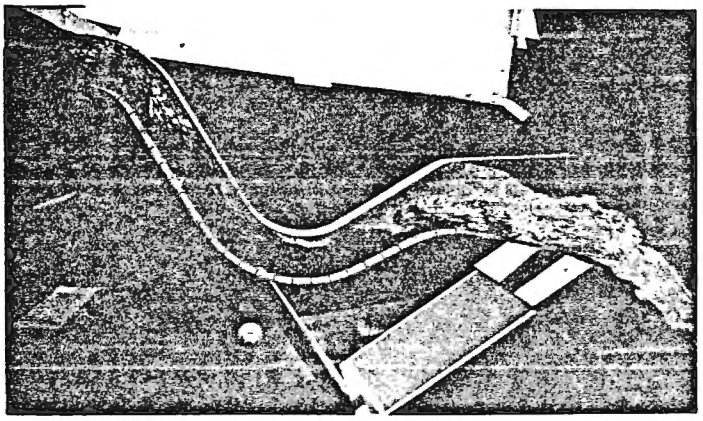

(e) Partialised flow

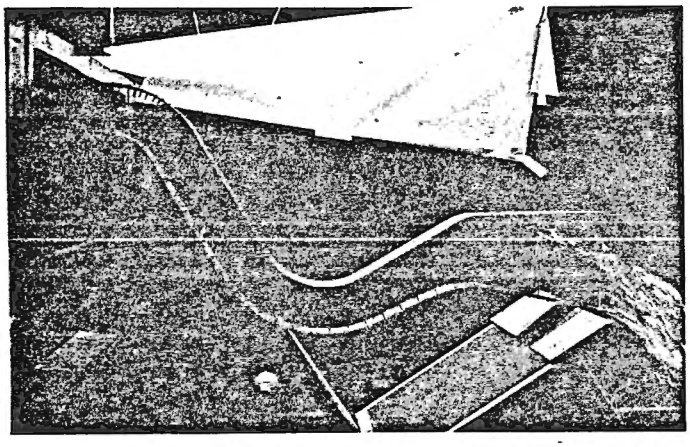

(f) Black water flow

FIG.3.26

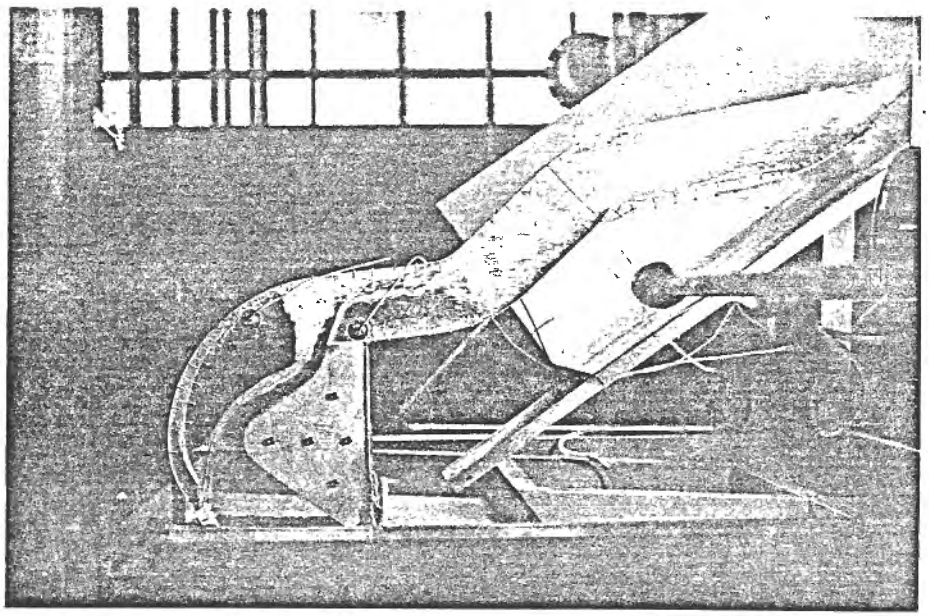

(b) Turbulent tongue appears

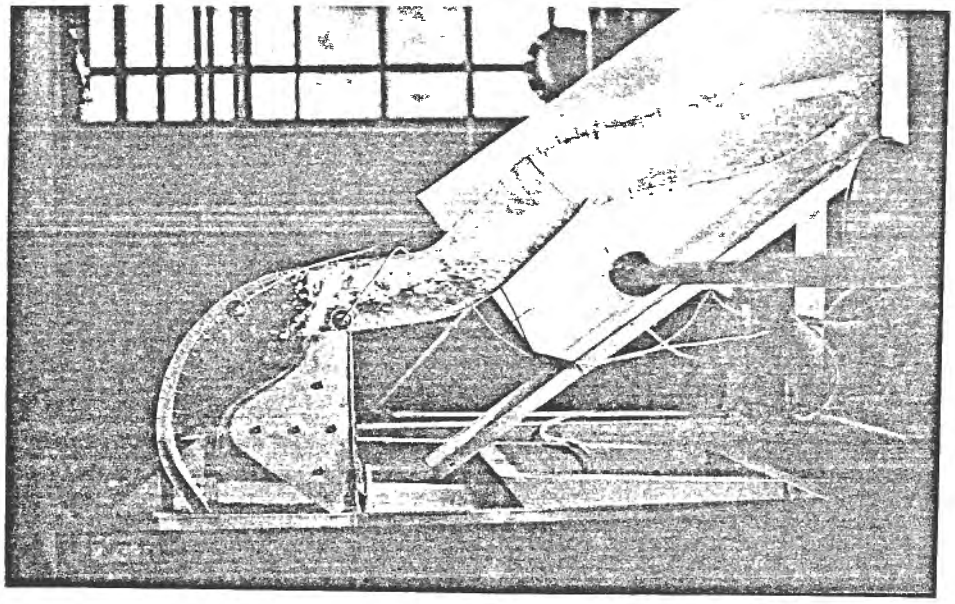

(a) Weir flow

FIG.3.26

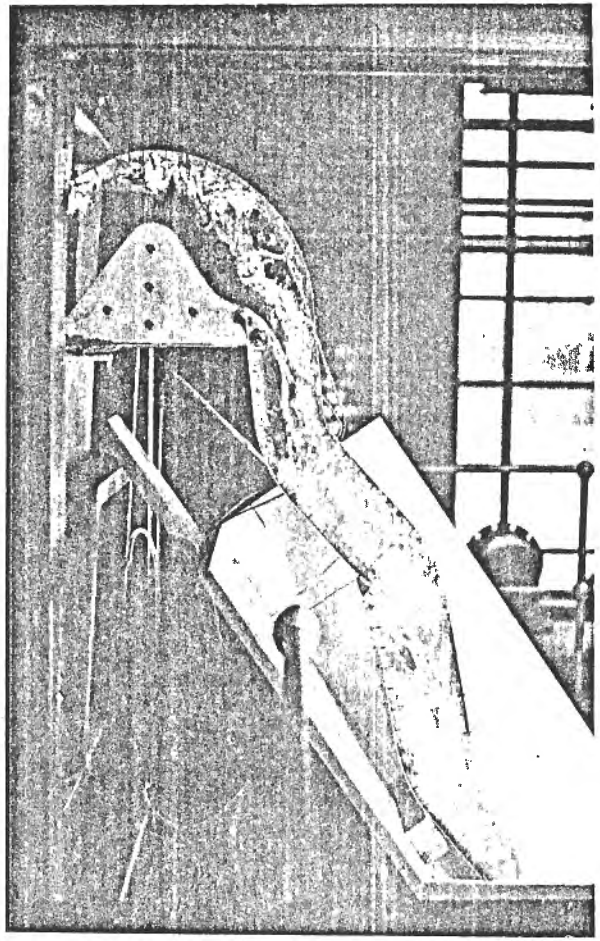

(c) Sub-atmospheric weir flow

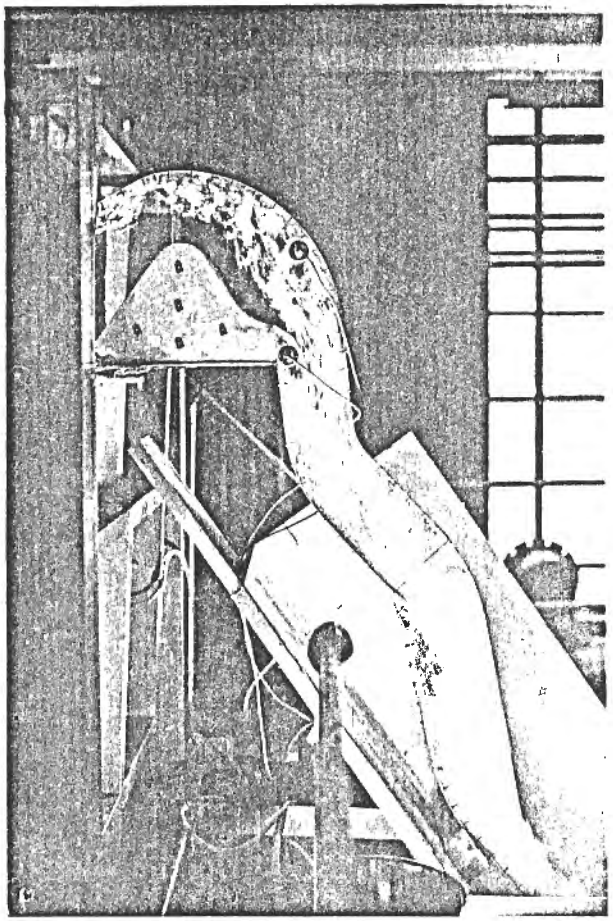

(d) Air pockets filling up.

FIG.3.24

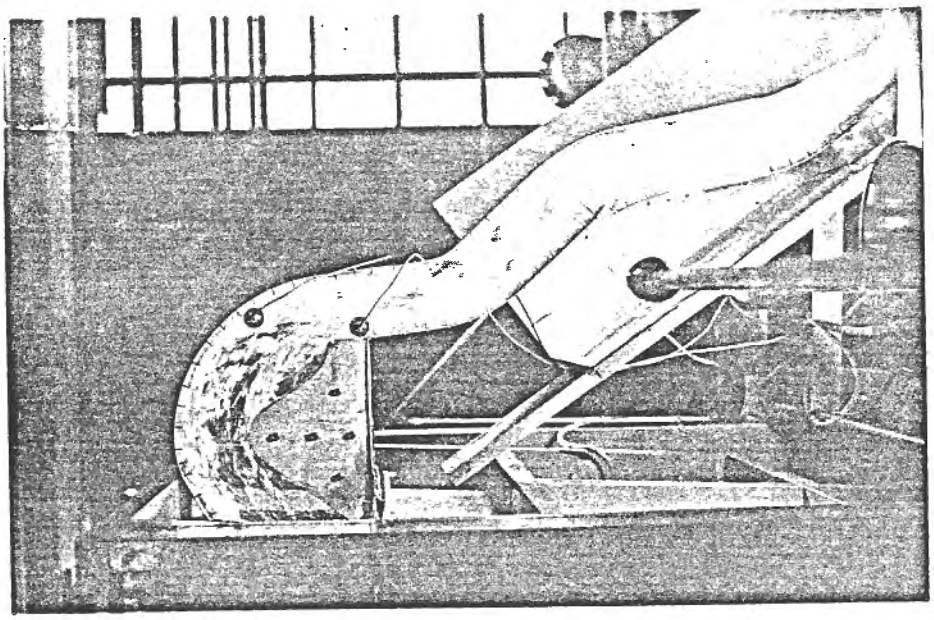

(f) Flow separation at crest

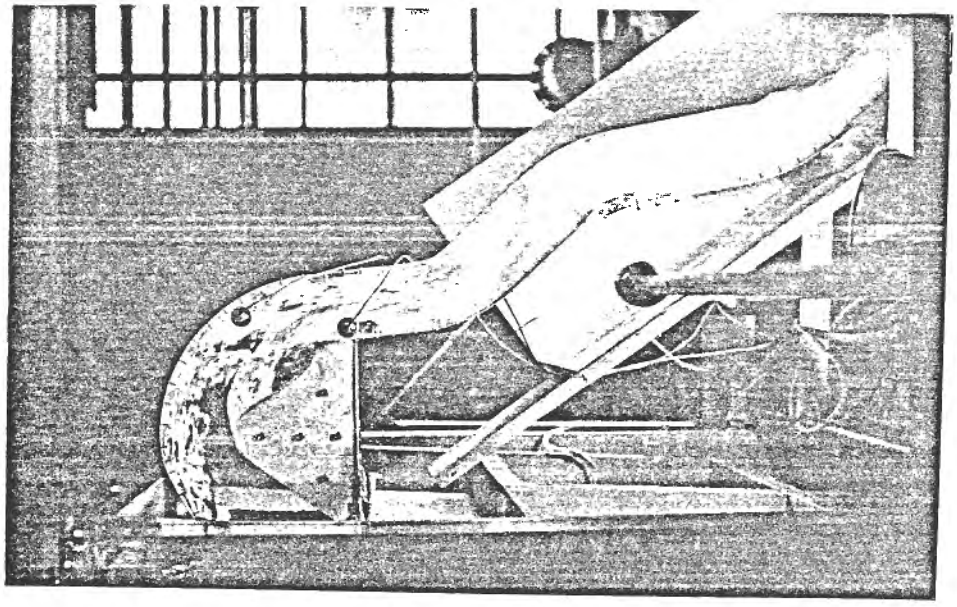

(e) Partialised flow

FIG. 3.26

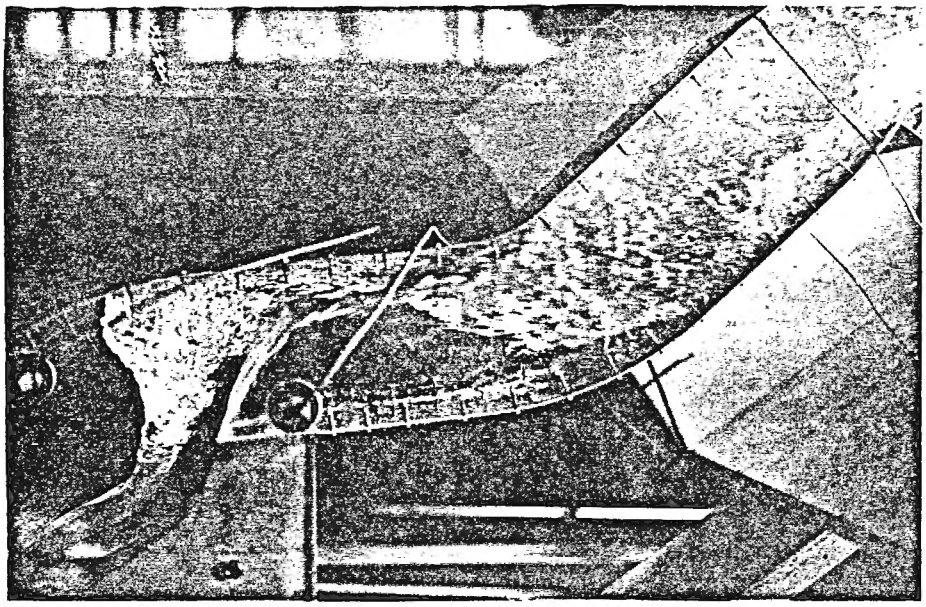

(h) Air entrainment by turbulent tongue (hydraulic jump effect)

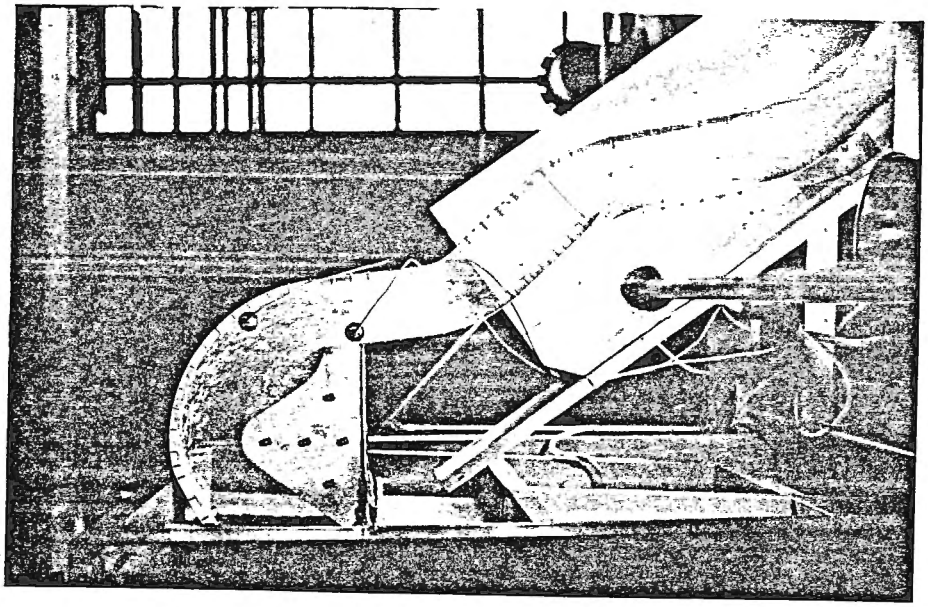

(g) Maximum flow (black water flow)

FIG.3.26.

whereas the high head siphons, at larger velocities, showed an increase in the air water ratio β_{an} approximately with $L_r^{1/2}$ or less. There was no consistent pattern with the scale effect. One thing did become clear, that siphons did not transport air according to Froude scaling. The reasons postulated for this by Ervine were:- (a) a minimum velocity (≈ 1 m/s) was required to entrain air initially, hence models operating at velocities around 1 m/s would entrain relatively little air. This effect would become progressively smaller as the velocity is the siphon barrel or the scale of the model increased, as witnessed by the high head siphons, (b) air evacuation would also depend on the ratio of the air bubbles rise velocity to the outlet water velocity in the siphon. As the bubble rise velocity U_{br} is approximately constant in all three scale models,

then U_{br}/U_o or $U_o - U_{br}$ is not scaled according to Froude law, and a distortion in air transport scaling results.

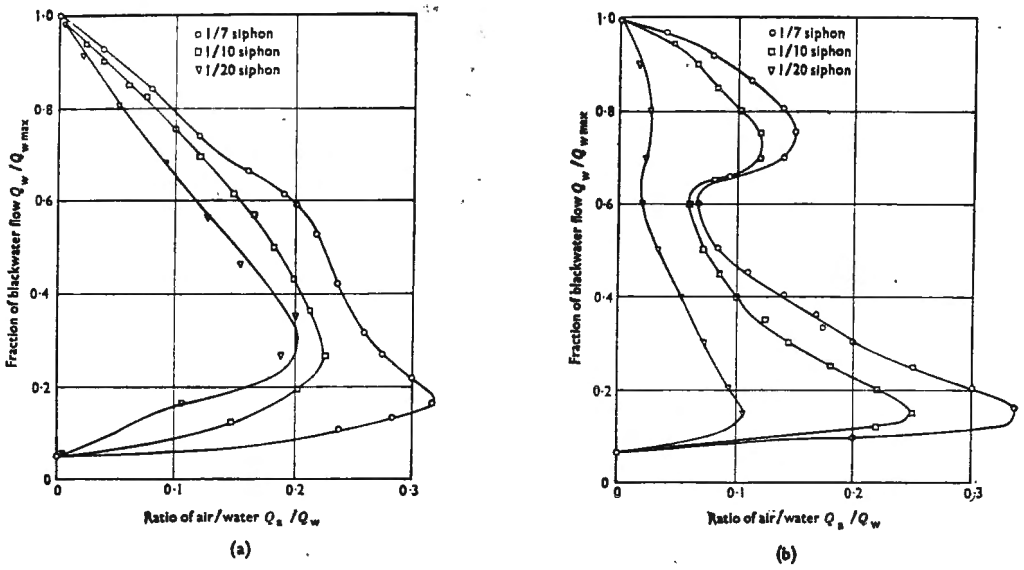

Typical air/water ratio curves for (a) the three high head siphons during priming, (b) the three low head siphons during priming

Figure 3.27

In 1975, Renner (Ref) reported on an experimental investigation into an aspect of siphon air entraining behaviour. This was also reported extensively by Kobus and Rao (Ref). A 2-dimensional jet issues from a slot impinging on a wall which may be inclined at any angle α to the horizontal. A turbulent surface roller is formed as shown on Figure 3.28 and according to Renner air is entrained at the toe of the roller. Thomas has since conjectured that air is in fact entrained into the roller itself as well as the toe of the roller. A proportion of the entrained air is transported along with the flow and the remainder is recirculated to the atmosphere. A correlation for two wall angles of the net rate of air transport is shown on Figure 3.28. From this it can be seen that for Froude Numbers less than 9, and for a given angle of wall α, the ratio of air to water can be given by

$$\beta_{en} = q_a/q_w = K Fr_1^2 \qquad \ldots\ldots (3.24)$$

or $q_{air} \propto U_1^3$ where U_1 is the jet velocity.

Kobus argues that air entraining situations which are not influenced by boundary scale, and where viscous effects are no longer significant, say $R_e > 10^5$, then we may write

$$q_a = f(u_1, \rho_w, g) \qquad \ldots\ldots (3.25)$$

or from dimensional analysis

$$\frac{q_a}{u_1^3 g} = \text{constant, which is the result of Renner.}$$

This result is very attractive because of its simplicity. The values of K reported by Renner are generally in the range 0.00172 and 0.00275 depending on the wall angle α.

Renner's result brings into question a lot of assumptions regarding air entrainment and transport outlined in Sections 2.2 and 2.3.

(1) What type of air entrainment mechanism is this? Type (1) entrainment due to jet surface roughness might give $\beta = K Fr_1^2 f(Tu)$ so we could assume that Renner's results were of the same order of magnitude turbulence intensity. Type (2) entrainment at higher velocities with a continuous layer of air at the toe of the surface roller would give $q_a \propto u_1^{3/2}$, which is obviously not the case from Renner's results. Type (3) entrainment due to a surface roller might give a correlation on Fr-1 for Froude Numbers less than 9, which appears not be be the case either.

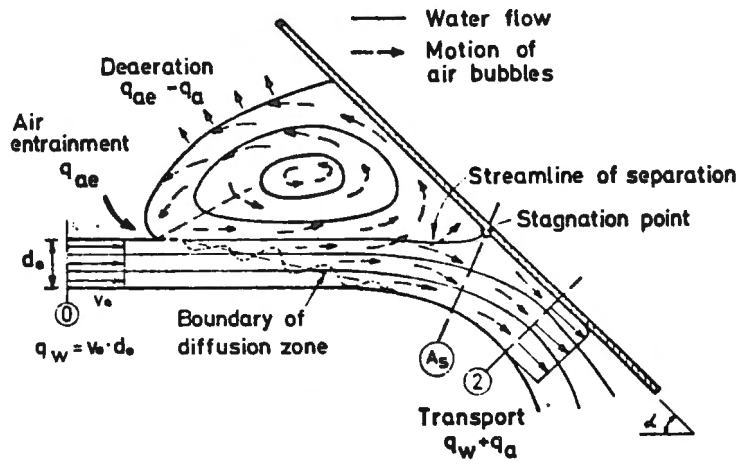

3.28
Fig. Illustrative sketch of air entrainment model (Renner)

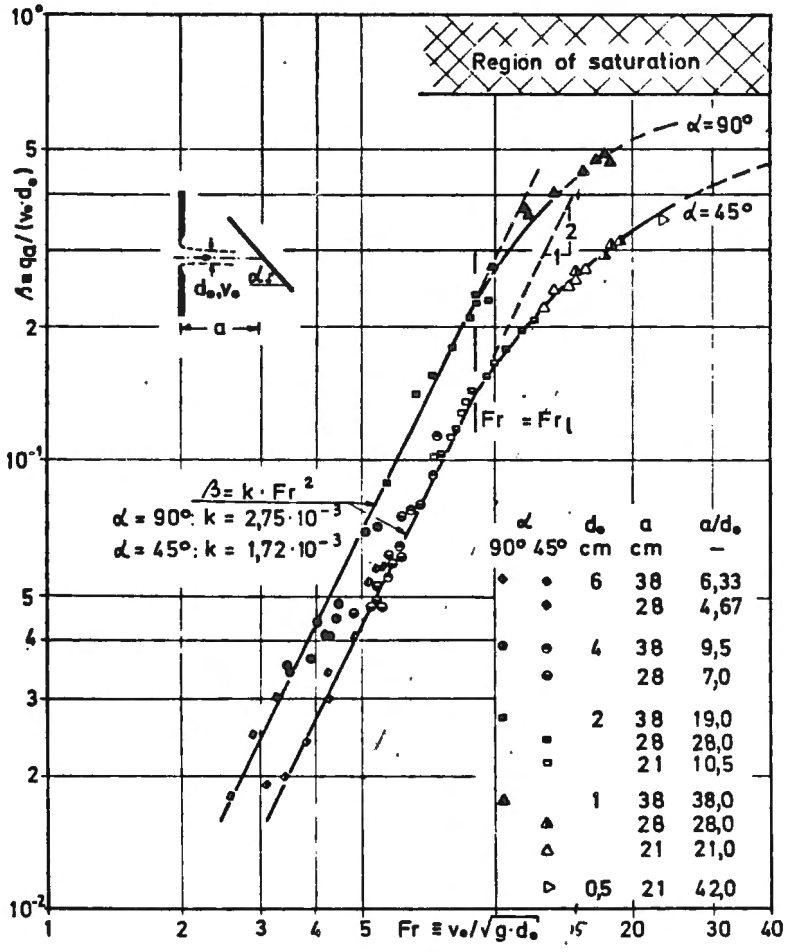

3.28
Fig. Relative rate of air entrainment for a free plane jet as a function of Froude number. (Renner)

(2) What type of air evacuation is this? The forces acting on an air bubble in the mixing region of the surface roller are inertial, buoyancy, vorticity and drag. Even is inertial and vorticity components are of no significance in this situation, buoyancy and drag will not scale on a Froude basis because of the same size of bubble in model and prototype. We can only assume that drag forces on the bubble say $\propto U_1^2$ are much greater than bubble buoyancy, which would only be the case at higher jet velocities, especially $U_1 > 2.5$ m/s. Renner tested only up to velocities of 5 m/s. Thus comparing with Thomas detrainment theory (Section 2.3) bubble detrainment appears with Renner's data to have no significance in this situation certainly with regard to scaling. This, in fact, might be the case in Renner's physical configuration as conventional penetrating shear layers are not occurring due to the proximity of the wall.

(3) Why does the angle of impingement into the wall have so much affect on the rate of entrainment? It can be seen from Figure 3.28 that a reduction in impingement angle from 90° to 45° causes a reduction in air entrainment ($\simeq$ 62%) at the same jet velocity. If, according to Renner, all the air is entrained at the toe of the roller, then at the same jet velocity, the same quantity should be entrained at 45° and 90° angles. Maybe more air is detrained at smaller wall angles. If on the other hand, air is entrained into the flow along the length of the surface roller, then this length will be reduced as the angle reduces from 90°. As a first approximation we might say that the length of the roller is proportional to the rate of change of momentum, then for a given U_1 and d the length will decrease approximately with $\sin\theta$. Thus the reduction in entrainment from 90° to 45° would be of the order, 100%:71% which is not as much as the measured value 100%:62% . Maybe more air is detrained at smaller impact angles.

(4) Renner noted from this data that jet thicknesss d < 10–15mm produced reduced rates of entrainment. This is in line with observations from other authors, Ervine and Ahmed (Ref) and Sene (Ref) etc. This is linked to the fact (not only of Re < 10^5) but a dampening of surface disturbances by surface tension when the scale of eddies is less than about four times the capillary length ($\simeq$ 11 mm) Hunt (Ref).

In 1977, Casteleyn, Van Groen and Kolkman (Ref), reported on air transport measurements in two model siphons at scale 1:20 and 1:7. The siphon design is shown on the sketch overleaf, with a total length of 100m (approx), a conduit dimension of 3.2m, and a variable level on the downstream side of the siphon.

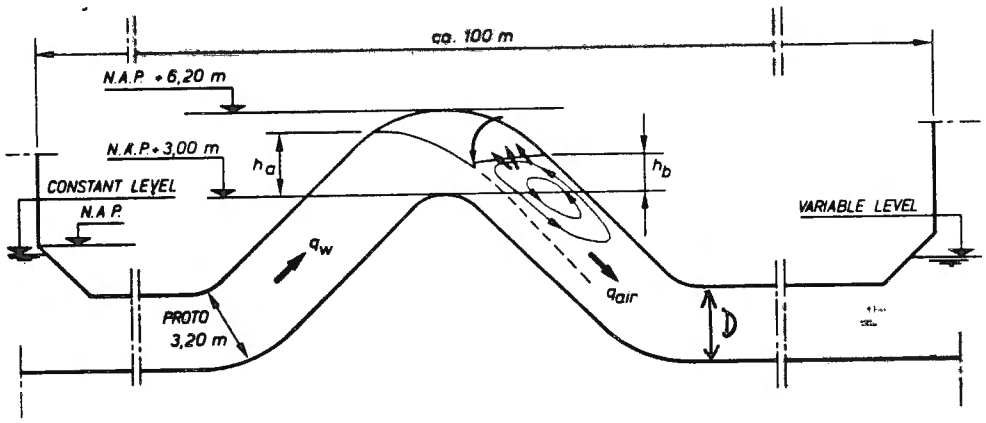

(Casteleyn, Van Groen and Kolkman – long Siphon)

Figure 3.29

Air entrainment (or air transport more correctly) measurements were made in the two scales of model siphon, with the downstream leg almost full, and the point of jet impingement generally just downstream of the point of criticality, i.e. the Froude Numbers at jet impact, $1 < u_1/\sqrt{gd} < 2.5$. An attempt was made at extrapolation of air transport measurements to prototype behaviour.

The physical reasoning for extrapolation was straight forward and similar in a sense to that of Thomas, Sene etc. If the rate of air entrainment q_a is proportional to the volume of air held in the jet surface disturbances and the jet velocity at impact, then we might have

$$q_a \propto u_1 f(\delta) \propto u_1 (u_1^2/g) = u_1^3/g \qquad \ldots\ldots (3.26)$$

Casteleyn et al found that in fact that for a given value of h_a/D, where h_a is defined on Figure 3.29, and D is the conduit dimension, that the rate of entrainment varied with, $q_a \propto U_1^{5.6}$. In order to generate a U_1^3 relationship, an additional term was introduced U_c, where $q_a \propto (U_1 - U_c)^3$. The value of U_c required to form this cubic relationship was 0.8 m/s, which by coincidence is the approximate jet velocity to entrain air into a flow. Using this revised cubic arrangement, the data from the $^1/20$ model and $^1/7$ model could be

correlated on one curve as shown below on Figure 3.30. (for the case of $h_a/D = 0.78$)

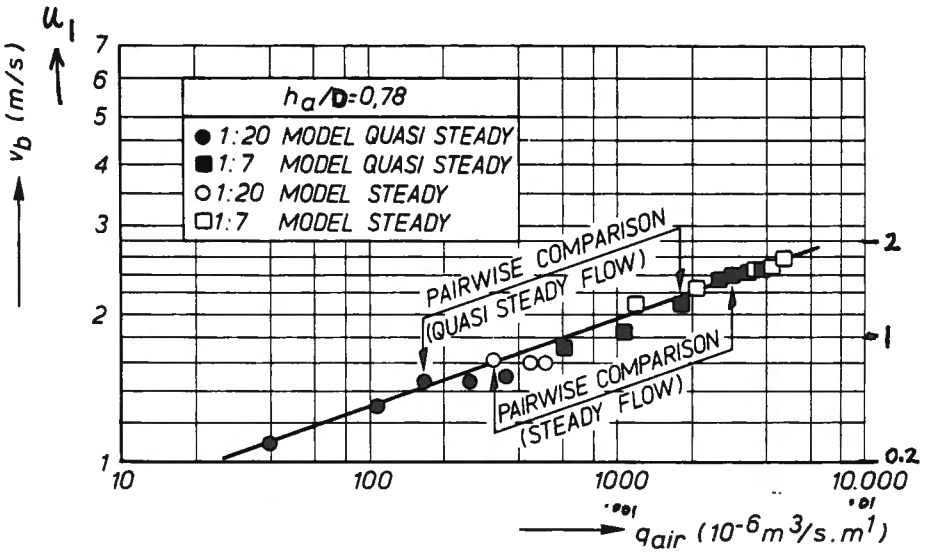

Figure 3.30

The correlation thus gave,

$$q_a = (u_1 - u_c)^3 \; f\left(h_a/D\right) \qquad \ldots\ldots (3.37)$$

and for h_a/D values greater than 0.6, this could be approximated to

$$q_a = 0.0005 \rightarrow 0.001 \left(u_1 - u_c\right)^3$$

This was later modified by Thomas to

$$\beta_{an} = 0.005 \rightarrow 0.01 \; Fr_1^2 \left(1 - \frac{u_c}{u_1}\right)^3 \qquad \ldots\ldots (3.28)$$

Prototype data confirming this relationship is still awaited.

Several points of interest emerge from Equation (3.28).

(1) Can the relationship $q_a \propto (U_1 - U_c)^3$ be sustained for prototype conditions where the velocity at impact U_1 is likely to be as high as 7 m/s? This would mean that surface roughness disturbances would have to increase with U_1^2/g. That is, for $U \propto 7$ m/s, $U_c/U_1 << 1$, then $\beta = 0.005 \rightarrow 0.01 Fr_1^2$. This is an abnormally high rate of entrainment by a jet entraining only on the upper surface. Sene (Ref) found an upper limit of $\beta \sim 0.004\ Fr_1^2$ which is approximately half of that to be expected from Kolkman's prototype data. Thus we must ask, in the light of Figure 2.9, Section 2.2, if the rate of entrainment will not be reduced from the $(U_1 - U_c)^3$ relationship when the jet velocity $U_1 > 5$ or

6 m/s corresponding to prototype conditions?

(2) Counterbalancing this possible reduction in air entrainment based on the $(U_1 - 0.8)^3$ relationship, (with higher prototype velocities) we have that possibility of greater air transport out of the penetrating shear layers in the prototype where the outlet velocities acting on entrained air bubbles will be greater. The drag forces on an entrained bubble are now much greater than buoyancy effects and scale effects from this source may be negligible compared with either the $^1/_{20}$ or $^1/_7$ scale model.

In terms of prototype predictions we may use the graph produced by Ahmed and Ervine (Figure 3.36) to give likely estimates of β_{an} for the case of Casteleyn et al siphons. Most of their siphon data gives $Fr_1 \simeq 1 \rightarrow 3$, and prototype velocities $5 \rightarrow 7$ m/s. Assume transport scale effects are negligible, then from Figure 3.36 we have for $Fr_1 \simeq 2$ and $U_1 \simeq 6$ m/s, $\beta_{an} \simeq 0.04$.

One point not mentioned by Casteleyn, Van Groen and Kolkman is the possibility of air pocket formation at the start of the horizontal outlet section of the siphon. Air bubbles from the entrainment mixing region may accumulate at the roof of the conduit with a possible blow-back tendency at low outlet Froude Numbers, say
It is assumed that this problem did not arise.

In 1978, Thomas (Ref) produced a scaling analysis for air transport out of a penetrating shear layer with a thick layer of foam on top of the shear layer, and air bubbles entrained into the shear layer along its upper length. This was subsequently reproduced and modified in a paper by Goldring, Mawer and Thomas (Ref) and a paper by Thomas in 1982 (Ref).

The analysis is presented in detail in Section 2.3, and the relationship presented by Thomas for the ratio of air to water β_{an}, is in the form of a scale independent entrainment into the shear layer term, and a scale dependent air bubble detrainment out of the shear layer term.

Entrainment into the shear layer is given as,

$\beta \propto (Fr - 1)$ for $Fr < 10$

and $\beta \propto Fr^2$ for $Fr > 10$

Bubble detrainment as indicated in section 2.3 is given by,

$$\left(1 - {}^{u_1^*}/_{u_1}\right)^2 \Big/ \left(1 - {}^{u_1^*}/_{3u_1}\right)$$

Thus for an air entraining situation with jet Froude Number less than 10,

$$\beta_{an} = K(Fr_1 - 1)\left[\left(1 - u_i^*/u_1\right)^2 \left(1 - u_i^*/3u_1\right)\right] \quad \ldots\ldots (3.29)$$

where the value of K according to Thomas ought to be around 0.025. This relationship is proposed for the net rate of air transport. One point of confusion in Thomas's relationship is connected with the value of U_i^*, which Thomas has called the entrainment inception velocity. It is not clear if this is meant to be the inception velocity to entrain air into the shear layer U_i^*, as discussed in Section 2.1, or the minimum velocity to commence air bubble transport $U_{1\,min}$ as discussed in Section 2.3. For Equation (3.29) to make any sense, the entrainment inception velocity should in fact be $U_{1\,min}$, below which there is no net air transport, but there may be entrainment into the shear layer and subsequent total detrainment.

Thomas used a value of $U_{1\,min}$ of 1 m/s to correlate the data of Casteleyn, Van Groen and Kolkman. This is smaller than predicted values of $U_{1\,min}$ in Section 2.3, because the shear layer in the Delft siphons is reaching the exit of the conduit, or to be more precise, the start of the horizontal length. Thus the minimum jet velocity to transport air $U_{1\,min}$ is practically as small as the inception velocity to entrain air U_i^* for this particular case. Generally, though, for long conduits the value of $U_{1\,min}$ in the Thomas equation should be around 1.5 → 2.5 m/s.

The correlation of Equation (3.29) with Casteleyn et al siphon data is shown in Figure 3.31, indicating excellent correspondence with both model scales (and a prototype extrapolation.) Thus for the prototype case of $Fr_1 \simeq 2$ and $U_1 \simeq 6$ m/s we obtain, $\beta \sim \frac{1}{40}(2-1)\left[(1-\frac{1}{6})^2/(1-\frac{1}{15})\right]$ which is $\beta_{an} \simeq 0.02$. This value is half of that predicted by Ervine and Ahmed ($\beta \simeq 0.04$).

Thomas correlation of CKs data

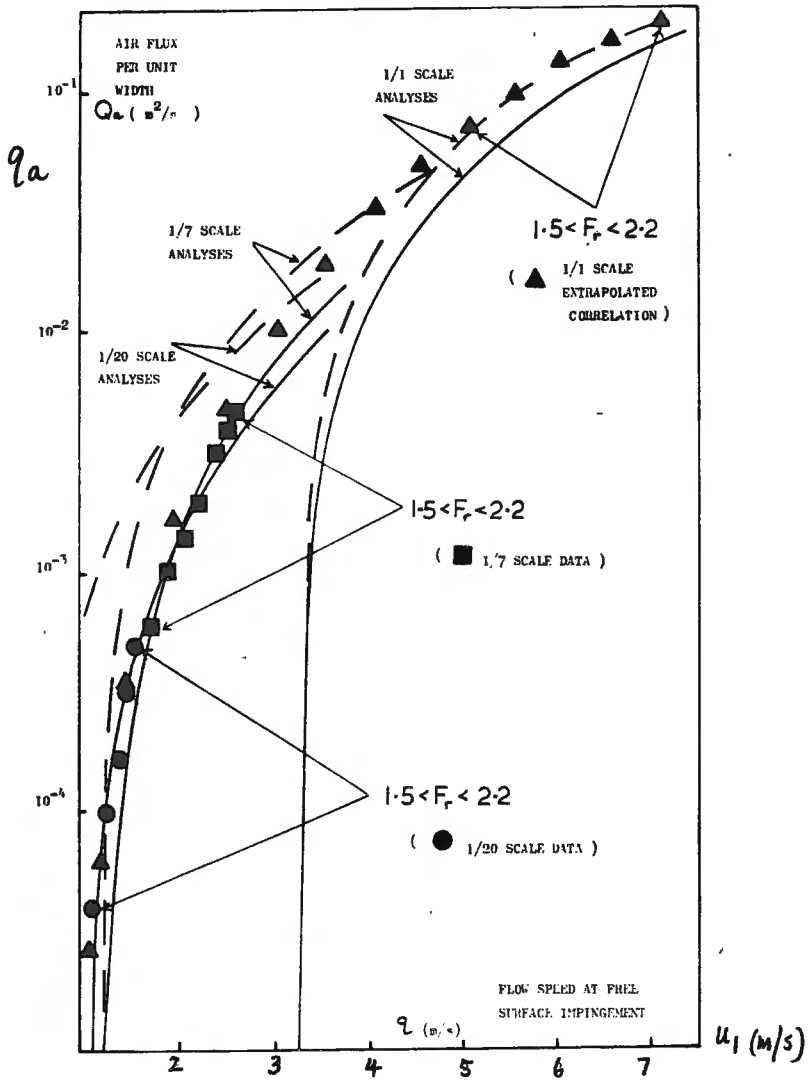

Figure 3.31

In his paper in 1982, Thomas compared data correlations from three separate siphon configurations

Renner $\beta_{an} \sim 0.00172 \rightarrow 0.00275\ Fr_1^2$ ..... (3.30)

Goldring $\beta_{an} \sim 0.0025\ Fr_1^2 \left(1 - u_1^*/u_1\right)^3$ ..... (3.31)

Castelyn + Kolkman $\beta_{an} \sim 0.005 \rightarrow 0.01\ Fr_1^2 \left(1 - 0.8/u_1\right)^3$ ..... (3.32)

in an attempt to obtain an explanation for the large ranges of K(.0017 → .01) obtained in the above correlations.

Thomas argued from photographic evidence and experiments at Cambridge, that two types of flow were possible, (1) when the shear layers penetrate into the flow and are almost plane as in the case of the Casteleyn et al siphons, and (2) where the shear layers are strongly curved and reattach either on the free surface or just a small distance along the conduit. This is generally accompanied by a thick layer of foam and is characteristic of the air-entraining siphon flow of Goldring. Goldring's siphon also exhibited curvature of the free surface impinging jet, which in turn contributed to the curvature of the shear layer and the reduced amount of air bubble transport compared with the Delft siphons. Thomas postulates that detrainment effects are comparable in Goldring's model compared with Casteleyn et al's model, but entrainment into the shear layer from the jet is greatly reduced in Goldring's model. This is still open to question.

Goldring investigated the priming performance of a siphon which constituted a component part of a cooling water outlet system for a power station, as shown on Figure 3.32. This work was reported both for model and prototype data in Reference , (1979) and Reference (1984), and Ref. (1980)

If we concentrate on Goldring's air entrainment work, he measured the rate of air transport through the siphon by indirect means using a step-by-step procedure based on the time taken for the siphon to prime and assuming hydraulic criticality at the siphon crest. That is, the air entrainment rate was assumed from one of the known formulae and checked against the actual rate of air removal from the air void in the siphon crown.

A correlation was attempted first with the model siphons using Equation (3.28) by Thomas. The best fit relationship was found to be,

$$\beta \sim 0,0066(Fr-1)\left[\left(1-\tfrac{1}{4}u_1\right)^2\Big/\left(1-\tfrac{1}{3}u_1\right)\right] \quad \ldots\ldots (3.33)$$

from which it is noted that the K value ($\simeq 0.0066$) is approximately one quarter of that used in the correlation of Casteleyn et al siphons. As already discussed, Thomas postulated the bi-model entrainment structure to explain this difference. Also Goldring used $U_{i\,min}$ of 1 m/s to commence air bubble transport which must be also open to question, as it coincides with the velocity required to entrain air into the shear layer. Thses are two separate criteria.

Goldring correlated model results with the empirical relationship developed by Casteleyn, Van Groen, and Kolkman, finding,

$$\beta \sim 0.0025\ Fr_1^2 \left(1 - 0.8/u_1\right)^3 \qquad \ldots\ldots (3.34)$$

Again the coefficient K ($\simeq$ 0.0025) is only one third to one quarter of Casteleyn et al. Again we have the assumption that air bubble transport occurs when $U_1 \simeq 0.8$ m/s which is open to question.

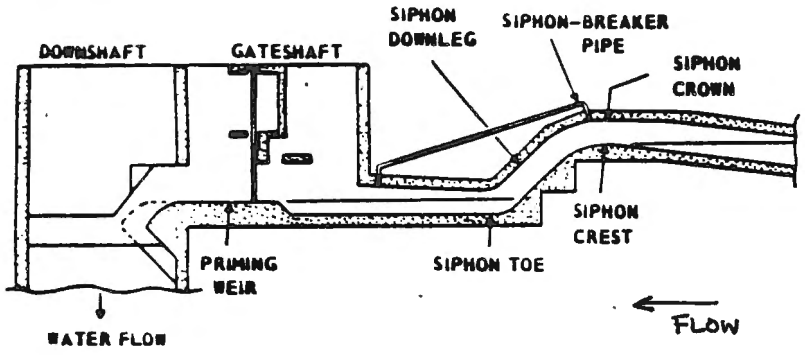

LONGITUDINAL SECTION THROUGH SIPHON SEAL WEIR
(GOLDRING)

Figure 3.32

Goldring in his 1984 paper (Ref) discussed prototype measurements of air entrainment in the siphon design which had been subject to the previous model tests. The surprising conclusion was that the Thomas equation which had proved satisfactory for model correlations, proved unsatisfactory in correlating prototype data. The value of K which had correlated as 0.0066 for model results, varied substantially in the prototype, 0.007 to 0.017, depending on D-d, (the conduit dimension less

the jet thickness). The non-correlation with prototype data was attributed by Goldring to the fact that Thomas's correlation can not be applied to Mode 2 flows (i.e. curved shear layer attaching on the opposite conduit wall) which leaves the obvious question as to why it proved satisfactory for scale models.

Goldring's model and prototype data obviously requires further analysis to find an explanation for this discrepancy. Perhaps the Thomas equation is more applicable not only in plane shear layers as opposed to curved, but also at lower water velocities in the shear layer where shearing vortices have a less coherent structure. This model data correlations with a small value of U_1 (jet velocity) (for Casteleyn et al this was < 2.5 m/s) may not translate into prototype velocities with more coherent vortex structures. (Sene, Ref)

Ervine and Ahmed (Ref and) carried out on an extensive series of air entrainment tests in a square conduit (0.14 m square) with the conduit angle ranging from 10° to the horizontal to vertical. Although this work is intended to be as applicable to dropshafts as siphons, a description of the work will be included below under siphons, and referred to (briefly) under dropshaft entrainment.

The purpose in testing such a wide range of conduit angles was to make the result applicable to dropshafts, siphons, hydraulic jumps in conduits, etc. The final result for air transport in closed conduits probably suffers from the fact that it attempts to include all types of entrainment and detrainment at all angles of conduit in a single expression.

A schematic diagram of the conduit is shown on Figure 3.33 with the experimental parameters appended. At each conduit angle, the total rate of air entrainment into the shear layer (q_{at}), and the net rate of air transport out of the shear layer downstream (q_{an}) were measured independently over a range of jet velocities up to 6 m/s and jet thickness up to 120 mm. All the results (from Section 2.3) could be said to be low velocity (i.e. < 10m/s). Working on the premise that entrainment due to jet surface undulationscales on U_1^3, and a minimum jet velocity of 0.8 m/s was required to entrain any air, a correlation for total air entrainment was attempted along the lines $q_{at} \propto (U_1 - 0.8)^3$. The constant of proportionality here proved not be a constant, but varied with the Froude Number $U_1/\sqrt{gd}$ and the conduit angle, as shown on Figure 3.34. This variation in K has many parallels with the variation in K found by

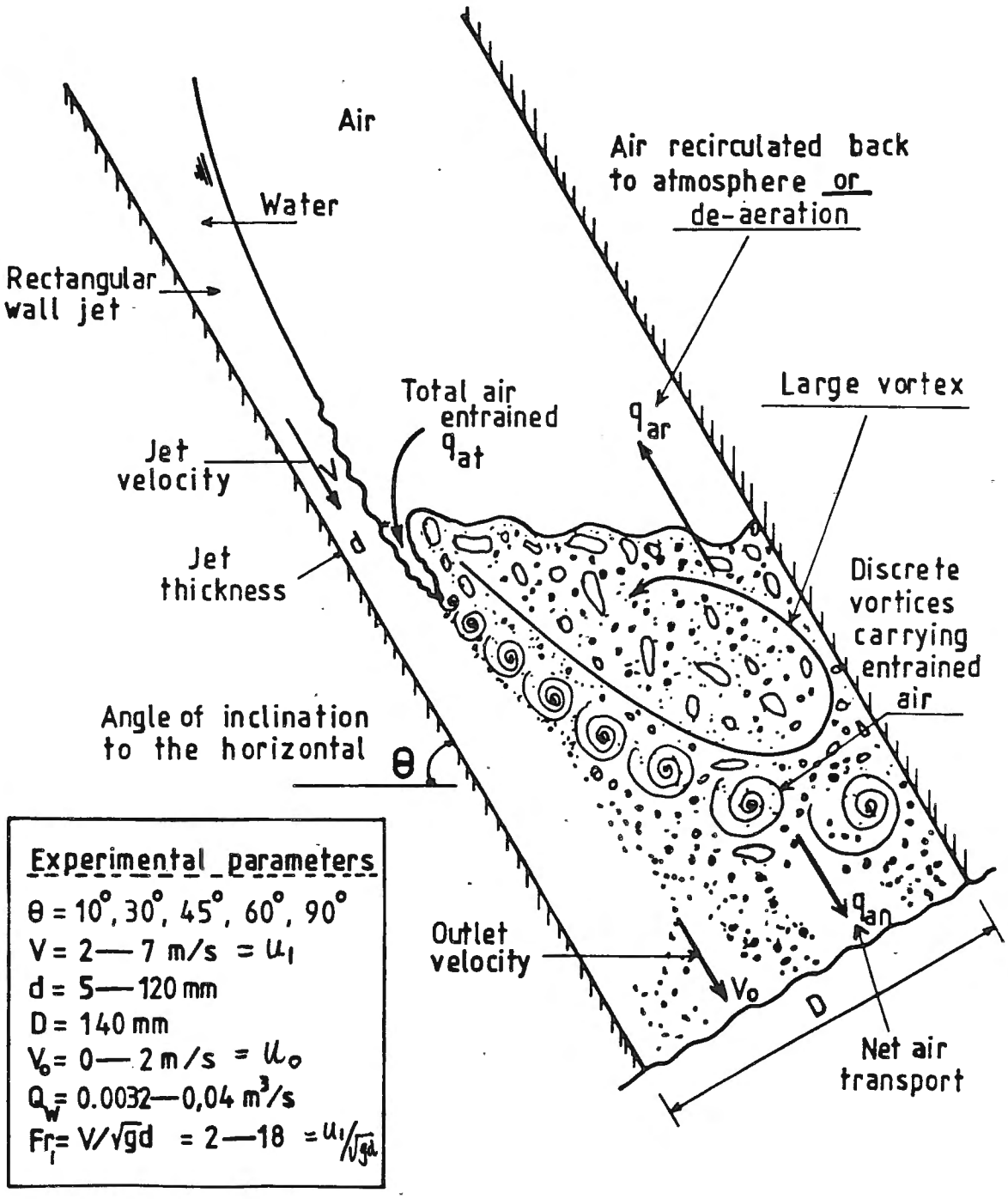

Fig. 3.33 Aeration by a supercritical jet in a closed conduit hydraulic structure.

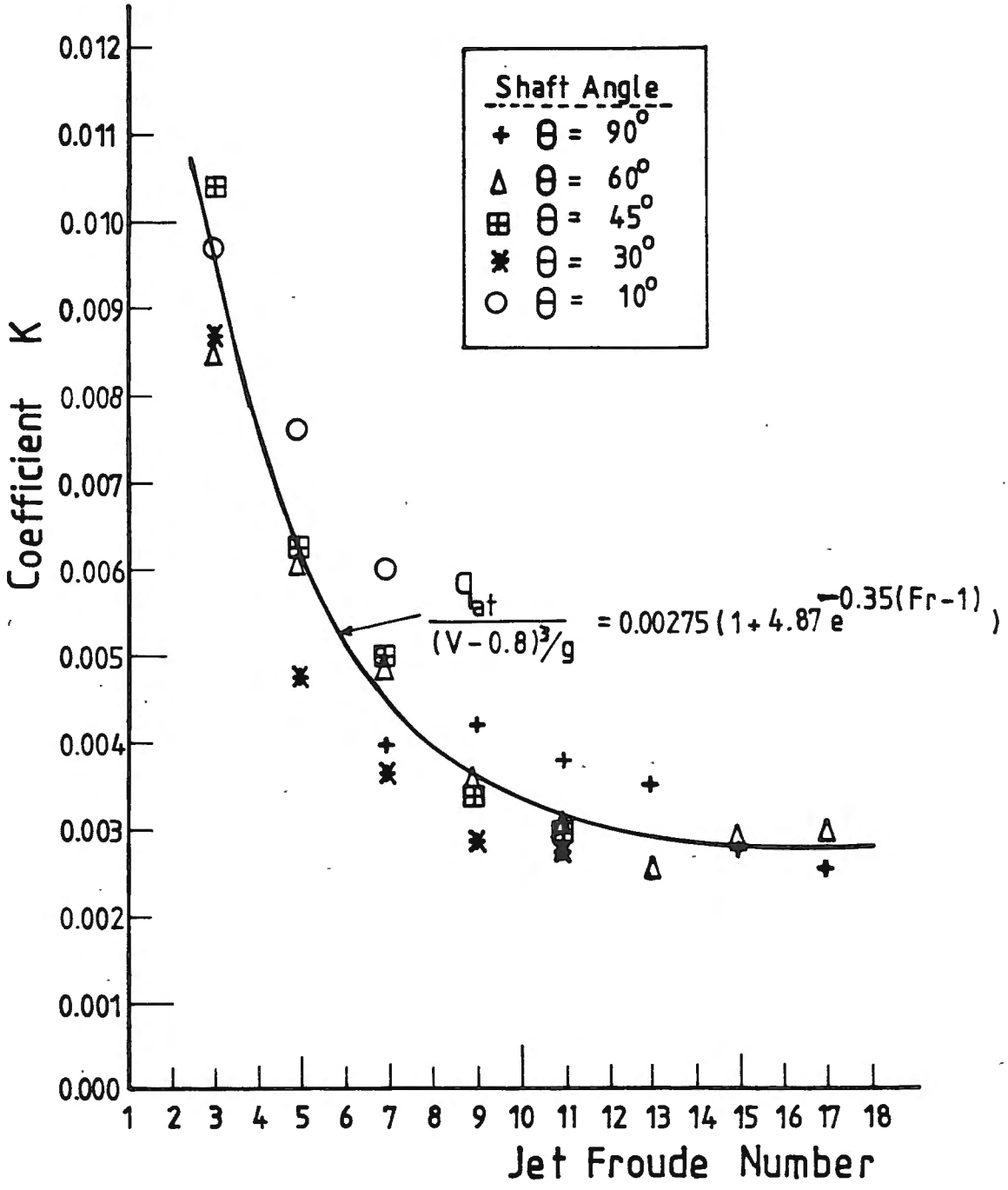

FIG. 3.34 Variation in K with Froude Number $U_1/\sqrt{gd}$ and angle θ (Ahmed + Ervine)

Goldring in his prototype data. Further more, the value of K found by Casteleyn et al for Froude Numbers around 2, was 0.01 which was very similar to the values on Figure 3.34. The value of K appears to be constant only for high Froude Number Flows ($Fr_1 > 10$).

The net air transport downstream out of the shear layer was plotted as a ratio of the net air transport to the total air entrainment (q_{an}/q_{at}) against a team incorporating the outlet velocity in the conduit, $(U_o - U_{o\ min})/U_{br}$. $U_{o\ min}$ is the conduit full outlet velocity required to commence air bubble transport and has been already described in Section 2.3. $(u_{o_{min}} = u_{l_{min}}\ d/D)$ The result for all conditions tested is shown on Figure 3.35, where it is clear that full transporting capacity of entrained air is effectively possible for $(u_o - u_{o_{min}})/u_{br} > 1$ That is, when the outlet velocity in the shaft exceeds the minimum outlet velocity to transport air by a value equal to the bubble rise velocity in still water, ≈ 0.25 m/s.

Ahmed and Ervine have thus proposed two separate scale factors for air transport, (1) a scale factor for entrainment into the shear layer $\left(1 - 0.8/u_1\right)^3$ and (2) a scale factor for transport out of the shear layer $f(u_o - u_{o_{min}}/u_{br})$ A final relationship was produced in the form

$$\beta_{an} = K\, Fr_1^2 \left[\left(1 - 0.8/u_1\right)^3 \left(1 - e^{-2(u_o - u_{o_{min}})/u_{br}}\right)\right] \quad \ldots\ldots (3.35)$$

where $K \approx 0.00235\left(1 + 4.87\, e^{-0.35(Fr_1 - 1)}\right)$

This complicated form is plotted on Figure 3.36 for a range of velocities U_1, but with the transport scale factor considered negligible. This relationship has proved reasonably accurate in correlating experimental data from Casteleyn et al siphons, as well as dropshaft data from Whillock and Thorn (see Ref).

It can be seen from Figure 3.36:-

(a) Air entrainment scale effects are small for jet velocity $U_1 > 5$ m/s.

(b) The upper limit for air entrainment is very similar to prototype data Campbell and Guyton, etc. $\beta_{an} \approx 0.04\ (Fr_1 - 1)^{0.85}$.

(c) Previous correlations based on $(Fr - 1)^n$, and Fr^2, generally cross velocity bands when the jet Froude Number is increased. This has resulted in spurious correlations as air entrainment is only partly governed by Froude scaling, and partly scales on the absolute velocities acting.

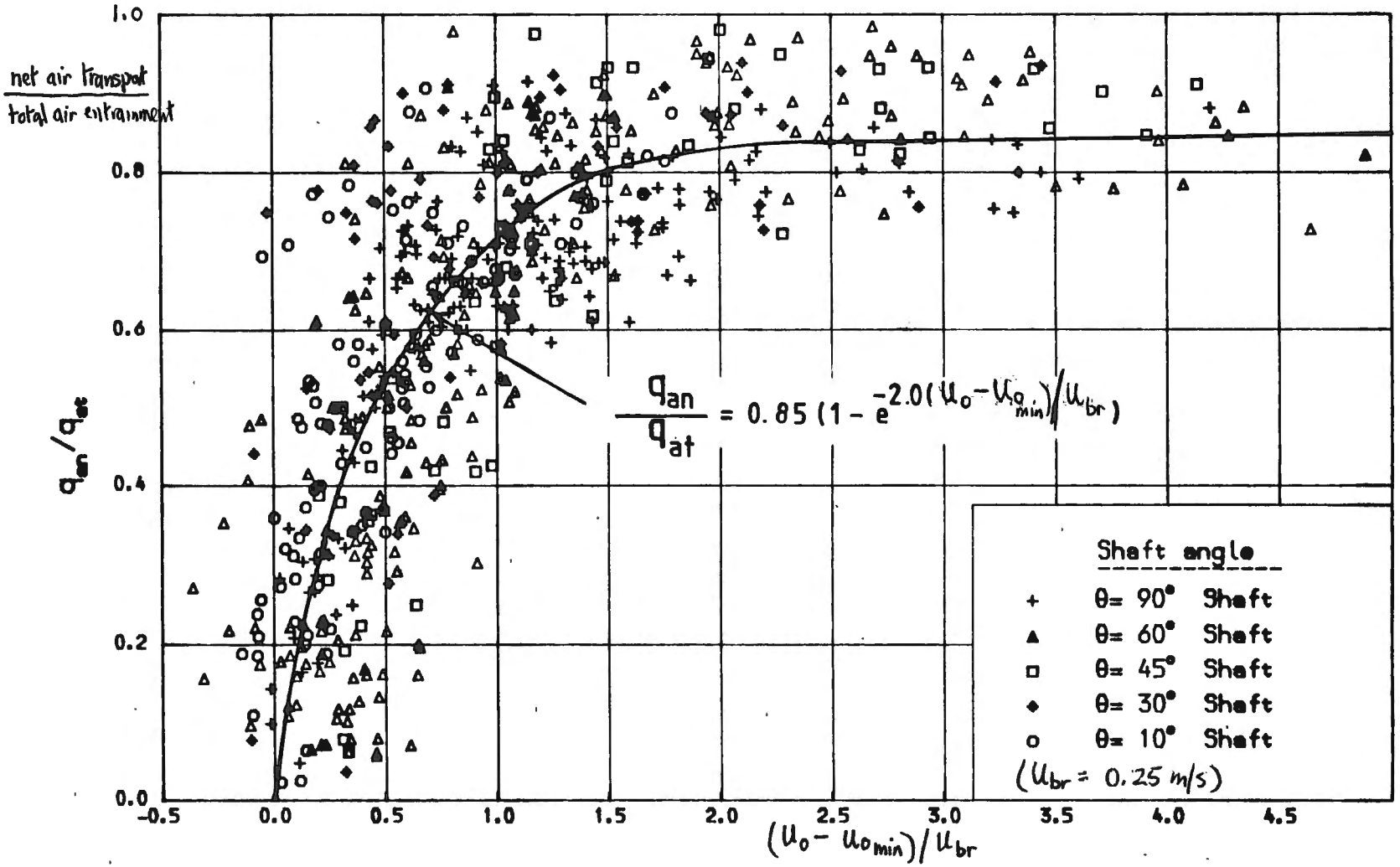

FIG 3.35 Air transport ratio against excess outlet velocity in conduit. (Ahmed + Ennine)

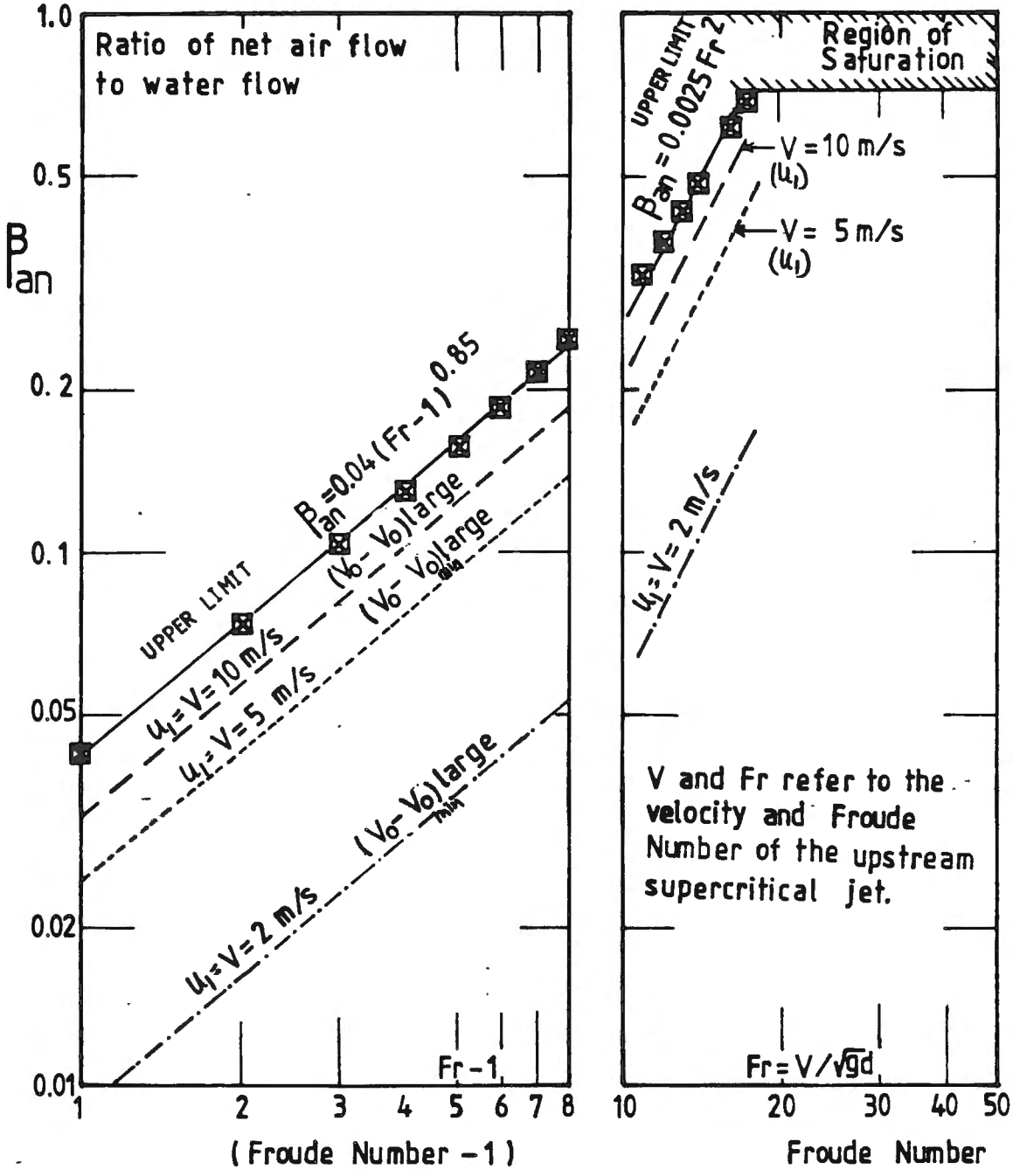

FIG 3.36 Plot of Equation (3.35) for a range of jet velocity $u_1 (= V)$ and $(u_o - u_{o_{min}})$ large (Ahmed + Ervine)

The behaviour of dropshaft with regard to air entrainment and transport

Dropshafts have generally been associated with the outlets of large dams where excess floodwaters are transferred from reservoir level via a circular vertical shaft to a horizontal conduit passing under the dam. Other applications include vertical flow structures in sewer systems, and more recently cooling water outlets of nuclear power stations have been included dropshafts (See Figure 3.37).

The air entraining characteristics of dropshafts are generally more complex than lower velocity, shorter length siphons. In fact their behaviour is also more complex than disintegrating jets plunging through the atmosphere. The reasons can be summarised as follows.

(1) During low flows, the hydraulic gradient in the outlet tunnel usually produces a low shaft-full level somewhere close to the shaft/tunnel junction. The annulus jet plunging down the dropshaft, may often produce high velocity entrainment at the plunge point.

(2) The plunging jet may also be partly disintegrated due to large plunge lengths, and pre-entrainment of the jet may have occurred, as in the case of free surface aeration.

(3) For low shaft-full levels the rate of air entrainment or air transport into the horizontal tunnel may be as high as the total entrainment rate at the plunge point. This is because the mixing region extends to the tunnel section.

(4) Air pockets may form at the tunnel/dropshaft junction at the conduit roof and 'blow-back', or at least cause instabilities and reduced discharge.

(5) For higher flows, the shaft-full condition is closer to the upper end of the dropshaft. the plunge length is less but all the problems mentioned above may still occur.

(6) Only when the shaft is completely submerged at the upper inlet will air entrainment problems cease. One method of overcoming some of the problems above has been the use of vortex inlets producing lower rates of air entrainment at the plunge point. This has met with partial success.

Before we consider some of the experimental and empirical correlations for dropshaft entrainment, perhaps we might consider some of the author's speculations for scaling of dropshaft entrainment. Like the case of siphons the process can be sub-divided into total entrainment into the

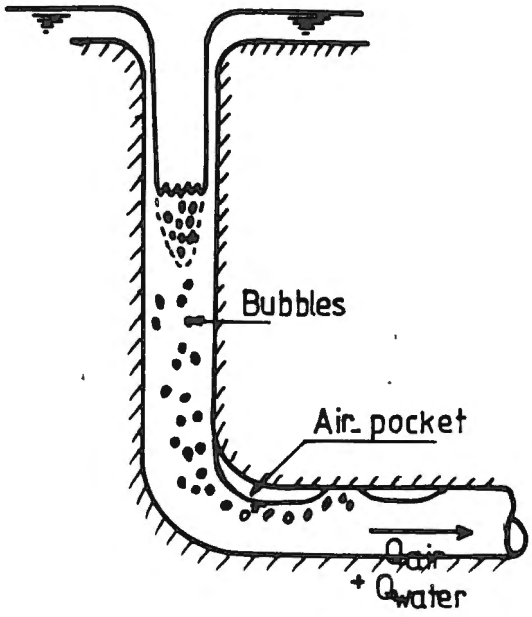

a- Typical dropshaft.

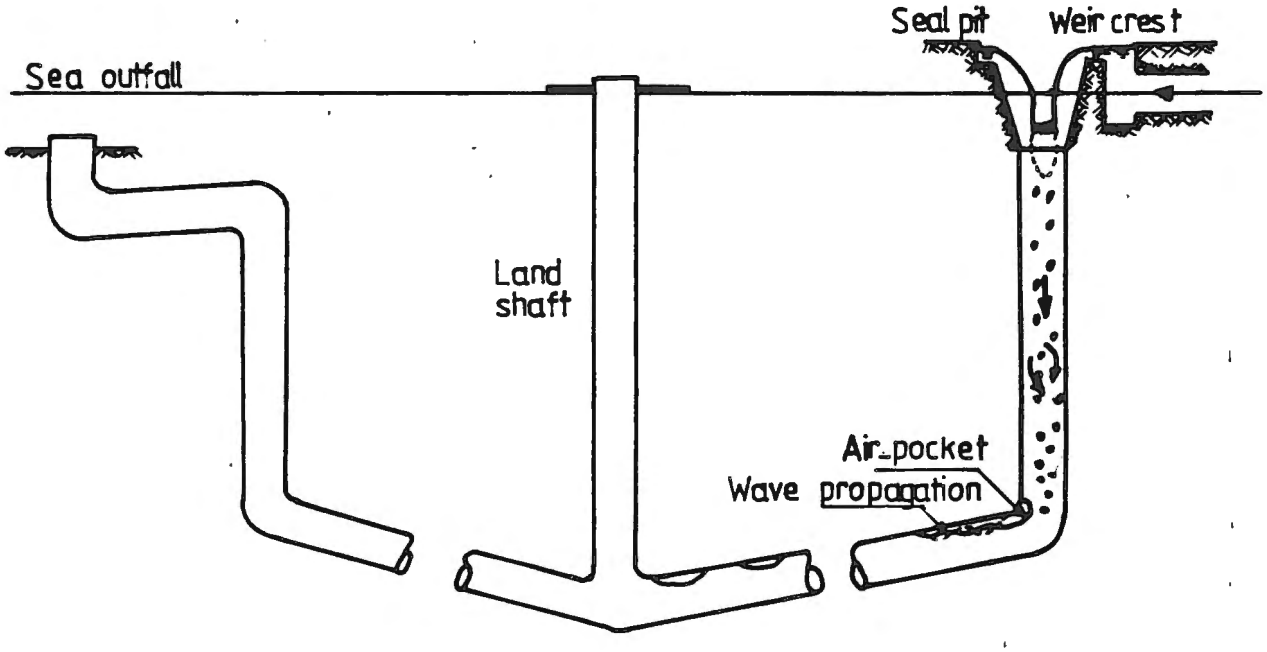

b-Cooling water outfall system for a Power Station. (Townson)

FIG 3.37. Typical dropshaft arrangements

shear layer, bubble detrainment and bubble transport downstream of the shear layer along the shaft.

(a) Total entrainment into the shear layer.

Consider a circular annular jet plunging down the drop shaft and impinging on the shaft full condition as shown on the sketch below.

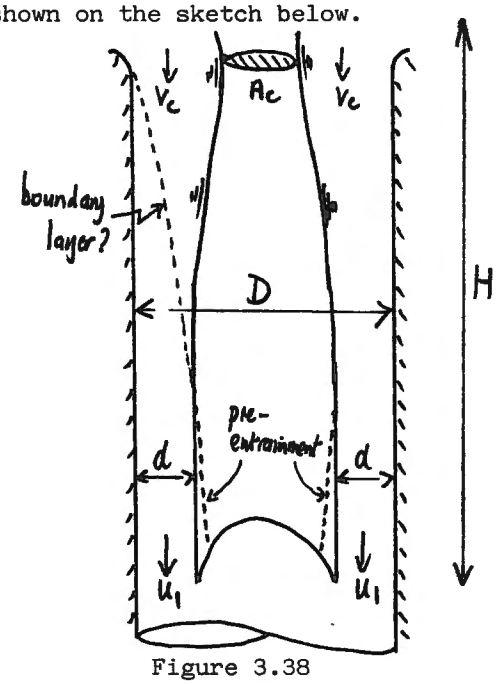

Figure 3.38

As in Section 2.2 we need to consider the rate of air entrainment per unit surface area. In this case the surface length entraining air is given by,

$$\pi (D - 2d)$$

where D is the conduit diameter and d the jet thickness.

Thus $q_a = Q_a / \pi D(1 - \frac{2d}{D})$

The value of q_a will depend primarily on the jet velocity at the plunge point. For low velocity jets $q_a \propto U_1^3$ and for high velocity jets $q_a \propto U^{3/2}$??

(excluding pre-entrainment)

Let us consider first, the likely effect of testing a series of scale models at increasing scale for a given value of H/D, the droplength over the conduit diameter. The likely variation in q_a with jet impact velocity is shown in the sketch below.

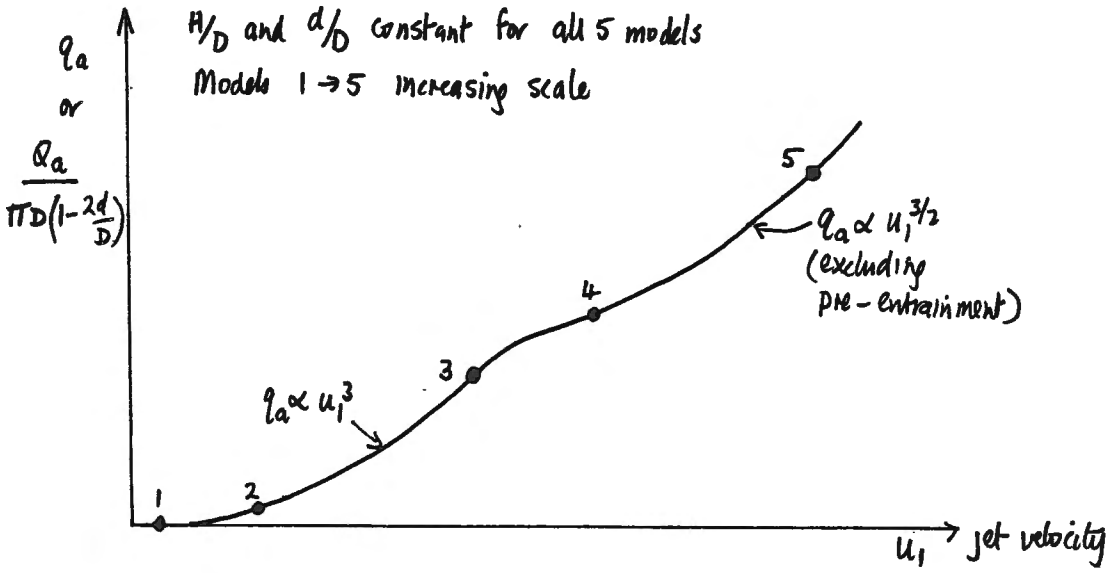

Figure 3.39

Consider five models with increasing scale (1 → 5), and hence increasing U_1 at a constant value of H/D.

Model 1 is extremely small and is entraining no air because the inception velocity to entrain air has not yet been reached $U_1 < 1$ m/s. This model will give $\beta_{at} = 0$, which is an underestimate of prototype entrainment!

Model 2 is larger than model 1, but may still give a low rate of air entrainment into the flow, as the jet velocity at impact U_1 is only slightly larger than U_1*, the inception velocity. If we attempted to correlate β_{at} on Fr^2, for model 2, and underestimate of β_{at} for the prototype may still be obtained.

Model 3 is considered to be operating close the the upper limit for low velocity jets where entrainment is due to surface undulations. In this region $q_a \simeq kU_1^3$ or $\beta \propto Fr^2$. The value of β_{at} obtained from model scale 3 is usually larger than the value of β_{at} obtained from models 1 and 2. At point 3, approximately the same value of β_{at} would be obtained for all model scales if, $q_a \propto U_1^3$ remained the case for increasing jet velocities beyond this point. This in fact may not be the case.

Models 4 and 5 may have now entered a new regime of air entrainment where ultimately $q_a \propto U_1^{3/2}$ for very high jet velocities? Thus it would be possible to obtain, in terms of the model scale ratio $L_r = L_{proto}/L_{model}$,

$$q_a = k U_1^{3/2} \text{ or } \beta = \frac{k U_1^{1/2}}{d} \propto \frac{L_r^{1/4}}{L_r} = \frac{1}{L_r^{0.75}}$$

That is, for models tested in the high velocity range only, the value of air/water ratio β_{at} may <u>decrease</u> with increasing model scale for a constant H/D and d/D. Thus, it is quite possible for model (scale) 3 to overestimate prototype total entrainment, and great care must be placed in correlating low and high velocity dropshaft entrainment data. It will be seen later in this section that larger scale dropshaft models often produce smaller air/water ratios than smaller dropshaft models, especially if pre-entrainment is not evident in any of the models.

A further problem in correlating total air entrainment data for dropshaft models, is the effect of increasing water discharge in a given model. There are two main effects (1) the droplength H decreases, hence does the jet velocity at impact U_1, and hence the rate of entrainment per unit surface length decreases, (2) the value of jet thickness increases, hence $(D - 2d)\pi$ decreases, (the surface length available for

entrainment), hence the total volume of air entrained (Q_{at}) also decreases. Thus an increase in water discharge will invariably produce a decrease in total air entrainment rate. This argument of course will not hold for small jet thickness at the impact point, say d < 10 mm, where the jet thickness itself will influence surface disturbance growth, eddy lengths and also air entrainment rate. That is, for jet thickness d < 20 mm, the rate of air entrainment may well increase with jet thickness, etc.

A further phenomenon of circular dropshafts at increasing water discharges is illustrated in Figure 3.38. The diameter of air core at top of the shaft may become too small to cope with the quantity of air being entrained at the plunge point. The plunging jet, if it remains attached to the dropshaft walls will also continue to accelerate under gravity until it reaches a terminal velocity, comparable to normal depth in open channel flows. Thereafter the jet might increase in thickness due to pre-entrainment if surface tension is overcome by turbulent fluctuations. The shape of the air core is now similar to a Venturi. If the air core becomes small, and the total air demand cannot be satisfied, then a sub-atmospheric air pressure will exist in the air core and accelerate air through the core from the atmosphere. In this case $Q_a > A_c V_c$, the air flow is greater than the area of the core times the water velocity at that point. For the case of an annular hydraulic jump occurring at the plunge point, the quantity of air passing the core will be required to satisfy only the net air transport (which is typically $\beta_{an} \simeq 0.1$ to 0.5), with a large proportion of the total air entrained, detraining and recirculating in the air core back to the plunge point.

(b) Dropshaft bubble detrainment and transport.

The total entrainment into an annular hydraulic jump will depend primarily on the jet velocity at the plunge U_1, and the turbulence intensity (U^*/U_1), Reynolds Number and jet thickness (for d < 20 mm and Re < 10^5) At long droplengths and smaller values of d/D, the ratio of air to water (β_{at}) often exceeds one and in some cases is as high as 2 or 3. (This is comparable to plunging jet entrainment). Clearly, the shaft-full flow downstream of the plunge point is incapable of transporting this ratio of air to water. Wallis (Ref) indicates that the maximum void ratio (α) for bubbly flows is around 0.42, which gives an upper limit of β_{an} for vertical bubbly flow of 0.72. Even this value is uncommon in vertical downward flows. Typical upper limits of downward bubbly flows appear to be around 0.4 to 0.5 for β_{an}. Thus, a large

proportion of entrained air must be immediately detrained. This is sketched below indicating a possible increase in air transport when the mixing region reaches the conduit exit.

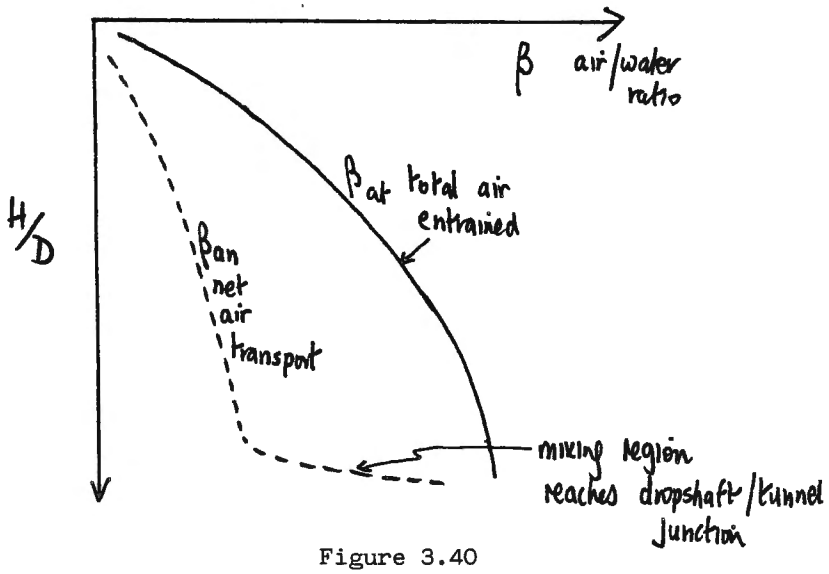

Figure 3.40

This type of detrainment cannot be prodicted by analyses such as Thomas (Ref), as bubble buoyancy terms $U_{br}\cos\theta$ and $U_{br}\sin\theta$ are negligible compared with velocities in the shear layer. It is much more informative to compare bubble rise velocities with the shaft full velocity U_{br}/U_o. We might assume for instance that the real bubble downward velocity in the shaft full condition is approximately $U_o - U_{br}$ (where U_{br} ≃ 0.2 to 0.3 m/s), in which case, as the air concentration (α) increases towards 0.42, there will be an increasing tendency towards bubble coalescence; air pockets may form and blow back to the free surface due to increased buoyancy. This type of air pocket formation and blow back is likely until the downward Froude Number of the flow $U_o/\sqrt{gD}$ exceeds 0.4 to 0.5, beyond which, even air pockets may be transported with the flow.

To the author's knowledge, no satisfactory entrainment or detrainment analysis exists for dropshafts. Recourse must be made therefore to experimental/empirical correlations.

Viparelli (Ref) presented a correlation for net air transport in vertical dropshafts in the form,

$$\beta_{an} \simeq 0.022 \left(h/D\right)^{0.6} \qquad \ldots\ldots (3.36)$$

where h is the height of fall of the plunging wall jet and D the conduit diameter.

This is a crude correlation on two counts:

(1) β_{an} increases ad infinitum for large $^{h}/D$ values.

(2) The relationship is essentially a Froude scaled phenomenon for air entrainment which might only be true for high velocities, turbulence level, $Re > 10^5$, $d > 20$ mm etc. etc. Even at high velocity there is a suspicion ($q_a \propto U_1^{3/2}$) that Froude scaling is not necessarily applicable for β_{an}. After the point of jet impingement air bubbles do not travel at the same speed as the water, and hence it is difficult to see how Froude scaling might apply in comparing model + prototype. However the correlation may provide rough estimates of entrainment rate. Wijeyesekera (1969) (Ref) carried out a series of experiments on a dropshaft at five different scales, measuring both total entrainment and net air transport downstream of the annular hydraulic jump. This result is shown on Figure 3.41 revealing that values of β_{at} for total entrainment are often as high as 1 to 2, but decrease with increasing water discharge (or $^{d}/D$). The net air transport downstream of the plunge point did not exceed 0.4 for β_{an} in any of the dropshafts, and conformed closely to the correlation presented by Viparelli. By implication, large amounts of air are detrained, with an exception possibly at small values of $^{H}/D$ when β_{at} is of the same order as β_{an}.

The Hydraulics Research Station, Wallingford, U.K. (Ref) carried out an investigation into the net air transport in a vertical dropshaft for Plover Cove, Hong Kong. Three models were tested at scales 1:10, 1:20 and 1:30, with the results plotted as β_{an} against $^{H}/D$ shown on Figure 3.42. An attempted extrapolation to prototype conditions is also shown. The most interesting feature of this correlation is decreasing air/water ratio with increasing model scale. The curves shown represent the upper limit of air transport in each model and therefore correspond to a high outlet water velocity where the slip velocity of air bubbles is not significant. Why then is there a scale effect in the entrainment rate? In order to find the answer, a complete analysis of the plunging jet profile would be required to be carried out for each model scale after the fashion of Dawson and Kalinske (Ref). The jet velocity U_1 and the jet surface length available for entrainment $\pi(D - 2d)$ could then be calculated for each plunge length. A graph of q_a or $Q_a/\pi D\left(1-\frac{2d}{D}\right)$ against U_1 could then be plotted for each dropshaft model. As a first order of magnitude however, if the dropshaft wall roughness is modelled correctly, the jet velocity at impact (U_1) should scale on a Froude basis ($L_r^{1/2}$) and hence U_1 for 1/10 model will be higher than the $^{1}/10$ and $^{1}/30$ models, and if β_{at} scales on Fr_1^2 or $(Fr - 1)$ then the same air/water ratio will be obtained for all 3 scale models. If on

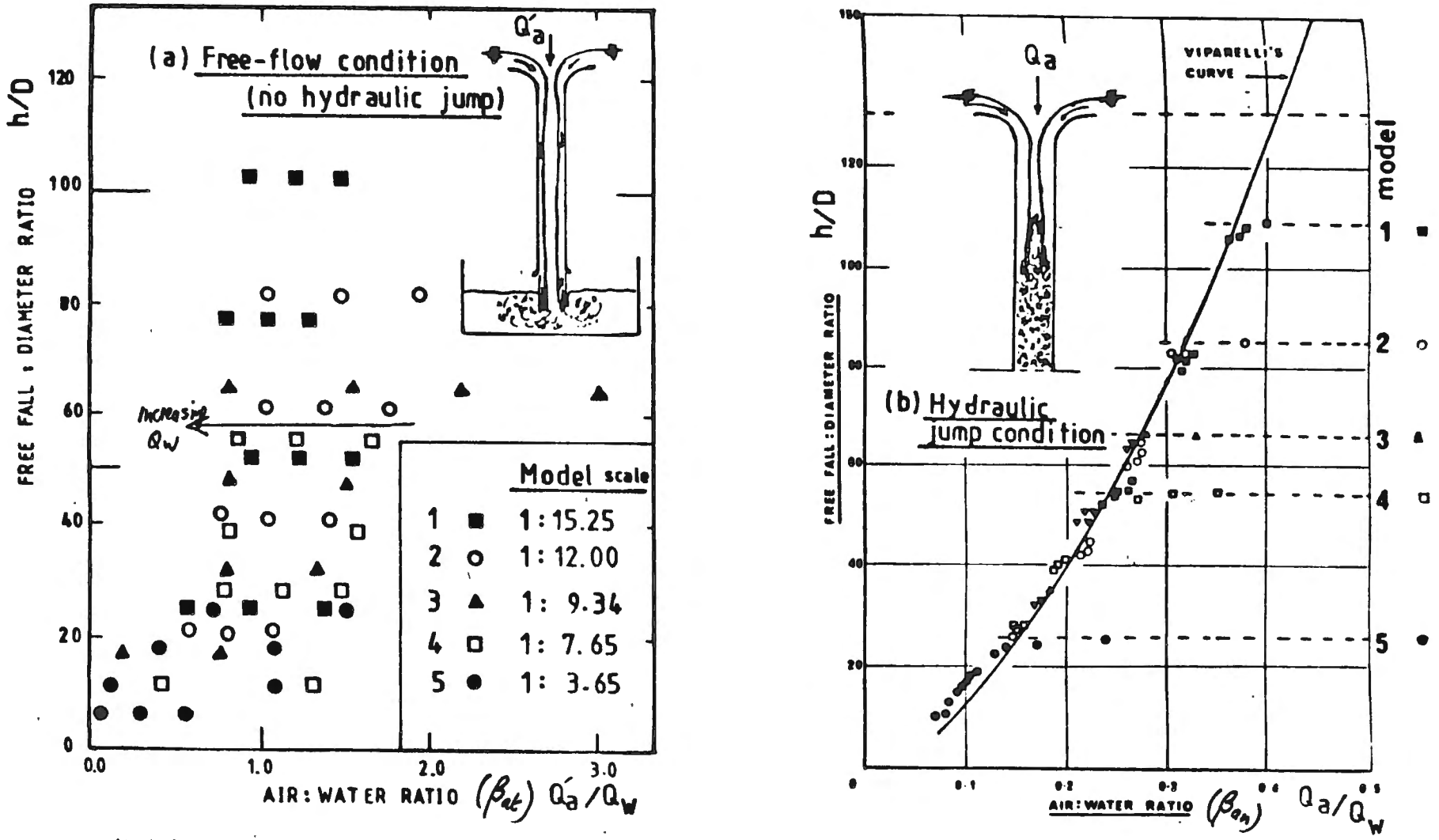

Fig(3.41) Experimental results for five different shaft model scales under two conditions: (a)Free-flow codition (b) Annular hydraulic jump condition, (Wijeyesekera, 1969)

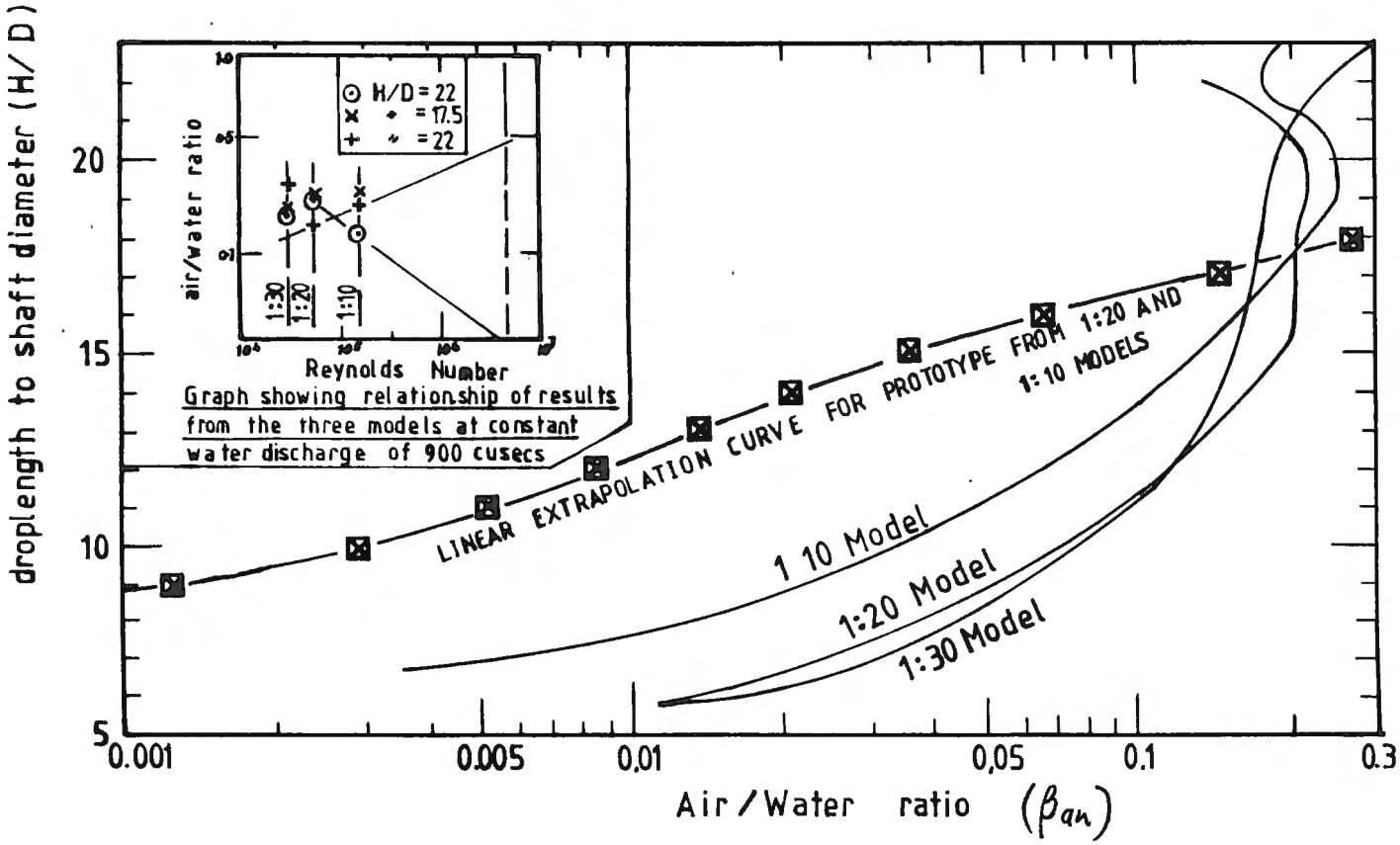

Fig (3.42) Comparition of results from three models at a constant water discharge together with a prediction of performance at full scale.

(HYDRAULICS RESEARCH STATION, U.K. — PLOVER COVE)

the other hand, the higher velocities in the $^1/10$ model produce a different regime of air entrainment (say $q_a \propto u_1^{3/2}$) whilst the $^1/20$ and $^1/30$ models scale on $\beta_{at} \propto Fr_1^2$ then the result shown on Figure 3.42 might result.

A simpler explanation based on wall surface roughness might be employed. Assuming that each model was constructed in the same material (say perspex), then wall roughness will be underestimated in the larger model. That is for Froude models, Mannings 'n' scales on $L_r^{1/6}$, which in comparing the $^1/30$ to $^1/10$ models should give $n_{(1/10)}/n_{(1/30)} \simeq 1.2$ or the model material should have a Mannings 'n' value 20% higher than the $^1/30$ model. If this is not the case, the $^1/10$ model will effectively overestimate the droplength required to reach terminal velocity and will overestimate terminal velocity.

Therefore the larger model, if it is too smooth, may overestimate jet thickness and underestimate velocity during the gradually varying section of its flow profile, even though the terminal velocity is higher in the smoother model. This is hardly likely to account for such a wide discrepancy in air/water ratios?

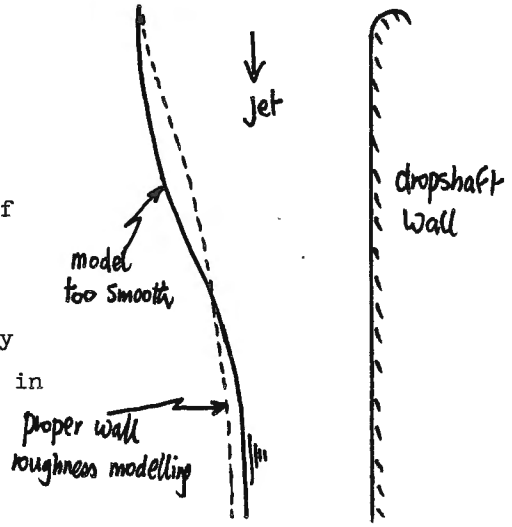

Whillock and Thorn (1973, Ref) carried out a more fundamental study of dropshaft air entrainment, using square dropshafts (to reduce the number of variables) at sizes ranging from .15 m square x 1.94 m long, to 0.3 m square x 3.88 m long. The net air transport was measured in each case, with a sketch of the apparatus shown on Figure 3.43 (a). The jet thickness can be controlled independently of the jet velocity, providing a more comprehensive range of data. Results for the .15 x .15 x 3.78 m long shaft are shown on Figure 3.43 (b) and the 0.3 x 0.3 x 3.88 m long shaft on Figure 3.43 (c), with the data plotted as the air/water ratio β_{an} against droplength H. The first point of interest is the increase in net air transport with water discharge (or outlet velocity U_o) until a limiting condition is reached where no further air transport is achieved. This can be seen by taking a horizontal line across at any given droplength H. The limiting condition for air transport corresponded to an outlet shaft-full velocity of $\simeq$ 0.5 m/s. Whillock and Thorn showed that the minimum outlet velocity

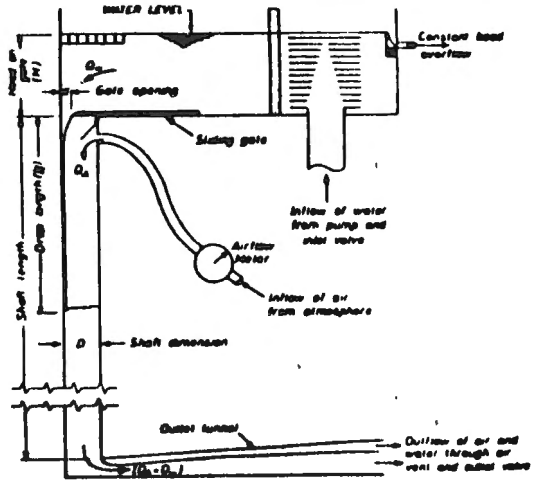

(a) SCHEMATIC LAYOUT OF VERTICAL PLUNGE MODEL

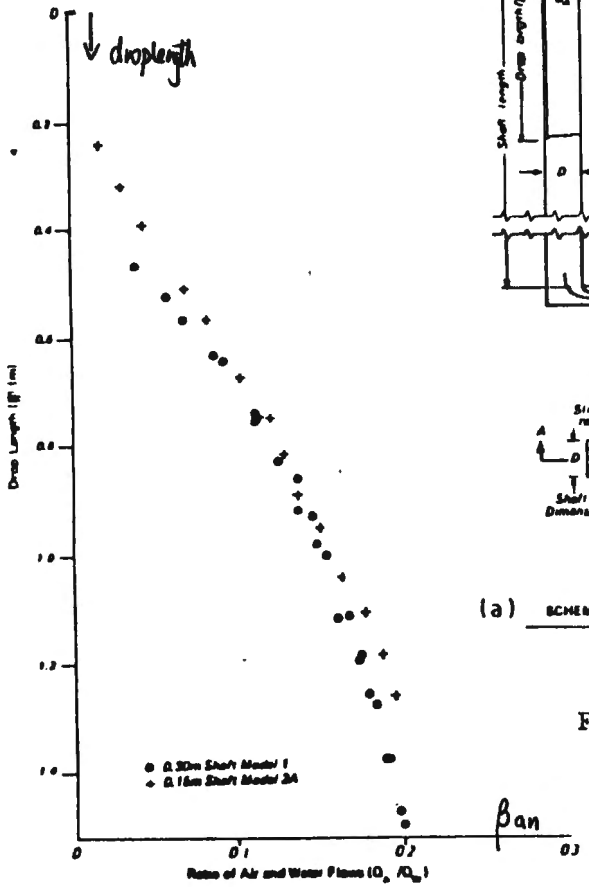

(d) COMPARISON OF DATA FROM LIMITING AIR DEMAND CURVES

Fig(3.43) Two-dimensional Dropshaft experimental results, (according to Whillock and Thorn, 1973)

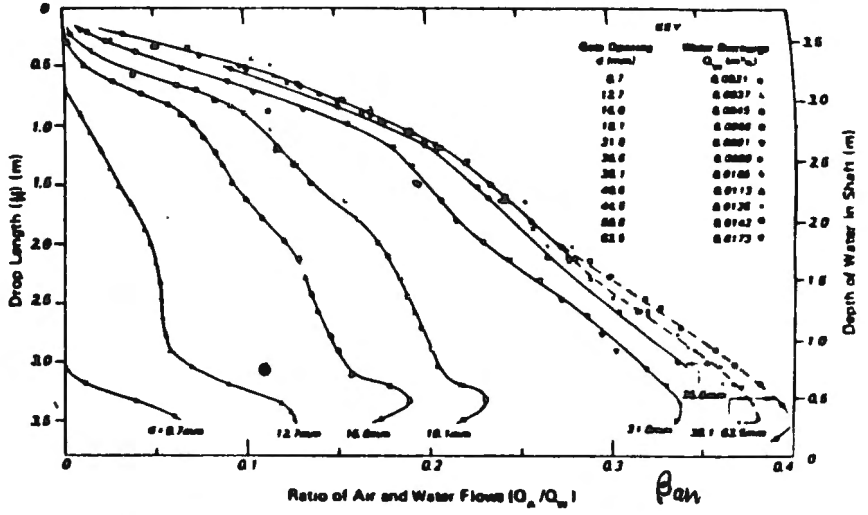

(b) AIR DEMAND CHARACTERISTICS (FOR SHAFT 0.15m SQUARE BY 3.78m DEEP)

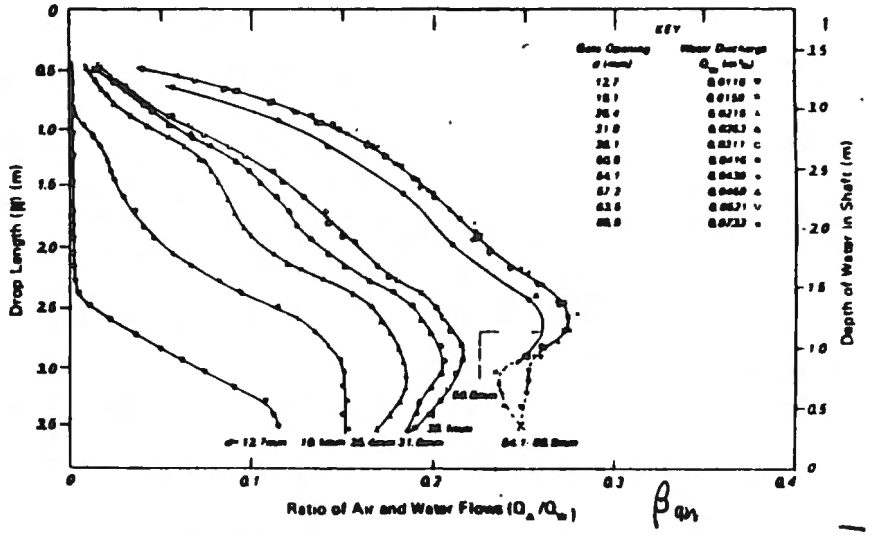

(c) AIR DEMAND CHARACTERISTICS (FOR SHAFT 0.30m SQUARE BY 3.88m DEEP)

to transport any air was approximately 0.15 m/s, hence maximum transport capacity is achieved at

$$\frac{U_o - U_{o\,min}}{U_{br}} \simeq \frac{0.5 - 0.15}{0.25} = 1.4$$

If we now compare this with the result of Ervine and Ahmed on Figure 3.35 we obtain excellent correspondence, as full transport is achieved at ≈ 1.5.

The other point of interest is the comparison of air/water ratios for the two models (b) and (c). The larger model appears to give lower values of β; this is misleading. Ervine and Kolkman (Ref) and Ahmed and Ervine (Ref) have calculated the water surface profiles for each of Whillock and Thorns dropshafts, revealing that the jet Froude Number at a given value of H is often lower in the larger model than the smaller one. Hence if $q_a \propto U_i^3$, for jet surface entrainment, then $\beta \propto Fr^2$, then the larger model may seem to give lower entrainment.

The data of Whillock and Thorn was compared for all three models against the relationship developed by Ahmed and Ervine

$$\beta_{an} = K\,Fr_1^2\left[\left(1-\frac{0.8}{U_1}\right)^3\left(1-e^{-2(U_o-U_{o\,min})/U_{br}}\right)\right] \quad \ldots\ldots (3.37)$$

where $U_{o\,min}$ was taken around 0.15 m/s as suggested by Whillock and Thorn. The result for all three scale models is shown on Figure 3.44, giving good correspondence at each model scale. It is possible that a comparable correlation could be achieved using the Thomas equation possibly in the form,

$$\beta_{an} = K\,Fr_1^2\left[\left(1-\frac{U_{1\,min}}{U_1}\right)^2 \Big/ \left(1-\frac{U_{1\,min}}{3U_1}\right)\right] \quad \ldots\ldots (3.38)$$

where the value of U_{min} could be estimated as $U_{o\,min}{}^{D/d} \simeq 0.15^{D/d}$. The value of K in the Ervine and Ahmed equation varies with Froude Number but is generally 0.003 - 0.004 for this set of data. This is in close correspondence with the estimates of Sene (Ref).

If it not possible to include all the vast range of literature on air entrainment in vertical shafts. The reader is referred to the review by Falvey (Ref) Whillock and Thorn (Ref) and the review by Haindl (Ref) for more detailed information. Of particular interest is the work of Hack (Ref) in predicting dropshaft air flow ratio when the outlet is not pressurised and free flow exists, the work of Haindl (Ref) predicting the rate of air transport downstream on an annular hydraulic jump $\beta_{an} = 0.02(Fr_1 - 1)^{0.86}$, and the work of Curtet and Djonin (Ref) in

predicting the length of a deaeration zone (L) downstream of a plunge point $\frac{U_o(1+\beta)}{\sqrt{gL}} \simeq 0.06$ for small values of bubble slip velocity (< 0.2m/s).

There is considerable scope for reanalysis of past dropshaft air entrainment data. More attention requires to be given to the following points:-

(a) The plunging jet condition, its profile calculation, (d and U_1), its boundary layer thickness (δ^*/d) for estimation of pre-entrainment. Its turbulence level (U^*/U_1), Reynolds, Froude and Weber Number at the jet at impact.

(b) Plotting is required for the rate of entrainment per surface length q_a, (or $Q_a/\pi D(1-2d/D)$ for an annular jet) against the jet velocity U_1, to determine if $q_a \propto U_1^3$, ($\beta \propto Fr^2$) or if the jet has reached high velocity entrainment region $q_a \propto U_1^{3/2}$? Care must be exercised in extrapolating not only from low velocity tests, but also from small jet thicknesses d < 20 mm, when for higher jet thickness q_a is independent of jet thickness.

(c) Attention is also required to detrainment and transport characteristics, with the model operating as far as possible with the outlet velocity as close to the prototype outlet velocities as possible, or at least U_o(model) $\geq$ 0.5 m/s. This ensures that the effect of bubble slip velocity is negligible.

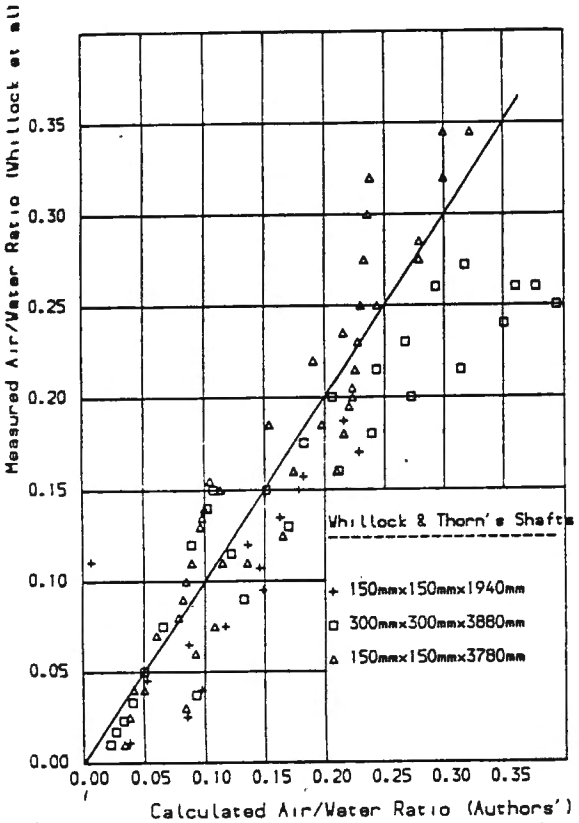

FIG. 3.44 Correlation with Whillock and Thorn's results

Section 3.3 Hydraulic jump entrainment and transport

This section, which may prove to be somewhat speculative in nature, will concentrate on air entrainment and transport by hydraulic jumps in closed conduits when the conduit slope, is horizontal, or in the upward or downward direction, and the conduit is filled by the downstream depth of the jump. Even a cursory review of previous data correlations will reveal a standard correlation

$$\beta_{an} = K (Fr_1 - 1)^n \quad \ldots\ldots (3.39)$$

where n seems to vary anywhere between 0.85 and 1.4

Fr_1 the upstream Froude Number $\left(u_1/\sqrt{gd} \text{ or } u_1/\sqrt{gA_1/B_1} \right)$

and K varies from 0.0066 to 0.04.

Equation (3.39) appears to be satisfactory:-

- for a wide range of conduit angle.
- for all almost all conditions of the upstream supercritical flow, velocity U_1, turbulence intensity (U^*/u_1), pre-entrainment, Reynolds Number, etc.
- bubble detrainment appears to have no significance (or it scales on the jet Froude Number) in the reattaching mixing region of the jump.
- bubble transport capacity downstream of the jump also appears to scale on the jet Froude Number.
- the inception condition for air bubble transport appears to be a supercritical jet ($Fr_1 > 1$).

Let us consider some of these points in more detail.

(1) The conduit angle

It is the author's opinion that this is one of the most sensitive parameters governing the amount of air transport along a conduit downstream of a hydraulic jump. Assuming for the time being that air entrainment into a jump is correlated at β and Fr - 1 as suggested, then let us look at the transport capacity of the flowing mixture downstream of the jump.

(a) For an upward sloping conduit angle, entrained air is easily transported (due to buoyancy) and a (Fr - 1) correlation may be possible.

(b) For a horizontal conduit ($\theta = 0$), air is again easily transported downstream in the absence of buoyancy effects.

(c) For a downward sloping conduit, $\theta < 20°$, a completely different regime of behaviour occurs in long conduits. Air is initially transported downstream of the jump in the form of air bubbles which soon rise to the conduit roof forming air pockets (or slugs). We will see in Section 4 that once an air pocket forms, a certain conduit-full Froude Number is

required to transport the pocket along the conduit, otherwise the pocket simply grows in size and will eventually blow back. This limiting Froude Number to clear air pockets depends not only on the conduit slope θ, but also the air pocket depth H/D. (See Figure 4.22). As an order of magnitude we will assume that even for small downward sloping angles (say 1°), the required Froude Number $V_o/\sqrt{gD}$ is in the region of 0.5 to 0.7 as shown on Figure 4.22 or 5.6. Thus, air transport will not commence until this Froude Number downstream of the jump is reached. For initiation of air transport for downward sloping pipes $\theta > 0°$ we may write

$$U_o/\sqrt{gD} \simeq 0.6 \quad \text{where } U_o A_p = U_1 A_1 \qquad \ldots\ldots (3.40)$$

U_1 and A_1 are upstream velocity and Area of flow

Ap is the full pipe area $\pi D^2/4$.

The upstream Froude Number may now be calculated to achieve this condition, (for various values of d/D, fractional depth)

Taking the case of a circular pipe, we obtain from (3.40)

$$U_1/\sqrt{gA_1/B} \simeq 0.6 \left(A_p/A_1\right)^{3/2} \sqrt{\frac{4 \sin a}{\pi}} \qquad \ldots\ldots (3.41)$$

where the upstream Froude Number is calculated on the basis of a flow depth, equal to the area of flow divided by the surface width.

The angle 'a' is specified on the sketch opposite.

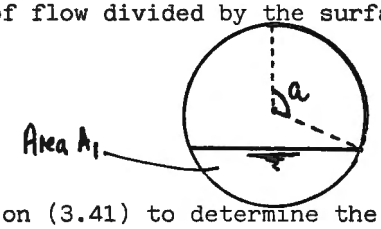

The author has used Equation (3.41) to determine the upstream Froude Number required to transport air, and compared the result with the data of Kalinske and Robertson (Ref). The result is shown on Figure 3.45 giving a good correspondence.

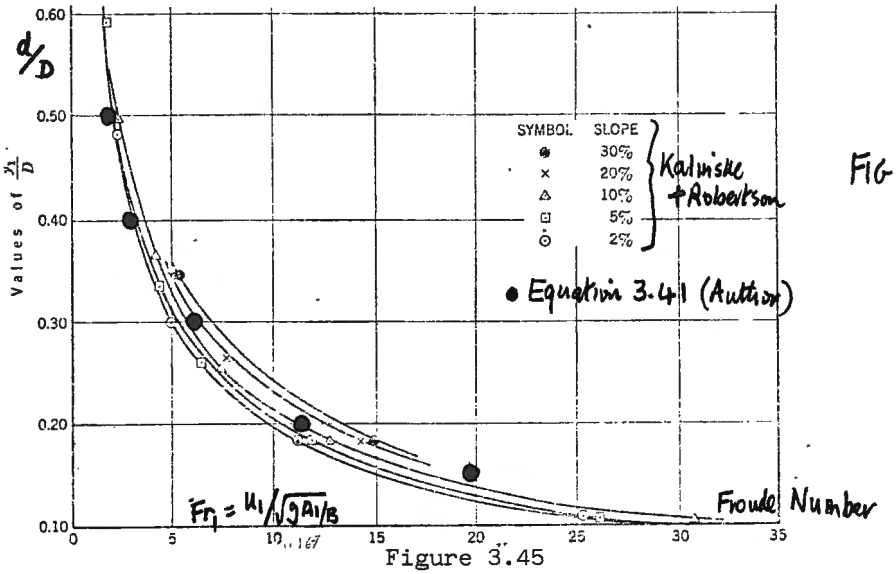

FIG 3.45

Figure 3.45

This has important implications for the transport of air downstream of a jump. If d/D is 0.2 (say) then a Froude Number of 10 will be required to commence air transport along a long conduit, that is, for conduits even at a slight downward angle. If the conduit is horizontal or sloping slightly upwards, no such limitation exists..

Even for a fractional depth of one half (d/D ≈ 0.5) an upstream Froude Number in excess of 2 is required to commence air transport in downward sloping pipes. Any correlations of air entrainment and transport by hydraulic jumps should therefore make careful reference to the slope of the conduit and a correlation for downward sloping pipes should contain an air pocket 'detrainment' or blow back term (albeit on a Froude basis) to account for the limiting Froude Number to transport air. Thus we might write for downward sloping pipes

$$\beta_{an} = K(Fr_1 - 1)^n \; f(Fr_1 - Fr_{1(limit)}) \qquad \ldots\ldots (3.42)$$

where the value of $Fr_{1(limit)}$ is given approximately by Figure 3.45.

(2) Bubble detrainment from the reattaching shear layer.

So far we have discussed a limiting condition for air pocket blowback downstream of a jump when the conduit slopes at a downward angle. However, at any conduit angle (upwards, horizontal or downwards) air bubbles have a natural propensity to detrain as already seen in the analysis of Thomas (Section 2.3). Thomas's analysis was for plane penetrating shear layers, unlike the case of a hydraulic jump with a strongly curving reattaching shear layer, as shown below.

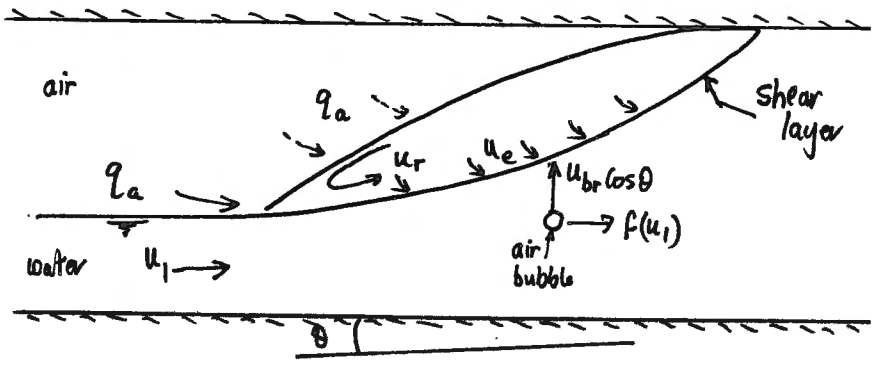

FIG 3.46. Hydraulic jump ($u_{br}\sin\theta$ is small)

The principle however remains the same. If we ignore contributions from vorticity holding air bubbles in their cores, then a bubble rise velocity

of U_{br} cos θ exists, tending to detrain air bubbles out of the shear layer, whilst at the same time and entrainment velocity U_e exists, tending to carry bubbles into the shear layer. As a crude approximation we might say that bubbles are detrained when U_{br} cosθ > U_e, or the point of commencement of air bubble transport is $U_{br}\cos\theta = U_e$. Of course, the real velocity required may be less than this as air bubbles can be ret ained in vortex cores for at least the length of the shear layer. According to Sene this influence becomes prevalent when ΔU is 5 - 10 times the bubble rise velocity, or $U_1 \simeq$ 1.25 - 2.5 m/s. $(\Delta u = u_1 - u_r \simeq u_1)$

Thomas specified the entrainment velocity U_e as εU_1, where ε is the half angle of the spreading shear layer which is aproximately equal to the turbulence intensity in the shear layer. Thus for air bubble transport we need $U_1 > U_{br}\cos\theta/\varepsilon$, when the value of ε might be 1/10 to 1/5 for a jump, and hence for shallow angles $U_1 > 1 \rightarrow 2.5$ m/s for commencement of air bubble transport downstream of the jump.

In any case, at slightly higher jet velocities bubble transport may still be influenced by detrainment, and we may speculate for horizontal and upward sloping conduits.

$$\beta_{an} = K(Fr_1 - 1)^n \quad f\left(1 - \frac{u_{br}\cos\theta}{\varepsilon u_1}\right) \qquad \ldots\ldots (3.43)$$

and for downward sloping conduits

$$\beta_{an} = K(Fr_1 - 1)^n \quad f\left(1 - \frac{u_{br}\cos\theta}{\varepsilon u_1},\ Fr_1 - Fr_{1(min)}\right) \qquad \ldots\ldots (3.44)$$

For downwards sloping conduits we must take account not only of air bubble detrainment, but air pocket blow back. At upstream jet velocities say greater than 2.5 m/s, detrainment may not be significant if air bubbles are transported by vorticity.

(3) Bubble entrainment into a hydraulic jump.

Consider first the inception correlations to entrain air into the flow. In previous sections we have seen that a velocity is required U_1^* to entrain air bubbles in a flow, for steeper conduits. In shallow conduits with a hydraulic jump, the only criterion for air entrainment is a breaking surface roller ($Fr_1 \simeq 1.3$) and air is carried into the shear layer. If $Fr_1 \simeq 1.3$ also coincides with a low supercritical velocity, say < 1 m/s, then entrained air is simply detrained and no transport occurs along the conduit. That is, for U_1 < 1 m/s, then U_{br} cosθ > U_e generally, and also vortex cores are not sufficiently developed to tranpsort air,

$\Delta u_1 < 5 - 10\ U_{br}$. Thus as an order of magnitude for hydraulic jumps, a dual criterion for air bubble transport occurs which is $U_1 > 1$ m/s and $Fr_1 > 1$ and this applies only horizontal and upward sloping conduits, as downward sloping conduits have a further limitation for blow back, in that $U_0/\sqrt{gD} > 0.5$ approximately.

Secondly, in order to obtain a correlation for air entrainment into a jump we must decide on the predominant mechanism for entrainment. There are three possible mechanisms:-

(a) Entrainment at the toe of the jump, with air entrainment coming from the volume of air held in the jet surface undulations. This has been dealt with in Section 2.2 with the conclusion that the air flow rate q_a is proportional to the jet velocity U_1^3 ($q_a \propto U_1^3$) and independent of jet thickness, with the exception of small jet thickness, $d < 20$ mm say. An alternative way of expressing this quantity of air entrained is in the form, $q_a/q_\omega = K\ Fr_1^2$ as seen in previous sections. Thus, for the case of air entrainment by surface undulations at the jet surface (whose volume scale on U_1^2/g,) we have the case as illustrated on the sketch below.

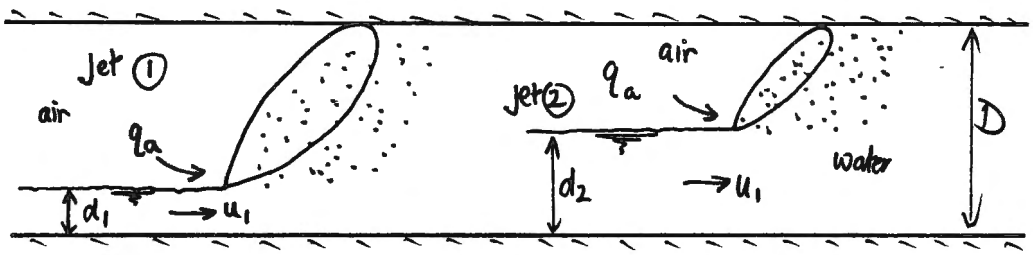

Figure 3.47

Jets of the same velocity entrain the same quantities of air, but when expressed as an air/water ratio β, jet (1) has a higher β than jet (b) by virtue of its higher Froude Number (or smaller depth).

One point noted by Ahmed and Ervine (Ref), albeit for steeper flows, is that for jet Froude Numbers less than about 10, (and incidentally for larger values of d/D) the value of K in the relationship $\beta = K\ Fr_1^2$, did not remain constant. An inspection of Figure 3.34 reveals that for $Fr_1 < 10$, the value of K varies approximately as $1/Fr_1$, or $K \simeq 0.03/Fr_1$, giving an approximate value for β of $\beta \simeq 0.03\ Fr_1$ if we ignore the term $(1 - 0.8/U_1)^3$ for first order magnitudes. Replotting the data for $Fr_1 < 10$, did in fact reveal a correlation for β on $Fr_1 - 1$, as shown on Figure 3.36. This is the same form as hydraulic jumps, even though it was derived from wall jet entrainment at steeper conduit angles.

(b) Surface roller entrainment.

Thomas (Ref) has hinted at a possible physical reasoning for correlations of β on $Fr_1 - 1$, for low Froude Number jumps. This has not been published and is merely surmised here by the author. Thomas assumed entrainment into a low Froude Number hydraulic jump occurred possibly by the mechanism of free surface entrainment into the surface roller. along its length This may be similar to natural surface aeration in high velocity flows and will depend therefore on surface tension forces being overcome by highly turbulent fluctuating components, U*. (A droplet of water is ejected by the turbulence, which entrains an air bubble as it reenters the flow). Alternatively, air bubbles may be entrained into the surface roller by the action of small breaking waves, etc. Air bubbles are then entrained into the shear layer from the layer of foam at a rate which must be dependent on the entrainment velocity U_e into the shear layer. We can state further that $U_e \propto U_1$ the upstream jet velocity. The rate of entrainment q_a must also be dependent on the length of the roller which Thomas denoted by D-d, (or $y_2 - y_1$ in hydraulic jump notation). In reality, the length of a jump is generally $\simeq$ 4 (D-d), but for the time being we may write

$$q_a = K (u_1)(D-d)$$

$$\text{or } \beta = q_a/q_w = K(D/d - 1) \qquad \ldots\ldots (3.45).$$

In the case of an open channel hydraulic jump, D/d scales on the Froude Number Fr_1 and we obtain $\beta = K (Fr - 1)$. This argument would only hold for the case of the sequent depth of the jump being approximately equal to the conduit dimension.

It is not absolutely certain if Thomas postulated the exact argument outlined above.

An equally valid argument can be put forward for scaling on Fr-1 based on observations of Ervine and Ahmed for low Froude Number jumps. If we refer again to Figure 3.47 with hydraulic jumps occurring at the same velocity but different fractional depths d/D, we may assume that entrainment occurs primarily at the toe of the jump based on $q_a \propto U_1^3$ or $\beta \propto Fr_1^2$ as outlined in Section 2.2 and 3.2. When d/D is increased, the length of the roller available for detrainment decreases. Thus we might assume that less detrainment and hence more air bubble transport occurs in Jump (2) with higher d/D. We may write as a speculation

$$\beta \propto Fr_1^2 \; f(d/D) \qquad \ldots\ldots (3.46)$$

for a closed conduit when $Fr_1 < 10$.

Now for hydraulic jump flows, $D/d \propto Fr_1$ as a first order approximation, and hence from (3.46), $\beta = f(Fr_1)$ and thus scaling of β on Fr-1 may be possible. This has certainly been attempted for the data of Ervine and Ahmed as already shown in Figure 3.36 where $\beta \simeq 0.04\,(Fr_1 - 1)^{0.85}$ f(Scale factors), although this is generally for steeper flows. If we attempt to linearise this expression for (Fr-1) we obtain $\beta \simeq 0.03\,(Fr_1 - 1)$ f(Scale factors). In any case, correlations on $(Fr-1)^{1.4}$ are only possible by crossing velocity bands as in the work of Kalinske and Robertson. It is most likely that β scales on $Fr_1 - 1$ for low Froude Number jumps, but some account must be made for air pocket detrainment, etc., highlighted in (1) under"conduit angle".

(c) High velocity entrainment.

This has been discussed in Section 2-2, where it has been proposed by Sene (Ref) that high velocity supercritical flows may produce a continuous layer of air under the roller (Type (2) entrainment, Fig 2.7). In this case $q_a \propto U_1^{3/2}$, and hence would not scale on the Froude Number. This type of correlation may well be relevant to prototype jump data.

Empirical correlations for hydraulic jump entrainment

The first reported work on closed conduit hydraulic jump entrainment was by Kalinske and Robertson (ref). Experimental studies were carried out in a 150 mm diameter pipe with a downward slope ranging from 0-30%. As already discussed, Kalinske and Robertson found a Froude Number $u_1/\sqrt{g A_1/B}$ below which only a small proportion of air was transported, this limiting Froude Number varying with d/D (Fig 3.45). They proposed a relationship for net air transport, presumably once the limiting Froude Number was exceeded, in the form,

$$\beta_{an} = 0.0066\,(Fr_1 - 1)^{1.4} \qquad \ldots\ldots (3.47)$$

No air pocket blow-back term was incorporated, which is surprising as an outlet Froude Number $u_o/\sqrt{gD}$ of at least 0.5 is required to transport air over most of the conduits slopes tested. By implication Equation (3.47) would reveal the air entrainment rate to vary approximately with $U_1^{2.5}$, but also to give increasing q_a with larger upstream flow depths, or as only one pipe was used, larger d/D values. The air entrainment rate into the shear layer should be independent of upstream flow depth d, but entrainment and/or detrainment may well be influenced by the length scale of the roller ($\propto$ D-d), perhaps best correlated in the form, f(d/D).

Further correlations for air transport were carried out by Campbell and Guyton (Ref) and Wisner (Ref) producing separate scalings for low and high Froude Number jumps.

For $Fr_1 < 8$ $\quad \beta_{an} \simeq 0.04 (Fr_1 - 1)^{0.85}$ ..... (3.48)

For $Fr_1 > 8$ $\quad \beta_{an} \simeq 0.014 (Fr_1 - 1)^{1.4}$ ..... (3.49)

the latter equation being in the same form as Kalinske and Robertson Equation (3.47) but the constant 0.014 twice as high as that given in Equation (3.47). Of course Wisner used larger dimension models than Kalinske and Robertson, the largest size being 0.5 m x 0.5 m which is of order 3 to 4 times greater. This in turn would imply jet velocities approximately twice as high for Wisner's data. It is of interest therefore to compare the correlation for steeper flows proposed by Ervine and Ahmed on Figure 3.36 predicting higher values of β_{an} for higher absolute jet velocities. That is, providing air pocket transport problems do not exist, and U_o is large.

Haindl (Ref) and (Ref) carried out extensive testing of hydraulic jump entrainment, again correlating β_{an} on a $(Fr_1 - 1)$ basis. His data is shown on Figure 3.48 , together with that of Wisner, and other published prototype data. Haindl suggests an upper envelope for all data in the form

$$\beta_{an} = 0.015 (Fr_1 - 1)^{1.4} \quad \text{..... (3.50)}$$

In conclusion,

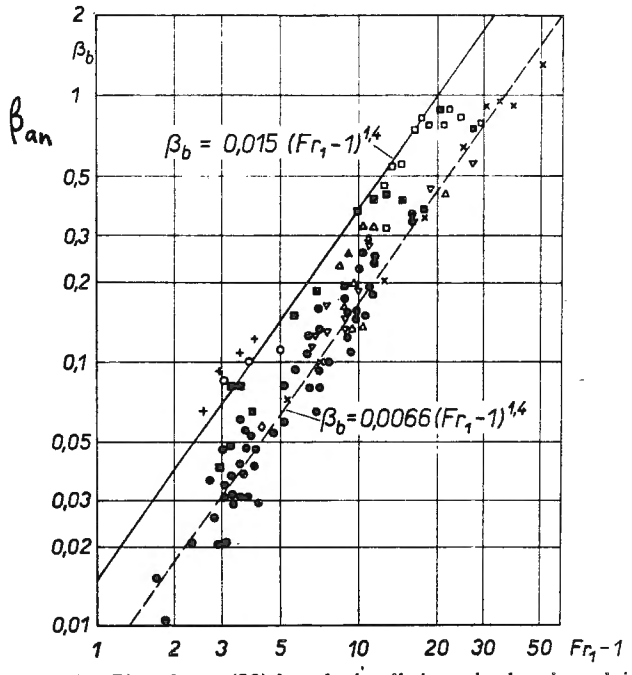

FIG. 10. Plot of eqn. (23) for a hydraulic jump in closed conduits.

+	Denison	9′ × 19′	2·74 m × 5·79 m
○	Hulah	5′ × 6·5′	1·52 m × 1·98 m
▽	Norfork	4′ × 6′	1·22 m × 1·83 m
■	Pine Flat	5′ × 9′	1·52 m × 2·74 m
◇	Tygart	5·67′ × 10′	1·73 m × 3·05 m
×	Ikari	7·9′ × 7·9′	2·4 m × 2·4 m

Laboratory model:

△ □	Wisner	25 cm × 25 cm 50 cm × 50 cm
●	Haindl	26·6 cm × 20 cm

FIG 3.48 Haindl's correlation of hydraulic jump air entrainment data.

SECTION 4

AIR POCKET FLOWS - THEORETICAL MODELS

4.1. Behaviour of air pockets in closed conduits (General)

(a) Vertical conduits

(b) Horizontal conduits

(c) Inclined conduits

4.2 Extension of Benjamins analysis to single air cavities in stationary and moving water conditions.

4.3. Analysis of air pocket 'blow-back' and air pocket 'clearing' in downward sloping pipes.

Major symbols used in Sections 4 and 5 on air pocket flows

A	area of flow under an air pocket
A_p	cross-sectional area of pipe
B	width of flow at surface in a circular pipe
C_o, C_1	constants used in air pocket flows in moving water
C_1	speed of an air pocket (used by Benjamin, Bacopolous, etc.)
D	conduit diameter
Fr_1	Froude Number of flow under an air pocket or upstream of a jump
Fr_o	Pipe-full Froude Number, $V_o/\sqrt{gD}$
g	gravitational constant
H	depth of air pocket
$\langle j \rangle$	volumetric flux for slug flows $(Q_A + Q_W)/A_p$
L	Total length of an air pocket
L^*	Length of air pocket from nose to point where pocket reaches maximum depth, H.
n	non-dimensional air pocket volume = $Vol/\pi D^3/4)$
Q_a	Air flow rate
Q_W	Water flow rate
R	bend radius at dropshaft/tunnel junction
R_b	bubble radius
Re	Reynold's Number
V_b	air pocket velocity in moving water conditions
V_r	air pocket velocity in stationary water conditions
V_∞	rise velocity of air pocket in vertical pipe (stationary water)
V_c	pipe-full water velocity required to clear an air pocket
V_o	pipe-full water velocity required to prevent air pocket blow-back
V_1 (or U_1)	water velocity under an air pocket or upstream of a jump
We (or Wb)	Weber Number

Y_1	depth of flow under an air pocket or upstream of a jump
Y_e	equivalent depth of flow in a circular pipe (A/B)
α	void fraction
β	ratio of rate of air flow to water flow (Q_a/Q_w)
ϕ	angle between nose of an air pocket and pipe wall
μ	absolute viscosity
ν	Kinematic viscosity
ρ_a	density of air
ρ_w	density of water
σ	surface tension coefficient.

Section 4.1. The behaviour of air pockets in closed conduits

In Sections 4 and 5, discussion will be limited to the behaviour of larger air bubbles, plug flow and slug flow, as illustrated in the sketches opposite, presented by Falvey (Ref.). The classical air pocket shape as encountered in many Civil Engineering applications is also sketched below in Fig.4.1.

The lower limit of air pocket sizes is difficult to define, but if we stipulate that the bubble behaviour is dominated by inertia and buoyancy, then a suitable limit would be bubbles of equivalent diameter of over 10 mm, thus excluding all of Sections 2 and 3.

The upper limit is equally difficult, but moving air pockets rarely exceed $H/D > 0,5$ in the Civil Engineering context especially at shallower conduit angles. Pure slug flow, say $H/D > 0.5$, does however sometimes occur, especially in cases such as blowbacks in vertical conduits, etc.

The term "air pocket" is thus used to cover any of the categories above, and a wide diversity of theory and practice is employed from slug flow research, air bubble research and air pocket research.

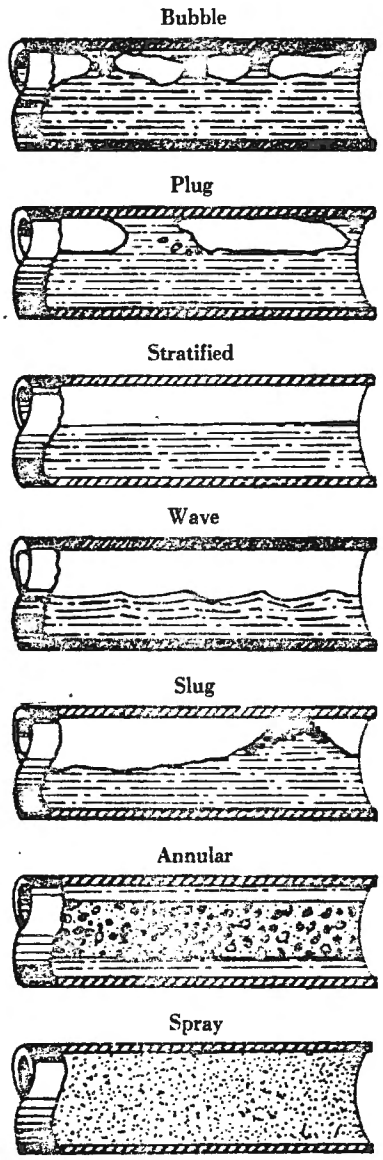

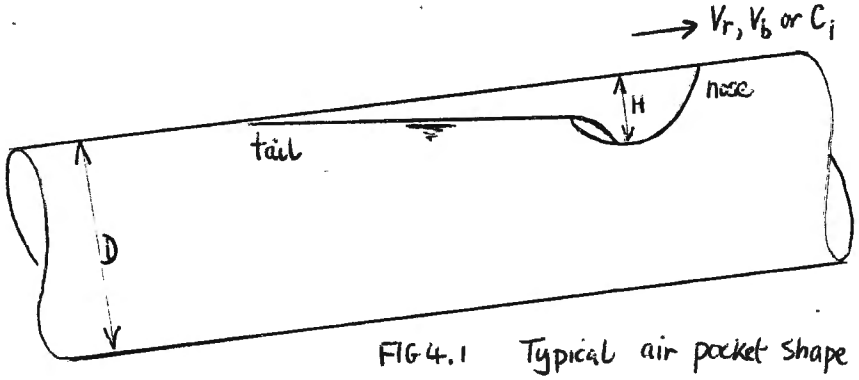

FIG 4.1 Typical air pocket shape

(a) The behaviour of air pockets in a vertical conduit

If we consider first the case of stationary water in a vertical conduit, then the behaviour of an air pocket will be governed by the balance between inertia, buoyancy, viscous and surface tension forces. Wallis (Ref.) has proposed three non-dimensional numbers describing the ratio of buoyancy to the other three forces,

$$\frac{\text{Inertia}}{\text{buoyancy}} \qquad \frac{\rho_w V_\infty^2}{gD(\rho_w - \rho_a)} \qquad \text{.....(4.1)}$$

$$\frac{\text{Viscosity}}{\text{buoyancy}} \qquad \frac{V_\infty \mu_w}{gD^2(\rho_w - \rho_a)} \qquad \text{.....(4.2)}$$

$$\frac{\text{Surface tension}}{\text{buoyancy}} \qquad \frac{\sigma}{gD^2(\rho_w - \rho_a)} \qquad \text{.....(4.3)}$$

It can be seen that for $\rho_a \ll \rho_w$ and $V_\infty \propto \sqrt{gD}$, Equations (4.1), (4.2) and (4.3) above, become a type of Froude Number, Reynolds Number and Weber Number respectively.

For the case of viscosity and surface tension effects considered negligible then from Equation (4.1)

$$V_\infty = K_1 \sqrt{\frac{\rho_w - \rho_a}{\rho_w}} \sqrt{gD} \simeq K_1 \sqrt{gD} \qquad \text{.....(4.4)}$$

for the case of air and water.

The value of K_1 is of the order of 0,345, with 0,35 being a commonly excepted value. Equation (4.4) is an important result in air pocket behaviour with its implicit suggestion of Froude scaling provided viscous and surface tension is neglectable. Definitions of its applicability will be given overleaf.

It is of interest to note that the rising velocity of single air bubbles in an infinite body of water was shown by Davies and Taylor (Ref.) to be $V_\infty = {}^2/_3 \sqrt{gR_c}$, applicable to bubbles greater than 10 mm diameter. R_c is the radius of curvature of the bubble nose. With the bubble spherical nose making an angle of approximately 100°, the volume of the bubble can be calculated, and the rise velocity V_∞ related to the equivalent bubble

radius R_b. The result gives $V_\infty = \sqrt{gR_b}$

When such bubbles rise in a pipe of diameter D, the rise velocity of the bubble can be expressed as a function of d_b/D, where d_b is the equivalent bubble diameter ($= 2R_b$). Collins (Ref.) has shown that the rise velocity for larger bubbles can be given by

$$\frac{V_r}{V_\infty} = 0{,}496 \left(\frac{D}{2R_b}\right)^{\frac{1}{2}} \qquad \text{.....(4.5)}$$

and when combined with $V_\infty = \sqrt{gR_b}$, yields, $V_r = 0.35\sqrt{gD}$, which is the same resust as that obtained for slug flow.

For the case of viscosity being the dominant force, we have from equation (4.2),

$$V_\infty = K_2 \frac{\rho_w - \rho_a}{\rho_w} gD^2 \simeq K_2 \frac{gD^2}{\nu} \qquad \text{.....(4.6)}$$

for air and water, where ν is Kineimatic viscosity (of order 10^{-6}) and K_2 of order 10^{-2} (Wallis, Ref.).

We may now eliminate the air pocket velocity in Equations (4.1) and (4.2) by taking the square root of Equation (4.1) and dividing by Equation (4.2).

The resulting term is the dimensionless inverse viscosity, denoted by N_f.

$$N_f = \frac{\left[D^3 g(\rho_w - \rho_a)\rho_w\right]^{\frac{1}{2}}}{\mu_w} \simeq \frac{(gD^3)^{\frac{1}{2}}}{\nu} \qquad \ldots\ldots\ldots\ldots\ldots\ldots (4.7)$$

Viscosity is dominant when $N_f < 2$, which, for an air/water mixture corresponds to a pipe diameter of less than 1 mm. Viscosity has an influence, however, for values of N_f up to 300 at least, giving a corresponding pipe diameter of 2 mm. It would appear that viscosity is not an important factor in the Civil Engineering context for air/water flows, although Wisner et al (Ref.) have detected viscous influence (for air pockets rising in a pipe inclined at 18°), for Reynolds Number up to 10^5, where $Re = V_r D/\nu$. If we translate the result of Wisner to the vertical case where $V_r \simeq 0{,}35\sqrt{gD}$, we obtain Viscous influence up to $0.35\frac{(gD^3)}{\nu} \sim 10^5$, which gives a pipe diameter of 200 mm.

For the case of surface tension being the dominant force, Equation (4.3) may be used in the form $(\rho_w - \rho_a)gD^2/\sigma$, known as the Eötvös Number. Wallis recommends this value to be greater than 100 in the vertical pipe case, giving a pipe diameter in excess of 27 mm to have neglectable surface tension effects. Experimental work by Zukowski (Ref.) indicates that this criterion may be sufficient for the vertical pipe case, but is inadequate for horizontal or inclined pipes where the air pocket rises along the conduit wall. It can be seen from Fig. 4.2 that a pipe diameter of 150 mm to 200 mm would be required to produce negligible surface tension effects, giving an Eötvös Number criterion of $N_{E\ddot{o}} > 3000$.

Translated into the Civil Engineering context, and physical modelling in particular, we may state that pipes of diameter approximately 150 mm or greater should produce negligible surface tension or viscous effects, and the rise velocity of an air pocket in a vertical conduit dominated by inertia and buoyancy, can be given by

$$V_\infty \simeq 0{,}35\sqrt{gD} \qquad \ldots\ldots\ldots\ldots\ldots\ldots (4.8)$$

Equation (4.8) is applicable to the stationary water case only and requires to be modified if the water is moving either upwards or downwards along the pipe. For the upward flow case, Wallis (Ref.) proposes a simplified relationship based on the drift flux model. The air pocket velocity is given by

$$V_r = j + V_\infty \qquad \ldots\ldots\ldots\ldots\ldots\ldots (4.9)$$

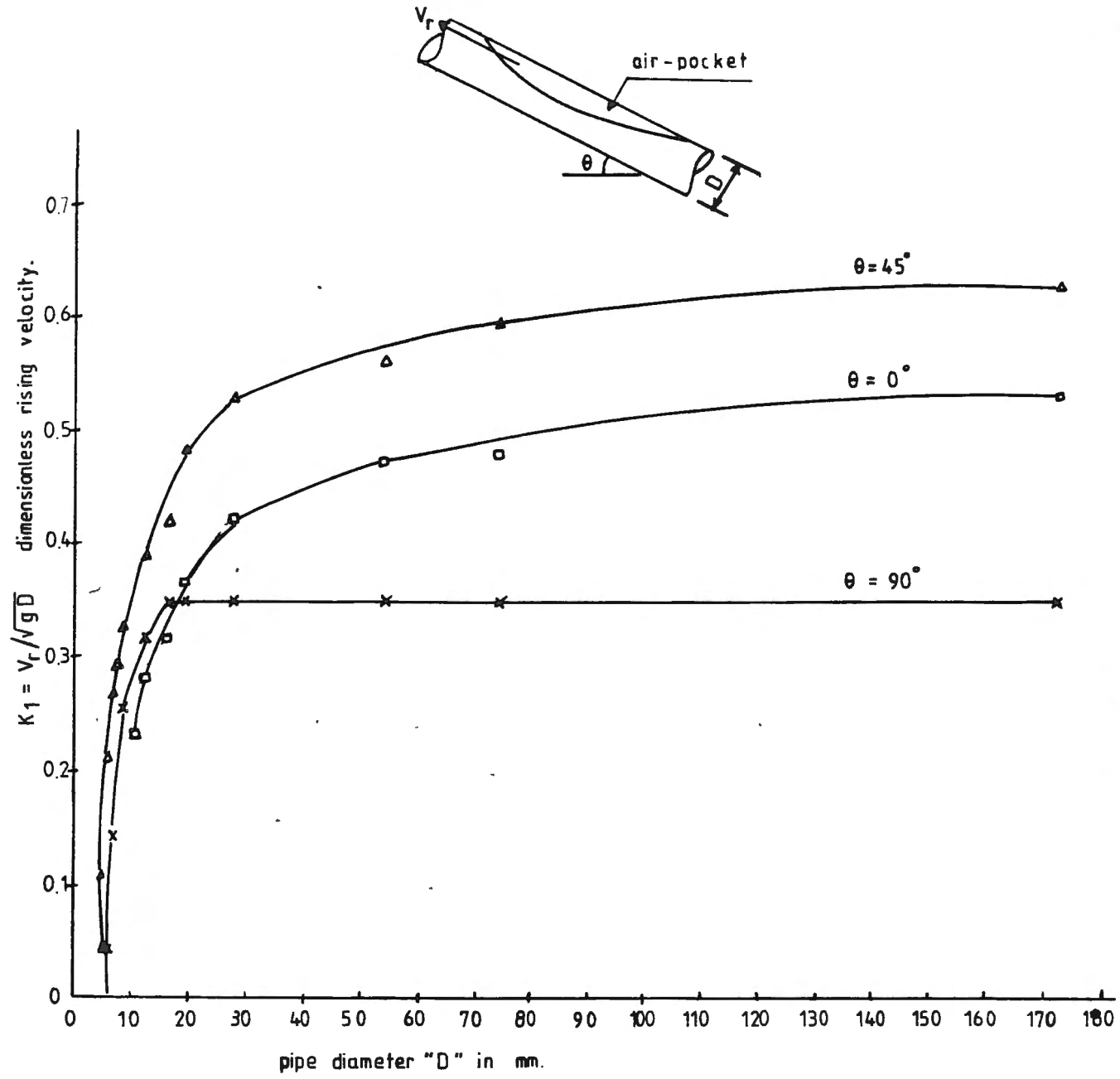

Fig. 4.2 Effect of surface tension on the rising velocity of air-pocket through stationary water in closed conduits (after Zukoski).

where j is the volumetric flux of the flowing mixture $(Q_A+Q_W)/A$, i.e. the air flow plus water flow rate averaged over the pipe area A. Equation (4.9) requires further modification to account for the fact that the air pocket moves relative to the actual water velocity profile in the pipe, (a function of Reynolds Number and pipe wall roughness) and not just the average velocity weighted over the pipe area. A more accurate representation of the air pocket velocity is thus

$$V_r = C_o \langle j \rangle + C_1 V_\infty \qquad \text{.....(4.10)}$$

C_o is approximately 1.2 for higher Reynold's Number flows ($Re_j > 8x10^3$, and $Re_j = jD/\nu$) . C_1 is unity, except for the case of the air pocket rising along the vertical pipe wall when $C_1 \simeq 1.4$ (Martin Ref.). Thus, the rise velocity of an air pocket in upward moving vertical flows is given by

$$V_r \simeq 1,2 \left(\frac{Q_A+Q_W}{A_p}\right) + 0,35\sqrt{gD} \qquad \text{.....(4.11)}$$

or in the case of the air pocket rising along the pipe wall,

$$V_r \simeq 1,2 \left(\frac{Q_A+Q_W}{A_p}\right) + 0,495\sqrt{gD} \qquad \text{.....(4.12)}$$

For the case of downward water flow, air pockets may either rise or descend, depending on the relative magnitudes of the air and water velocities. An investigation of this phenomenon has been carried out by Samuel Martin (Ref.), in three vertical pipes of diameter 0.026 m, 0.1016 m and 0.14 m. In each case water flowed vertically downward, and the air pocket (or slug) would then either ascend, descend or remain stationary. A typical result for the pipe 0.14 m diameter is shown in Fig. 4.3 below.

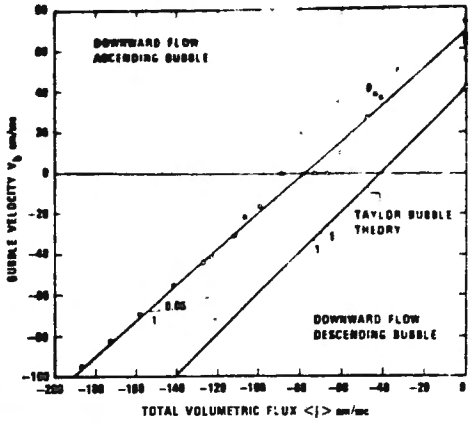

Fig. Bubble velocity—flux plane for D = 14 cm

FIG. 4.3 (MARTIN)

For downward velocity flux (of the mixture) up to 0.8 m/s, the air pocket ascended the pipe, and for velocity fluxes above 0.8 m/s in the downward direction, the air pocket descended. In this case, the point of air pocket equilibrium is when $V_b = 0$, and $V_o \simeq 0.8$ m/s and hence $V_o/\sqrt{gD} \simeq 0.68$, or a downward Froude Number in excess of 0.68 is required to ensure downward air pocket movement. This work has important implications for blow-back and clearing studies and will be discussed further in Section 5. The other point concerns the correlation of air pocket velocity. This is given by Martin as

$$V_b = C_o \langle j \rangle + C_1 \sqrt{gD} \qquad \text{.....(4.13)}$$

For the case shown, $C_o \sim 0.86$ which is very much smaller than (i) the 1.2 found for upward moving water flows, (ii) the value of 1.0 to 1.2 commonly found in horizontal slug flows and (iii) 1.05 to 1.11 found by Ervine and Himmo for a pipe inclined at $+1.5^\circ$ above the horizontal. Martin attributes the lowering of C_o values for downward flows to the tendency for the air pocket to become eccentrically shifted from the pipe axis and hence it is moving relative to a velocity smaller than the cross sectional average.

The value of C_1 shown is 0.58 which is a good deal larger than either Equation (4.11) or (4.12) for upward flows, but in fact comparable to data of Ervine and Himmo in Section 4.2.

(b) The behaviour of air pockets in horizontal conduits

In this work, it is intended as far as possible to treat the behaviour of air pockets in horizontal or slightly inclined conduits in the same manner as density currents or gravity currents, after the example of Brooke Benjamin (Ref.). Numerous observations of air pockets in shallow conduits reveal great similarities in behaviour as shown in the sketch below, especially when the air pocket depth (H) occupies less than half the pipe diameter (D), or $H/D < 0{,}5$. For values of $H/D > 0{,}5$, the flow regime will be that of fully developed slug flow, with analysis outlined by Wallis (Ref.), and in any case is not particularly relevant in the Civil Engineering context.

[In Benjamins analysis C_1 is the air pocket speed not to be confused with the constant C_1 in slug flows, as in Equation 4.13]

FIG. 4.4(a)

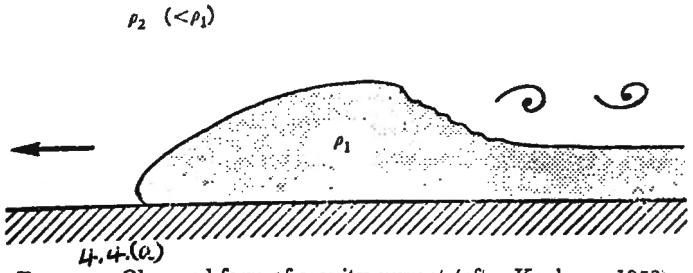

4.4.(a)

FIGURE ... Observed form of gravity current (after Keulegan 1958).

FIG4.4(b)

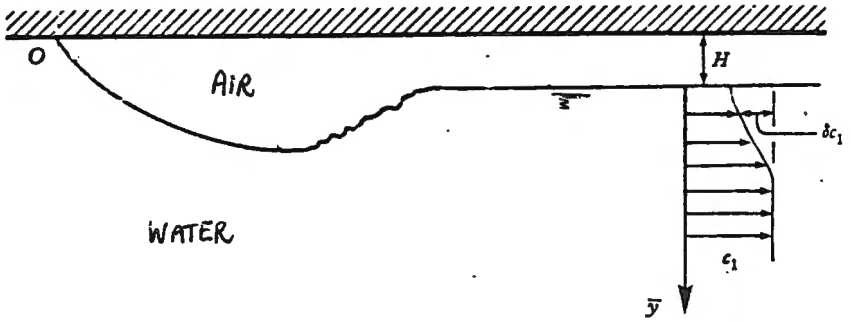

FIGURE 4.4.(b) . Illustration of real flow, showing breaking head wave and velocity profile of ensuing wake.

- Let us consider first, energy conserving flow for the simple two-dimensional case below, where an air void is propagating along the conduit atcelerity C_1, conduit dimension D, and air pocket depth H. The air void is continuous to the exit of the conduit, such as in the case of liquid emptying from a long horizontal conduit.

FIG 4.5

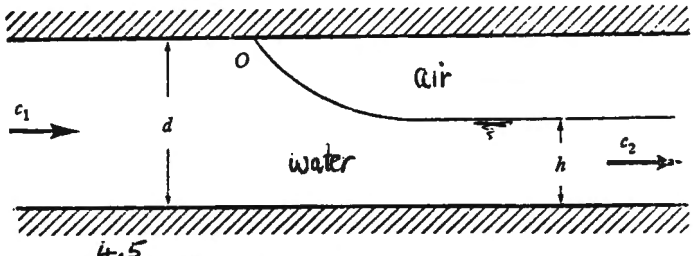

FIGURE 4.5 . Specifications of analogous steady flow past a cavity.

We may bring the air void to 'rest', by applying relative velocity C_1 to the water just upstream of the stagnation point O, with the relative velocity under the cavity becoming C_2.

Applying Bernoulli along the free surface (at atmospheric pressure) to the stagnation point, we have

$$C_2^2 = 2gH = 2g(D-h) \qquad \text{.....(4.14)}$$

The flow force at a point upstream obtained by adding pressure forces to the momentum flux gives,

$$S_1 = \tfrac{1}{2} \rho_w (C_1^2 D + gD^2) \qquad \text{.....(4.15)}$$

and similarly at a point downstream gives,

$$S_2 = \rho_w (C_2^2 h + \tfrac{1}{2} g h^2) \qquad \text{.....(4.16)}$$

Combining Equations (4.14), (4.15) and (4.16) with continuity $C_1 D = C_2 h$, and with $S_1 = S_2$, Benjamin found that for flow with no loss of energy,

$$C_2^2 = \frac{g(D^2-h^2)D}{(2D-h)h} \qquad \text{.....(4.17)}$$

which yields the solutions,

$h = D/2$ or $H = D/2$, the air pocket occupies exactly one half of the conduit depth, and,

$$\frac{C_1}{\sqrt{gD}} = \tfrac{1}{2} \text{ and } \frac{C_2}{\sqrt{gh}} = \sqrt{2} \qquad \text{.....(4.18)}$$

It can be noted that for energy conserving flows in a horizontal conduit $C_1 = 0.5\sqrt{gD}$, which gives a higher air pocket velocity, than the vertical conduit case ($0.35\sqrt{gD}$), and also the receding stream Froude Number $C_2/\sqrt{gh} > 1$ and hence is supercritical.

Benjamin extended this simplified analysis to the 2-dimensional case where energy loss occurs. It can be seen from Fig. 4.4 that most of the energy loss is likely to occur at the jump just behind the cavity nose. Denoting the head loss by Δ, Equation (4.14) becomes

$$C_2^2 = 2g(D-h-\Delta) \qquad \text{.....(4.19)}$$

and again combining with equations of momentum and continuity, an expression was found for the head loss Δ which had a maximum value of $\Delta/D \simeq 0{,}021$. The revised expression for the non-dimensional air void speed is given by,

$$\frac{C_1}{\sqrt{gD}} = \left[\frac{h(D^2-h^2)}{D^2\,(2D-h)}\right]^{\frac{1}{2}} \qquad \text{.....(4.20)}$$

which is plotted on Fig. 4.6 in the form of $C_1/\sqrt{gD}$ against either h/D (the depth of flow beneath the cavity) or H/D (the air cavity depth).

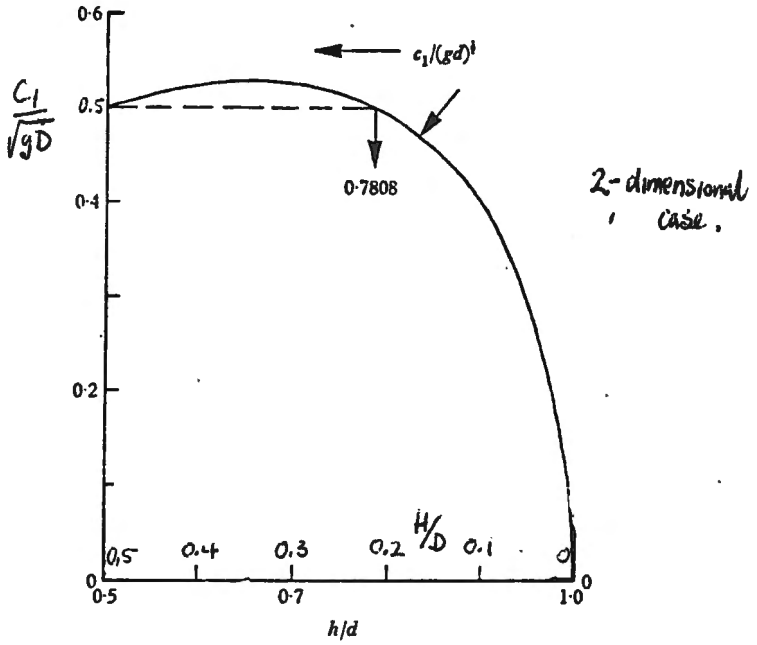

FIG. 4.6 (Benjamin) Variation of $C_1/\sqrt{gD}$ with H/D.

Several points emerge from this graph:-

(a) For a given conduit angle (in this case horizontal), the air pocket speed can be given in the form $C_1/\sqrt{gD} = f\,(H/D)$ as shown on Fig. 4.6.

(b) For small air pocket depths, H/D small, (h/D large), the air pocket speed increases with increasing H/D until at maximum air pocket speed is reached. In this case for the conduit horizontal, $(C_1/\sqrt{gD})$ maximum = 0,527, when H/D = 0,3473. Further increases in H/D up to 0,5 reduce the air pocket speed to the value of $C_1/\sqrt{gD}$ = 0,5 as in the energy conserving case. Values of $H/D > 0,5$ require an energy input in order to sustain a stable air pocket flow.

(c) the speed of an air cavity, void or pocket, can also be related to the pocket depth rather than the conduit dimension. This is shown on Fig. 4.7 plotting $C_1/\sqrt{gH}$ against H/D, giving the result that

$$C_1 = 1/\sqrt{2} \rightarrow \sqrt{2}\ \sqrt{gH} \quad \text{as } H/D \text{ varies from 0.5 down to zero.} \qquad \text{.....(4.21)}$$

Therefore, gravity currents at great flow depths have an upper limit of celerity of $C_1 \leq \sqrt{2gH}$.

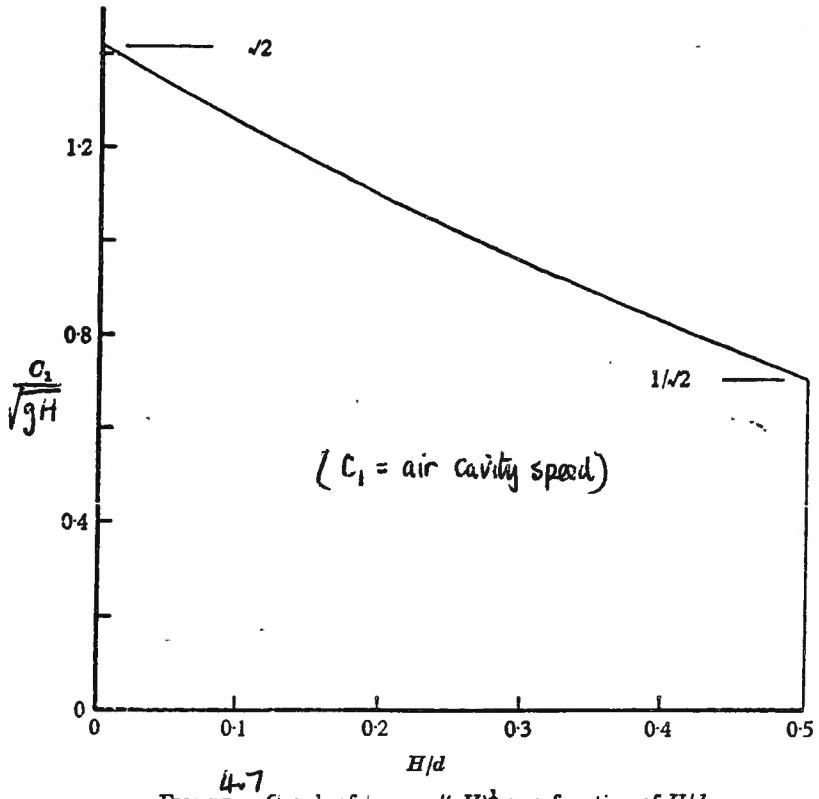

4.7
FIGURE . Graph of $c_1/(gH)^{\frac{1}{2}}$ as a function of H/d.

(d) Benjamin extended this concept to the case of energy conserving flow emptying from a horizontal circular pipe of radius R, or diameter D. Applying the same principles as the 2-dimensional case argued above, Benjamin found the maximum speed of the continuous cavity to be

$$C_1/\sqrt{gR} = 0{,}767 \quad \text{or} \quad C_1/\sqrt{gD} = 0{,}542 \quad \text{for } \theta = 0 \qquad \text{.....(4.22)}$$

which was later confirmed in experiments by Zukowski (Ref.) For circular pipes, the zero energy loss case occurs at $^{H}/_{D} = 0{,}437$.

The important point about Benjamins analysis, is that it may provide a powerful method for analysing the behaviour of air pockets in the Civil Engineering context. If the analysis can be extended to sloping pipes, to single air pockets (rather than the continuous air pocket type which occurs on emptying shallow pipes), to non-uniform velocity profiles, to incorporate wall shear stress, etc., then it may well prove to be more useful than the simple application of empirical correlations which has been a feature of most of the Civil Engineering work to date. The first step in this direction has been taken by Bacopolous (Ref.) under the guidance of Dr. J. Townson. This will be discussed in Section 4.2.

Meanwhile it is clear that most Civil Engineering interest in air pocket behaviour in horizontal pipes would not necessarily involve a continuous cavity as described by Benjamin above, but a single air pocket or single air pockets driven by a water velocity. This situation has not been analysed as such, but it is now open to analysis following the work of Bacopolous (Section 4.2). The application of force/momentum - continuity - energy principle would yield the speed of an air pocket for various air pocket depths ($^{H}/_{D}$) and values of water velocity.

Conventional analyses of slug flows in horizontal pipes (Wallis Ref.) generally involve much larger air pockets than those generally encountered in Civil Engineering. For instance, Wallis proposes a model shown on the sketch below, where the area taken up by a passing air slug is given by

$$A^{1} = \pi\left(\frac{D}{2} - \delta\right)^{2} \qquad \text{.....(4.23)}$$

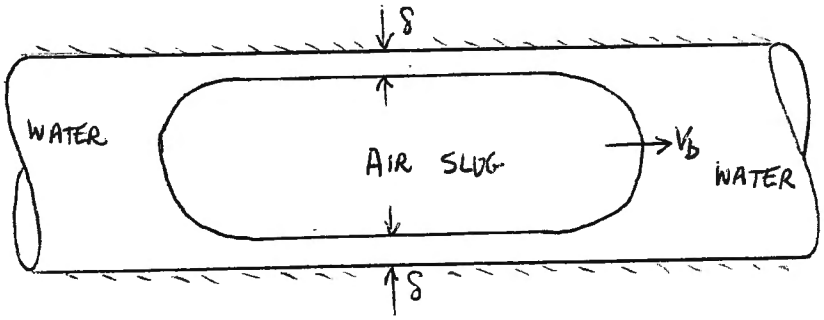

FIG. 4.8 (Wallis)

Assuming no pressure drop along the length of the pocket, the water film on the wall is substantially stationary and we obtain by continuity

$$V_b A^1 = j A_p \quad \text{or} \quad V_b = \frac{A_p}{A^1} j \qquad \text{.....(4.24)}$$

or the air pocket speed $V_b > j$ as $A_p/A^1 > 1$

Wallis quotes for $Re_j > 3000$, $V_b \simeq 1.2\ j$

$$\text{or} \quad V_b \quad 1.2 \left\langle \frac{Q_A + Q_W}{A_p} \right\rangle \simeq 1.2\ V_o\ (1+\beta) \qquad \text{.....(4.25)}$$

It is not yet clear how relevant this is to Civil Engineering type air pocket flows.

(c) Behaviour of air pockets in inclined conduits

Most Civil Engineering interest in air pocket behaviour in inclined pipes has generally centred on :-

(i) velocities required to remove or clear air pockets downstream from a pipe high point, siphon, dropshaft, etc.

(ii) air pocket blow-back studies.

Almost all this work has been experimental, Edmunds (Ref.), Gandenberger (Ref.), Kalinske and Bliss (Ref.), Kalinske and Robertson (Ref.), Kent (Ref.), Wisner et al. (Ref.), Sailer (Ref.), Zukowski (Ref.) to name but a few.

An analysis of air pocket 'blow-back' and air pocket "clearing" in inclined pipes will be carried out in Section 4.3, with experimental evidence presented in detail in Section 5.1. This section, 4.1(c), will concentrate therefore on general aspects of air pockets in inclined pipes, and in particular, deal with rising velocity of continuous and single air cavities in inclined pipes.

In 1965, Zukowski (Ref.) carried out an experimental study on the effect of viscosity, surface tension and conduit angle on the speed of continuous air cavities moving along conduits containing stationary water. Zukowski showed that air pocket propagation rates were substantially unaffected by viscous effects when $Re_o > 200$, where $Re_o = V_r R/\nu$, or put in an alternative manner, when $V_r D/\nu > 400$. If we substitute a typical value of rising velocity $V_r \sim 0.5 \sqrt{gD}$ we obtain that the pipe diameter only requires to be 4-5 mm.

Even the substitution of very small rise velocities $V_r \sim 0.1\sqrt{gD}$, means that the pipe diameter only requires to be 11-12 mm to render viscous effects negligible. This will be discussed in more detail in the light of data from Wisner et al (Ref.) who detected viscous effects in rising single air pockets up to $V_r D/\nu \sim 10^5$.

According to Zukowski, surface tension effects are much more significant at least for continuous air void behaviour. This is clearly illustrated in Fig. 4.2, a plot of the air void rising velocity with pipe diameter assuming fluid properties remain constant. It is clear that for conduit angles other than vertical, surface tension remains an influence even for pipe diameters in excess of 150 mm diameter.

The effect of conduit angle on the rise velocity of continuous voids is shown on Fig. 4.9. Zukowski's results are clearly indicated, and if we ignore the effect of increasing pipe diameter (decreasing surface tension effect) and discuss only the results for the largest 0.178 m diameter pipe, denoted by ⊛. The following points of interest emerge:-

(i) for the vertical case ($\theta = 90^\circ$), the rise velocity is given by $V_r/\sqrt{gD} \simeq 0.35$ which is the same result as obtained by several other authors discussed in (a) under vertical conduits. Presumably the air void is rising up the centre line of the pipe rather than a pipe wall. This gives the apparently strange result that an air void propagates slowest up a vertical pipe.

(ii) for the horizontal case ($\theta = 0^\circ$) the air void propagation rate is $V_r/\sqrt{gD} \simeq 0,53$ which is 2% less than the propagation rate predicted by Benjamin for movement with no energy loss. (Eqn. 4.22)

(iii) the effect of conduit angle is clearly shown, with maximum air pocket velocities at a conduit angle generally between 30° and 60° to the horizontal.
This can be at least partly predicted as shown on the sketch below. ϕ is the angle the nose of the cavity makes with the pipe wall.

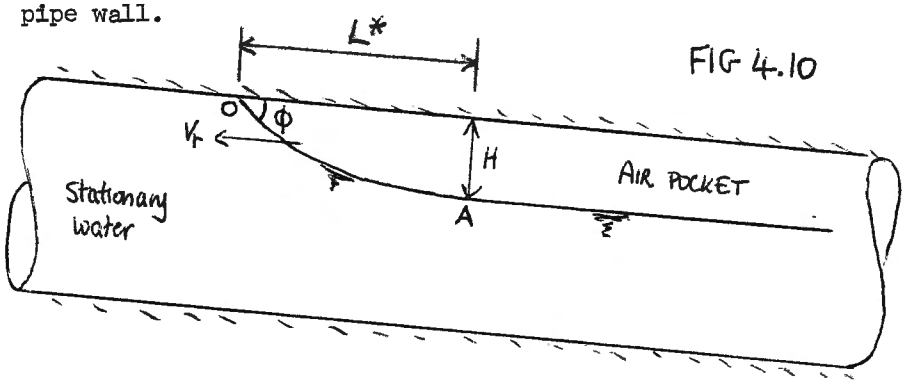

FIG 4.10

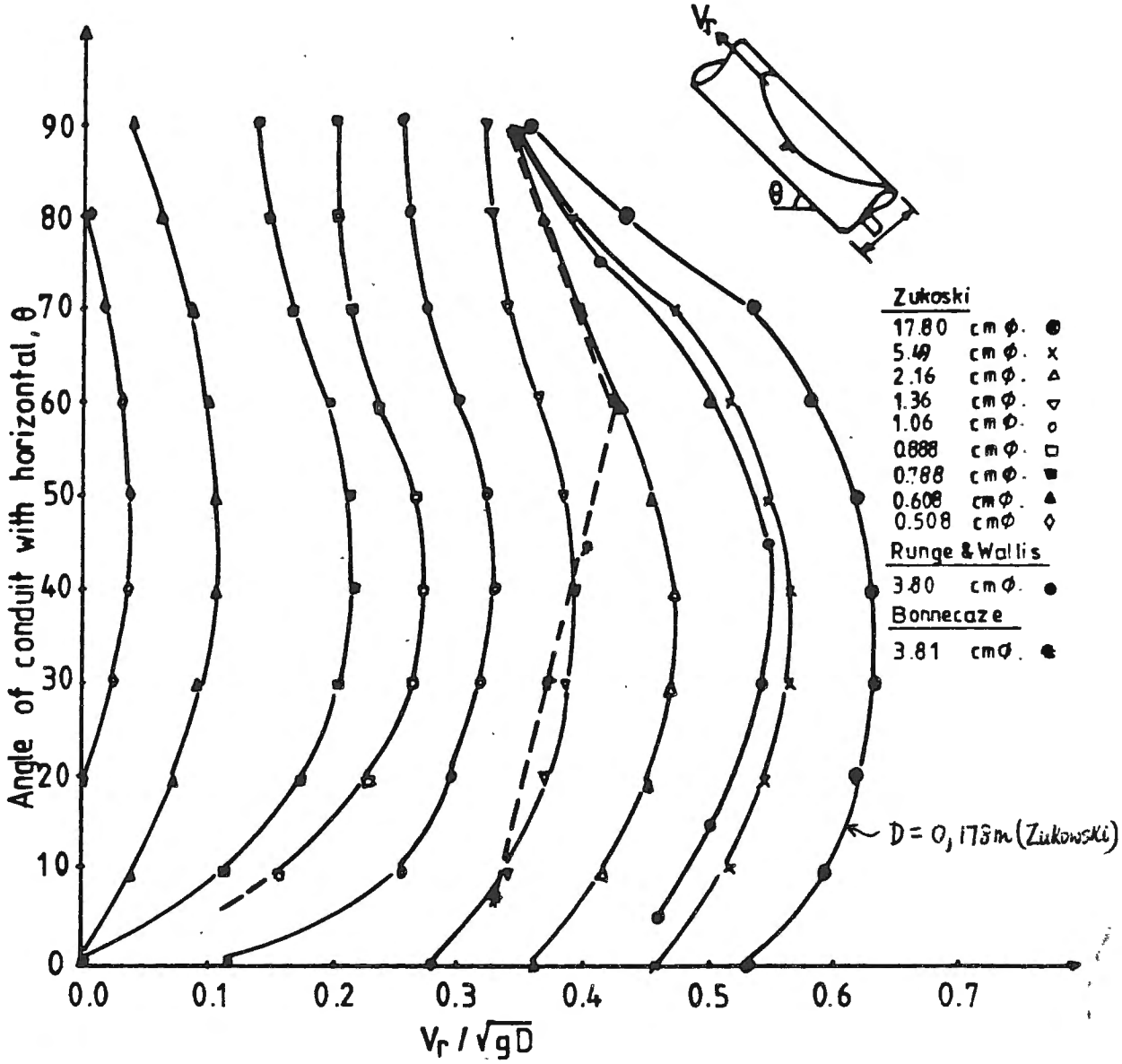

Fig. 4.9 -Variation of pocket rise velocity with conduit angle and pipe diameter, illustrating surface tension effect.

The vertical distance between 0 and A is H Cosθ + L*Sinθ, and applying Bermoulli between 0 and A, with 0 a stagnation point

$$H \cos\theta + L^* \sin\theta = V_A^2/2g \quad \text{where} \quad V_A A_A = V_r A_p \qquad \ldots\ldots\ldots(4.26)$$

This yields $$V_r/\sqrt{gD} = \frac{A_A}{A_p}\sqrt{2H/D \cos\theta + 2L^*/D \sin\theta} \qquad \ldots\ldots\ldots(4.27)$$

If we assume the shape of the nose is parabolic and asymptotic to A, then for $\phi = 60^\circ$, $L^*/D \simeq 1.15 H/D$ or more generally $L^*/D = \frac{2}{\tan\phi}\frac{H}{D}$. The author has plotted below the form of Equation (4.27) for the particular case of $H/D = 0{,}437$, $A_A/A_p = 0{,}58$ and $\phi = 60^\circ$, which is the energy conserving case of Benjamin. It can be seen from Fig.4.11 that Equation (4.27) is a good approximation to Zukowski's data especially for $\theta < 30^\circ$ but Equation (4.27) has been plotted for H/D, L^*/D and ϕ constant. The variation of $V_r/\sqrt{gD}$ with conduit angle θ, is at least illustrated to be a function of the vertical distance between the nose of the cavity and the point of maximum depth of air pocket.

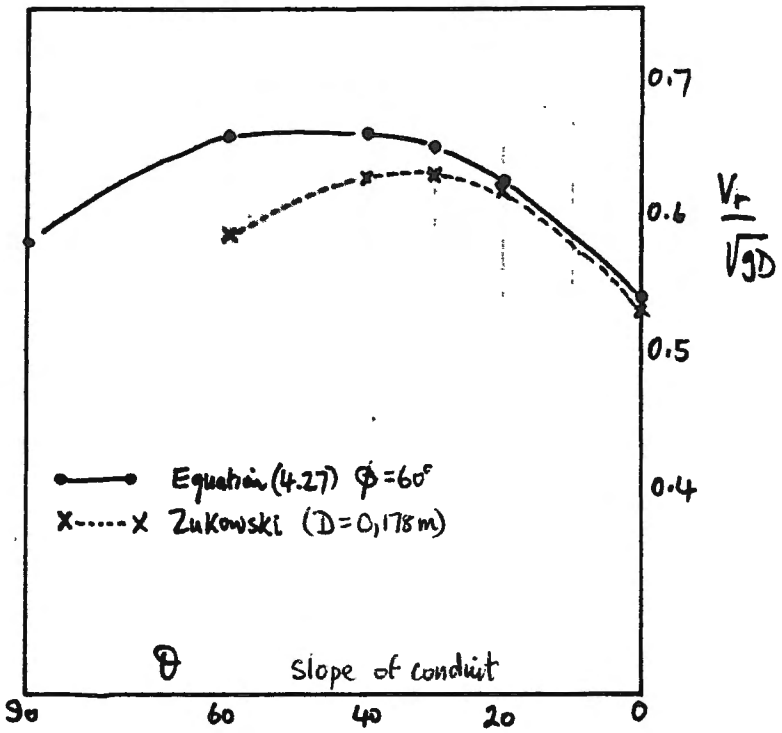

Fig. 4.11

Runge and Wallis (Ref.) investigated the parameters which affect the rise velocity of slugs in still water in an inclined pipe. They concluded that

$$V_r/\sqrt{gD} = f(N_F, N_{E\ddot{o}}, \theta) \qquad \text{.....(4.28)}$$

where N_F is the inverse viscosity term and N_{Eo} the surface tension Eötvös Number already discussed under vertical pipes. Fig. 4.12 shows a plot of $V_r/V_{r(90^\circ)}$ against the conduit angle for large values of $N_{E\ddot{o}}$ and N_F, so that surface tension and viscous effects are small. The pattern for slugs is very similar to the pattern of Zukowski's data for continuous air voids. This is again shown on Fig. 4.9 (alongside Zukowski's data) for a pipe diameter of 0.038 m.

As a preface to experimental work on clearing velocities for air voids in a downward sloping pipe, Wisner et al (Ref.) conducted tests of the rise velocity of single air pockets in stationary water, in a pipe 244 mm diameter and sloping at 18.5°. The result is shown in Fig. 4.13 where the non-dimensional rise velocity is plotted with the Reynolds Number in the form V_rD/ν, for various air pocket volumes. n is a measure of air pocket volume equal to Vol./$\pi D^3/4$. This is a dubious measure, employed both by Gandenberger and Wisner, as it incorporates both the length (L/D) and depth (H/D) of the pocket. It can be seen from Fig. 4.13 that the value of $V_r/\sqrt{gD}$ only exceeds 0.5 for large air pocket sizes for single air voids, and a comparison with Zukowski's data at 18.5° reveals $V_r/\sqrt{gD}$ to be in excess of 0.6. This may be due to differences in character between continuous and single air pockets. Wisner's data relates more to the slug flow data of Runge and Wallis.

The other point of interest in the data of Wisner et al, is that their data has been combined with some of Gandenberger's data to produce the variation in rise velocity with Reynolds Number. A Reynolds Number of 10^5 is required to render viscous effects negligible, which is in sharp contrast to Zukowski's claim that viscous effects are negligible for Re>400. This remains an open question, but it surely might be of interest to plot Wisner's data with the Weber Number ($\rho V_r^2 D/\sigma$) as surface tension effects are thought to be more significant.

Bacopolous (Ref.) conducted experiments on the rise velocity of single air cavities in stationary water for pipe slopes up to 1.65% or 0.945° and a pipe diameter of 0.219 m. The result is shown on Fig. 4.14 for slopes of 1.25%, 1.5% and 1.65%, corresponding to conduit angles θ = 0.716°, 0.86° and

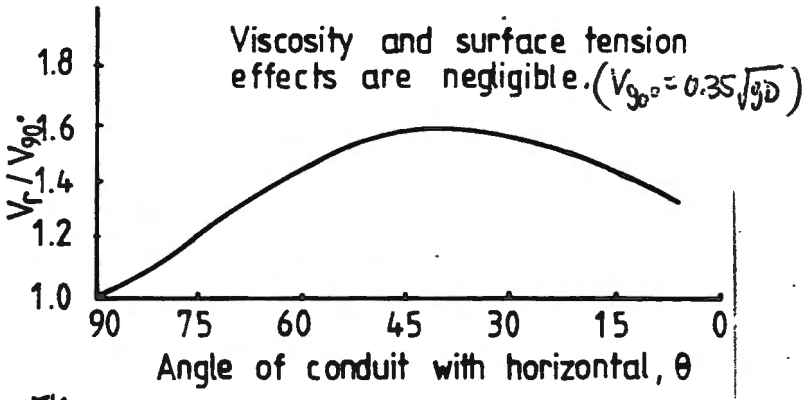

FIG 4.12 - Slug flow in inclined pipe. (after Runge & Wallis)

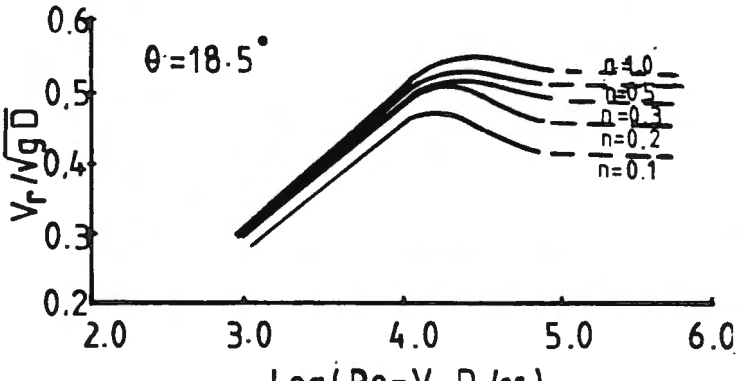

FIG 4.13 - Variation of rising velocity with pocket size. (after Wisner et.al.)

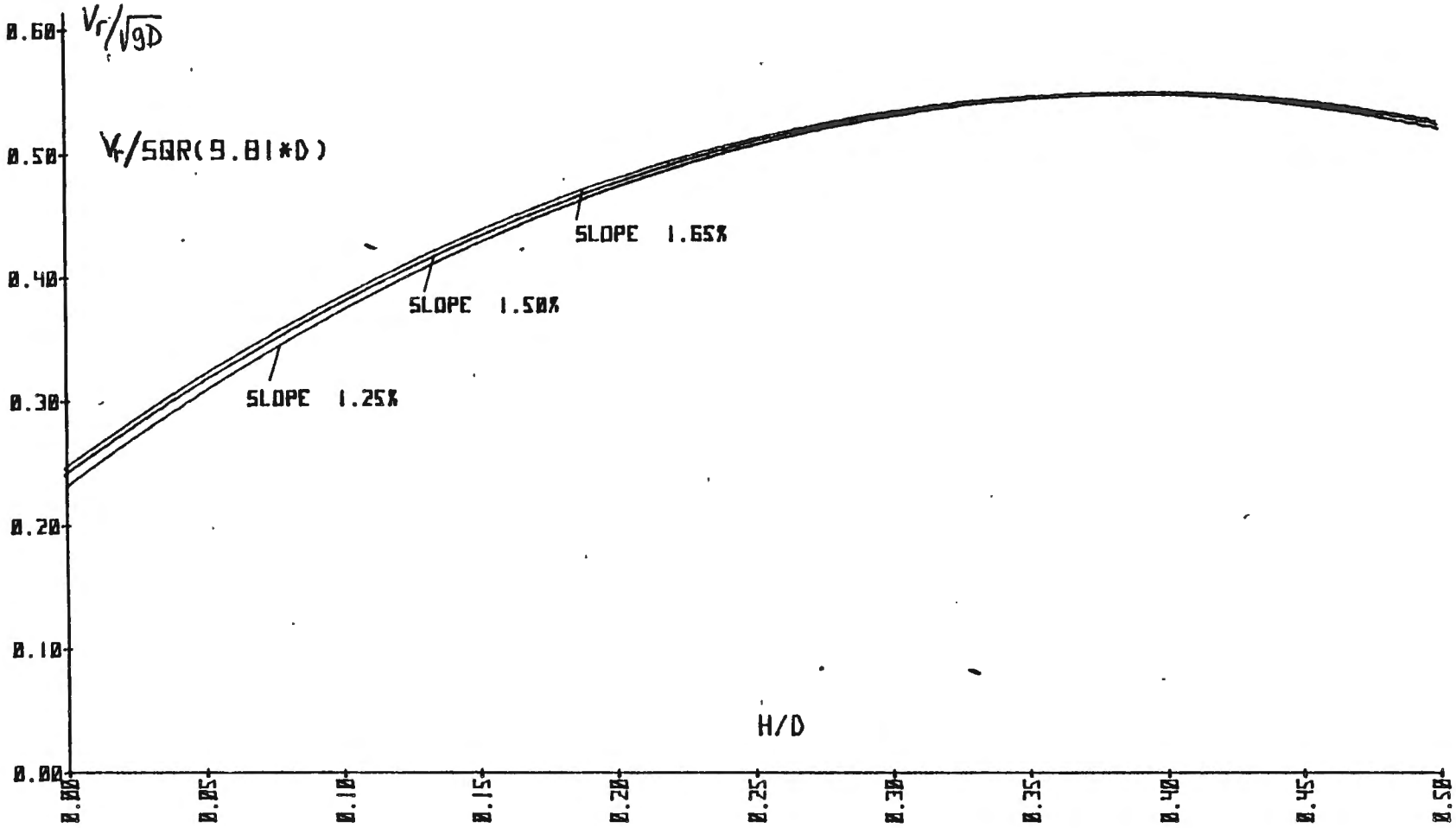

FIGURE 4.14 (BACOPOULOUS) EXPERIMENTS SINGLE AIR CAVITY

0.945°. The result is plotted with the cavity depth parameter, H/D. It should be noted that Bacopolous also attempted correlations of the air pocket rise velocity $V_r/\sqrt{gD}$ with the overall length of the air pocket (L/D) and also the air volume $Vol/\pi D^3/4$. The most significant correlations (at least for shallow conduit angles) are with cavity depth, H/D, and the author feels that this should be adopted in future correlations, rather than the cavity volume. It can be seen from Fig. 4.14 that the air pocket velocity varies significantly with H/D, in a similar pattern to that of Benjamin (Fig. 4.6), with the maximum values of $V_r/\sqrt{gD}$ well in excess of 0.5. This corresponds closely with Zukowski's data for continuous cavities at the same conduit slope, suggesting that Wisner's data may represent a slight underestimation of cavity speeds, possibly due to differing experimental conditions or techniques.

For the case of air pockets travelling in an inclined conduit under moving water conditions one would expect a correlation similar to the drift flux model outlined for vertical conduits,

$$V_b = C_o \langle j \rangle + C_1\sqrt{gD} \qquad \text{.....(4.29)}$$

where C_o might be 1,2 as for vertical and horizontal conduits and C_1 might vary with H/D and the angle θ as discussed under stationary flow conditions above. Typical values of C_1 for Zukowski's data (Fig. 4.9) are 0.35→0.63, Runge and Wallis C_1 = 0.35→0.56, etc.

Bonnecaze(Ref.) investigated slug flow under moving water conditions for a pipe sloping from +10° in the upward direction to -10° in the downward direction. The data correlates,

$$V_b \simeq 1.2 \langle j \rangle \pm 0.35\sqrt{gD} \qquad \text{.....(4.30)}$$

where the + sign is used for upward sloping pipes and - for downward sloping pipes. It is not certain why C_1 = 0.35 remained constant for all pipe slopes, as almost all other research reveals a substantial variation with conduit slope.

Ervine and Himmo (unpublished) conducted experiments in a pipe (152 mm diameter) sloping at 1.5° in the upward direction. This will be discussed in some detail in Section 4.2. The results were correlated in bands of air cavity depth H/D, with the plot of V_b against $\langle j \rangle$ shown on Fig 4.19. The correlations in Equations (4.41) to (4.44) reveal,

$$V_b \simeq 1.05 \rightarrow 1.11 \langle j \rangle + f\left(H/D\right)\sqrt{gD} \quad \ldots\ldots\ldots\ldots\ldots\ldots (4.31)$$

where $f(H/D)$ is very similar to the pattern produced by Bacopolous for stationary flows. For H/D varying from 0.1 to 0.35, the value of C_1 varied from 0.4 to 0.581.

Thus for Civil Engineering type air pocket flows we might speculate that the speed of an air pocket in pipes sloping upwards (at angle θ) and under moving water conditions, is given by,

$$V_b \simeq 1 \rightarrow 1.2 \langle j \rangle + f\left(H/D, \theta\right)\sqrt{gD} \quad \ldots\ldots\ldots\ldots\ldots\ldots (4.32)$$

where $\langle j \rangle = (Q_a + Q_w)/A$ pipe

$f(H/D)$ is approximately as predicted by Benjamin or Bacopolous

$f(\theta)$ is approximately as predicted by Zukowski, with Zukowski's curve for pipe diameter 0.178 m representing the maximum air cavity speeds for any value of H/D?

Section 4.2. Extension of Benjamin's analysis to the case of single air pockets in mildly sloping pipes

This problem has been recently tackled by Bacopoulos (Ref.) under the general supervision of Dr. J. Townson at the University of Strathclyde, Glasgow. Bacopolous formulated theoretical models for both continuous and single air cavities. We will confine our discussion to the case of a single air cavity shown overleaf on Fig. 4.15. Several important assumptions are made as follows:-

(a) The cavity moves at a constant speed along a long circular pipe of diameter D, the pipe sloping at angle θ to the horizontal.

(b) The water ahead of the cavity is stationary, but the cavity moves at speed C_1. The cavity is brought to rest by applying a relative velocity backwards of C_1.

(c) For convenience of analysis the cavity is sub-divided into four zones as indicated

- Zone OA is of length L_1, and is assumed to be a parabola making an angle 60° at point O, and approaching asymptotically a line parallel to the pipe axis at point A. The maximum depth of the cavity (H) occurs at point A.

- Zone AE is of length L_2 and is a low Froude Number hydraulic jump which may either be an undular jump or incorporate a breaking wave. Bacopolous used an experimental expression for the jump length L_2, in the form

$$L_{2/D} = 0.45 + \left(\frac{H/D - 0.14}{0,27}\right) 0.55 \qquad \text{.....(4.33)}$$

- Zone EZ is of arbitrary length $2D (= L_3)$

- Zone Z to the end of the cavity is simply the horizontal interface between air and water, and is effectively the tail of the air cavity.

(d) the velocity profile at section AA_1 (see Fig. 4.15) is assumed to be rectangular on account of its proximity to the nose of the cavity OO_1, where the water starts moving. The resistance to flow in the region $OO_1 AA_1$ is unknown, but Bacopolous tries three possibilities -

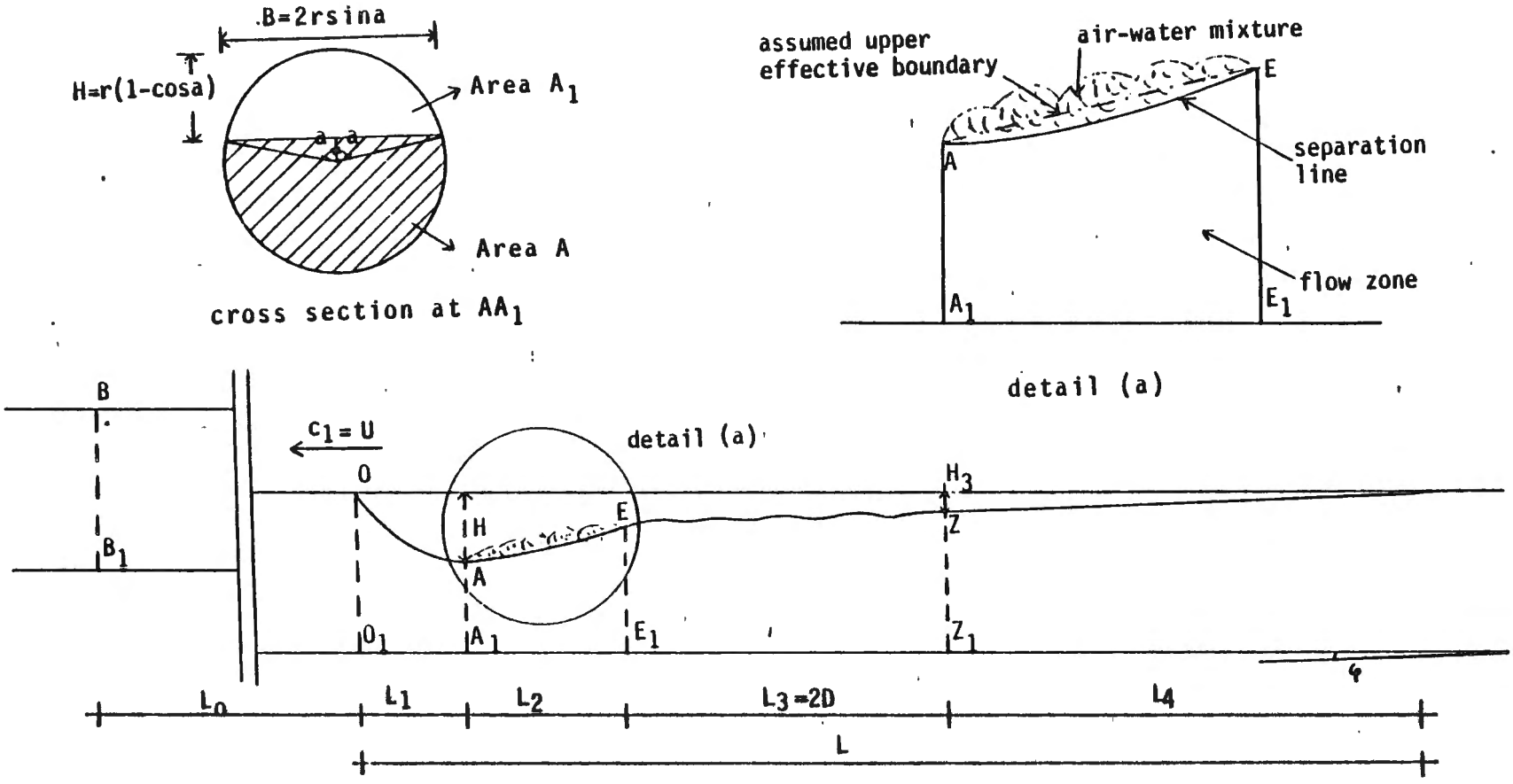

Figure 4.15 Single air cavities. Section along the pipe axis.

(i) No resistance present

(ii) $^2/_3$ of water weight in OO_1 AA_1 balanced by resistance,

(iii) resistance from D'Arcy-Weisbach using estimates of friction factor λ.

(e) the water velocity profile at section ZZ_1 (Fig.4.15) is assumed to be parabolic which seems a reasonable first estimate in view of the difficulty in estimating boundary layer growth from the front end of the cavity to the point ZZ_1 for this 3-dimensional case. Bacopolous goes to some lengths to calculate the momentum correction factor for section ZZ_1 to provide a more accurate assessment of the momentum flux at that point.

The analysis (force/momentum, etc.) of the sections AA_1 and ZZ_1 was attempted again using the three possibilities of resistance to flow outlined above, under (d).

Let us now consider the analysis for the relationship between the cavity speed $C_1/\sqrt{gD}$ and the cavity depth, H/D.

Applying Bernoulli's equation between point B, some distance upstream where only a relative velocity of C_1 is occuring, and point O at the nose of the cavity. Point O is considered to be a stagnation point with zero velocity, and also the datum point for the analysis.

$$\frac{P_B}{\rho g} + \frac{C_1^2}{2g} + L_o \sin\theta = \frac{P_{air}}{\rho g} + \frac{0}{2g} + 0 \qquad \text{.....(4.34)}$$

The pressure in the air pocket is denoted by P_{air}, and no resistance to flow occurs over this length L_o. Hence we obtain,

$$\frac{P_B}{\rho g} - \frac{P_{air}}{\rho g} + L_o \sin\theta = -C_1^2/2g \qquad \text{.....(4.35)}$$

We now apply force/momentum balance between sections BB_1 and AA_1

(Pressure at BB_1) + (Momentum flux at BB_1)
- (Pressure at AA_1) - (Momentum flux at AA_1)
+(Water weight between BB_1 and OO_1) + (Water weight between OO_1 and AA_1)
-(Resistance between OO_1 and AA_1) = 0

.....(4.36)

Assuming the velocity at Point AA_1 is C_2, the area at AA_1 is given by A, and the pipe is of radius r, we obtain,

$$(P_B \times \pi r^2 + \pi r^2 \times \rho g r \cos\theta) + (\rho \pi r^2 C_1^2)$$

$$-(P_{air} \pi r^2 + \rho g r \cos\theta [A \cos a + {}^2/_3 r^2 \sin^3 a]) - (\rho A C_2^2)$$

$$+ (\rho g \pi r^2 L_o \sin\theta) + (\rho g \sin\theta \times \text{Volume water between } OO_1 \text{ and } AA_1)$$

$$- (\text{Resistance between } OO_1 \text{ and } AA_1) = 0 \qquad \ldots\ldots\ldots\ldots\ldots\ldots (4.37)$$

It should be noted here that the area of flow (A) in a partially filled circular pipe is given by

$$A = \pi r^2 \left(1 - \frac{a}{180} + \frac{\sin 2a}{2\pi}\right) \qquad \ldots\ldots\ldots\ldots\ldots\ldots (4.38)$$

where a is the half angle illustrated on Fig.4.15.

The resulting hydrostatic pressure force from a partially filled pipe is given by

$$F = \rho g r (A \cos a + {}^2/_3 r^2 \sin^3 a) \qquad \ldots\ldots\ldots\ldots\ldots\ldots (4.39)$$

so that when the pipe is full, a = o and $F = \rho g r A = \rho g \pi r^3$.

Finally, the energy equation (4.35) can be combined with the force-momentum equation (4.37) and also with the continuity equation ($C_1 \pi r^2 = C_2 A$) where A is the area of section AA_1, to provide a relationship between the speed of an air cavity and its depth H/D. To complete this analysis, Bacopolous calculated the volume of water between OO_1 and AA_1 assuming the parabolic shaped cavity nose. As pointed out previously, three values of resistance between OO_1 and AA_1 were used. The final resulting relationship for a conduit slope of 1.65%, is shown on the table (FIG 4.16) below for various values of H/D.

$\frac{H}{D}$	0.10	0.20	0.30	0.40
a) no resistance present	0.4239	0.5367	0.5716	0.5597
b) $\frac{2}{3}$ of water weight component is balanced by resistance	0.4213	0.5335	0.5682	0.5565
c) resistance is given by the equation of turbulent flow.	0.4239	0.5367	0.5716	0.5597

Fig. 4.16. Variation of dimensionless air cavity velocity $\frac{C_1}{(gD)^{1/2}}$ with resistance condition. Slope of pipe = 1.65%.

A few points of interest emerge from Table 4.16 above,

(i) The inclusion of a flow resistance term from Section OO_1 to AA_1 makes no difference to the eventual cavity speed.

(ii) The air cavity velocity varies with the value of H/D as shown. The trend is the same as that predicted by Benjamin for the 2-dimensional case (see Fig. 4.6) of a continuous air cavity.

(iii) The parameter H/D is much more significant in correlating air cavity behaviour than other parameters, such as L/D (the cavity length) or the air volume held in the cavity. This was illustrated in the experimental correlations of Bacopolous (Ref.).

(iv) The author has plotted the theoretical result of Bacopolous (for a pipe slope of 1.65% and stationary water) alongside experimental data for the same condition. This is illustrated on Fig. 4.17 by the points denoted X (theoretical) and + (experimental). It is clear that for the range shown, the theoretical prediction of air cavity speed overestimates the experimental values. This occurs at least for H/D values less than 0.4, but the reverse is the case for H/D from 0.4 to 0.5. (not shown).

Bacopolous continued his single air cavity analysis by calculating a theoretical length of the cavity, L/D, and plotting the result against the cavity depth, H/D. The total length of the cavity was calculated by summing theoretical estimates of the four separate zone lengths, $L = L_1+L_2+2D+L_4$. The result, for a pipe slope of 1.65% is shown on Fig. 4.18, again for the three flow resistance estimates. For this particular angle of conduit, most of the air pocket lengths are in the region of 10-15 pipe diameters, although this must decrease for steeper conduit angles and increase for shallower conduit angles.

The analysis of Bacopolous and Townson may prove to be a useful tool in predicting air pocket behaviour. So far it has been applied only for shallow conduit angles, up to 1.65% or 0.945°, and to stationary flow conditions. It would be of interest to see if this work could be extended over the full range of conduit angles and also under moving water conditions which is much more commonly the case.

after Bacopoles { × theoretical (no resistance) ; slope=1.65% , θ = 0.945°
+ experimental , slope = 1.65% , θ = 0.945

Himmo + Ennie { ⊙ experimental, slope = 2.62% , θ = 1.50°

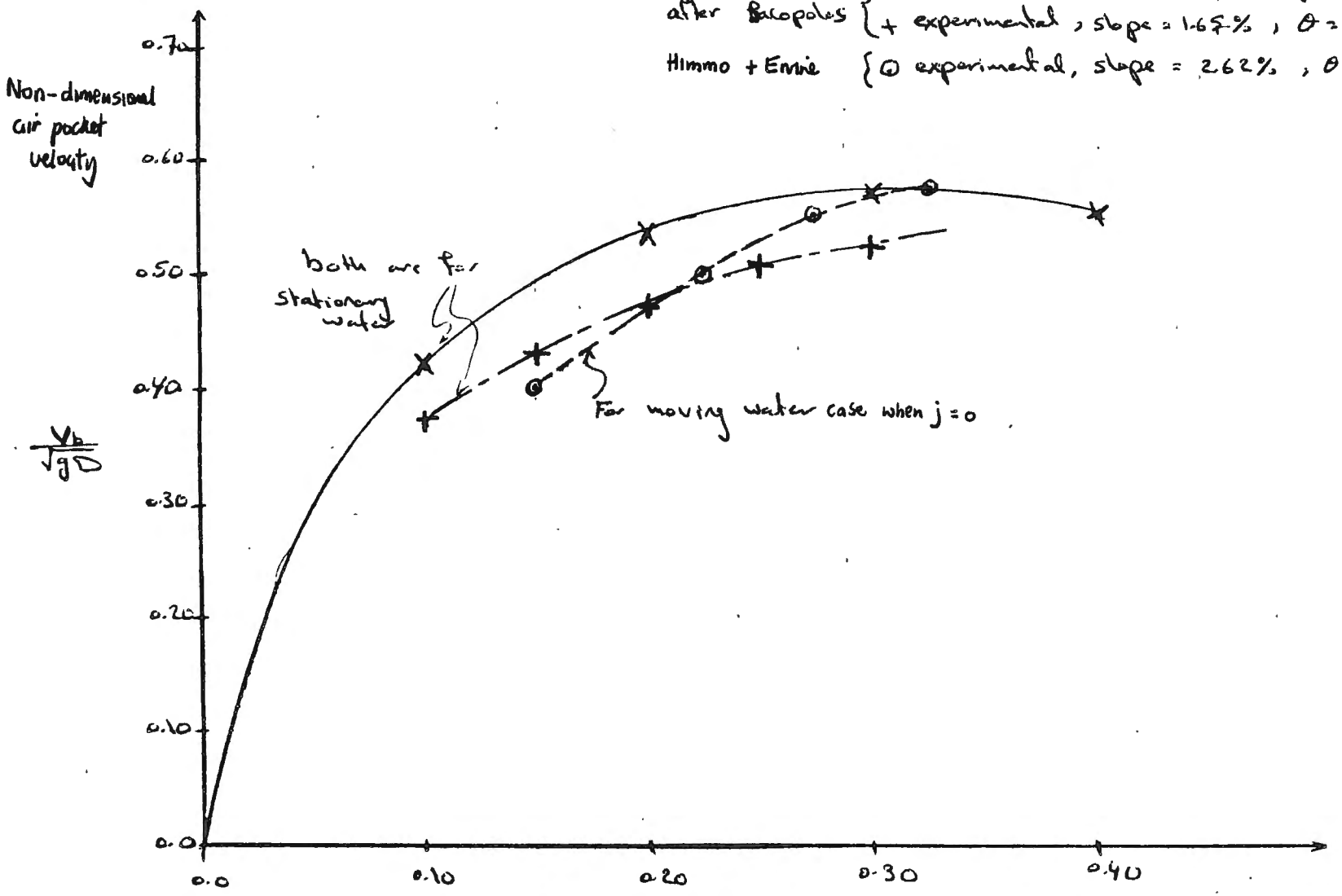

FIG 4.17

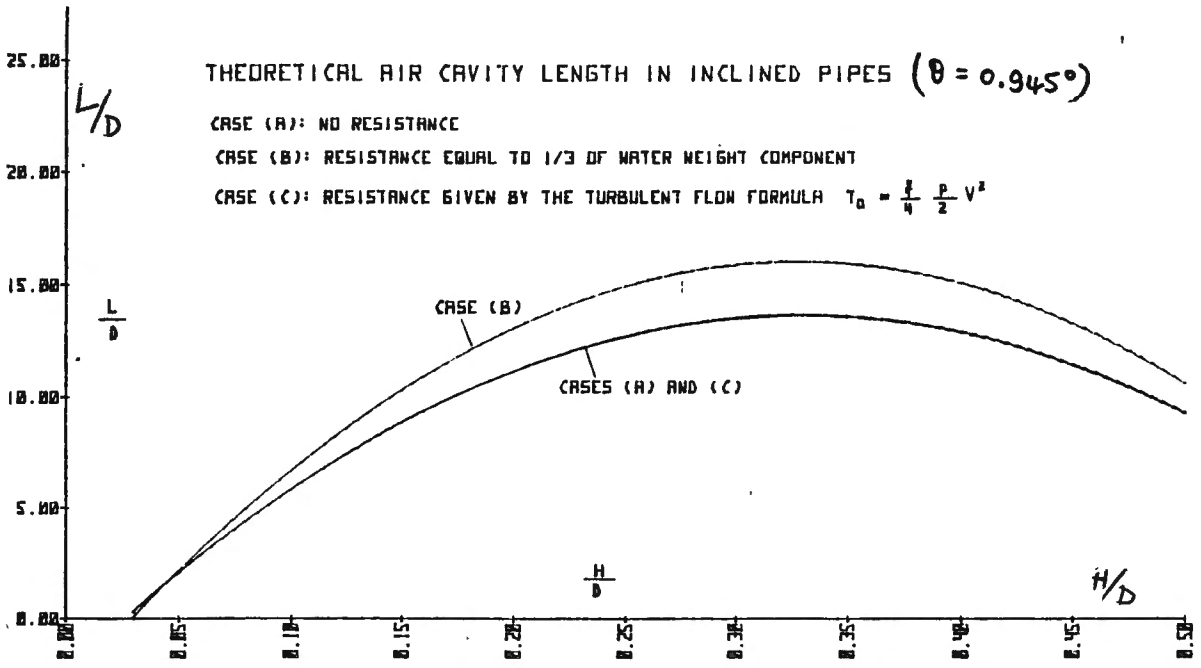

FIGURE 4.18 SINGLE AIR CAVITIES

Certainly for the case of a shallow angle of conduit, the work of Bacopolous could be easily extended for the moving water case, when an allowance for pipe wall friction between sections BB_1 and OO_1 would be required.

Regarding the speed of air cavities under moving water conditions, Ervine and Himmo (not yet published) have recently measured air pocket speeds along a perspex pipe (152 mm diameter) over a wide range of water velocities. The work(which will be described in detail in Section 5.2,) is a study of air pocket formation at the junction of a vertical dropshaft and a horizontal or almost horizontal tunnel outlet. A series of successive air pockets travel along the tunnel under the influence both of buoyancy and moving water, as shown on Fig.5. . The tests described below apply to the tunnel section inclined at an upward angle of 1.5° which is slightly steeper than that of Bacopolous (0.945°), and with the air pockets shape and speed measured by Churchill wave probes.

The air pocket shape approximates very closely to that sketched by Bacopolous on Fig. 4.15 with three discernible sections, the initial nose, the hydraulic jump and the tail of the pocket. Before discussing the experimental data of the air pocket speed V_b, we should note that the speed of air pockets (or slugs) has been shown by previous authors to have the

form,

$$V_b = C_o \langle j \rangle + C_1 \sqrt{gD} \qquad \text{.....(4.40)}$$

where $\langle j \rangle$ is the mean velocity of the whole air-water mixture $(Q_A + Q_W)/Ap$, which is a better measure for the case of successive air pockets passing along the pipe. We have already seen that for the vertical pipe case at high Reynolds Numbers $C_o \sim 1.2$ and $C_1 \sim 0,35$, whereas for inclined pipes C_1 at least increases above 0.35.

The experimental results of Ervine and Himmo are shown on Fig. 4.19 which is a plot of the air pocket speed V_b against the mean velocity of the flowing mixture $\langle j \rangle$. The slope of this data should then be equal to C_o and the intercept equal to $C_1\sqrt{gD}$, where D = 0.152 m. On inspection of the data, it was found that a series of almost parallel lines could be drawn, corresponding to each range of the cavity depth, H/D, which was also measured. The value of C_o which was expected to be 1,2 varied slightly with each range of H/D between 1.055 and 1.11. Regression analysis of each band of H/D revealed,

$0.1 < H/D < 0.2$,

$$V_b = 1.11 \langle j \rangle + 0.4 \sqrt{gD} \qquad \text{.....(4.41)}$$

$0.2 < H/D < 0.25$,

$$V_b = 1.076 \langle j \rangle + 0.501 \sqrt{gD} \qquad \text{.....(4.42)}$$

$0.25 < H/D < 0.3$,

$$V_b = 1.055 \langle j \rangle + 0.556 \sqrt{gD} \qquad \text{.....(4.43)}$$

$0.3 < H/D < 0.35$,

$$V_b = 1.096 \langle j \rangle + 0.581 \sqrt{gD} \qquad \text{.....(4.44)}$$

all for a conduit slope of 1.5°. This indicates quite clearly that although the value of C_o may be approximately constant, the value of C_1 varies with H/D, for a given conduit slope. We have already seen that C_1 varies with slope of conduit in Section 4.1. The author has plotted the experimental values of C_1 above with the experimental and theoretical data of Bacopolous ($\theta = 0.945°$) on Figure 4.17 (points marked ⊙), showing good agreement. By implication, if the work of Bacopolous can be extended to any conduit angle θ, then accurate values of C_1 can be predicted for the full range of H/D and conduit angle, and because C_o remains fairly constant between 1 and 1.2 we may be able to predict air pocket speeds accurately over a wide range of conditions.

Air-pocket rising velocity for a tunnel at +1.5° with horizontal

FIG. 4.19

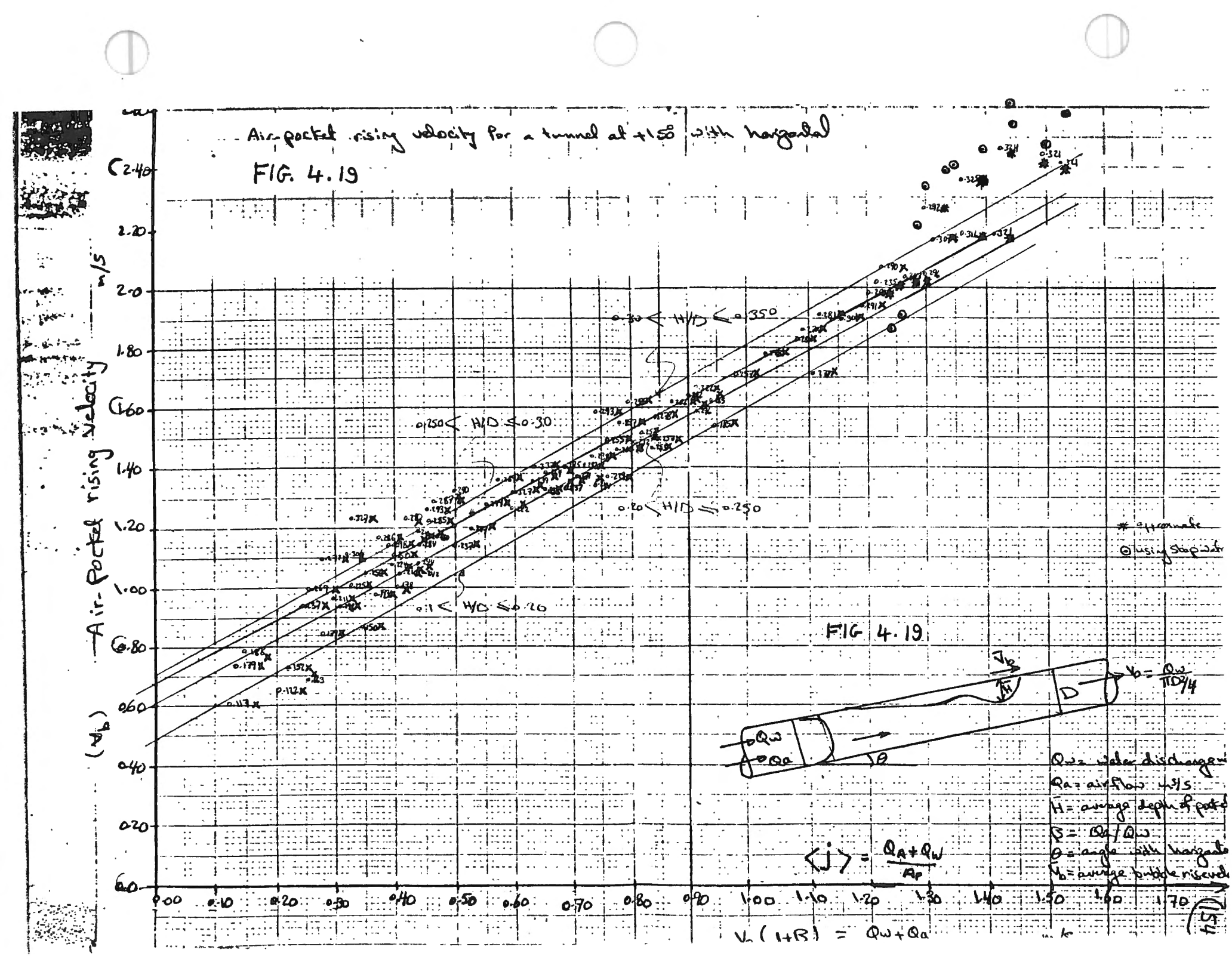

Section 4.3. Analysis of air pocket 'blow-back' and cleaning conditions for downward sloping pipes

In Sections 5.1 and 5.2 we will investigate experimental evidence for blow-back and cleaning conditions for air pockets at a dropshaft/tunnel junction (5.2) and downward sloping pipes (5.1). Both scenarios are sketched below, and in each case the air pocket may remain stationary, blow backwards against the flow, or be cleared downstream with the flow.

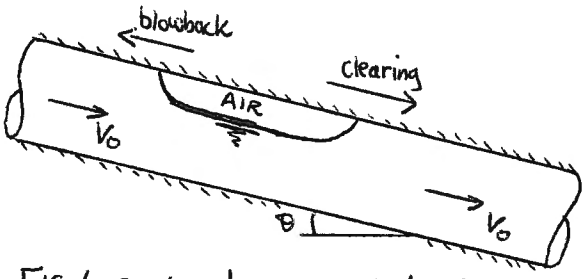

FIG 4.20 (a) downward sloping pipe

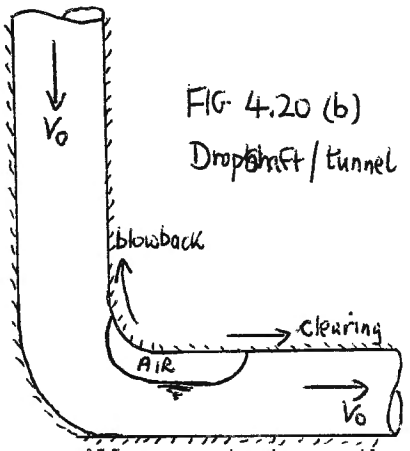

FIG 4.20 (b) Dropshaft/tunnel junction

For the case of the dropshaft/tunnel junction we will concentrate on the work of Townson (Ref.), Golding (Ref.) and Ervine and Himmo (Ref.) in Section 5.2.

For the case of high points and downward sloping pipes we will concentrate on the work of Kalinske and Robertson (Ref.), Kalinske and Bliss (Ref.), Edmunds (Ref.), Gandenberger (Ref.), Wisner et al (Ref.), Kent (Ref.), Sailer (Ref.) and Golding (Ref.), in Section 5.1.

In this section it is intended to explore a slightly more fundamental approach to the problems of blow-back and cleaning, although this may prove somewhat speculative in nature.

Blow-back

The author proposes below a tentative scheme to predict air pocket blow-backs in a straight downward sloping pipe, where the air pocket is formed by a coalescence of entrained air bubbles, downstream of a hydraulic jump, for instance. Air bubbles are assumed to be uniformly distributed passing section OO_1 and are assumed to have coalesced into the air pocket at a distance L_1, as shown in Fig. 4.21. The water velocity averaged over the entire pipe area is V_o, but is modified to account for the volume occupied by air bubbles to give a velocity $\frac{V_o}{1-\alpha} = V_o(1+\beta)$, where β is the ratio of air to water. The air pocket is assumed to be stationary, but on the point

of blow-back, so that it might take up a shape similar to that sketched. The velocity to be calculated V_o is, therefore, the velocity required to keep the air pocket stationary, and velocities less than this would allow blow-back to occur. Two methods of analysis which might be employed are (i) simplified energy method and (ii) force/momentum balance

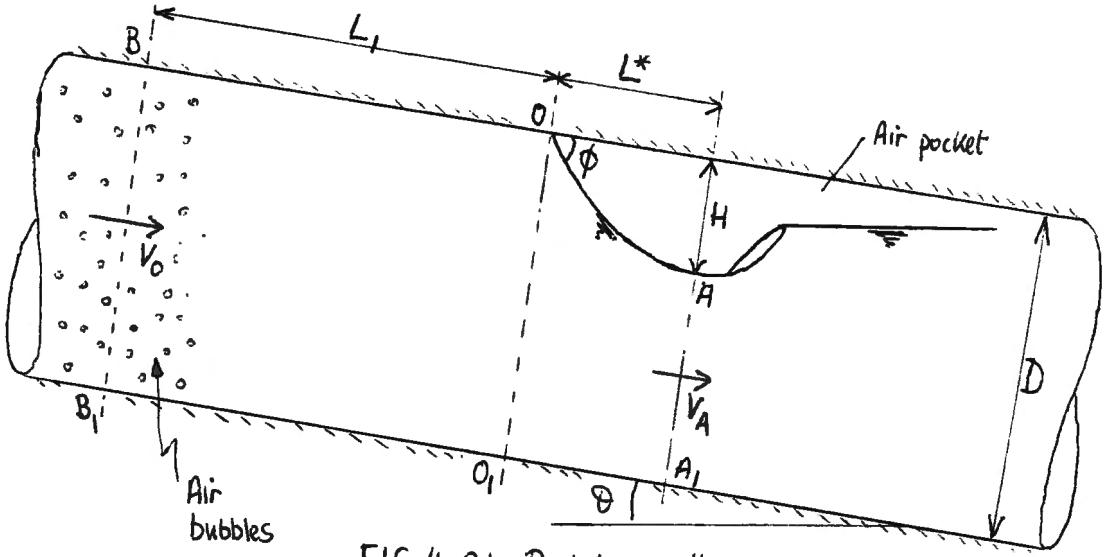

FIG 4.21 Pocket on the point of blowback.

(1) Simplified energy procedure

Assuming no energy loss occurs between O and A on the air pocket surface (energy loss is concentrated in the jump) and assuming that Point O is a stagnation point, we may apply Bernoulli between these two points. If the pocket length between O and A along the pipe is L* and the pocket depth normal to the pipe wall is H, then the vertical distance between O and A is given by $H\cos\theta + L^*\sin\theta$. The application of Bernoulli assuming the same air pocket pressure at O and A gives

$$H\cos\theta + L^*\sin\theta + \frac{0}{2g} + \frac{P_{air}}{g} = 0 + \frac{V_a^2}{2g} + \frac{P_{air}}{g} \qquad \text{.....(4.45)}$$

which becomes

$$\frac{V_A^2}{2g} = H\cos\theta + L^*\sin\theta \qquad \text{.....(4.46)}$$

If we now apply continuity between BB_1 and AA_1, with a distribution of air bubbles at Section BB_1 we obtain

$$V_o(1+\beta)\,A_p = V_A\,A_A \qquad \text{.....(4.47)}$$

where A_p is the full pipe area, and A_A the area of flow at Section AA_1 A_A is dependent on H/D, and is given by $A_p\,(1 - \frac{a}{180} + \frac{\text{Sin}2a}{2\pi})$, as already discussed under the work of Bacopolous in Section 4.2. Combining equations (4.46) and (4.4) we obtain

$$\frac{V_o(1+\beta)}{\sqrt{gD}} = \frac{A_A}{A_p}\sqrt{2\,H/D\,\text{Cos}\theta + \frac{2L^*}{D}\,\text{Sin}\theta} \qquad \text{.....(4.48)}$$

where A_{A/A_p} is given by $1 - \frac{a}{180} + \frac{\text{Sin}2a}{2\pi}$. (a is defined in Fig 4.15)

This relationship when solved for a range of H/D values (and hence A_A/A_p values) will give the water velocity required to keep a pocket from blowing-back in a straight downward sloping pipe. The main point of difficulty is an estimation of the value of L^*/D. Using the reasoning of Bacopolous that the curve OA is a parabola with vertex at A and passing through O, making an angle ϕ at that point. It can be shown that

$$L^*/D = 2\,H/D\;\;1/\tan\phi \qquad \text{.....(4.49)}$$

A value of ϕ proposed by Von Karman and also Benjamin is 60°, whereas visual observations (photographic) reveal the angle of the nose often to be less than 60°. If we simply assume $\phi \sim 60^\circ$ meanwhile, then $L^*/D \sim 1.15\,H/D$. The author has used equation (4.48) for conduit angles up to 30° and for values of H/D between 0.1 and 0.5, to predict the velocity (or Froude Number) required to keep an air pocket stable. The result, using the energy equation and $\phi = 60^\circ$, is shown on Fig. 4.22 by the dashed line, revealing that for downward sloping pipes $\theta < 30^\circ$, for typical air pocket depths $0.1 < H/D < 0.5$, a Froude Number of the region of $0.5 \rightarrow 0.7$ is required to keep an air pocket from blowing-back. This is a first order estimate showing that blow-back conditions are strongly dependent on the cavity depth H/D and the conduit slope θ. Fig. 4.22 does obscure possible variations in the angle of the nose of the air pocket ϕ. For steeper conduit slopes it is quite possible the ϕ may reduce from 60°. If we take an extreme reduction in ϕ say from 60° to 30° then from equation (4.49), L^*/D will increase from $1.15\,H/D$ to $3.46\,H/D$. When this is substituted into the energy equation we obtain much higher values of the Froude Number required to prevent blow-back in a straight downward sloping pipe. In fact, a wide range of values of $V_o/\sqrt{gD}$ can be obtained, depending on the choice of ϕ, θ, and H/D.

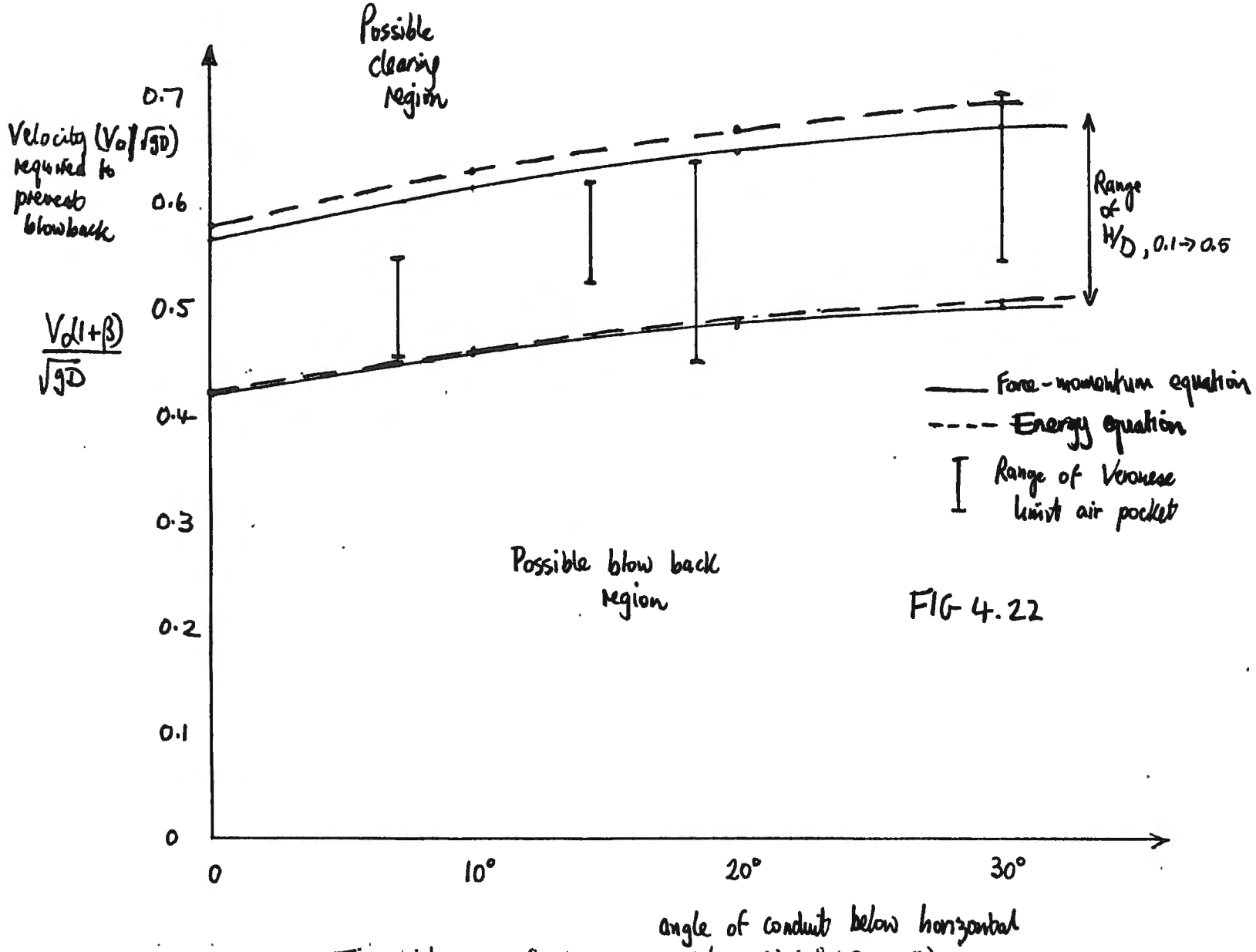

FIG. 4.22

FIG. 4.22 Theoretical curves for blow-back ($\phi = 60°$) ($0° < \theta < 30°$)

(ii)

The author has also analysed this situation using a force/momentum balance and continuity between BB_1 and AA_1 combined with Bernoulli applied between B and O. The analysis is similar to that of Bacopolous (Section 4.2) and reveals a solution for the Froude Number required to prevent an air pocket from blowing back in the form

$$\left(\frac{V_o}{\sqrt{gD}}\right)^2 = \frac{\cos\left(1-{}^{A}/_{A_P}\cos a-{}^{2}/_{3}\ \sin^3 a\right) + \left(\text{Wt. water from } OO_1 \text{ to } AA_1 / \rho g A_P {}^{D}/_{2}\right)}{(1+\beta)^2\ \left(2({}^{A_P}/_{A_A})-1\right)} \qquad \text{.....(4.50)}$$

Further details may be obtained from the author, but the result is shown on Fig. 4.22 represented by the solid lines for $0.1 < {}^{H}/_{D} < 0.5$, and for a constant angle of the front nose of the cavity $\phi = 60^\circ$. The theoretical curves presented on Fig. 4.22 are in close agreement with the "limit bubble" data of Veronese and in the same region as the void removal and blow-back data plotted by Golding and shown on Fig.5.

Clearing

In the section above, the velocity (or Froude Number) required to keep an air pocket stable or from "blowing-back" was discussed. It might be postulated that velocities higher than this would cause clearing of the pocket downstream along the conduit. The problem is more complicated than this, for the reasons outlined below.

(1) The velocity required to clear an air pocket (V_c) must be somewhat greater than the velocity required to hold the air pocket from blowing-back. This is due to the fact that an air pocket must change shape before clearing, as shown below

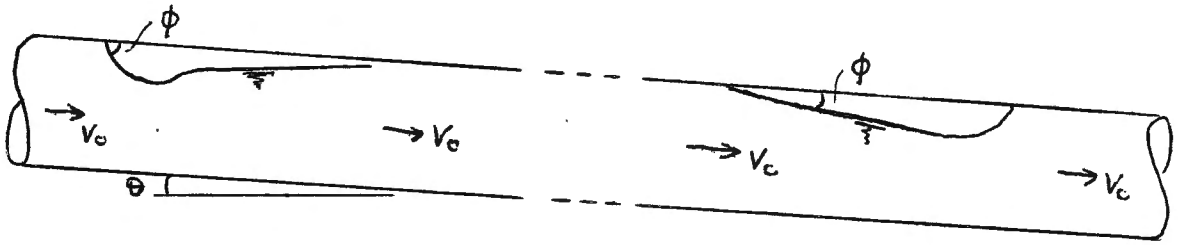

Fig. 4.23 (a) Pocket stationary but on the point of blow-back.

Fig.4.23 (b) pocket stationary, but on the point of clearing.

The nose of the cavity facing the oncoming flow must flatten, so that $\phi < 60^\circ$ for clearing. We have already used the energy principle for blow-backs

($\phi \simeq 60^\circ$), illustrating that the blow-back velocity is a function of H/D, θ and ϕ. Suppose that the energy principle can be used for clearing, this time with $\phi < 60^\circ$ with the nose facing the oncoming flow still approximating to a parabola of shape $L/D = 2/\tan\phi . H/D$. This is put forward without much justification. If we assume, as an order of magnitude, that ϕ reduces to 30° say, then $L/D \simeq 3.46\ H/D$, and the energy equation for clearing becomes

$$\frac{V_c}{\sqrt{gD}} = \frac{A_A}{A_p}\sqrt{2\ H/D \cos\theta + 3.46\ H/D \sin\theta} \quad \ldots\ldots\ldots\ldots\ldots\ldots (4.51)$$

where H is the maximum cavity depth and A_A is the area of flow under the cavity at this point. The author has calculated $V_C/\sqrt{gD}$ for various conduit slopes θ, with the result shown on Fig. 4.24 for $H/D = 0.1$ and $H/D = 0.3$. Equation (4.51) is also compared with experimental data from Kent, Wisner and Gandenberger. For $H/D = 0.3$, the equation is very similar to the data of Kent, and is practically identical to the median value of Wisner's data. Gandenberger's data for larger air volumes (say $n > 0.5$) corresponds approximately to $H/D \sim 0.2$. Clearly it is possible to use Equation (4.51) to correlate any experimental cleaning velocity data, depending on the choice of ϕ and air pocket depths, H/D. A question which remains, can ϕ or H/D be predicted for any experimental set-up? This is presently being investigated.

(11) Air pocket clearing downstream in a downward sloping pipe is further complicated by concept of partial clearing by hydraulic jump entrainment at the downstream end of the air void. This is illustrated in the sketch below, Fig. 4.25. It is often the case with substantial upstream Froude numbers $V_o/\sqrt{gD}$ and larger air pocket depths (H/D), that the Froude Number under the air pocket $V_1/\sqrt{gA/B}$ is greater than one, a hydraulic jump forms, and air is carried out of the jump by entrainment. The entrained air may further coalesce at some point downstream but may well be transported because the values of H/D are much smaller than the main air pocket. See Equation (4.51). When this occurs, and the main air pocket is not fed with air transport from upstream, then the cavity may reduce in size until it's H/D value is small enough for the pocket to be clear bodily. The rate of air transport from the jump may be calculated either from Kalinske and Robertson's equation, Thomas equation or the Ervine and Ahmed equation, all discussed in Sections 3.2 and 3.3. This type of entrainment will cease when the Froude

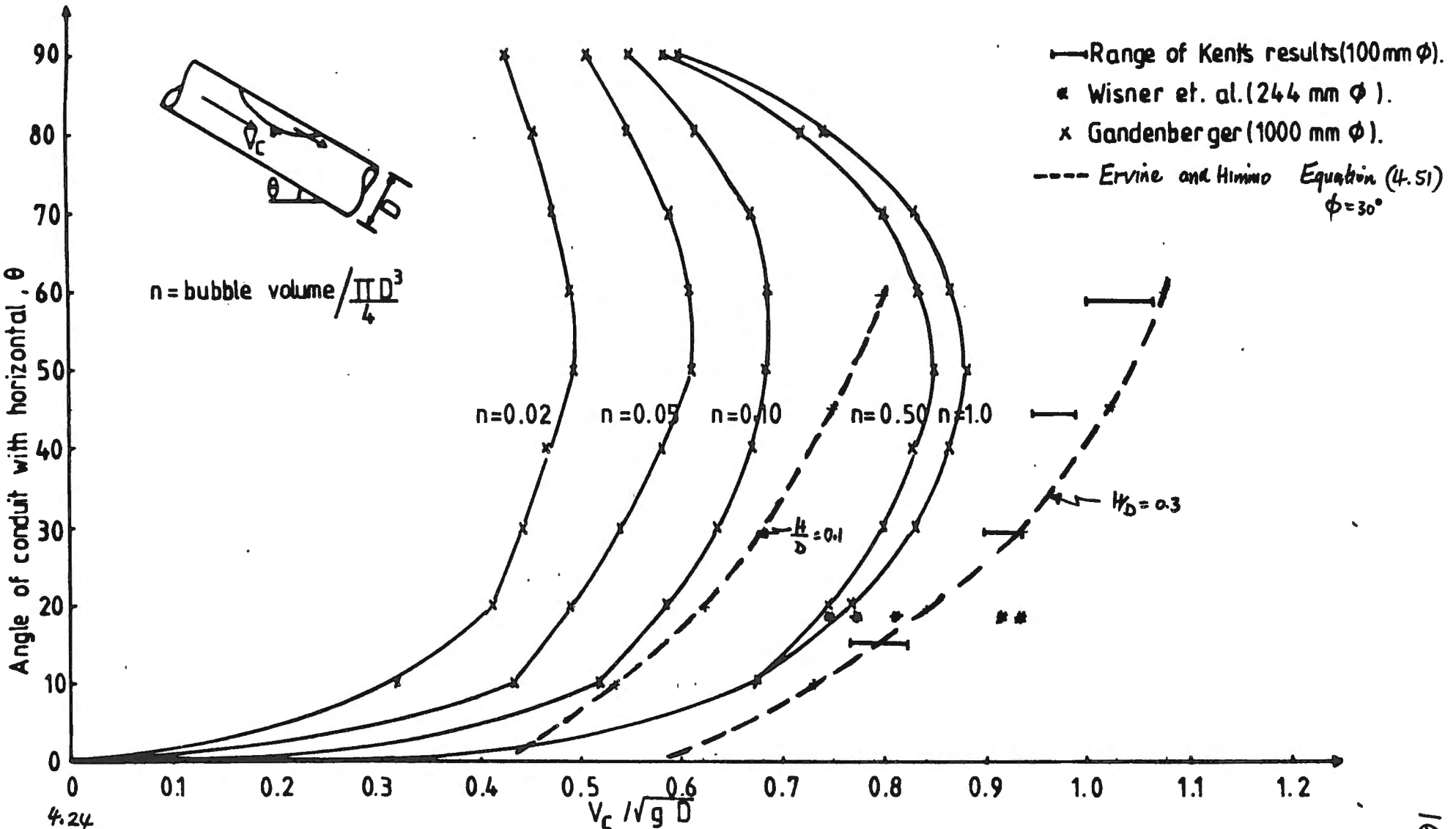

4.24

FIG(8) Non-dimensional water velocities required to clear an air pocket downstream in a pipe sloping at θ° below the horizontal. (ERVINE & HIMMO)

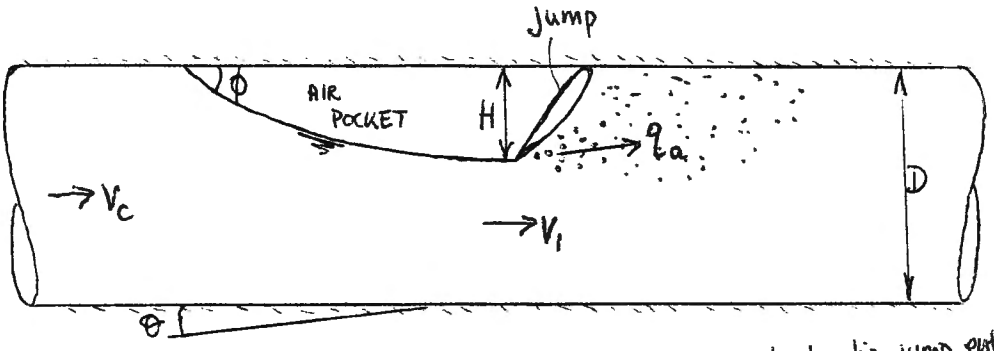

$q_a/q_w = \beta \propto (Fr_1 - 1)$

where $Fr_1 = V_1/\sqrt{gA_1/B_1}$

FIG. 4.25 Clearing by hydraulic jump entrainment

Number under the pocket <1, and removal of the pocket may then proceed in the manner described in (i), using the energy equation (4.51).

SECTION 5

AIR POCKET FLOWS - Experimental evidence and empirical relationships.

5.1. Air pocket blow-back and clearing in downward sloping pipes.

5.2. The formation, blow-back and clearing of air pockets forming at dropshaft/tunnel junctions. Analysis and experimental evidence.

Section 5.1. Air pocket blow-back and clearing in downward sloping pipes

The type of air pocket formation to be discussed in this section is illustrated in Fig. 5.4(a)-(c). In (a), pockets may form downstream of a hydraulic jump due to the coalescence of small air bubbles, and the resultant air pockets may 'blow-back' towards the jump, remain stationary or clear downstream. In (b) a pocket may form at a high point in a pipe-line or siphon and removal of the pocket might proceed either by entrainment of air at a jump, or the bodily sweeping out of the pocket. In (c), a stationary or equilibrium void might occur, where buoyancy and drag forces are in balance.

Several experimenters have investigated clearing of air pockets, but, to the authors knowledge, no investigation to date has been set up specifically to look at air pocket blow-back. When blow-back has been mentioned in past experiments, it usually features as a side-effect, with an inadequate set of flow parameters for detailed analysis.

Some photographs are presented overleaf, Fig. 5.1, 5.2 and 5.3, illustrating air pocket clearing and blow-back in a downward sloping pipe with angle 1.5° below the horizontal. Fig. 5.1 illustrates how an air void might be removed by the gradual entrainment of air at the downstream end of the void. Fig. 5.2 shows a typical small air void being swept along the conduit in the same direction as the flow. Fig. 5.3 shows small air pockets blowing-back against the direction of the flow. In many cases, whether sweeping out or blowing back, a small breaking wave often exists at the downstream end of the pocket. The purpose of this section, therefore, is to determine the conditions and flow parameters which lead to the various modes of air pocket behaviour.

Blow-backs and clearing in downward sloping pipes - experimental evidence

This problem has been recently reviewed by Goldring (Private Communication - Feb.1985) in which he states that the specific problem of blow-back has received little or no attention. Most of the work is concentrated on either air entrainment or air pocket removal in downward sloping pipes. Goldring highlights three types of experiments which have been carried out, as shown on Fig. 5.4. Fig. 5.4(a) is the only one where the flow parameters at blow-back were measured and published, Fig. 5.4(b) relates to experiments designed to determine the flow parameters to remove an air pocket from a high point in a pipe line and, Fig. 5.4(c) relates to flow parameters designed to keep an air pocket stationary.

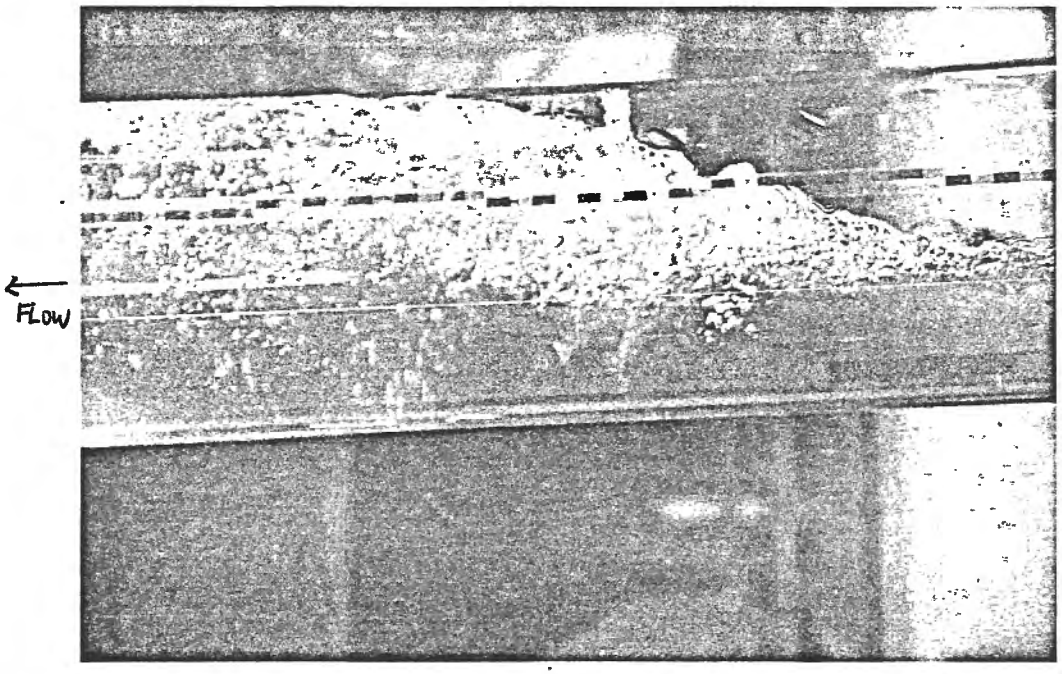

FIG-5.1 Partial clearing of deep air void by hydraulic jump entrainment
Pipe sloping downward 1.5°

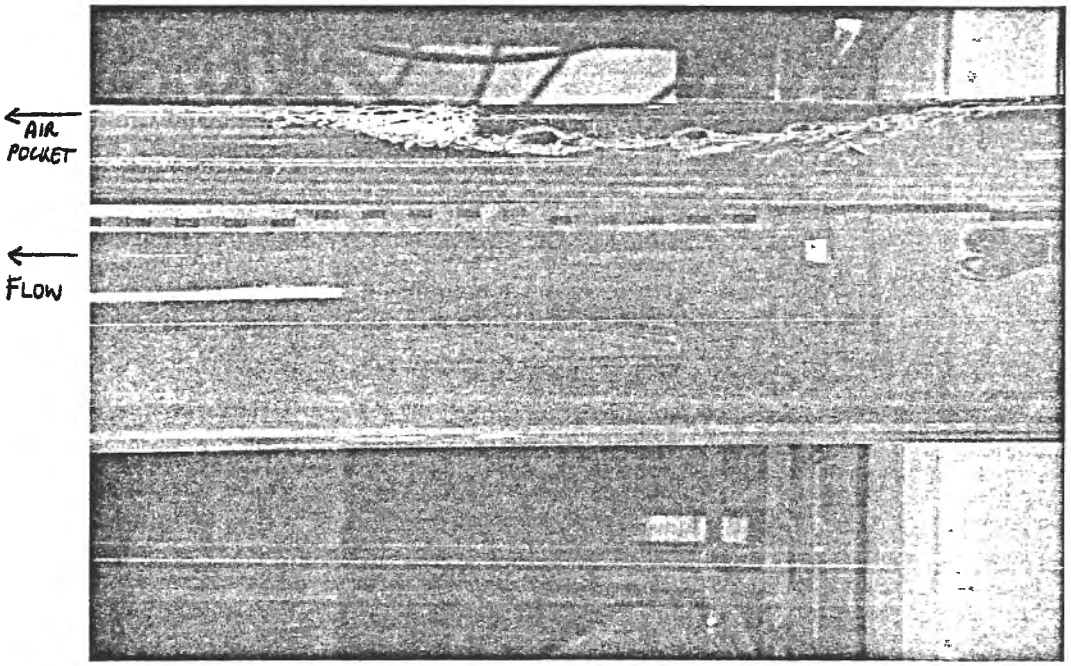

FIG-5.2 Air pocket sweeping out of downward sloping pipe ($\theta = 1.5°$)

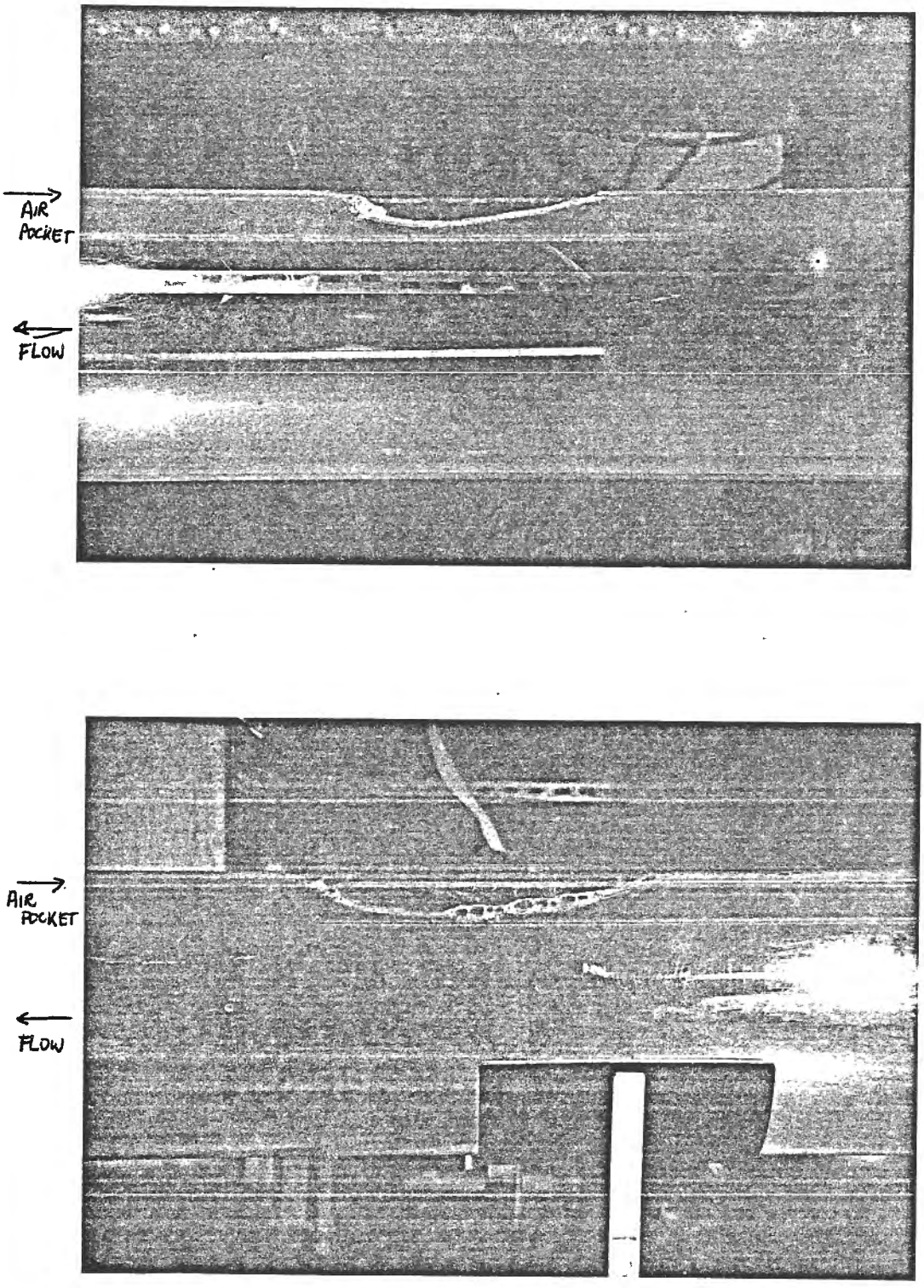

FIG-5.3 Small air voids "blowing-back" up a downward sloping pipe ($\theta = 1.5°$)

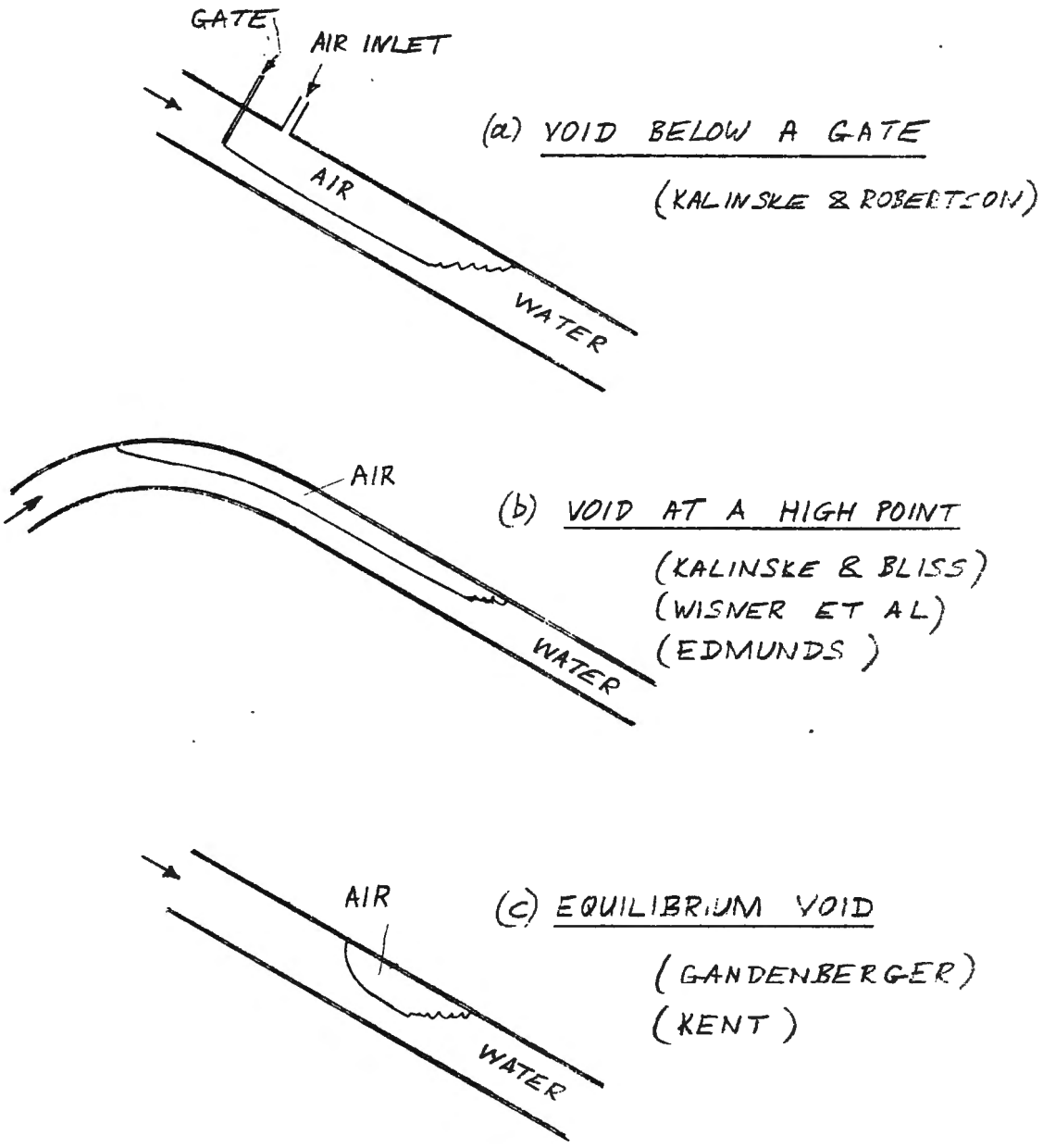

FIG. 5.4 AIR VOID CONFIGURATIONS (Goldring)

The earliest reference to "blow-back" is highlighted in a paper by Kalinske and Robertson (Ref.), while investigating the air entraining capacity of a hydraulic jump formed downstream of a gate in a downward sloping circular pipe ($\theta \leq 16.7^{\circ}$) and pipe diameter 0.15 m. "The air pumped by the jump would form a large bubble just beyond the jump..... periodically this large bubble would blow out over the jump.....". They show a graph, Fig. 5.5, which is a plot of the fractional depth $Y_{1/D}$ and the Froude Number just upstream of the jump $V_1/\sqrt{gA_{1/B_1}}$, below which only a fraction of the entrained air would be transported. We may assume that blow-backs occur up to this limiting Froude Number. As the fractional depth ($Y_{1/D}$) has been specified, we may translate this limiting upstream Froude Number, Fr_1, into a limiting pipe-full Froude Number $V_o/\sqrt{gD}$ <u>below which</u> blow-backs will occur. This is shown on Fig. 5.6 and compared with the authors theoretical equation for blow-back Eqn. 4.48 and 4.49 with ϕ constant at 60°. The data of Kalinske and Robertson represents an upstream fractional depth of 0.15 and 0.3 respectively.

It can be seen from Fig. 5.6 that the authors energy equation for $\phi = 60^{\circ}$ is generally an underestimate of the limiting Froude Number for blow-back except for very shallow conduits, say $\theta < 1^{\circ}$. The reason for this must be related to the author's naive energy model, where the length of the cavity L* to the point of maximum cavity depth H, (see Section 4.3) is assumed in this case to be $L^*/D = 2^{H}/_{D}\ ^{1}/_{\tan\phi}$, where ϕ is the angle of the cavity nose to the pipe wall. (60°). A good correlation with Kalinske and Robertson's data can be achieved by the simple expedient of increasing L* in the energy equation (4.48), by reducing ϕ from 60° to somewhere around $30\text{-}40^{\circ}$. Unfortunately, Kalinske did not provide enough data on the shape, depth and length of the air cavity downstream of the hydraulic jump to provide a meaningful comparison with theory. It is of interest to note, however, that the limiting Froude Number $V_o/\sqrt{gD}$ increases with the upstream fractional depth, $Y_{1/D}$, as shown on Fig. 5.6 for the cases $Y_{1/D} = 0.15$ and $Y_{1/D} = 0.3$. According to Kalinske's data, when $Y_{1/D} = 0.15$, $Fr_1 \sim 15\text{-}20$, and the air/water ratio approaching the air cavity should be around 0.3-0.4. When $Y_{1/D} = 0.3$, $Fr_1 \sim 5\text{-}7$ and the ratio of air to water for 0.06-0.1. If we now return to the full energy Equation (4.48), it has been shown that

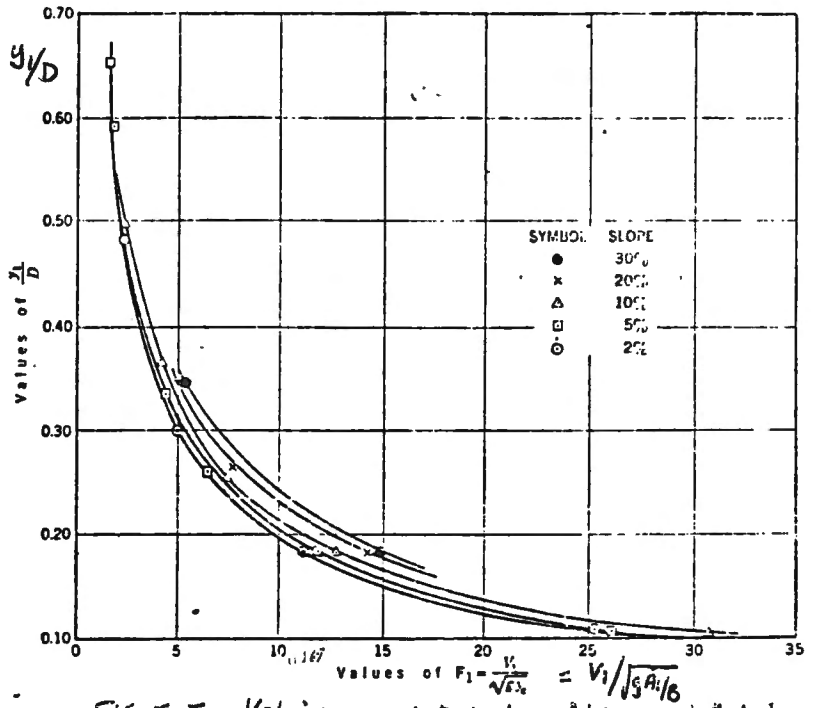

FIG 5.5 Kalinske and Robertson "blowback" data

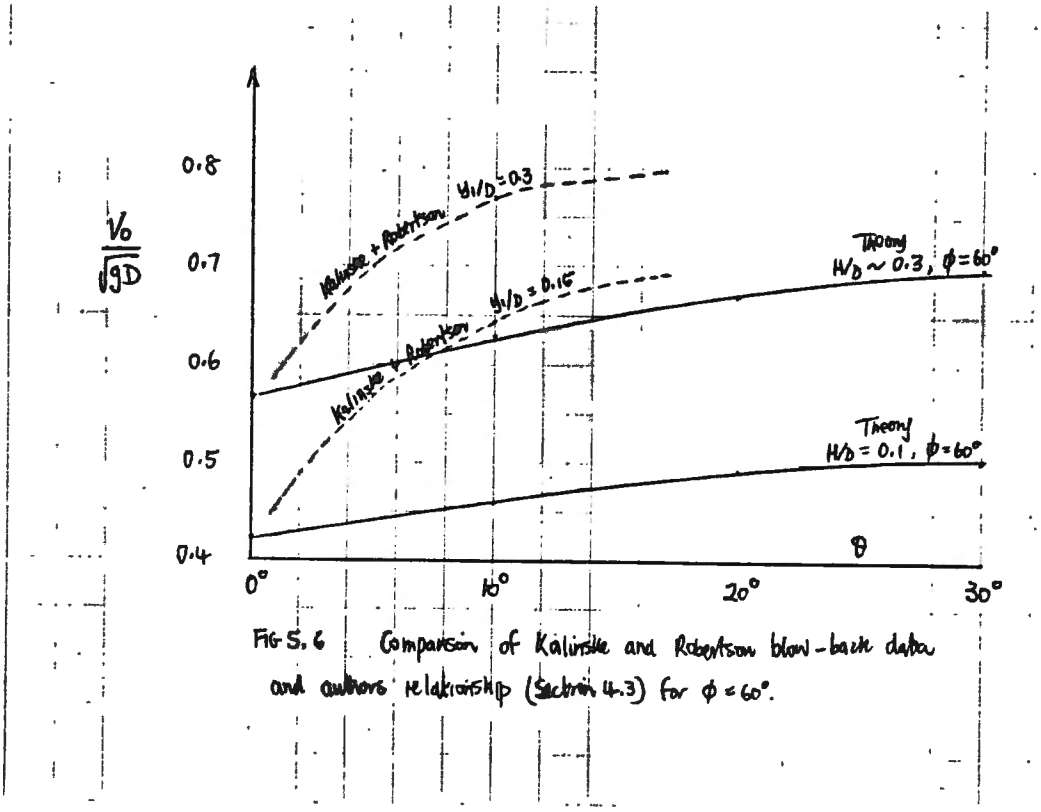

FIG 5.6 Comparison of Kalinske and Robertson blow-back data and authors relationship (Section 4.3) for $\phi = 60°$.

$$\frac{V_o(1+\beta)}{\sqrt{gD}} = \frac{A_A}{A_p}\sqrt{2^{H}/_{D}\cos\theta + 2^{L^*}/_{D}\sin\theta} \quad \text{.....(5.1)}$$

indicating that the limiting blow-back Froude number will decrease with increasing β. In this particular case, $V_o/\sqrt{gD}$ should ratio on $(1 + 0.35)/(1 + 0.08) \sim 1.25$, which is approximately the case for the two values of $Y_1/_D$ shown. Clearly a more definite study of blow-back is required before the influence of the upstream air/water ratio, the cavity depth $H/_D$, the cavity length $L^*/_D$ and the angle of the cavity nose ϕ can be properly ascertained. The important point meantime, is that Kalinske and Robertson propose that blow-back will occur when the Froude Number is less than the limiting Froude Number.

This is in sharp contrast to the findings of Sailer (Ref.) who reported that the U.S.B.R. had analysed the flows in the downslopes of 21 different siphons ranging from 0.61 m to 2.82 m diameter. The results were plotted on the same graph as Kalinske and Robertson (Fig. 5.7), indicating that blow-backs occurred when the flowing Froude Number was greater than the limiting Froude Number, whereas conditions, on, or less than Kalinske and Robertson's curves did not produce blow-back. Goldring has translated Sailer's upstream Froude Numbers into pipe-full Froude Numbers $V_o/\sqrt{gD}$, and has proposed, tentatively, as shown on Fig. 5.8, that Sailer's blow-back problems were confined to flows where the pipe-full flow is supercritical, and hence it is not possible for a hydraulic jump to form. ($V_o/\sqrt{gD} > 1$). If the hydraulic jump cannot form at the downstream end of the air pocket, then the pocket cannot even partially clear by air entrainment, and hence it is probable that an air pocket in the downstream leg of the siphon would develop a large cavity depth $H/_D$, a long length $L^*/_D$, and would only be removed by bodily sweeping. This is the worst possible condition and a warning perhaps to avoid supercritical pipe-full flows if possible. Sailer did not have any problems with blow-backs in sub-critical pipe full flow as illustrated by points marked Δ on Goldring's graph (Fig. 5.8).

Kalinske and Bliss (Ref.) investigated air void removal from a high point in a pipeline as shown on Fig. 5.4. Two pipes of 0.1 m and 0.15 m diameter were used and downward slopes up to 8.5° were tested. Their data line is shown on Goldring's graph (Fig. 5.8) and essentially represents an equilibrium air-void line above which air pockets would be removed downstream. Their work was similar to the previous work of Kalinske and

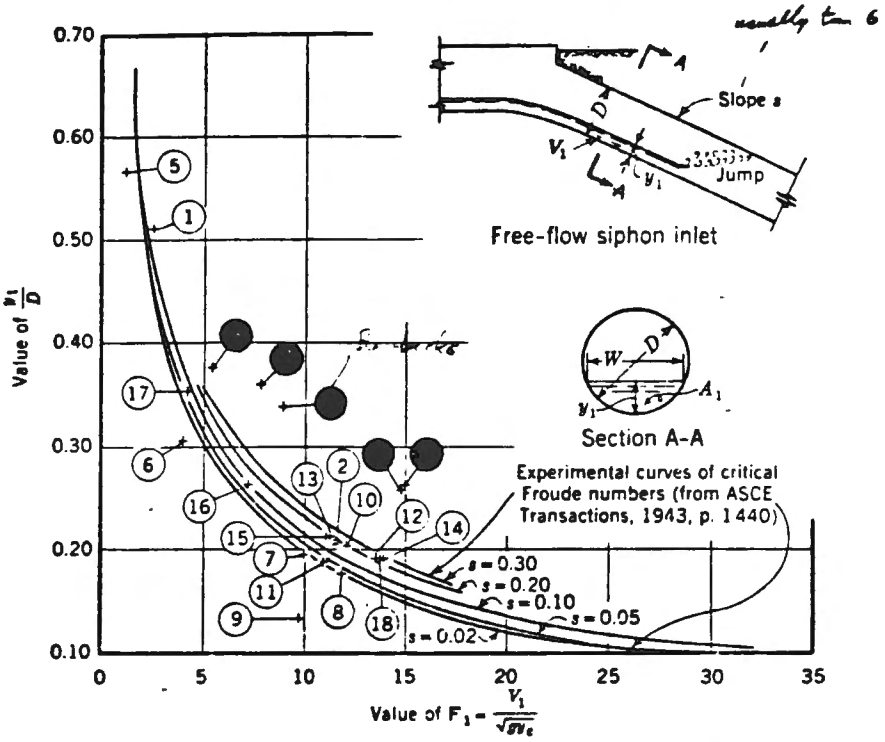

FIG 5.7. Sailers data for "blow-backs"
(Problems with blowbacks indicated by dark circles)

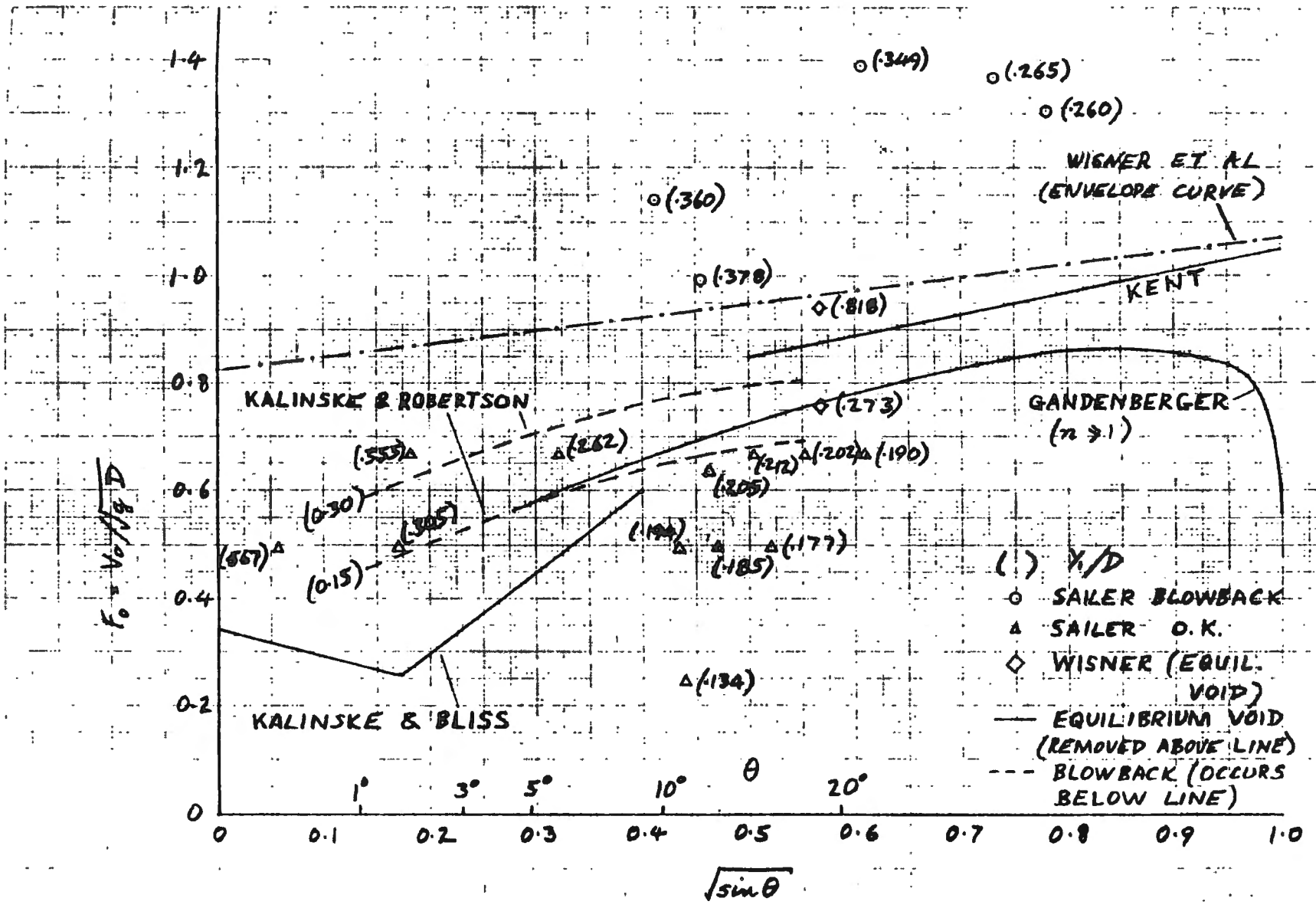

FIG. 5.8 VOID REMOVAL AND BLOWBACK IN CIRCULAR PIPES (Goldring)

Robertson, except that fractional depths $Y_{1/D}$, were not controlled by a sliding gate mechanism. They employed a simplified drag/buoyancy relationship to show that the velocity required to clear an air pocket downstream could be given by

$$\frac{V_c}{\sqrt{gD}} = \sqrt{\frac{KS}{C_d}} \qquad \text{.....(5.2)}$$

where K is a constant, S the downstream slope of the pipe and C_d the drag coefficient of the water on the air pocket. This relationship was used by Kalinske and Bliss to show that if C_d could be considered constant, then the clearing Froude Number would be proportional to $\sqrt{\tan\theta}$ or $\sqrt{\sin\theta}$.

Unfortunately, Kalinske and Bliss did not produce enough data on Fractional depths, upstream Froude Numbers, shape and size of air pockets, etc. to make a detailed analysis. We are simply left with the curve shown on Fig. 5.8 and to speculate on the obvious questions of (i) why smaller Froude Numbers are required for clearing than the blow-back Froude Number data of Kalinske and Robertson, and (ii) why their data does not coincide with comparable data of Gandenberger, Kent, etc.

Kalinske and Bliss indicate that a hydraulic jump occurred at the downstream end of the upper air void, entraining air and transporting along the sloping conduit. If the conduit is relatively short, then a large or substantial proportion of air may have been transported in the form of small bubbles (as in Sections 2 and 3), although it is clear that secondary air voids did occur downstream of the jump, and were responsible for blow-backs into the upper air void. This type of bubbly mixture transport (if it did occur) does not scale on Froude Number $V_o/\sqrt{gD}$, as the size of bubbles produced at the plunge point are similar in model and prototype. The bubble transport phenomenon is dependent on absolute velocities, whereas air pocket transport scales on Froude Number. What happens if a mixture of the two types of transport occurred, not only with Kalinske and Bliss but also Kalinske and Robertson?

Suppose, hypothetically, that small air bubble transport was dominant, then according to Thomas (Ref.) the upstream jet velocity to transport air might be given by $U_{1min}/U_{br} \simeq \cos\theta/\mathcal{E}$, where $\mathcal{E}$ the turbulence intensity is say $1/20 \rightarrow \frac{1}{4}$. For small angles $\cos\theta \rightarrow 1$ and we find $U_{1min} \simeq 4 \rightarrow 20 U_{br}$, or U_{1min} anywhere from 1 to 5 m/s. The pipe full velocity to transport air is then given by $V_o = U_1 A_{1/A_p} = f(U_1 Y_{1/D})$, and thus will increase with

increasing fractional depth. This is illustrated for the data of Kalinske and Robertson, Fig. 5.9, for Y_1/D varying from 0.1 to 0.5. For bubbly mixture transport only, $V_o/\sqrt{gD}$ will vary with varying conduit dimension D, as V_o remains constant for a given θ and Y_1/D value irrespective of the conduit dimension.

The other end of the spectrum requires that all air transport is in the form of air pockets and will thus scale on a Froude Number $V_o/\sqrt{gD}$. The main effect of Y_1/d would then be the amount of air entrained by the jump, β, and its effect on possible blow-back conditions. That is, small Y_1/D values generally correspond to high upstream Froude Numbers, Fr_1, corresponding to high β values, corresponding to lower blow-back Froude Numbers. A secondary effect might be the positioning of the secondary air pocket downstream of the wake of the jump.

Thus we cannot make definitive analyses of this work as details of the mode of air bubble transport are not given. It is surprising that the Kalinske and Bliss data falls on one curve, and may be an indicator that only a small range of values of Y_1/D were obtained for the limiting Froude Number, and also that these values of Y_1/D would appear to lie in the region of 0.05 to 0.2 as shown on Fig. 5.9. As already pointed out, Kalinske and Bliss had no control of Y_1/D values.

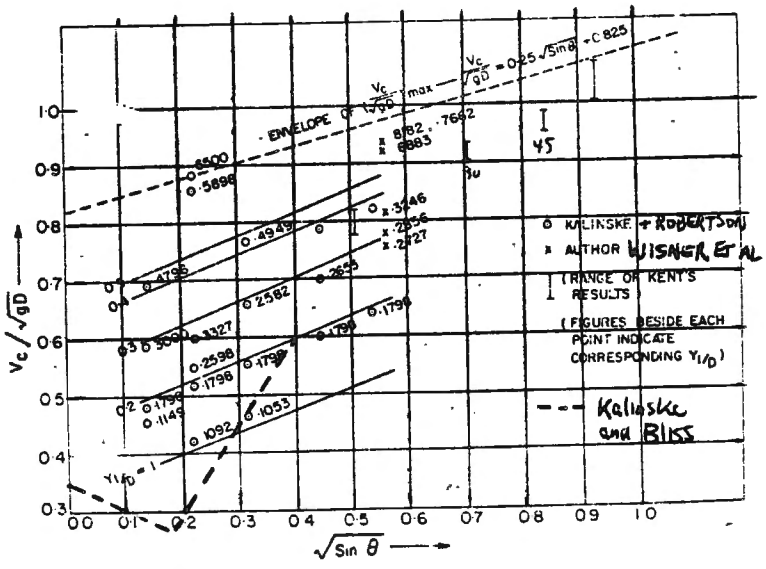

FIG 5.9

Extrapolation of the Kalinske and Bliss curve beyond 8.5° slope is not advisable as it is not clear how the limiting Froude Number varies with the fractional depth Y_1/D, for steeper angles.

Kent (Ref.) carried out an experimental study of air pocket movements in a 4" diameter (0.1 mØ) downward sloping pipe at angles ranging from 15° to 60°. The type of experiment is essentially the equilibrium void type as shown on Fig. 5.4(c), and the emphasis rests on the pipe-full water velocity required to keep the air void stationary. Velocities greater than this limiting value would cause the air void to move downstream.

Using a buoyancy-drag analysis, Kent proposed,

$$(\rho_w - \rho_a)\, g \forall \sin\theta = \tfrac{1}{2} C_d A^1 \rho_w V_o^2 \qquad \text{.....(5.3)}$$

where $\forall$ is the air pocket volume

θ is conduit angle

A^1 is the area of the pocket exposed to the oncoming flow

C_d is a drag coefficient

V_o is the velocity required to keep the pocket stationary.

Assuming that $\forall/A^1$ is proportional to the air pocket length L, which in turn has geometric similarity with the conduit dimension D, Equation (5.3) reduces to

$$V_o = K\sqrt{gD \sin\theta} \qquad \text{.....(5.4)}$$

where K is a function of the drag coefficient and given by Kent to be equal to $1.62\sqrt{\xi}$. The value of ξ is 0.58 for air pocket lengths greater than $L/D > 1.5$. That is, for longer air pockets, $L/D > 1.5$, Equation (5.4) becomes,

$$V_o \simeq 1.234\sqrt{gD\sin\theta} \quad \text{or} \quad \frac{V_o}{\sqrt{gD}} \simeq 1.234\sqrt{\sin\theta} \qquad \text{.....(5.5)}$$

This is an approximate fit to Kent's data, which is illustrated on Fig. 4.24, Fig. 5.8 and Fig. 5.9. Kent's data for air pockets of $L/D \geq 1.5$, differs from other data in the sense that it does not indicate a broad range of equilibrium Froude Numbers corresponding to a range of fractional depths under the air pocket Y_1/D. One can only assume that Y_1/D just upstream of the jump did not vary significantly, otherwise a wider spread of results would have occurred. The other important point is that for a conduit angle of 60°, Kent required supercritical pipe-full Froude Numbers to keep the pocket stationary. It must be re-emphasised here, that a hydraulic pump is

unlikely to occur at the downstream end of the air pocket in this case, and a different mechanism might be assumed to be operating.

In any case we are in a position to make use of the authors energy equation in Section 4.3 combined with an experimental observation of Kent. This observation is that the velocity required to hold the pocket stationary is independent of the pocket length once it exceeds a value of $L/D \geqslant 1.5$. The geometrical parameters are sketched on Fig. 5.10 below,

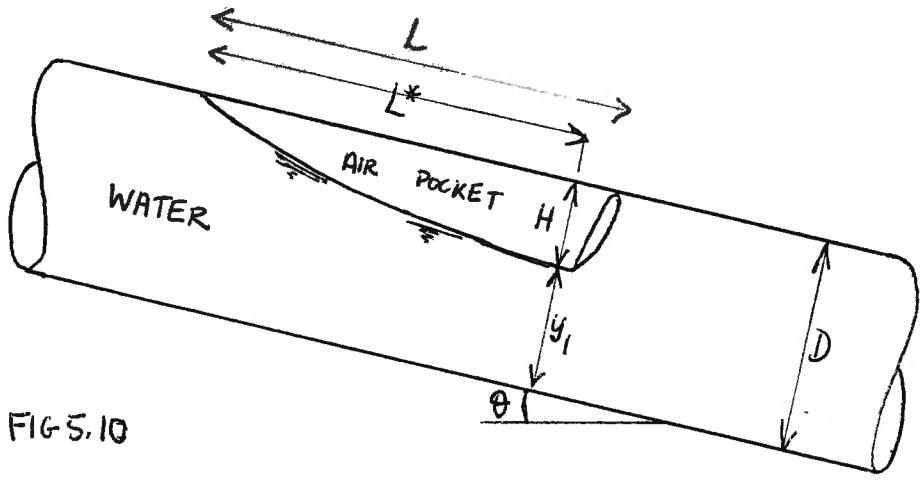

FIG 5.10

If we assume that L/D for Kent's air pockets is approximately equal to L^*/D required for the energy equation, i.e. L* is the pocket length from the upstream nose to the maximum cavity depth point H, then we might assume that $L^*/D \sim 1.5$ and the energy equation (4.48) (ignoring β meanwhile) is then given by,

$$V_o/\sqrt{gD} \simeq A_A/A_p \left(2\, H/D \cos\theta + 3 \sin\theta\right)^{\frac{1}{2}} \qquad \ldots\ldots\ldots\ldots\ldots\ldots (5.6)$$

A_A is the area of flow at the point Y_1.
Kent tested the angles $\theta = 15°, 30°, 45°$ and $60°$, but did not publish either H/D or Y_1/D at the downstream end of the void. However an approximate fit using Equation 5.6 is shown below for Kent's data using $H/D \sim 0{,}4$ and $L^*/D \sim 1{,}5$.

Using constant values of H/D and L^*/D is a crude approximation but it does illustrate (Fig. 5.11) that a close approximation to Kent's data may be obtained. Furthermore, the assumption of $H/D \sim 0.4$, implies $Y_1/D \sim 0,6$, and when comparing Kent's data with Kalinske and Robertson's data on Fig. 5.9 we see that Y_1/D of 0,6 is not an unreasonable mean estimate.

We can also see from Fig. 5.9 why Kent's data predicts apparently higher equilibrium Froude Numbers than Kalinske and Bliss. The flow depth parameter under the air pocket, Y_1/D, is much greater in the case of Kent's work, i.e. Kent must have been operating almost exclusively in the higher range of Y_1/D, say comparable to $Y_1/D > 0.5$ in Kalinske and Robertson's work, whereas Kalinske and Bliss appear to have been operating in the range $Y_1/D < 0,2$.

There is also some doubt over the form of Kent's empirical relationship $V_o/\sqrt{gD} = K\sqrt{\sin\theta}$, as it will grossly under-predict equilibrium Froude Numbers for small conduit angles and over-predict for angles approaching 90°. For the vertical conduit ($\theta = 90°$), Kent predicts an equilibrium Froude Number $V_o/\sqrt{gD} \sim 1,234$, whereas Martin (Ref.) and other authors have shown that air voids may clear vertically downwards at Froude Numbers $V_o/\sqrt{gD} > 0,7$.

Wisner, Mohsen and Kouwen (1975, Ref.) examined the removal of air from a downward sloping pipe at angle 18.5° and pipe diameter 0.244 m. Commencing with a dimensional analysis to determine the parameters governing the bodily sweeping out of an air pocket, they proposed the sweeping-out velocity in the form,

$$\frac{V_s}{\sqrt{gD}} = f\left(L/D, Re, \theta\right) \qquad \text{.....(5.7)}$$

and point out that the pocket length parameter L/D, might be replaced by the non-dimensional air volume, $n = \bar{V}/(\pi D^3/4)$. They also point out that Re (viscous effects) is not important when $Re > 10^5$. Equation (5.7) is over simplified in the sense (i) previous authors found surface tension effects more significant than viscous effects, and (ii) it is clear from the energy equation, that the cavity depth term H/D is just as significant as the cavity length term L/D, and it may be misleading to lump them both together in the form of an air volume. Therefore, bodily sweeping of an air pocket with no hydraulic jump at the downstream end of the pocket might be more accurately described by,

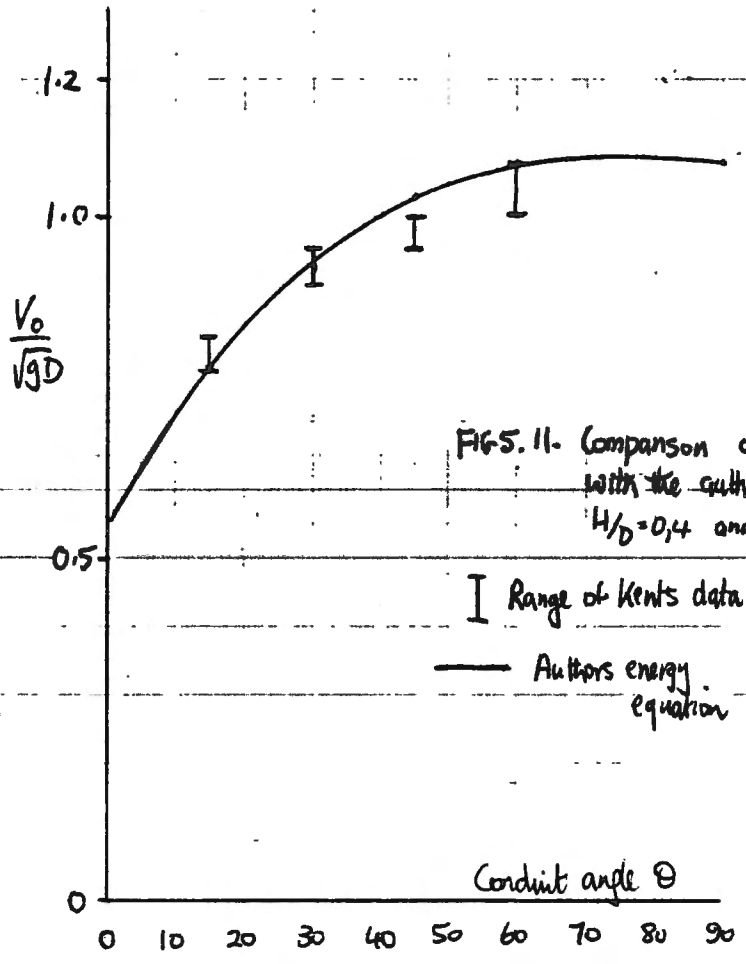

FIG 5.11. Comparison of Kents data with the authors energy equation $H/D = 0.4$ and $L_t/D = 1.5$.

$$\frac{V_s}{gD} = f\left({}^{L}/_{D}\,,\ {}^{H}/_{D}\,,\ \theta\,,\ \text{Re},\ \text{Wb}\right) \qquad \text{.....(5.8)}$$

For the case of air pockets clearing by a combination of air entrainment at a hydraulic jump at the downstream end of the pocket, together with an element of sweeping, we might propose,

$$\frac{V_c}{gD} = f\left({}^{L}/_{D}\,,\ {}^{H}/_{D}\,,\ \theta\,,\ \frac{V_1}{V_{br}}\,,\ \text{Re},\ \text{Wb}\right) \qquad \text{.....(5.9)}$$

Note that the fractional depth is not included, but is implicit in the term ${}^{H}/_{D}$. The term ${}^{V_1}/_{V_{br}}$, (water velocity just upstream of the jump over the bubble rise velocity), is included to account for undoubted scale effects associated with entrainment at the jump, giving a total of three possible scale effect terms, ${}^{V_1}/_{V_{br}}$, Re and Wb. Both Re and Wb will be insignificant for pipe diameters greater than 0.15 to 0.2 m. According to Kobus (Ref.) entrainment scale effects are negligible for $V_1 Y_1/\nu > 10^5$, where Y_1 is the flow depth at the upstream side of the jump. This reduces to $V_1 Y_1 > 0.1$. For a pipe say 0.2 m diameter, and the cavity taking up half the pipe depth, then $Y_1 = 0.1$ m, and V_1 would only have to be 1 m/s to satisfy the Kobus criterion. In the author's view, this is unreasonably low because of extensive detrainment out of the jump when $V_1 = 1$ m/s (see Thomas, Section 2.3). A more realistic criterion for negligible entrainment scale effects is likely to be $V_1 \simeq 2.5$ to 5 m/s, in the absolute sense, rather than being strictly related to a Reynolds Number term.

Wisner, Mohsen and Kouwen essentially investigated the removal of an air pocket from a high point in a pipeline, as illustrated in Fig. 5.4. Their data is shown on Fig. 5.9 with fractional upstream depths ranging from 0.273 to 0.818, and again on Golding's graph, Fig. 5.8. Apparently, the effect of ${}^{Y_1}/_{D}$ is not quite as significant as say Kalinske and Robertson, but of a comparable order of magnitude. They plotted their data with that of Kent, and Kalinske and Robertson, Fig. 5.9, and proposed a lower bound envelope for air pocket clearing in the form,

$$\frac{V_c}{\sqrt{gD}} = 0.25\sqrt{\sin\theta} + 0.825 \qquad \text{.....(5.10)}$$

In the author's view, this empirical relationship is an unreasonable over-simplification, in view of the fact that clearing of an air pocket is a complex phenomenon involving the pocket length, depth, fractional depth,

velocity under the pocket, etc. Golding (private communication) points out the following, and I quote,

"Wisner, Mohsen and Kouwen (1975) examined the removal of air from water lines by the water flow. They plotted the non-dimensionalised water velocity in a full pipe to just remove air voids versus the square root of the sine of the pipe slope. They used equilibrium void results from Kent (1952), blow-back results from Kalinske and Robertson (1943), and void-removal results from their own tests in a 0.245 m diameter pipe with an 18.5° downslope. They drew a straight line (an envelope curve) above all the plotted results and called this the "lower bound" for the clearing velocity so that void clearance would be assured if this lower bound was exceeded. However, they then say that "Values of the velocity parameter should not be much higher than the lower bound as this will introduce a problem of blow-back". In the subsequent discussion (Wisner et al, 1976), they enlarge upon this as follows. "When the velocity was increased significantly beyond that recommended by the envelope curve, a different flow pattern developed. In this pattern, large parts of the air pocket would tear and quickly rise to the high point. The collected air at the summit would again be forced down in smaller sizes. The back-and-forth movement of the air continued at a seemingly unpredictable rate and caused significant pressure pulsations". They found that "blow-back did not occur when the velocity parameter was within 5% of the lower bound". This work tends to corroborate Sailer's prototype findings, but the plotting of equilibrium void results and blow-back results on a 'void removal' axis is not particularly helpful".

In other words, clearing of an air void occurs just above the recommended envelope, but at higher velocities still, blow-back may occur. Presumably, this is the supercritical pipe-full Froude number problem already discussed under Sailer's work. It does serve to emphasise, however, that separate criteria may be required in properly describing sub-critical and super-critical blow-back and clearing.

Gandenberger carried out extensive testing on the water velocities required to clear air pockets along downward sloping pipes. His work was published in German (1953 and 1957) but summarised by Mechler in English (Ref.). Gandenberger's work stemmed from air pocket problems in two 900 mm diameter water mains from Lake Constance to Stuttgart, Germany. As well as observations in these pipelines, experiments were carried out in glass pipes

10.5 mm to 45 mm diameter, and a steel pipe 100 mm diameter, all of which may have been subject to either viscous or surface tension scale effects, albeit very small in the 100 mm pipe. His data covered the full range of conduit slope 0^{o} to 90^{o}, and a range of air pocket volumes n = 0.02 to n>1. The results are plotted below in the form of the water velocity required to clear air pockets along a 1 m diameter pipe.

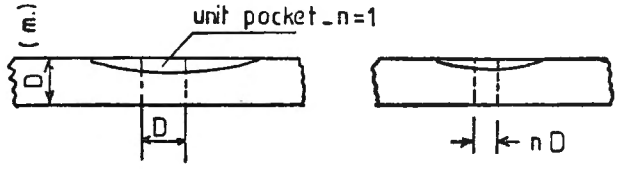

Pocket volume = $n\pi D^3/4$

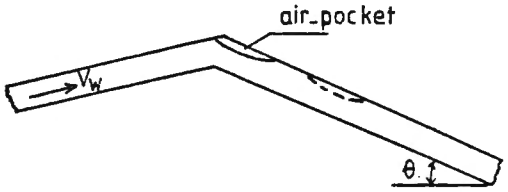

FIG. 5. 12
Gandenbergers data for air pocket clearing along a downward sloping pipe, for a pipe 1m. diameter

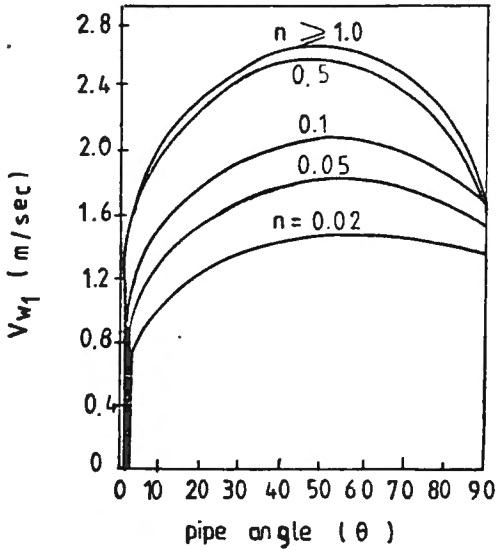

The clearing velocity for any other pipe diameter can be obtained thus

$$V_c = V_{W_1}\sqrt{D} \qquad \text{.....(5.11)}$$

Gandenberger's data has been replotted in a non-dimensional form on Fig. 4.24 and also on Golding's graph, Fig. 5.8, for n⩾1. It can be seen from Fig. 5.8 that Gandenberger's limiting Froude Number is less than Kent and

Wisner's comparable situation, and in fact fits more closely to the small fractional depth ($Y_{1/D}$) blow-back data of Kalinske and Robertson. It is unfortunate again that Gandenberger did not separate cavity depth and cavity length rather than employing the "global" air volume term, as detailed analysis still cannot be carried out on this set of data. The application of either force/momentum balance or energy principle requires more data on the shape and size of the air pocket.

Summary

Several points of interest emerge from our discussion in Section 5.1.

(i) No one (to my knowledge) has yet carried out a comprehensive study of either blow-backs or air pocket clearing where all the relevant parameters have been measured.

(ii) These parameters would include air pocket lengths L/D, depths H/D, upstream fractional depths $Y_{1/D}$, angle of the cavity nose to the pipe wall, ϕ, pipe slope θ, velocity profiles around the cavity, separate criteria for sub-critical and super-critical pipe-full flows, variations in the air/water ratio entering the upstream end of the air pocket, etc.

(iii) Scale effects are still not properly understood, especially the case of air pocket clearing by hydraulic jump entrainment. This might involve comparison between prototype and model studies, or at least model studies at different scales.

(iv) The author has put forward in Section 4.3 possible tentative analyses based on simplified force/momentum or energy principles. These could be verified if all the parameters are known, but this has not been the case to date.

(v) Goldring's graph, Fig. 5.8, highlights several discrepancies between previous investigations, and also highlights the necessity to differentiate between blow-back velocities, equilibrium-void velocities, and clearing velocities, which in the past have often all been plotted on the same axis.

Section 5.2. Air pocket behaviour at the junction of dropshaft and tunnel systems

Vertical dropshafts joining up with a horizontal (or nearly horizontal) tunnel system are often constructed at the outlet to dams, hydroelectric power systems, or more recently, the outfall systems of nuclear power plants. A plunging nappe in the upper part of the shaft will often entrain small air bubbles (<10 mm diameter) which may coalesce during downward movement in the shaft, or at the tunnel soffit at the dropshaft/tunnel junction. Continued coalescence at this junction gives rise to air pocket formation, which in turn may lead to discharge reduction (trapped air pocket), "blow-backs" (structural damage and possible mass oscillation), or "blow-backs" (may also lead to structural damage, vibration, mass oscillation, etc.).

The subject has received some attention in the past, mainly related to "morning-glory" spillways, (which will be reviewed very briefly), but is again attracting attention in the context of the outfall systems of nuclear power stations. We shall concentrate on the latter, and in particular the work of Townson (Ref.), Goldring (Ref.) and Ervine and Himmo (Ref.). A typical dropshaft/tunnel arrangement is shown opposite, indicating possible air pocket formation at the sharp bend. (Fig. 5.13).

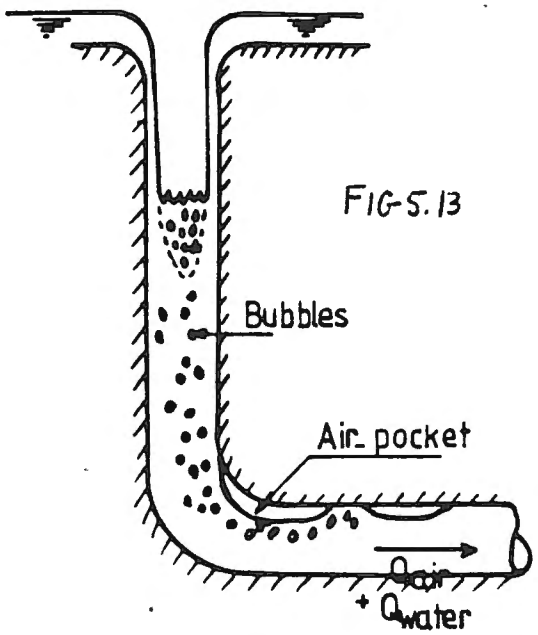

FIG-5.13

Unsatisfactory flow conditions leading to blow-backs and vibration were reported by Hall (Ref.) in 1944). The performance of two dams near Oakland, California, namely San Pablo dam and Chabot dam, were observed.

At the San Pablo dam, (constructed in 1917-1920), air entrainment caused serious problems in that small bubbles were carried down the vertical shaft and into the horizontal leg, where they accumulated in large air pockets along the roof. These pockets moved slowly along the grade of the tunnel towards the outlet and discharged periodically with explosive violence throwing water as spray to a height of about 15 m in the air. The vibration caused in the tunnel following each of these air discharges also led to serious difficulties.

In 1956, Bradley (Ref.) reported on the prototype behaviour of different shaft spillways one of which was the Owyhee Dam Spillway, completed in 1932 by U.S. Bureau Reclamation. In this dam an unusual phenomena was observed. For low heads, 0.3 m to 0.6 m above the inlet gate, the water fell in a solid sheet toward the centre of the shaft. Air was entrained faster than it could be released by the outlet end of the tunnel causing the pressure to increase until it was sufficient to "blow-back", when air emerged with sufficient force to carry spray 15 m or 20 m above the level of the gate.

More recently in early Spring 1982, a blow-back of compressed air damaged the intake of a Norwegian Power Station, see FIG (5.14). This information was sent to the author by Mr. Kare Trinnereim, Head of Norwegian Hydro-dynamic Laboratories, in a letter dated 14th October 1982.

In 1966 Colgate (Ref.) reported on the Canadian River project. The project included an aqueduct system, pumping plants and regulating reservoirs, with the water flowing in the main pipeline under gravity. The pipeline was designed so that at normal flow the hydraulic gradient will be parallel to the average ground profile with the water pressure not exceeding 30 m head. A tower-type check structure as shown on Fig. (5.15) was designed and situated in the main pipeline to prevent adverse conditions such as over-pressures, water hammer and surging caused either by the operation of filling, draining or air entrainment. Each tower consisted of an inverted U-tube with an air vent open to the atmosphere at the summit, and designed so that during normal operation the hydraulic gradient will be above the top of each tower causing the system to flow full. For flow less than normal, or no flow, this arrangement ensured the conduit

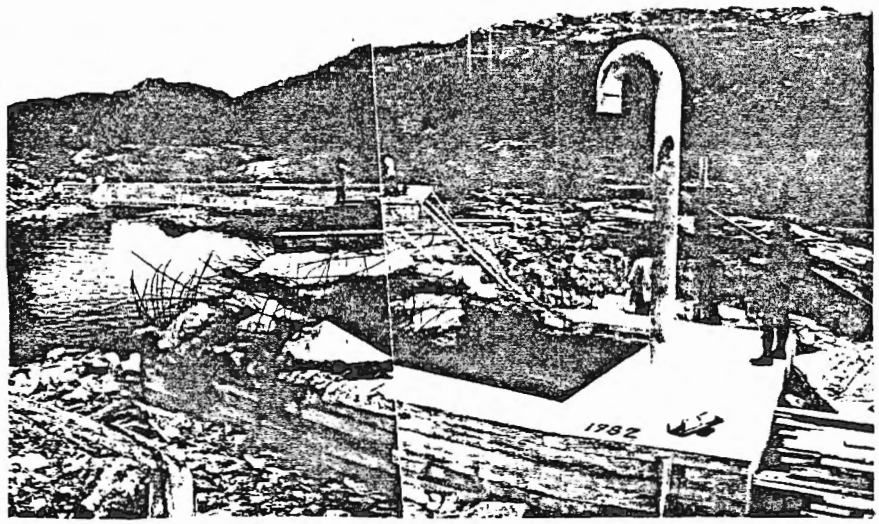

DAMAGE AT THE INTAKE EARLY SPRING 1982

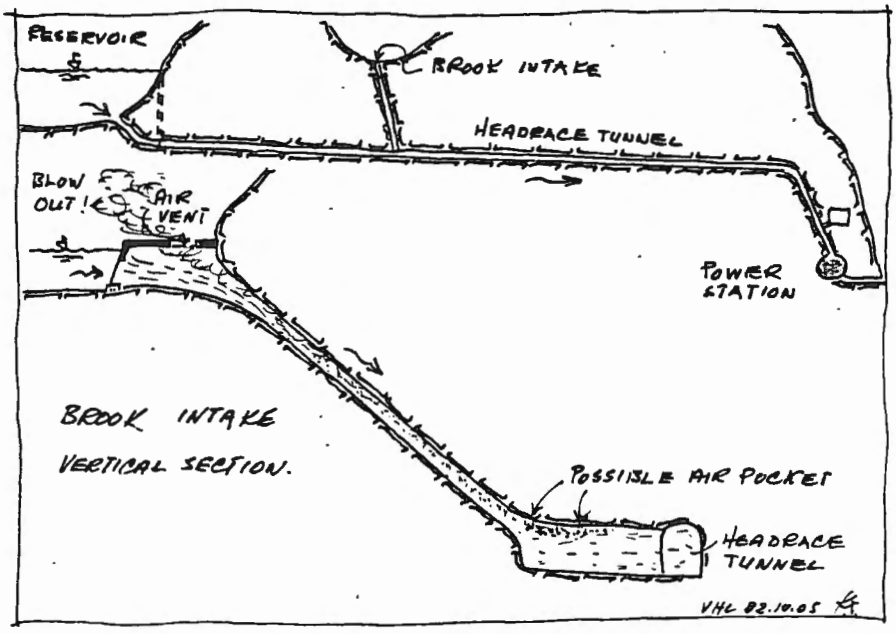

FIG. (5.14). Damage at the intake of a Norwegian Power Station.

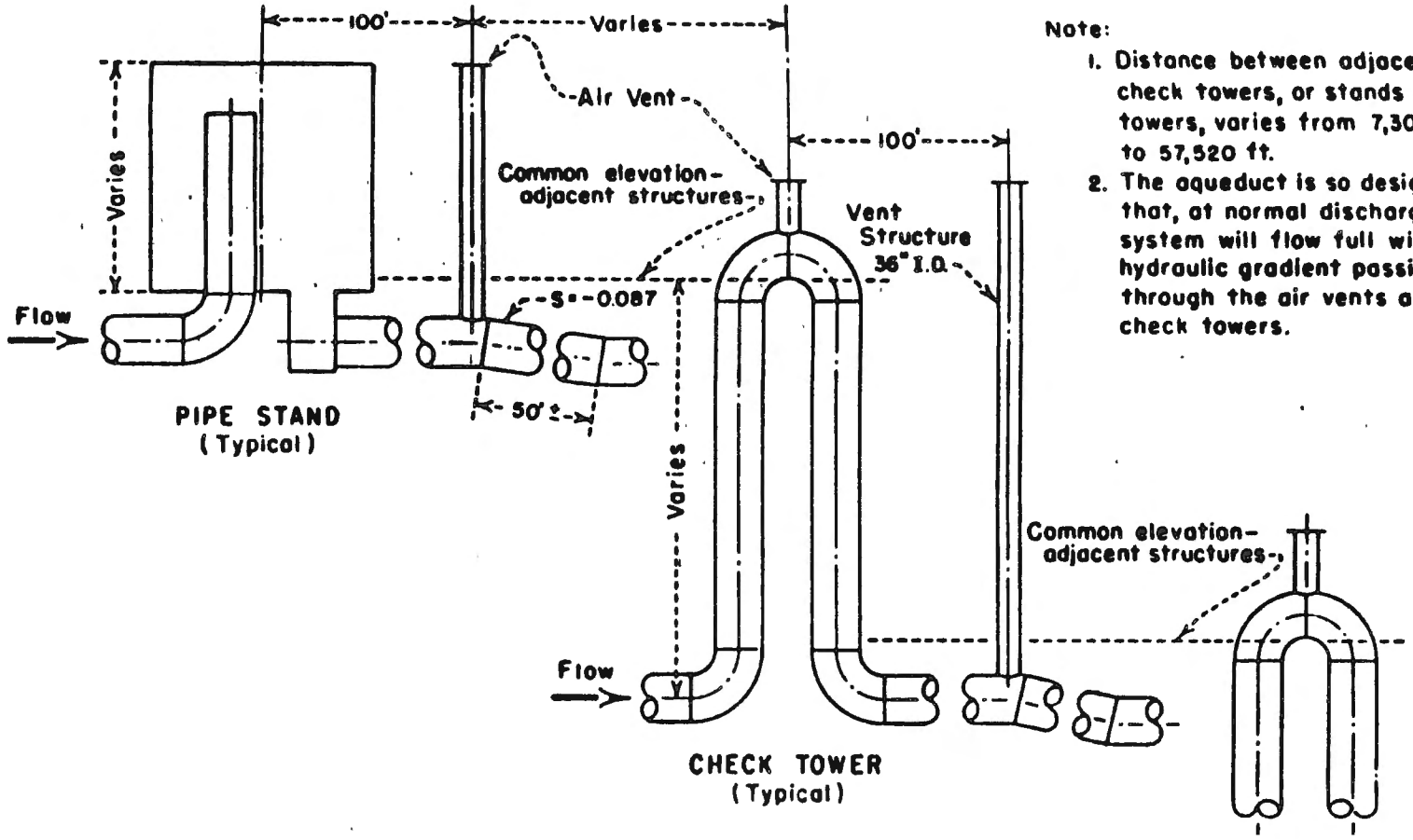

Fig(5.15) Check Towers and Vent Structures for Canadian River Main Aqueduct (Colgate ,1966)

between towers remained full. The open pipe at the top of the tower prevented over-pressure damages when there was surging in the conduit during transient conditions. The open air vent pipe also allowed air entrainment at low discharge in down-stream leg of tower when flowing partially full. Air passed through the vent and became entrained in the flow in the form of bubbles, which either moved upstream or downstream depending on the pipeline slope, discharge and bubble size. Studies were carried out to obtain the best conduit slope to allow the air bubbles to vent back upstream to the air vent and to be removed from the line. It was found that a downward conduit slope of 5^{o} downstream from the vent was enough to ensure that all entrained air was recirculated back to the vent.

Water level surges caused by air entrainment and air pocket formation was experienced at the out fall of several power stations and other hydraulic structures. For example, level instability and surging in dropshaft/tunnel systems has been reported within the U.K. on projects for the South of Scotland Electricity Board and CEGB by Goldring, (Ref.), Miller (Ref.), Brook et al., (Ref.), Maximum water level surges of 9 m have been reported. In these cases, water level surges have generally arisen by the collapse or blow-back of an air pocket at a dropshaft/tunnel junction, the air pocket having been formed in the first place by entrainment of air in the upper part of the dropshaft.

A new Central Electricity Generating Board (CEGB) project at Thameside Power Station (Ref.) exhibited flow instability in the downshaft, Fig. (5.16) during periods of certain air/water flow requirements. These level surges have caused anxiety among the CEGB engineers about the ability of such outfall structures to withstand this phenomenon for the life of the power station. Field data on localized pressure changes caused by the collapse or movement of air pockets have not been adequate for a civil engineering design appraisal and it has been suggested (Ref.) that a large scale instrumentation survey be mounted on at least one project to tain more insight into the structure - air pocket - level surge - damage relationship.

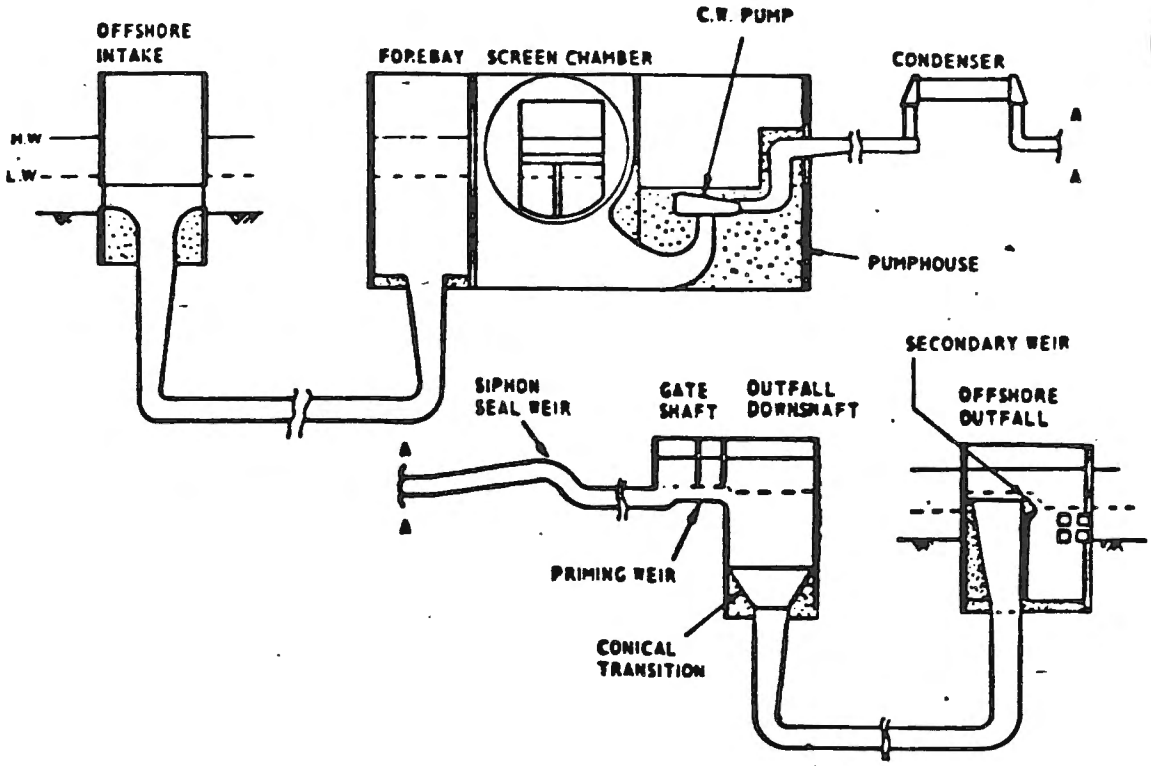

(b) Elevation sketch of cooling water system

Fig. (5.16) Cooling Water System in Thameside Power Generating Stations (Goldring, 1980).

The Hunterson "B" Power Station, Fig. (5.17), is another example which exhibited flow instability due to air entrainment and air pocket formation in the water filled shaft/tunnel system, and took the form of oscillations in both land and pit shaft as shown on Fig. (5.18). This was reported by Townson, 1975 (Ref.). These conditions increased gradually until the seal pit weir was submerged and spillage occurred at the land shaft. It was observed that oscillations were accompanied by variations in average shaft density and presence of an air cavity at the tunnel roof. From model scale studies it was found that entrained air was the main cause of the oscillations. In the shaft, air bubbles circulated in vertical direction according to their size and position in the flow. Some of the air returned to the surface while the rest was carried around the bend into the roof of the tunnel forming a cavity or air pocket, (see Fig. (5.18)).

Townson carried out a mass oscillation analysis of the system, shown on Fig. 5.19), by idealising it to a three shaft system, assuming the sea outfall end to have infinite area, and also introducing density variations in the intake shaft. On writing the equations of motion and continuity,

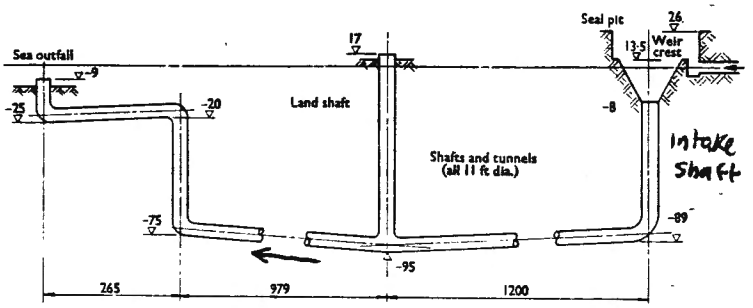

FIG 5.17 Longitudinal profile of outfall system (not to scale, levels in ft OD, distances in ft) (Townson)

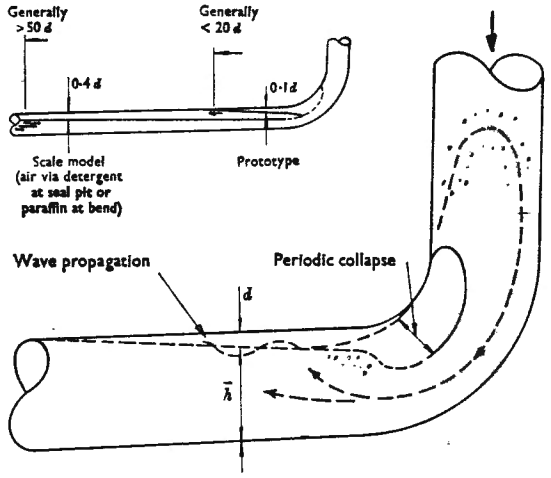

FIG. 5.18 Cavity mechanisms and comparative model/prototype sizes (Townson)

two modes of oscillation were predicted (for the case of infinite sea area), W_1 and W_2. These are shown on Fig. 5.19 below and compared with model and prototype data. It is clear that the lower frequency mode W_1, is sensitive both to the density ratio, (ρ_1 is the reduced density in the intake shaft due to the presence of air bubbles) and also the area ratio a_o/A. (a_o is the cross-sectional area of the intake shaft and A the tunnel cross sectional area). a_o was introduced into the analysis on account of the variation in intake shaft area, in the region of the conical diffuser.

The 1/32 scale model of the system using clear water revealed that the prototype mode of oscillation could be achieved, but quickly decayed, unlike the prototype. An injection of detergent at the seal pit weir was found necessary to simulate the large sustained oscillations found in the prototype. This, however, produced an adverse side effect of air "hold-up" in the tunnel system. Townson introduced paraffin oil at the tunnel soffit just downstream of the bend, so that the cavity behaviour could be

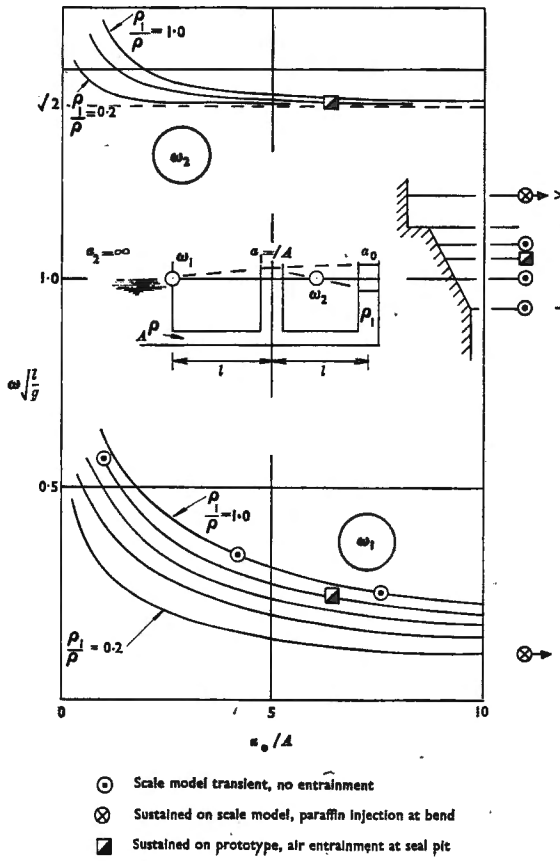

Variation of system response with shaft area and density

FIG. 19 Townson's analysis

studied in more detail, free from the chaotic nature of air bubble flows in the intake shaft and bend. The paraffin oil cavity test revealed that a periodic collapse of the cavity nose back in to the shaft, and the corresponding reduced density of flow in the shaft ρ_1, was coupled with natural frequencies of the system to produce sustained oscillations.

The following recommendations to avoid oscillation were reported:-

(a) Delay of oscillation could be achieved by covering the seal-pit weir nappe with rubber sheeting, thus reducing the degree of aeration. This has proved quite effective in prototype tests.

(b) Adjustments of length and diameter of shaft so that natural frequencies are small compared to cavity oscillation in separating zones.

(c) Control of separation zone size by local conduit geometry and/or venting.

(d) Allowing the air to be swept through the system to a point where it could be released.

Golding (1983, Ref.) has carried out an experimental investigation into the behaviour of air pockets at a dropshaft/tunnel junction for the particular case of the ratio of air to water (coming down the shaft) less than 2%. This is of particular relevance to systems with air coming out of solution, but of limited interest to dropshaft spillway studies, etc., where the ratio of air to water often exceeds 0.4 (40%). Golding tested up to four different pipe diameters, 0,072 m, 0.1 m, 0.14 m and 0.19 m Ø, and up to four bend radii for each pipe diameter, $^{R}/_{D}$ = 0.5, 0.75, 1.0 and 1.5. An $^{R}/_{D}$ of 0.5 is a completely sharp bend, with R measured from the centroid of the inner bend radius to the centre-line of the pipe.

Four regimes of behaviour were shown to exist:-

(a) At low Froude Numbers, any air pocket which started to form at the inside of the bend would vent back up the shaft.

(b) At higher Froude Numbers, a stable void formed with the upstream nose located on the curved inner radius of the bend and the tail (downstream end) in the form of a hydraulic jump. In this case the air pocket was short, with the jump almost drowning back to the bend. Golding referred to this as a partly ventilated void.

(c) At higher air flow rates, this stable void extended in length (and depth) with a stable jump forming at its downstream end. Golding referred to this as a fully ventilated void.

(d) At higher Froude Numbers still, the pocket at the bend cleared. These four regions are shown on the sketch below, in the form of a plot of the air/water ratio (<2%) against the upstream Froude Number, $V_o/\sqrt{gD}$.

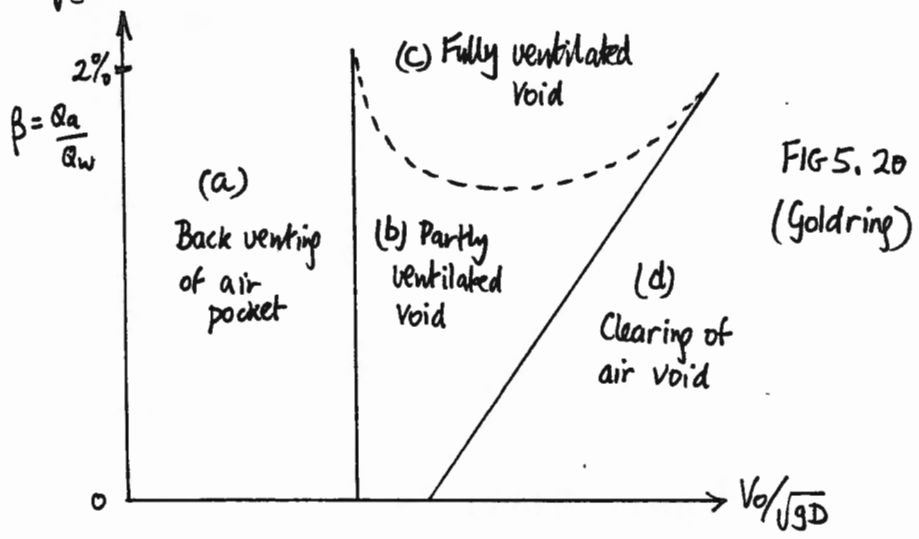

FIG 5.20 (Goldring)

The effect of bend radius R/D, is shown on Fig. 5.21 for the case of the 0.14 m diameter bend. It is clear that back-venting (vertical lines) is a problem in the sharp radius bend ($R/D = 0.5$) only up to a Froude Number of 0.3, whereas it is a problem in the smoothest radius bend ($R/D = 1.5$) up to a Froude Number in excess of 0.6. The same applies to air pocket clearing (inclined lines). An air pocket clears most efficiently in the sharpest bend and less efficiently in the smooth radius bends. On both counts, the sharpest bend is the optimum choice. Clearing Froude Numbers are generally 0.5 to 1.0, in a similar range to that of downward sloping pipes in Section 5.1.

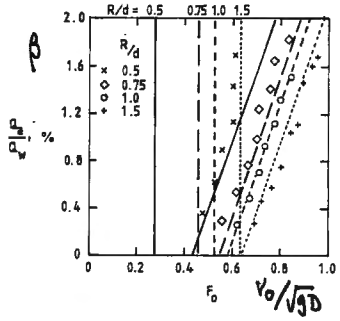

FIG. 5.21

FIG. 5.21—Void Behavior in Bends of Various R/d and 5.5 in. (0.14 m) diam; Correlations and Experimental Results (Goldring)

The effect of pipe diameter is shown on Fig. 5.22 for the four pipe diameters but a constant R/D of 1.0. It is clear from this diagram that larger pipe diameters produce lower clearing Froude Numbers, and an extrapolation of Goldring's data would produce a very low clearing Froude Number for large diameter conduits found in practice.

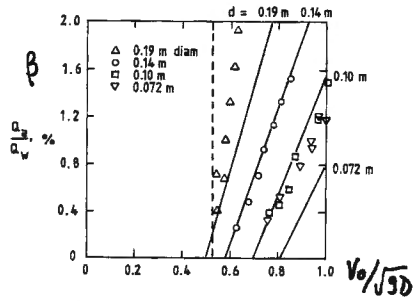

FIG. 5.22

FIG. 5.22—Void Behavior in Bends of R/d = 1.0 and Various Pipe Diameters; Correlations and Experimental Results (Goldring)

The concept of a greatly decreasing clearing Froude Number with increasing pipe diameter has not been commented on by previous authors in the case of downward sloping pipes. On Fig. 5.8 for instance, Wisner's data was obtained from a 244 mm ∅ pipe, and Kent's data from a 100 mm ∅ pipe giving roughly comparable data. In other words the scale effect is not apparent. Golding's data on Fig. 5.11 is therefore a novel departure for clearing of air pockets when clearing occurs by hydraulic jump entrainment at the tail of the pocket.

By way of explanation, Golding proposes essentially that an air void will clear from the bend when the flow velocity under the void is greater or equal to the minimum velocity to entrain air U_1^*, approximately 1 m/s. He proposed an empirical relationship describing the clearing Froude Number in the form,

$$Fr_c = \frac{(0.5 + 0.25\sqrt{\frac{r}{D}} + 20\beta)\ U_1^*}{\sqrt{gD}} \qquad \text{.....(5.12)}$$

Thus for a given r/D and β, the clearing Froude Number is proportional to $U_1^*/\sqrt{gD}$, and as U_1^* is a constant, then Fr_c will reduce greatly for larger pipe diameters, D. In the author's opinion, this represents an over-emphasis on the velocity under the pocket, with no reference to the fact that the Froude Number under the pocket must also be greater than unity, for the jump to form in the first place. Therefore, if we had a dual criterion for clearing,

$$U_1^* \geq 1 \text{ m/s}$$

and

$$Fr_1 = \frac{U_1}{\sqrt{gA_1/B}} > 1 \qquad \text{.....(5.13)}$$

then the second of these two criteria might mean that the clearing Froude Number $U_o/\sqrt{gD}$ for prototype sizes might be in the same range as the four pipes tested by Golding.

For instance, if we take the case of a typical air pocket depth $H/D \simeq 0.5$ at the tail of the pocket, or $Y_1/D \simeq 0.5$. That is, the pipe half-full. The value of Fr_1 then is given by $U_1 = 2U_o$, $A_1 = \pi D^2/8$ and B = D, hence Fr_1 becomes

$$Fr_1 = \frac{U_1}{\sqrt{gA_1/B}} = \frac{2U_o}{\sqrt{gD\pi/8}} \simeq 3.2\ \frac{U_o}{\sqrt{gD}} = 3.2\ Fr_o \qquad \text{.....(5.14)}$$

If the pocket clears when $U_1 > 1$ m/s and $Fr_1 > 1$, then assuming for a large diameter pipe that $U_1 > 1$ m/s is easily satisfied, then from (5.14) $Fr_c \simeq Fr_{1/3.2} \simeq 0.31$. For a large diameter pipe $Fr_c = 0.31$ is likely to give a much higher clearing Froude Number than the simple application of $U_1 \geq 1$ m/s, and the range is more in line with the experimental values of Golding.
λ

Clearly, much work still requires to be done, on the scale effects involved in clearing air pockets by entrainment, but Golding's work shows very clearly, not only the different regimes of air pocket behaviour and the regions of back venting, but also that clearing of such air pockets from a sharp bend may be less of a problem in a prototype structure compared with a Froude model. Himmo (together with the author) is currently carrying out an experimental study of air pocket formation at dropshaft/ tunnel junctions. The apparatus shown on Fig. 5.23 in longitudinal profile, consists of a dropshaft 152 mm diameter and a tunnel section 8.3 m long and again 0.152 m diameter. The tunnel section has been tested (a) in the horizontal position $\theta = 0$, (b) with the tunnel pipe inclined slightly upwards $\theta = +1.5^\circ$, and (c) with the tunnel pipe inclined slightly downwards, $\theta = -1.5^\circ$. The purpose of the variation in tunnel slope is to investigate not only air pocket formation at the sharp bend, but also air pocket behaviour in upward sloping pipes (See section 4.2) and air pocket behaviour in downward sloping pipes, i.e. blow-back and clearing properties.

The bend radius R/D has also been tested over the range 0.5, 1.0 and 1.5 for each of the three tunnel slopes -1.5°, 0°, $+1.5^\circ$, giving a total of nine geometrical configurations. Water and air flow are controlled independently as shown on Fig. 5.23, with 16 air inlets each 5 mm diameter ensuring a range of bubble sizes found in nature. The water flow can be increased up to 40 l/s, giving pipe full velocities as high as 2 m/s, and the air flow range up to about 20 l/s, giving an air/water ratio of 0.5, even at the highest water flow rates. Use is made of Churchill wave monitors, not only to measure air pocket depths (H/D), but also the speed of air pockets moving along the tunnel section and their shape development.

(i) Air pocket formation at the bend.

Regarding the formation of an air ppcket at the dropshaft/tunnel bend there appear to be several regimes of behaviour. These are shown on Fig. 5.24 for the particular case of the tunnel horizontal ($\theta = 0^\circ$) and a

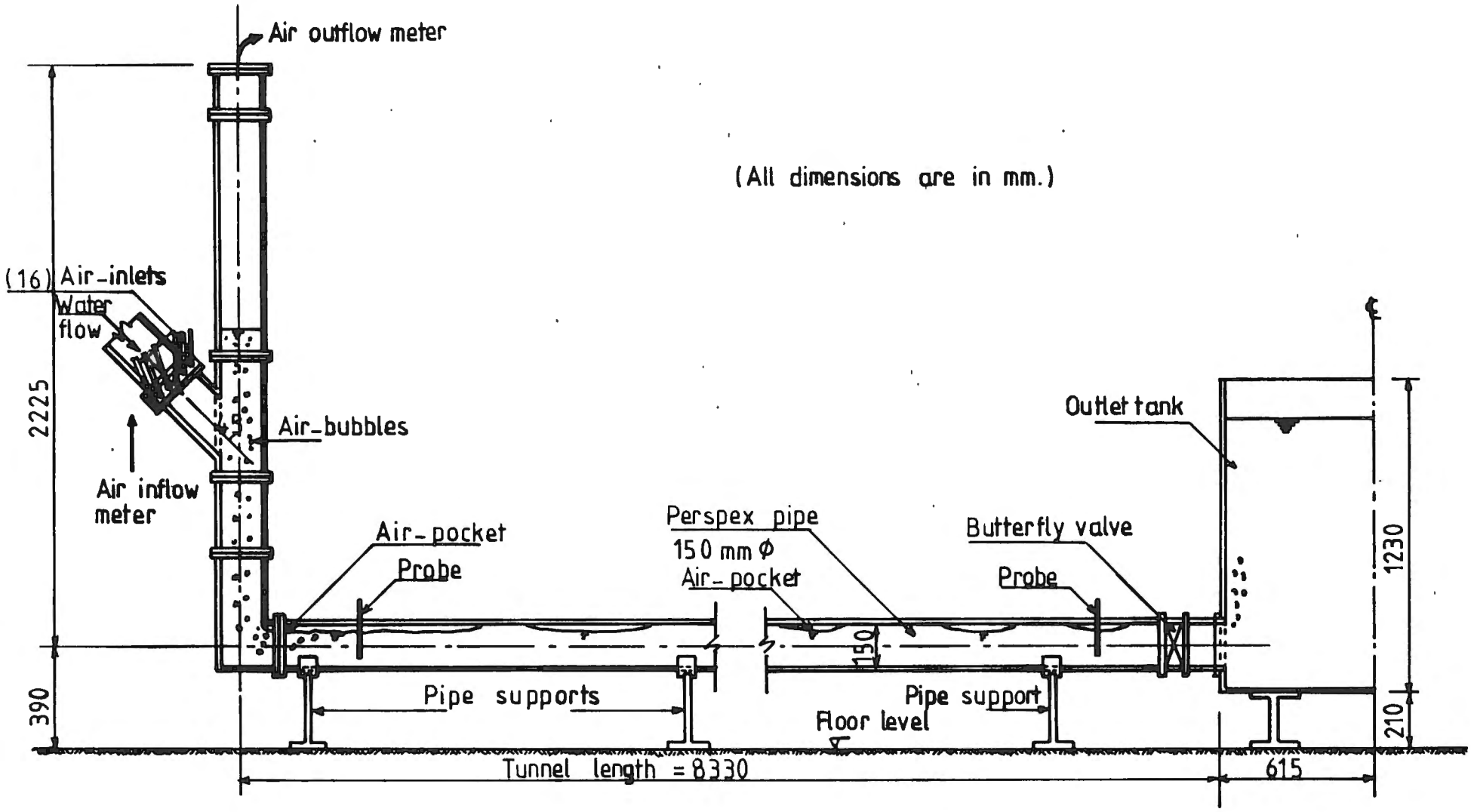

FIG 5.23 Himmo's experimental set-up for air pocket behaviour at a dropshaft/tunnel bend

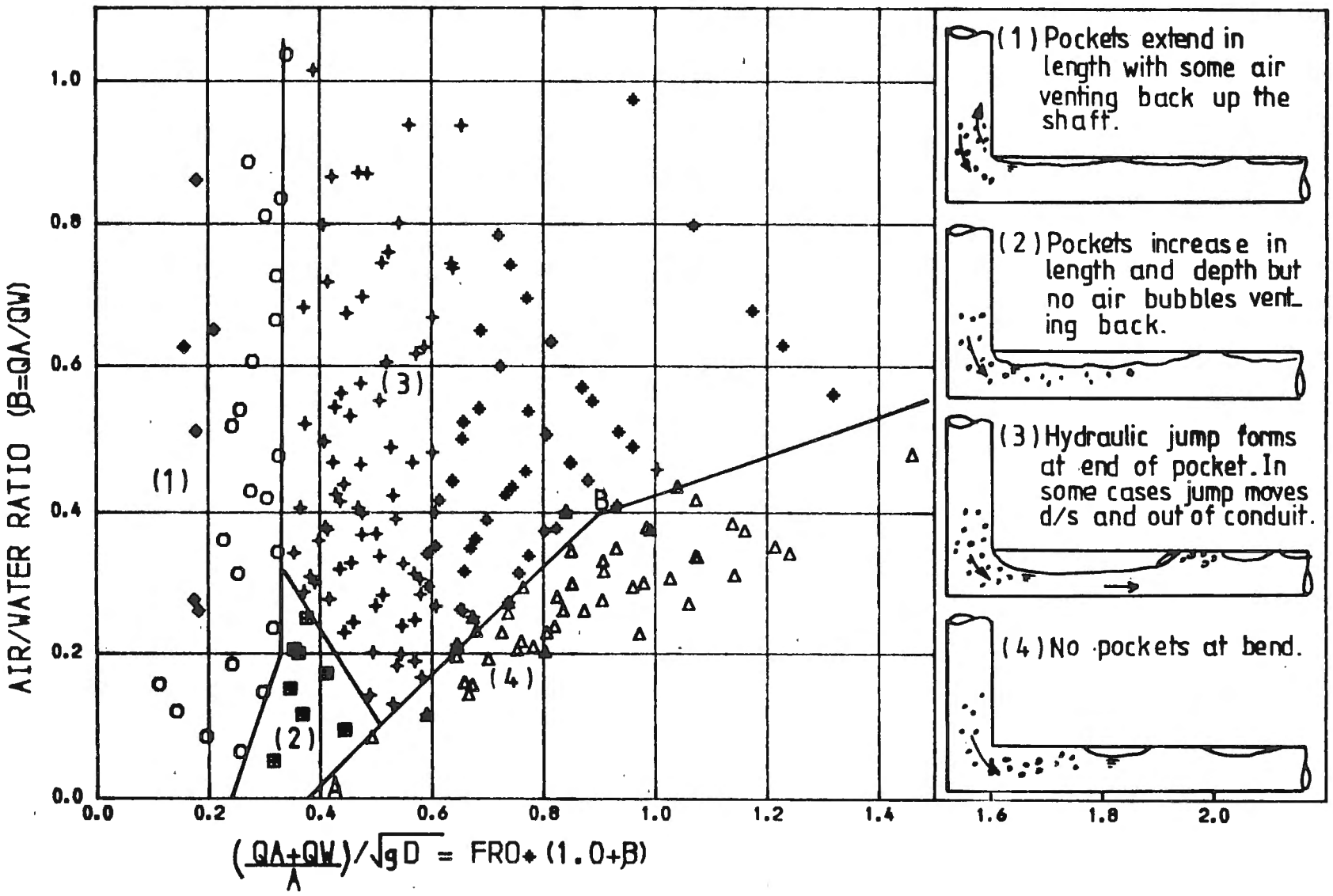

FIG 5.24. Regimes of air pocket behaviour for the particular case of tunnel horizontal (θ=0) and a sharp bend (R/D < 0.5)

single mitre sharp bend $R/D = 0.5$. The graph is plotted as the air/water ratio, β, against $\frac{\langle j \rangle}{\sqrt{gD}}$, or $\frac{Q_A+Q_W}{A_p\sqrt{gD}}$ or $Fr_o(1+\beta)$.

Regime (1) is the region where the air pocket forms, lengthening and deepening, but also having the capability to vent back into the shaft. This corresponds to the region $V_o/\sqrt{gD}(1+\beta) < 0.3\text{-}0.4$.

Regime (2) is similar to (1) except that back venting of the pocket into the shaft does not occur. The flow under the air pocket is still sub-critical, i.e. $V_1/\sqrt{gA_1/B} < 1$.

Regime (3) is characterised by supercritical flow under the air pocket with a hydraulic jump forming at the tail of the pocket. The jump may take up a position either (a) close to the bend where it behaves almost as a drowned jump, (b) in a stable position some distance downstream of the bend or (c) the jump may travel out of the tunnel section completely and blow into the end tank. In this case, stratified flow exists over the total 8.3 m length of the tunnel.

Regime (4) is characterised by the air pocket at the bend clearing completely. Further air coming down the shaft may form a new pocket at the bend, but this is again cleared, so that a succession of air pockets travel along the tunnel, with none remaining stable at the bend.

The line AB on Fig.5.24 thus represents clearing criteria for air pockets at a sharp bend, comparable with the clearing criteria outlined in Section 5.1 for downward sloping pipes.

(ii) Clearing and blow-back criteria.

Fig.5.25 shows the clearing and blow-back lines for the case of the horizontal tunnel and for three bend radii $R/D = 0.5$, 1 and 1.5. The graph is plotted as β against $V_o/\sqrt{gD}$, the pipe full Froude Number. We will discuss this graph along with Fig.5.26 which is a plot of the clearing and blow-back Froude Numbers for the same R/D values, but in this case the tunnel inclined upwards at an angle of $+1.5^\circ$. The following initial conclusions can be drawn.

- Clearing of the bend air pocket becomes increasingly more difficult as R/D increases from 0.5 (sharp bend) to 1.5 (smooth bend). This is related to the position and angle of the nose of the air pocket at the inner bend radius, and also the development of secondary currents and

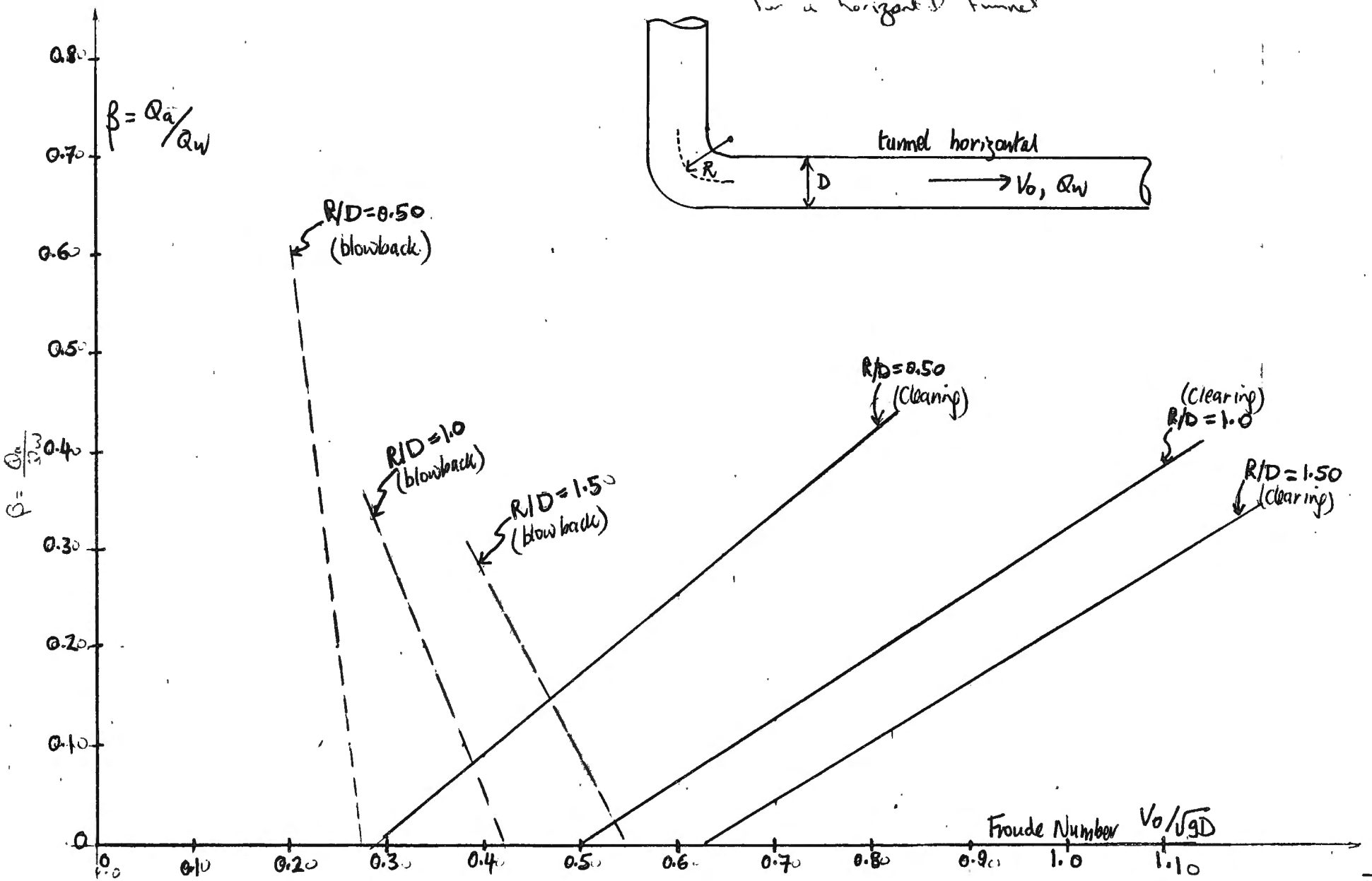

FIG 5.25 Blow back and cleaning lines for tunnel horizontal and three bend radii. (Himmo)

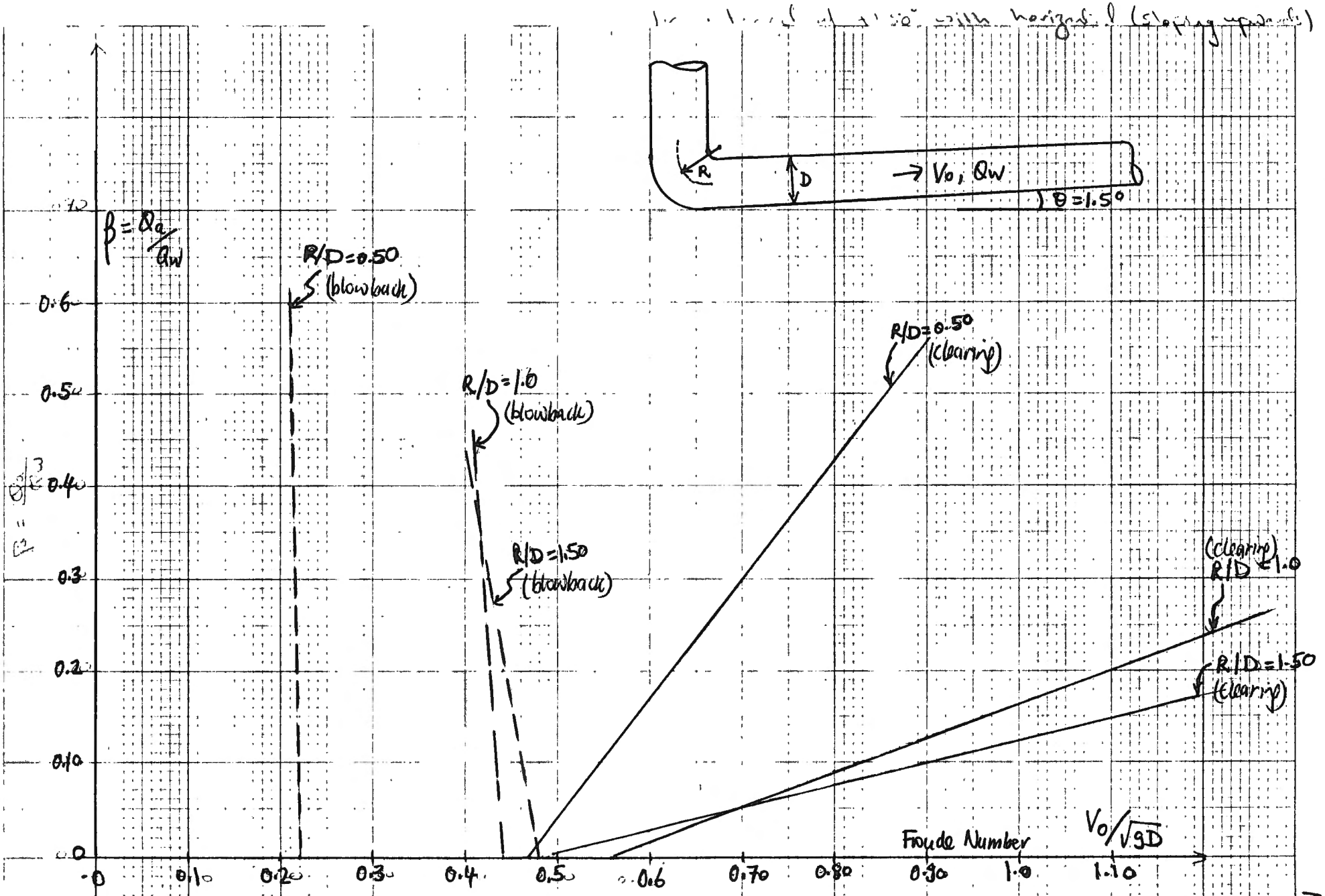

FIG 5.26. Blow back and clearing lines for the tunnel sloping upwards at 1.5° and various values of R/D

swirling for sharper bends.

- Clearing of the bend air pocket becomes increasingly difficult as the air/water ratio β (or void fraction) of the flow coming down the shaft increases. This is undoubtedly related to the fact that the air pocket volume, length and depth each increase for increasing air/water β, for a constant water discharge. It can be seen from Section 5.1 that larger air volumes, lengths and depths of the cavity require larger Froude Numbers for clearing.

- Comparing Fig. 5.25 and Fig. 5.26 it appears that clearing of an air pocket from a bend is more difficult with the tunnel section sloping upwards (+1.5°) compared with the horizontal. This is somewhat surprising in view of the fact that in the upward sloping pipe, air pocket buoyancy is acting in the same direction as the flow.

- the upper limit for back venting of the air pocket into the dropshaft is indicated by dashed lines on Figs. 5.25 and 5.26. It is clear that the bend radius R/D is significant, in that, the smoother and more gradual the bend (larger R/D), then back venting occurs of a larger range of Froude Numbers. In this case, smoother bends allow the air void to take up a position on the inner radius of the bend such that the nose of the air pocket is closer to the dropshaft and hence back venting more likely. For the single mitre sharp bend ($R/D = 0.5$), the nose of the pocket forms on the edge of the bend and hence back venting is much less of a possibility.

(iii) The depth of the air cavity at the dropshaft/tunnel bend.

The depth of the air cavity has been measured for the various geometrical configurations outlined, $R/D = 0.5$, 1.0, 1.5 and $\theta = -1.5°$, 0° and +1.5°. A schematic diagram showing the variation of H/D with Froude Number $V_o/\sqrt{gD}$ is shown on Fig. 5.27 overleaf. Three distinct patterns emerge -

(a) At low Froude Numbers corresponding roughly to Regimes (1) and (2) on Fig. 5.24 (when the flow under the pocket is generally subcritical) we obtain a region of increasing air pocket depth with increasing Froude Number. This is indicated as the "separation model" on Fig. 5.27 In this region the air pocket depth, H/D, also increases with air/water ratio, β.

THEORETICAL MODELS FOR AIR-POCKET BEHAVIOUR AT A DROPSHAFT/TUNNEL BEND.

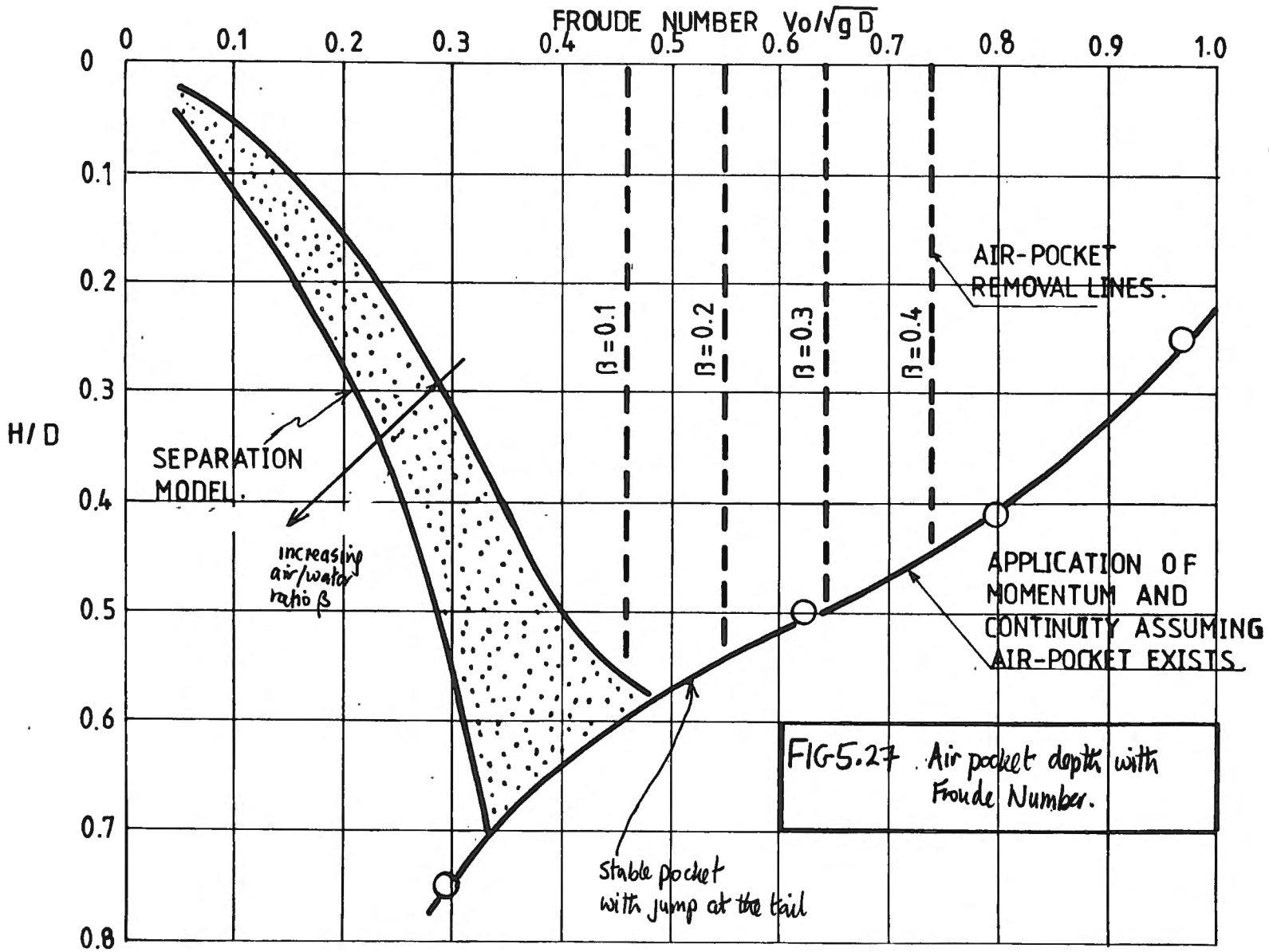

FIG 5.27 Air pocket depth with Froude Number.

(b) The second stage involves the formation of supercritical flow under the bend air pocket with a hydraulic jump at the tail. Air pocket depths fall on or around the curve indicated by -O- on Fig. 5.27 This is equivalent to Regime (3) on Fig. 5.24

(c) Finally, air pockets clear from the bend along vertical dashed lines as indicated, corresponding to the onset of Regime (4) on Fig. 5.24 It is possible, for low values of air/water ratio β, to proceed directly from "separation model" region to clearing, bypassing the second stage completely.

Himmo is currently engaged in developing theoretical models for each of these stages. Let us consider a theoretical model, using energy, force/momentum and continuity principles, for the case of Stage (b), with supercritical flow under the pocket, a stable air-fed air pocket at the bend, and a hydraulic jump at the tail of the pocket.

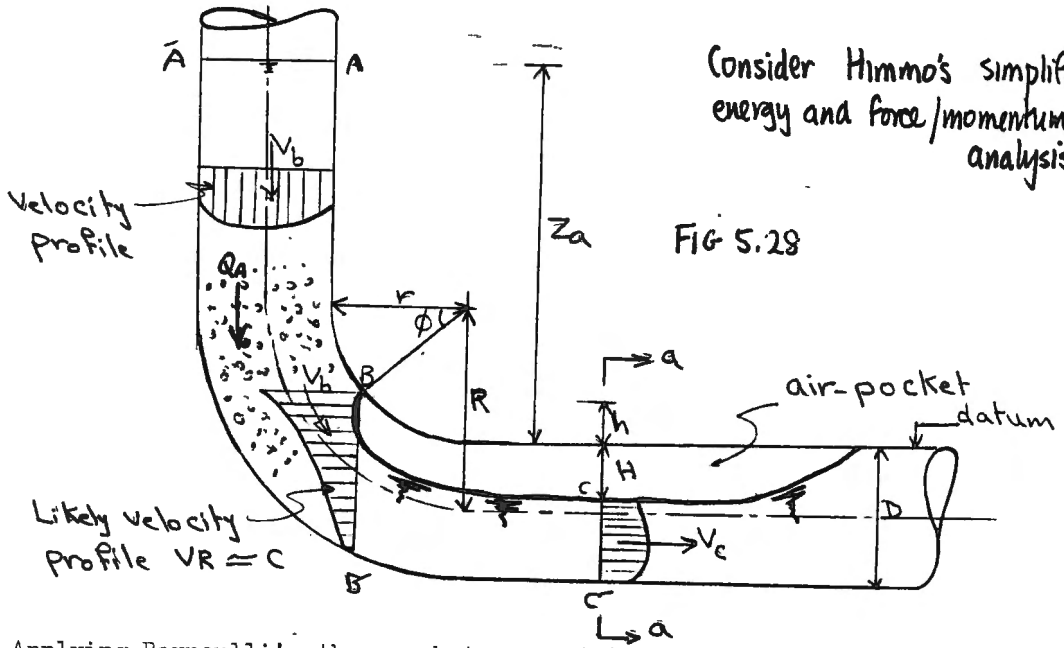

Applying Bernoulli's theorem between points A, B and C

$$\frac{P_A}{\rho g} + \frac{V_a^2}{2g} + Za = \frac{P_B}{\rho g} + \frac{\alpha_b V_b^2}{2g} + h + \Delta_1 = \frac{P_c}{\rho g} + \frac{\alpha_c V_c^2}{2g} - H + \Delta_2 \quad \ldots\ldots (5.15)$$

where P_A = pressure at point A = atmospheric pressure

V_A = velocity at point A = 0

Za = height of point A above the assumed datum at top of pipe

P_B = pressure at point B

V_b = velocity at B

α_b & α_c = velocity correction factors at B and C.

h = height of nose of pocket above datum = $r(1 - \sin\varphi)$

P_c = pressure at C = $P_B = P_{air}$

V_c = velocity at C

H = air-pocket depth

Δ_1 = losses at bend = $1.2 \frac{V_b^2}{2g}$

Δ_2 = Δ_1 + friction losses

$$= 1.2 \frac{V_b^2}{2g} + \lambda \frac{L}{D} \frac{V^2}{2g}$$

From Eq. (5.15) we get

$$\frac{P_B}{\rho g} = Za - \frac{\alpha_b V_b^2}{2g} - h - \Delta_1$$

$$P_B = \rho g \left[Za - \frac{\alpha_b V_b^2}{2g} - r(1 - \sin\varphi) - 1.2 \frac{V_b^2}{2g} \right]$$

$$P_B = \rho g \left[Za - r(1 - \sin\varphi) - \frac{V_b^2}{2g} (\alpha_b + 1.2) \right] \quad \ldots\ldots (5.16)$$

$$\frac{P_c}{\rho g} = Z_a - \frac{\alpha_c V_c^2}{2g} + H - \Delta_2$$

$$P_c = \rho g \left[Z_a - \frac{\alpha_c V_c^2}{2g} + H - \frac{1.2 V_b^2}{2g} - \frac{\lambda L}{D} \frac{\frac{(V_b + V_c)^2}{2}}{2g} \right] \ldots\ldots (5.17)$$

Applying <u>continuity equation</u> between section $B\acute{B}$ and $C\acute{C}$ $V_b A_p = V_c A_c$

where A_p = pipe area = πr^2

A_c = area of partially full pipe

$$= \pi r^2 \left(1 - \frac{a}{\pi} + \frac{\text{Sin } 2a}{2\pi}\right)$$

$$V_c = \frac{V_b A_p}{A_c} \quad \ldots\ldots (5.18)$$

a = angle in radians

1) If we have a 90° sharp edge bend then $r = 0$. Hence $h = 0$, also the point of separation is exactly at the bend.

The assumptions to be made here are as follows:

(a) Δ_1 and Δ_2 can be neglected

(b) $\alpha_b = \alpha_c = 1.0$

(c) resistance between $B\acute{B}$ and $C\acute{C}$ can be neglected

(d) Uniform pressure distribution at the bend (not correct)

From equations (5.16) and (5.17) where $P_B = P_c = P_{air}$

$$\rho g \left[Za - \frac{\alpha_b V_b^2}{2g} \right] = \rho g \left[za - \frac{\alpha_c V_c^2}{2g} + H \right]$$

$$\frac{\alpha_b V_b^2}{2g} + H = \frac{\alpha_c V_c^2}{2g} \qquad \text{---------- (5.19)}$$

Substituting for V_c from the continuity equation (5.18), we obtain

$$H/D = 0.5 \frac{V_b^2}{gD} \left[\left(\frac{A_p}{A_c} \right)^2 - 1 \right] \qquad \text{.....(5.20)}$$

$(\alpha_b = \alpha_c = 1)$

Due to the presence of air bubbles approaching the bend from the shaft, we must modify V_b to account for the presence of air bubbles. That is, if V_o is the shaft full water velocity averaged over the entire pipe area Q_w/A_p, then $V_b(1-\alpha) = V_o$, where α is the void fraction, and hence $V_b = V_o(1+\beta)$, or Equation (5.20) becomes

$$H/D = 0.5 \frac{V_o^2}{gD} (1+\beta)^2 \left[\left(\frac{A_p}{A_c} \right)^2 - 1 \right] \qquad \text{.....(5.21)}$$

(where $V_o^2/gD = Fr_o^2$)

Equation (5.21) has been solved for a range of Froude Numbers, and values of β, and compared with experimental data from the sharp bend case $R/D = 0.5$ when supercritical flow exists. The result is shown on Fig. 5.29 giving reasonable correlation between simplified theory and experiment.

We may attempt a similar analysis using simplified force/momentum balance using the same simplifying assumptions as above referring to Fig. 5.28 and,

Applying Momentum equation between $\acute{BB}$ and $\acute{CC}$:-

$P_{\acute{BB}} - P_{\acute{CC}}$ = Momentum at $\acute{CC}$ - Momentum at $\acute{BB}$ + resistance section $\acute{BB}$ and $\acute{CC}$ ..... (5.22)

PTO

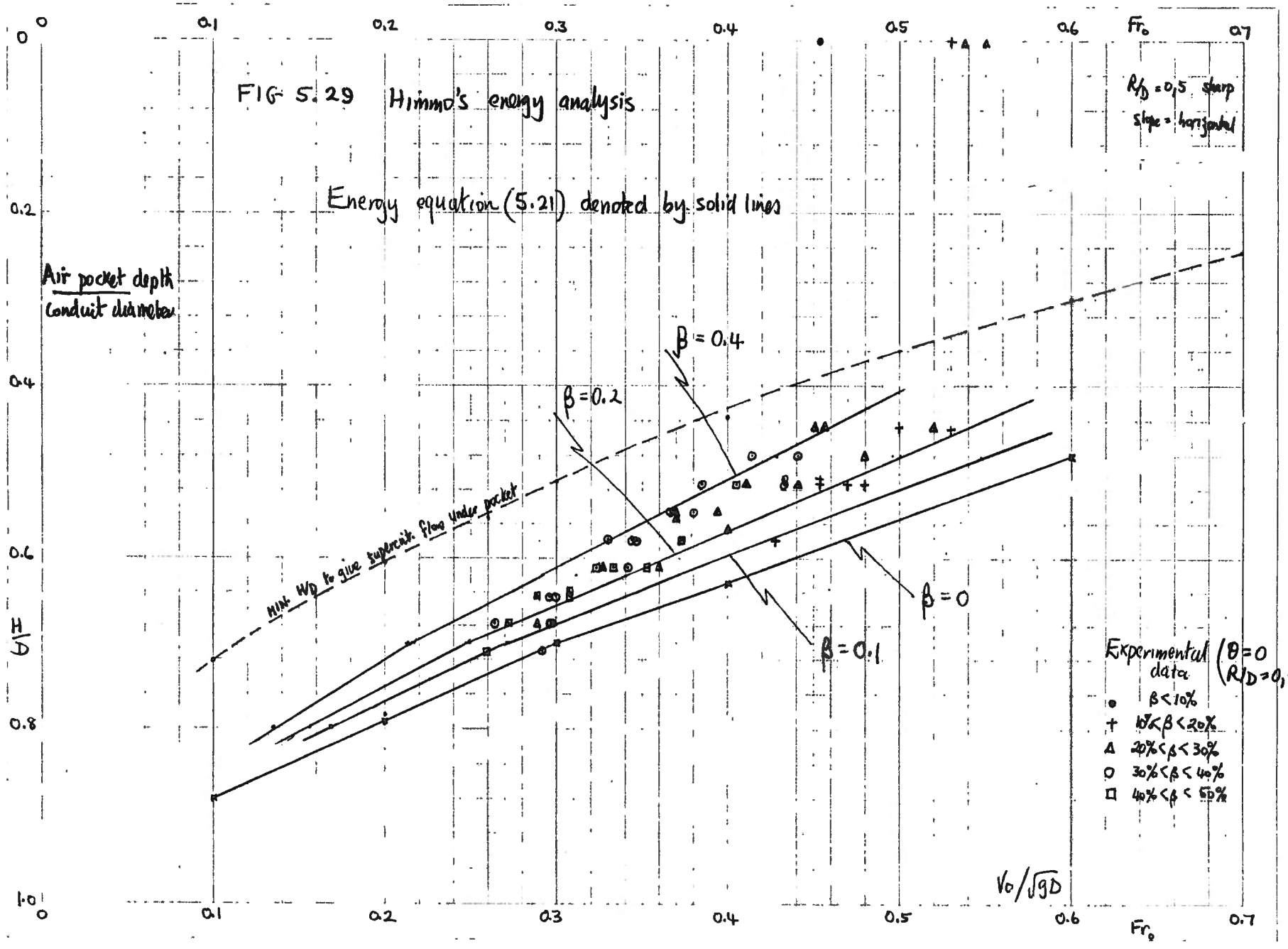
FIG 5.29 Himmo's energy analysis
Energy equation (5.21) denoted by solid lines
$R/D = 0,5$ sharp slope = horizontal
Air pocket depth / Conduit diameter
H/D
$V_o/\sqrt{gD}$
Fr_o
Min. WD to give supercrit. flow under pocket
$\beta = 0.4$
$\beta = 0.2$
$\beta = 0$
$\beta = 0.1$
Experimental data ($\theta = 0$, $R/D = 0,5$)
$\beta < 10\%$
$10\% < \beta < 20\%$
$20\% < \beta < 30\%$
$30\% < \beta < 40\%$
$40\% < \beta < 50\%$

where $P_{BB'} = P_B A_P + \rho g \frac{D}{2} A_P$

$= P_{air} A_P + \rho g r A_P$

$P_{CC'} = P_{air} A_P + \int_a^\pi \rho g h' \, dA$

From Fig.(5.30) section (a-a)

$h' = r \cos a + r \cos (\pi - \theta)$

$= r (\cos a - \cos \theta)$

$dA = 2 r \sin (\pi - \theta) \, dh'$

$= 2 r \sin \theta \, dh'$

$dh' = \sin (\pi - \theta) \, ds$

$= \sin \theta \, ds$

$= r \sin \theta \, d\theta$

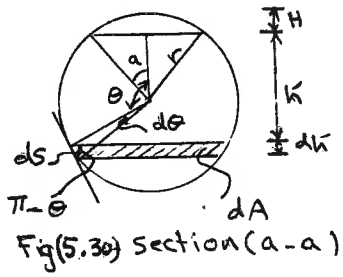

Fig(5.30) Section(a-a)

$\therefore \int_a^\pi \rho g h' \, dA = \int_a^\pi 2 \rho g r^3 (\cos a - \cos \theta) \sin^2 \theta \, d\theta$

$= \rho g r (A_c \cos a + \frac{2}{3} r^2 \sin^3 a)$

$\therefore P_{CC'} = P_{air} A_P + \rho g r (A_c \cos a + \frac{2}{3} r^2 \sin^3 a)$

Momentum at $BB' = \beta_o \rho V_b^2 A_P$ (β_o = M.C.F.)

Momentum at $CC' = \rho V_c^2 A_c$

Substituting into equation (5.22) ignoring resistance BB' CC'

$P_{air} A_P + \rho g r A_P - P_{air} A_P + \rho g r (A_c \cos a + \frac{2}{3} r^2 \sin^3 a)$

$= \rho V_c^2 A_c - \beta_o \rho V_b^2 A_P$

Divided by $(\rho g r A_P)$:-

$$1 + \frac{A_c}{A_P} \cos a + \frac{2}{3} \frac{r^2}{A_P} \sin^3 a = \frac{V_c^2}{gr} \frac{A_c}{A_p} - \beta_o \frac{V_b^2}{gr}$$

Sub. eq.(5.18) into the above equation for V_c

$$\therefore 1 + \frac{A_c}{A_P} \cos a + \frac{2}{3\pi} \sin^3 a = \frac{V_b^2}{gr} \frac{A_P}{A_c} - \beta_o \frac{V_b^2}{gr}$$

$$1 - \frac{A_c}{A_P} \cos a + \frac{2}{3\pi} \sin^3 a = \frac{V_b^2}{gr} \left(\frac{A_P}{A_c} - \beta_o\right)$$

Assuming $\beta_o = 1$ and $V_b = V_o (1+\beta)$, we obtain

$$1 - \frac{A_c}{A_P} \cos a + \frac{2}{3\pi} \sin^3 a = 2 Fr_o^2 (1+\beta)^2 \left(\frac{A_P}{A_c} - 1\right) \quad \text{-----(5.23)}$$

The simplified force/momentum equation (5.23) is shown plotted on Fig. 5.31 using the same experimental data but giving a poorer correlation.

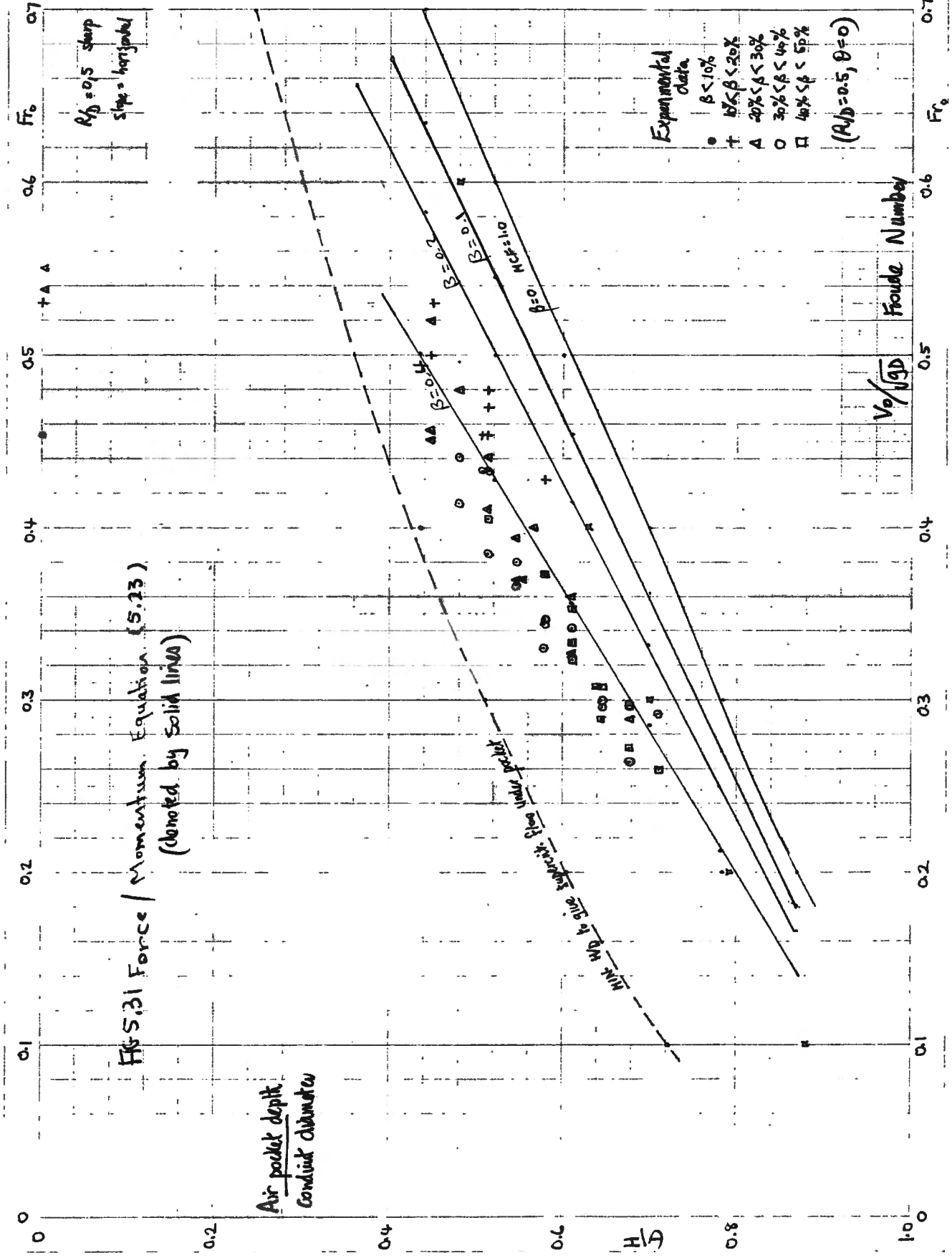

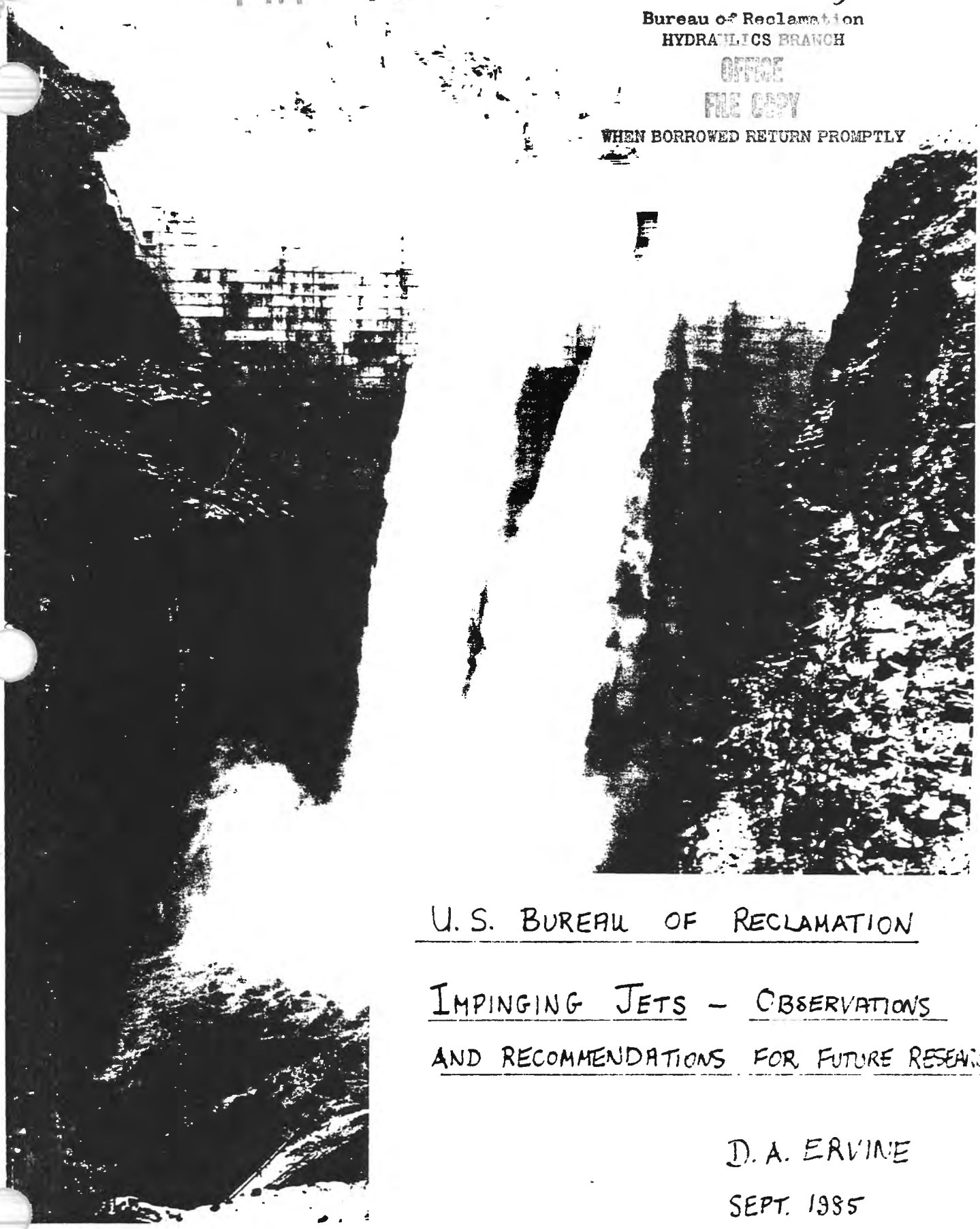

U. S. BUREAU OF RECLAMATION

IMPINGING JETS - OBSERVATIONS AND RECOMMENDATIONS FOR FUTURE RESEARCH

D. A. ERVINE

SEPT. 1985

IMPINGING JETS — OBSERVATIONS AND RECOMMENDATIONS FOR FUTURE RESEARCH

Summary

The purpose of this research work is primarily to make recommendations for future research work on impinging jets at the U.S. Bureau of Reclamation, Denver, Colorado.

The problem stemmed from uncertainty in "scaling up" from model data of pressures on a stilling basin or plunge pool floor, to the prototype situations. The characteristic of this type of plunging jet is a flow of water discharging under a sliding gate high up in a dam structure, plunging through the atmosphere into a plunge pool at the base of the dam, + generating pressures on the plunge pool floor, which can be separated into steady and fluctuating components.

Thus any recommendations will include behaviour of the flow before entering the atmosphere, a detailed study of the jet plunging through the atmosphere, the behaviour of the jet spreading in the plunge pool and the resulting analysis of of pressures experienced on the floor of the plunge pool.

This report commences with some simplified conjectures concerning the behaviour of jets including the influence of upstream turbulence intensity, free surface aeration and more basic parameters such as increasing jet velocity, jet dimensions, plunge length and plunge pool depth. This is followed by high speed photographs of spreading jets and initial lessons learned from such photographs. Some experimental data is presented on initial jet studies and the report concludes with recommendations for future research in this area.

Acknowledgements

Thanks to Hank Falvey for providing so many stimulating ideas for this discussion
Thanks to Warren Frizzell and Brent Mettford for assistance with the laser equipment
Thanks to Don Clem for speedy construction of the apparatus

CONTENTS

INTRODUCTION — SECTION 1

The two photographs overleaf (Page 6) show jets plunging through the atmosphere for a prototype situation (Morrow Point Dam) and a 1/24 scale model of the prototype. The main point of interest (to the USBR) is,

(1) How do pressures in the plunge pool in the prototype relate to those in the model

Other questions of interest are :-

(2) What factors affect the jet spread angle as it plunges through the atmosphere?
(3) What happens to the inner core of the jet?
(4) Why is air entrainment not evident in the model?
(5) What is the effect of air entrainment on plunge pool pressures?
(6) Why is there little or no spray in the model?
(7) How does the impinging jet spread in the plunge pool?
(8) What is the effect of plunge pool geometry?
(9) Are pressure fluctuations more important than mean pressures on the plunge pool floor?
(10) Can this prototype situation be simulated in a model study?
(11) What is the best way to carry out a model investigation of this phenomenon?
(12) Can a realistic math model be made of this situation?
(13) Can the K-ε model be adapted to this complex situation?

These, and many other questions come to mind. This document, in fact, is only a starting off position for some fundamental research into the problem which is soon going to be tackled by USBR, and puts forward some speculations on a few of the questions posed above.

MORROW POINT DAM

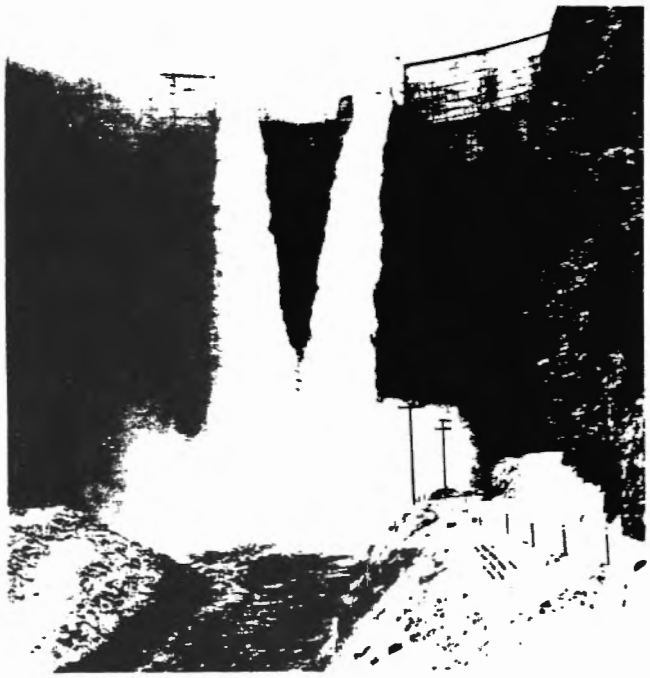

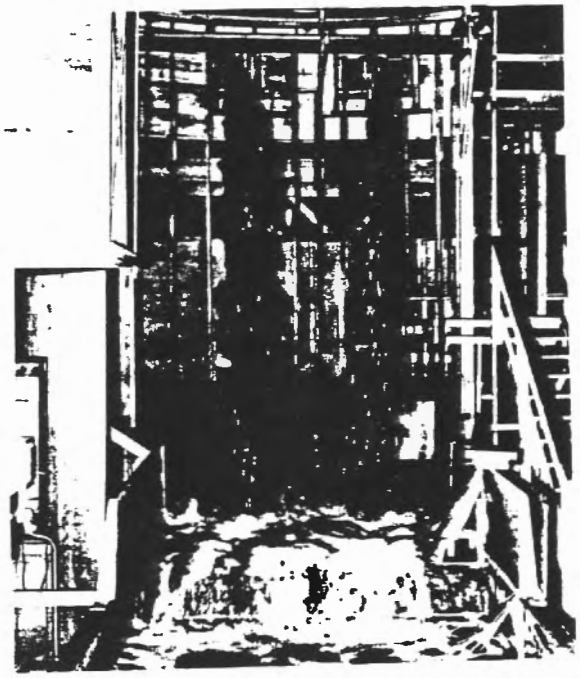

PROTOTYPE / MODEL VISUAL COMPARISON OF PLUNGING JETS

SHOWING APPROX EQUAL JET SPREAD ANGLES

MODEL SCALE 1 : 24 [PROTOTYPE REYNOLDS NO. UP TO 6×10^7 / MODEL REYNOLDS NO. UP TO 5×10^5]

PROTOTYPE MAX. DISCHARGE / JET ~ 280 m^3/s
GATE OPENINGS (MAX) ~ 4.57m x 4.57m

SECTION 2 – SIMPLE PHYSICAL CONJECTURES

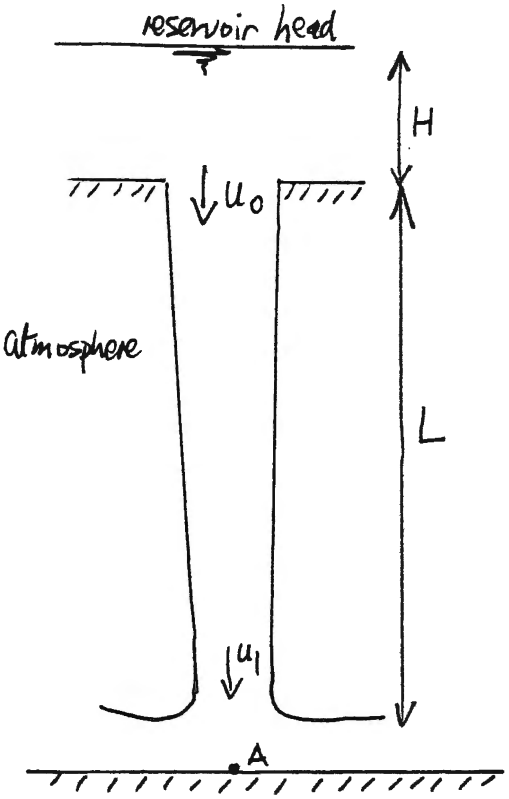

Consider first the grossly over simplified case shown opposite, of a circular, vertical plunging jet with zero turbulence and no air resistance. u_0 is the velocity on entering the atmosphere and u_1 the velocity at impact. Consider first the case of zero plunge pool depth

Accelerating under gravity $u_1^2 = u_0^2 + 2gL$

Max. pressure excluding fluctuations $= \frac{1}{2}\rho_w u_1^2$

Max pressure at A $= \frac{1}{2}\rho_w (u_0^2 + 2gL)$

$$\text{max head} = \frac{p}{\rho g} = \frac{u_0^2}{2g} + L$$

Assuming negligible loss at the reservoir exit, $u_0^2/2g \sim H$
and hence the max. head $\simeq H + L$.

This is unrealistic because of turbulence, air entrainment, definite plunge pool depth, etc.

Consider first the effect of introducing a definite plunge pool depth y.

On entering the plunge pool the jet will spread as shown overleaf, generating shear layers which we will assume to be linear. Little or no. past research has been carried out into this type of shear layer with air entrainment (air bubbles) but early indications reveal an outer spread angle ε, of the region of $\tan^{-1} 14°$ or 0.25. Thus the max. turbulence intensity in this type of shear layer is likely to be of the 0.25.

It can be seen from the diagram opposite that the stagnation pressure now generated $= \frac{1}{2}\rho u^2$
where $u \leq u_1$

It can also be seen that $u = u_1$ when the plunge pool depth is less or equal to y_c

or when $y < y_c$ $\quad p = \frac{1}{2}\rho u_1^2$ as before

It becomes important therefore to obtain an estimate of y_c

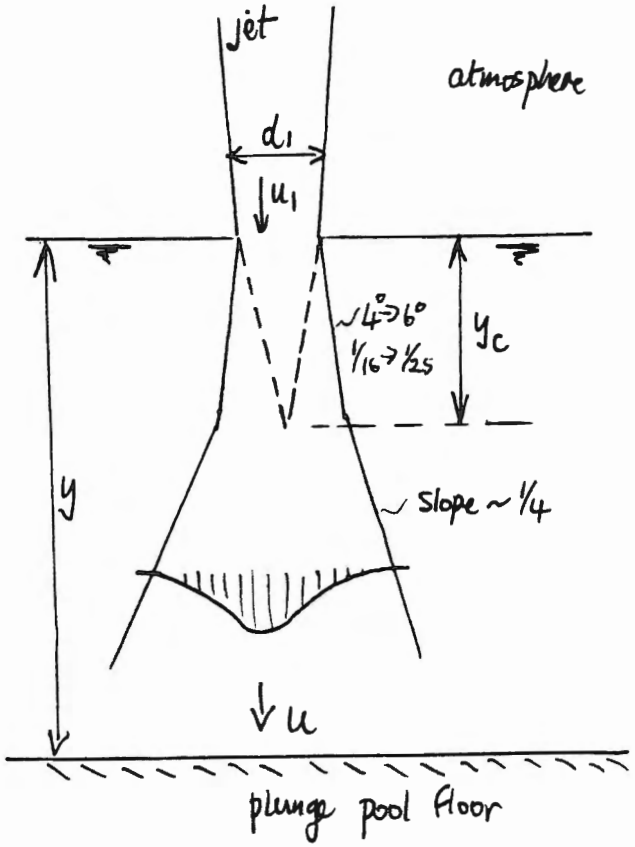

Classical work by Albertson (graph shown opposite) reveals that the maximum jet velocity is obtained for y/d_1 up to 6. This was obtained for circular submerged jets and is thought to be an overestimate for plunging highly turbulent jets (McKeogh)

i.e. for $y/d_1 < 6$, $u = u_1$,
and $p \sim \frac{1}{2}\rho u_1^2$

for $y/d_1 > 6$ $\quad u \sim 6u_1 \frac{d_1}{y}$
and $p = 18\rho u_1^2 (d_1/y)^2$

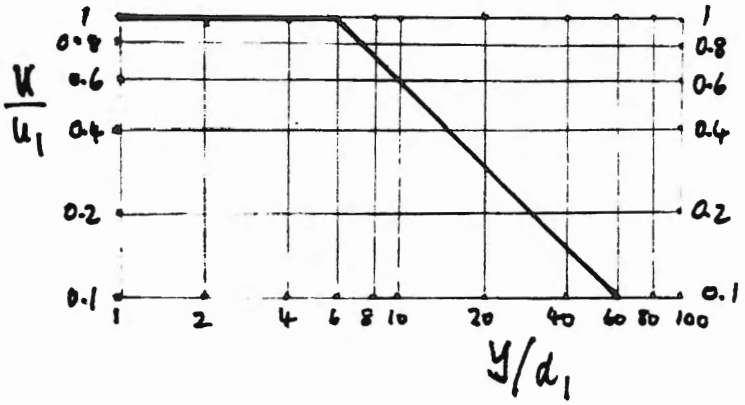

Erich Hausler (1983) postulates that based on prototype + model studies the best design evidence to date is that the core of the jet on entering the plunge pool maintains the core velocity to a depth of 5 d_u, where d_u is the theoretical diameter of the jet due to acceleration of gravity

Thus pressures experienced in this core can be up to $\frac{1}{2}\rho u_1^2$ or a head $\simeq$ L+H

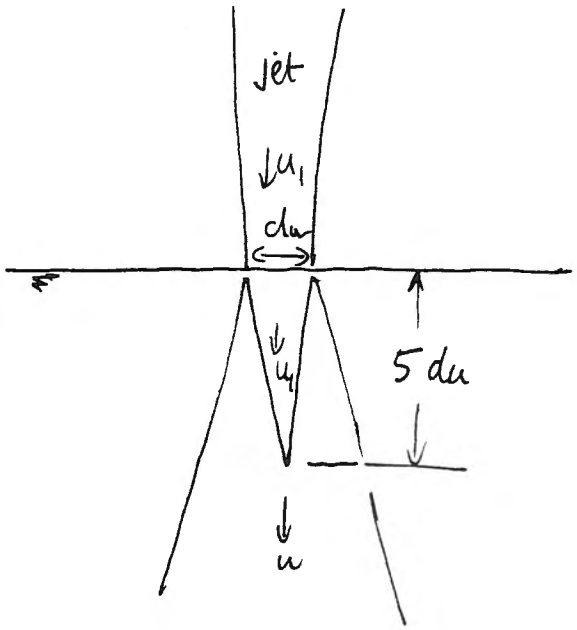

Thus for Morrow Point H+L ~ 120m, u_1 = 48 m/s, Q = 10000 ft^3/s and d_u ~ 2.7m
Therefore 5 d_u = 13.5m = 44 ft Morrow Point only ~ 60 feet deep so not a great deal of help from pool depth.

Using same argument as before $y/d_u > 5$ $u = 5u_1 d_u/y$ $p = 12.5\rho u_1^2 (d_u/y)^2$
or $p = 0.54\left(\frac{1}{2}\rho u_1^2\right)$ ~ 60-65m (= 200 ft)

This now becomes a top priority for research, i.e. the centre-line velocity decay with depth into the plunge pool, so that realistic estimates of max. pressures can be achieved. The should be investigated for the full range of upstream parameters etc

Let us now introduce turbulence into the jet at the point of jet exit into the atmosphere. Assume, to begin with, that the turbulence is homogeneous, isotropic and is generated either in the upstream flow system or the outlet device such as sliding gate / orifice plate, etc, or both together. The most relevant component of turbulent velocity in this case is the radial component $v'/\bar{u}_o$, but for initial assumption of isotropic turbulence, we may use axial turbulence component u'/u

Consider the case where the jet is <u>not</u> accelerating under gravity for the sake of initial simplified analysis. The RMS value to turbulence velocity is denoted by $u' = \sqrt{\overline{u^2}}$. The pressure on the jet surface due to turbulence = $\frac{1}{2}\rho u'^2$

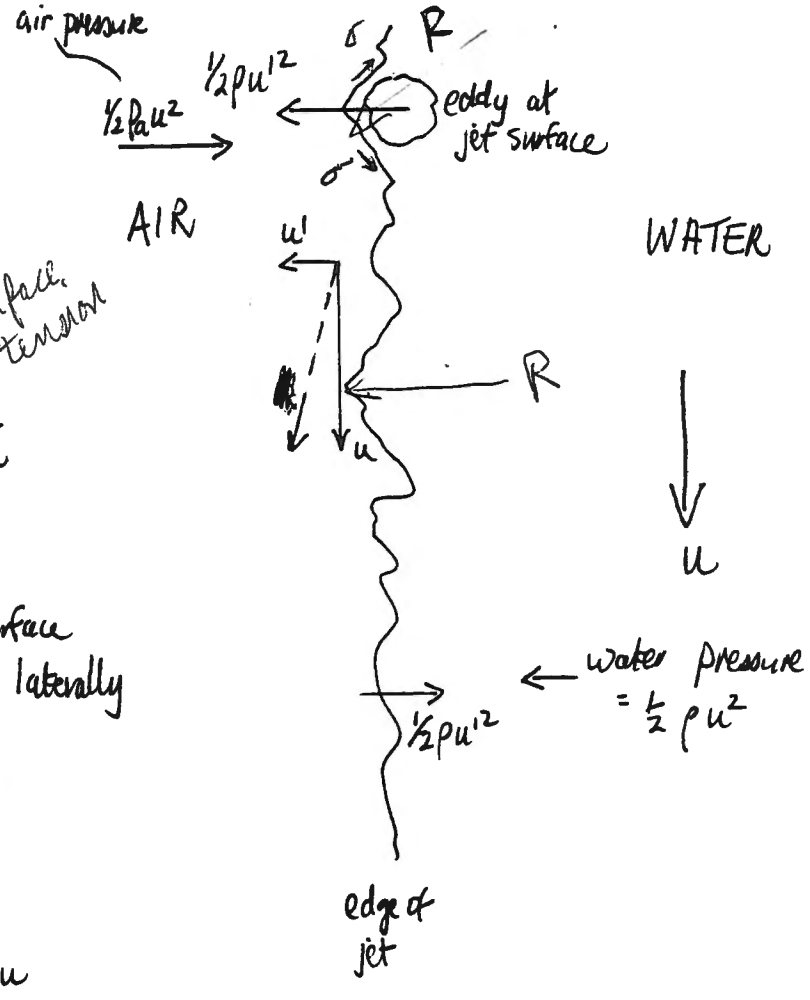

Outward jet surface movements

The outward pressure balance is given by

$\frac{1}{2}\rho u'^2 - \frac{1}{2}\rho_a u^2 - 2\sigma/R$ ← Surface tension

where $\frac{1}{2}\rho_{air}u^2$ is negligible and $2\sigma/R$ is the surface tension pressure

When turbulent energy overcomes surface tension the jet is free to expand laterally at a rate $\tan^{-1}(u'/u)$

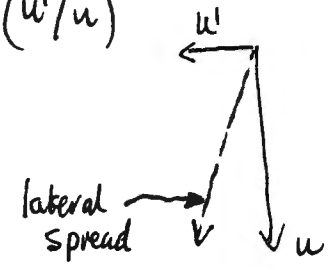

Say that the jet is free to spread, when $\frac{1}{2}\rho u'^2 > 2\sigma/R$. It is obvious that low velocity, low turbulence jets do not spread laterally, but infact contract under the influence of gravity. This will be shown in the photographs in Section, and from initial measurements of spreading angle. Thus we must establish some rough criterion for the initiation of jet spreading due to turbulence otherwise model studies at low velocity and turbulence will never simulate prototype performance.

$$\tfrac{1}{2}\rho u'^2 > 2\sigma/R$$

$\div \frac{1}{2}\rho u^2$ gives

$$\left(\frac{u'}{u}\right)^2 > \frac{2\sigma}{R}\frac{1}{\frac{1}{2}\rho u^2} \sim \frac{0.3}{1000u^2 R}$$

This presents a problem in estimating what value A should be at the transition from jet contraction to jet expansion. A further problem exists in defining u'/u. This in fact is the average turbulence intensity acting, and for Gaussian distribution turbulence, initiation of spreading is more likely to stem from peak values of u'/u, which are of the order of $3u'/u$. Furthermore a water droplet pushed out from the core of the jet is likely to have a diameter approximately twice the capillary length (2.7mm) and hence $R \sim 2.7$mm. Thus

$$\left(\frac{u'}{u}\right)^2_{peak} \sim 9\left(\frac{u'}{u}\right)^2_{mean} \sim \frac{0.3}{1000u^2\,\frac{2.7}{1000}} \sim \frac{1}{9u^2}$$

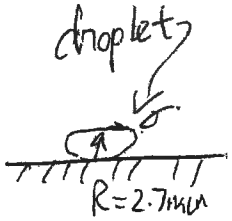

$$\therefore \left(\frac{u'}{u}\right)^2_{mean} \sim \frac{1}{81u^2}$$

Or for initiation of spreading $\left(\frac{u'}{u}\right)_{mean} \sim \frac{1}{9u}$ (or $u' \sim 0.11$)

$.1 \rightarrow .15$ u. m/s

Using the values of jet velocity used in the photographs

		Required turbulence level		Actual u'/u
when	$u = 3.2$ m/s	$u'/u \sim 3.5\%$	not achived	$2.5 \rightarrow 3\%$
	$u = 5$ m/s	$u'/u \sim 2.2\%$	achieved	$3-4\%$
	$u = 10$ m/s	$u'/u \sim 1.1\%$	achieved	8%

It is of interest to note here that in initial tests, the only jet which did not spread was the 3.2 m/s jet, which according to the estimates above should have had a turbulence level of 3.5% for spreading, but in fact had a turbulence level of $2.5 \rightarrow 3\%$. More tests required to be carried out in this area.

Thus we might speculate, that if turbulence is sufficient to cause a jet to spread, then the angle of spread might be $\simeq u'/u$. as shown overleaf denoted by δ_2.

The next, and more important question concerns the inner contraction of the jet core. i.e. if the jet is spreading laterally, then by continuity, the inner core is contracting laterally. (This is, as well as the effect of gravity). It is reasonable to assume that the inner core, ignoring the effect of gravity, contracts less quickly than the outer edge spreads. The rationale for this is embodied in the fact that outer spread is met only with surrounding air pressure whereas, inner spread is met by the jet core pressure ($\frac{1}{2}\rho u^2$).

Simplified continuity model for jet behaviour. (spreading jets only)

Initially the basic assumption is that the jet core is NOT contracting due to gravity. i.e. this might be similar to a high velocity jet entering the atmosphere with little or no effects of gravity over short distances from its point of exit. Assume the edge of the jet is fluctuating as shown on the sketch (this is based on high speed photographs to be presented later) Assume the outer spread is denoted by δ_2 and the inner core contraction by δ_1. Assume also that velocity is constant everywhere and equal to the initial jet velocity at exit to the atmosphere.

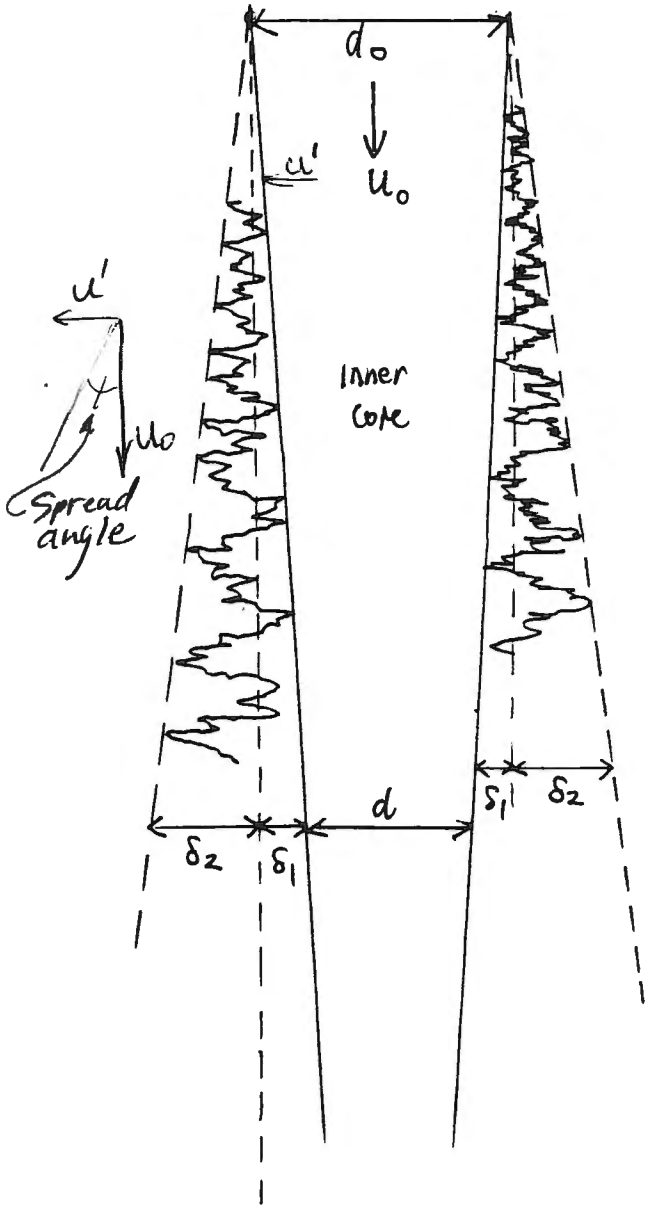

The unevenness in the jet surface due to turbulence as indicated in the sketch opposite, is also occurring in cross section as shown below

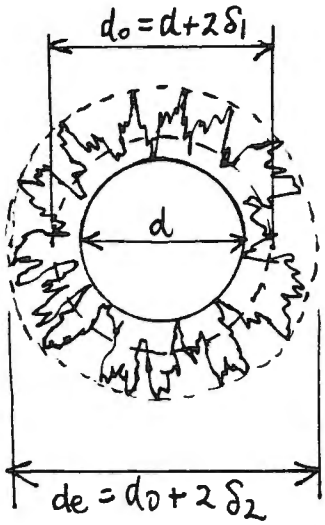

By continuity,

$$u_o d_o^2 = u_o d^2 + K_1 u_o (d_o^2 - d^2) + K_2 u_o (d_e^2 - d_o^2)$$

where $K_1 = P_1/100$, and P_1 is the average probability of having water in δ_1 and $K_2 = P_2/100$, and P_2 is the average probability of having water in δ_2 and $P_2 < P_1$. or $K_2 < K_1$.

Thus, $(d_o^2 - d^2)(1 - K_1) = (d_e^2 - d_o^2) K_2$

where $K_1 < 1$ and $K_2 < K_1$

Now $d_o = d_1 + 2\delta_1$ or $d = d_o - 2\delta_1$

hence $d_o^2 - d^2 = d_o^2 - (d_o^2 - 4d_o\delta_1 + 4\delta_1^2) = 4\delta_1 d_o - 4\delta_1^2$

Also $d_e = d_o + 2\delta_2$ or

$$d_e^2 - d_o^2 = d_o^2 + 4d_o\delta_2 + 4\delta_2^2 - d_o^2 = 4\delta_2 d_o + 4\delta_2^2$$

Thus $(4\delta_1 d_o - 4\delta_1^2)(1 - K_1) = (4\delta_2 d_o + 4\delta_2^2) K_2$

$$\div 4d_o^2 \quad \left[\delta_1/d_o - (\delta_1/d_o)^2\right](1 - K_1) = \left[\delta_2/d_o + (\delta_2/d_o)^2\right] K_2$$

Ignoring 2nd order terms meanwhile, we obtain

$$\delta_1/d_o (1 - K_1) \sim \delta_2/d_o K_2$$

$$\text{or} \quad \delta_1/\delta_2 \sim K_2/1 - K_1 \sim \bar{P}_2/100 - \bar{P}_1$$

where P_2 is the average probability in the outer part of the jet, etc.

The major question at this point therefore was concerned with the fact as to how to estimate probability for the edge of this type of jet. Early conjecture would suggest that surface disturbances on the jet are due to turbulence which is essentially Gaussian and hence probability at the edge of the jet is also likely to be approximately Gaussian

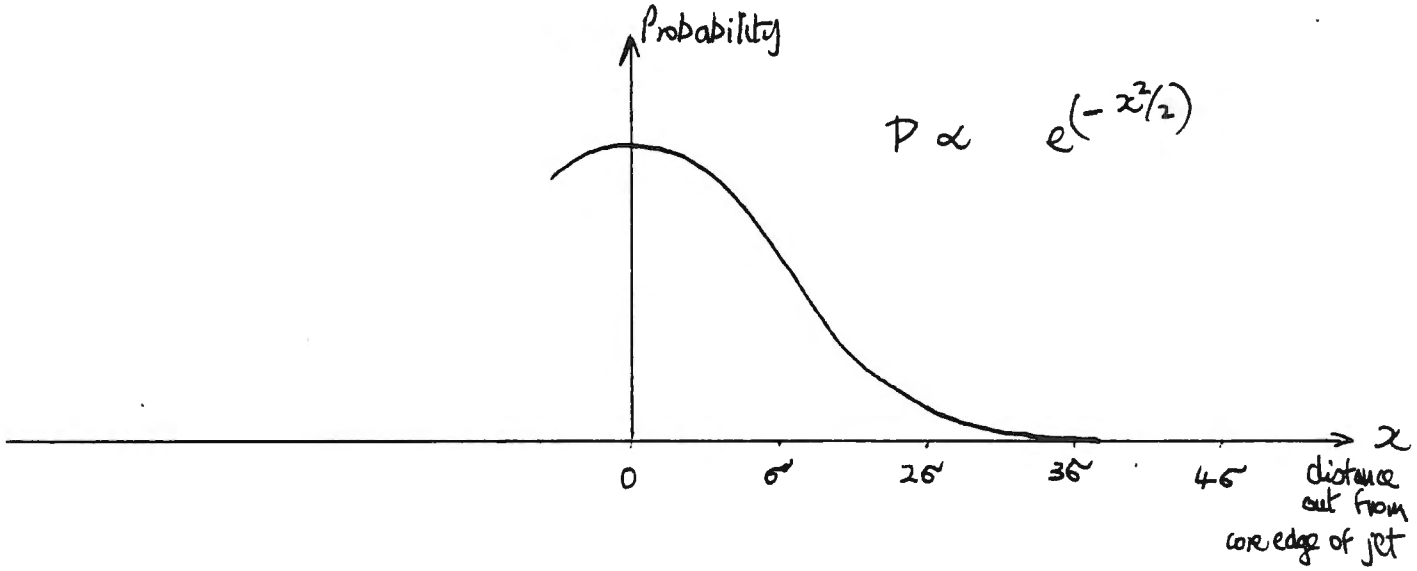

For initial verification, the author carried out a single test using Hank Falvey's probability probe on the edge of a jet, $U_{vc} = 8$ m/s, orifice diameter 50mm, $d_{vc} \sim 39$mm, distance downstream of orifice ~750mm. The probe was traversed from station 4 to station 10 as indicated on Fig overleaf each station 5mm apart. It can be seen that the experimental probability points are close to a Gaussian distribution apart from at great distances from the edge of the jet (see station 9 and 10, Fig)

The author would argue that the real probability for the purpose of calculating the discharge in the continuity equation above, is in fact the measured probability squared. That is, the measured probability is for longitudinal surface disturbances, whereas the same process is occurring around the jet perimeter. Thus we might obtain a reasonable estimate of δ_1 / δ_2 by using Fig and assuming the probability is the measured probability squared

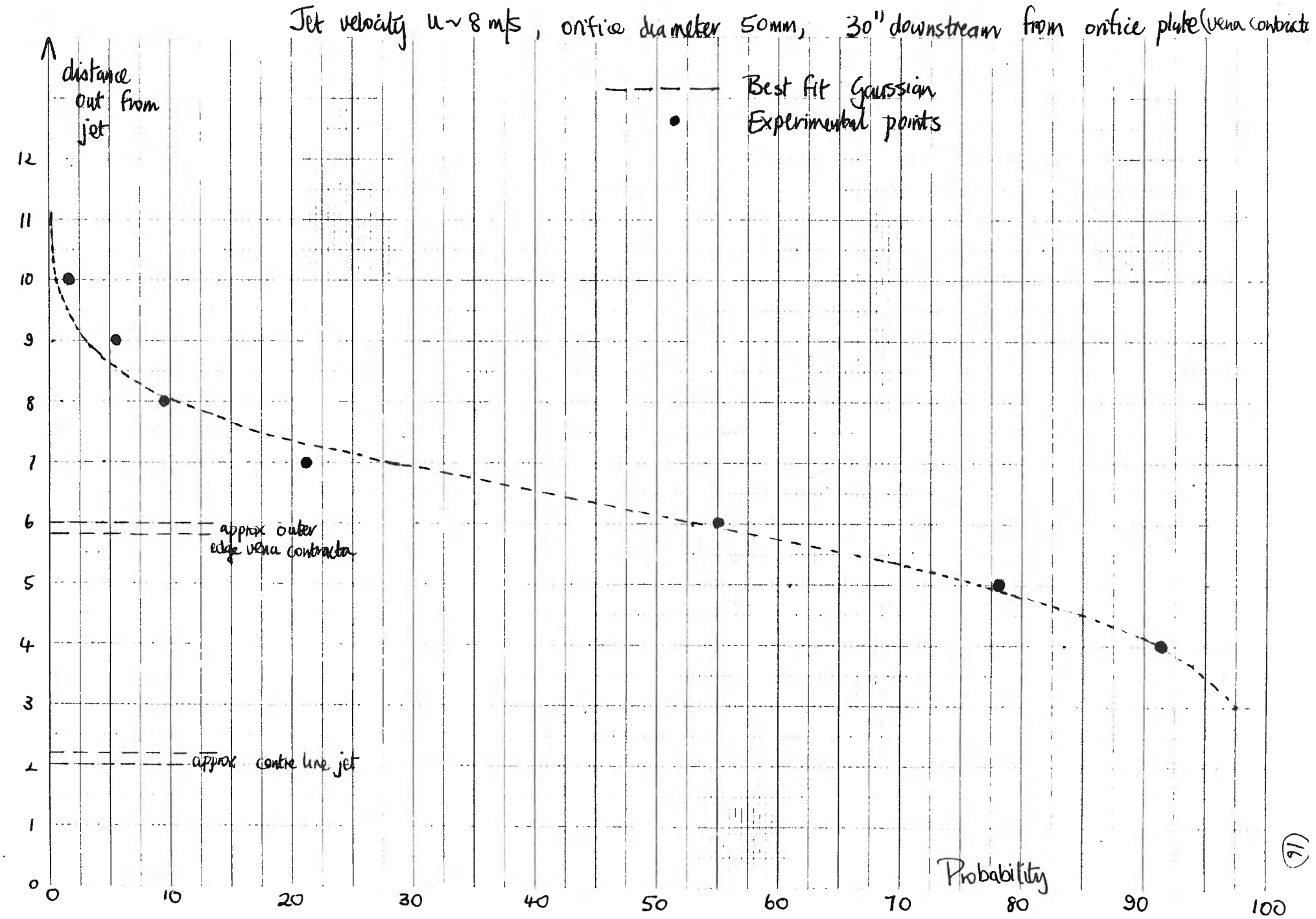
Jet velocity u ~ 8 m/s, orifice diameter 50mm, 30" downstream from orifice plate (vena contracta
distance out from jet
Best fit Gaussian
Experimental points
approx outer edge vena contracta
approx centre line jet
Probability
0
1
2
3
4
5
6
7
8
9
10
11
12
0
10
20
30
40
50
60
70
80
90
100

(91)

The rationale advanced for this is over simplified, but rests in the fact that the shape of surface undulations on the jet surface are assumed to be pyriamds as shown on the sketch below

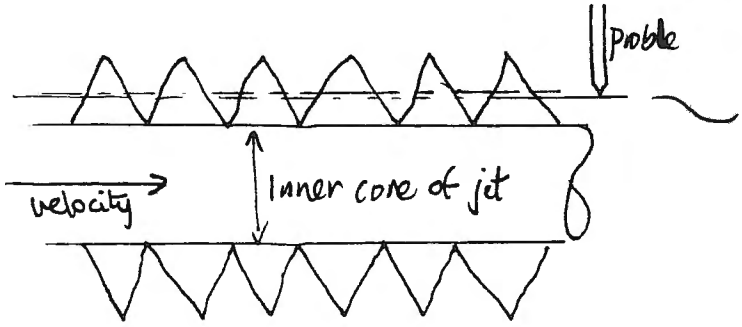

a probability probe placed here will measure 50% probability

however

when we look at a cross section of the jet as shown opposite, it is apparent that the discharge in an annulus around the position of 50% probability will give $Q = \frac{\pi}{4}(d_1^2 - d_2^2)u \frac{1}{2}$

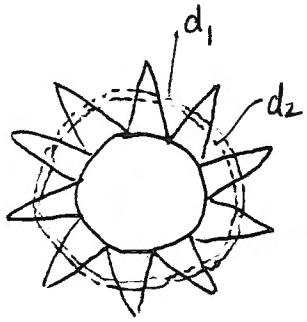

Cross section of jet

Thus when we take into account 50% probability longitudinally, the real discha in the annulus is $Q = \frac{\pi}{4}(d_1^2 - d_2^2)u\left(\frac{1}{4}\right)$

i.e. the "real" probability is 25%

This has important implications for the ~~spres~~ contraction of the inner core If we return to our probability graph, then a new probability graph may be constructed, which is essentially Probability "squared". The result shows that for the outer part of the jet i.e. outside the line of the vena contracta, the pr average probability "squared" is 4% and inside the line is 72%.

Thus we have as an order of magnitude, that

$$\delta_1/\delta_2 \sim P_2/_{100-P_1} = \frac{4\%}{100-72\%} = 1/7$$

i.e. the inner core contracts at a rate of only 1/7 of the outer spread

This has important implications for pressures on a plunge pool base. The smaller the core becomes at the point of impact on the plunge pool is smaller the pressures are likely to be

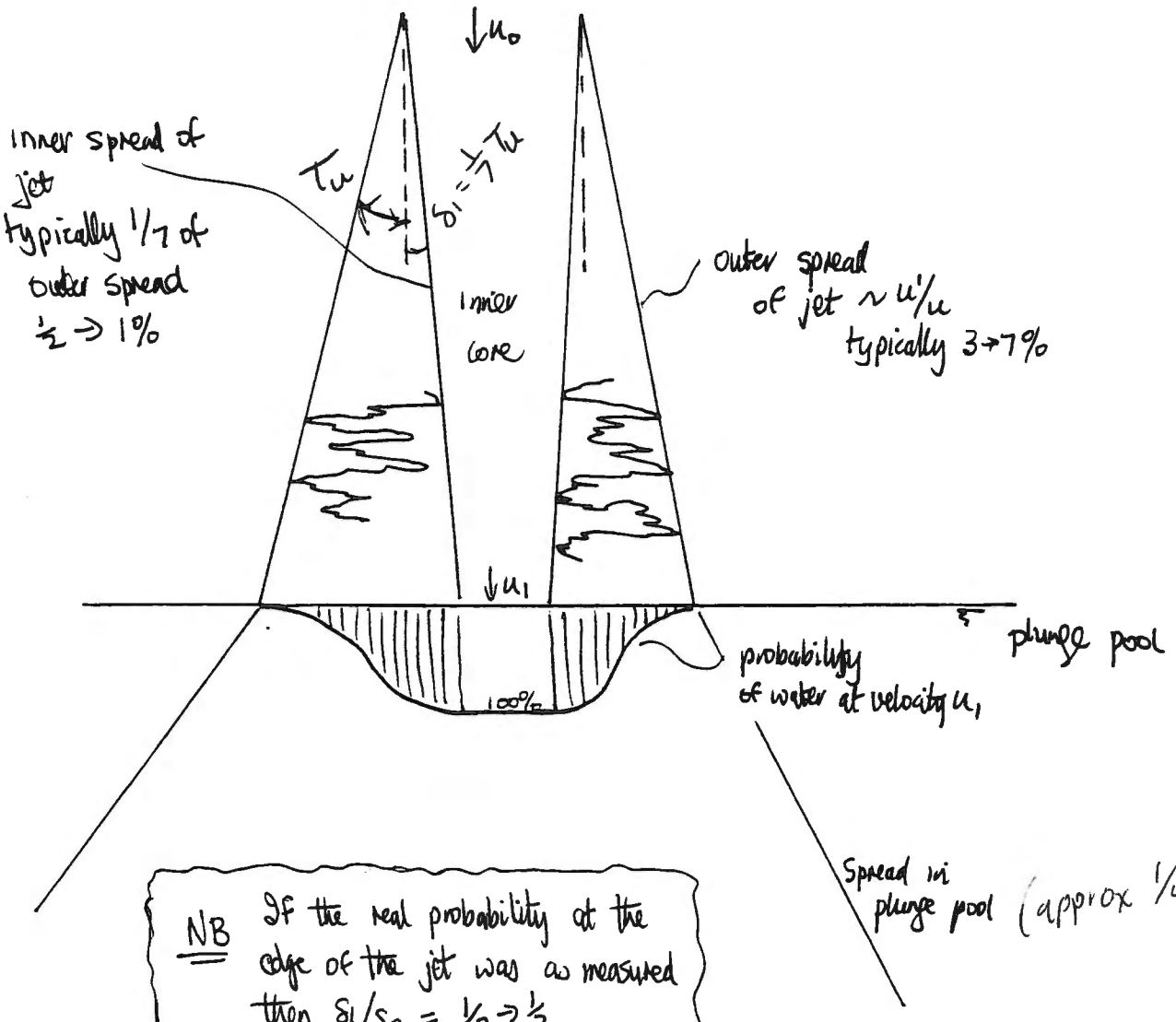

NB If the real probability at the edge of the jet was as measured then $\delta_1/\delta_2 = ½ \rightarrow ⅓$

The behaviour of such a jet (shown overleaf) spreading in a plunge pool is extremely complex. Most authors in fact approximate the jet to a simple solid core accelerating under gravity and having velocity u_1 at impact and diameter d_u (calculated from total discharge Q and velocity u_1)

What is really happening, is an inner solid core with diameter $d < d_u$ because of continuity of the outer spread. This inner core may have similar spreading characteristics in the pool to a submerged jet

Although Hausler recommends an inner core (in the plunge pool) contraction of 1/5, I believe high turbulent aerated jets may decay at 1/4 solely based on half angle of spread = $u'/u \sim 0,25$
Thus when $y > 4d_u$, $u = 4u_1\left(\frac{d_u}{y}\right)$

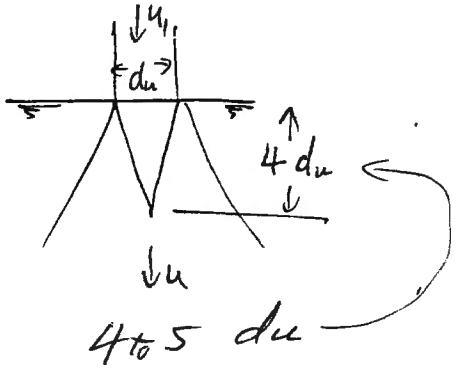

At the outer edges of the jet, water is entering in plunge pool as large droplets of water. Is the pressure of droplets felt at the plunge pool floor? One possible idea is that discrete droplets form waves on the plunge pool surface (say, the wave height $\propto$ water droplet size). Such waves would radiate out from the point of impact and pressure on the floor would essentially not be affected until the waves reached a substantial height relative to the plunge pool depth ie. for larger probabilities closer to the jet core. Such waves or surface undulations might show up simply as small amplitude, long wavelength pressure fluctuations on top of the mean pressure which must essentially be generated by the high probability central part of the core.

Thus we might advocate three components of pressure

on the plunge pool floor (1) the mean – due to high probability core (2) low amplitude surges due to surface waves and (3) high amplitude fluctuations due to turbulence in the shear layer

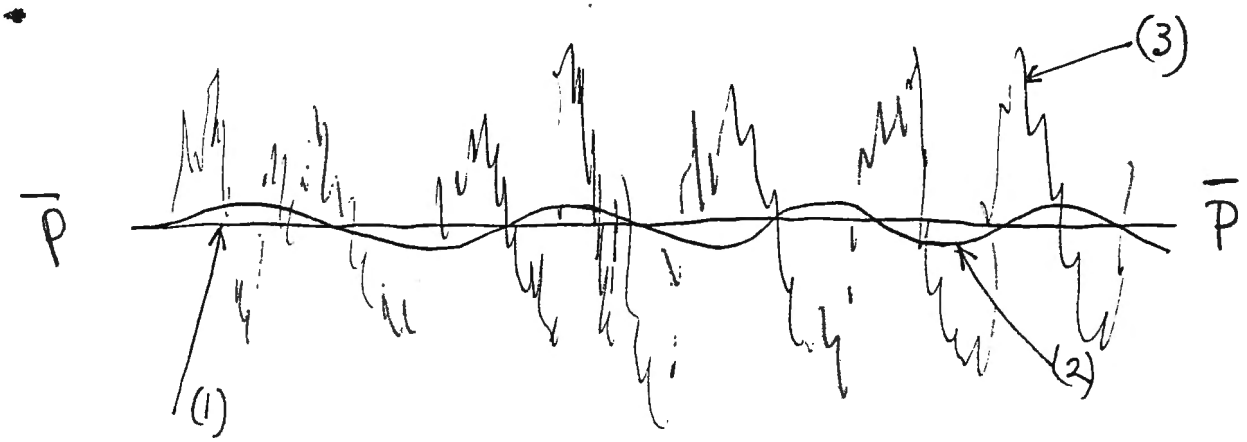

This is an area which to date seems devoid of any serious research work and thus could be incorporated into any future study at the USBR.

The influence of air entrainment

The influence of air entrainment on pressures generated on the plunge pool base is as yet unknown, but some speculations are presented in this section.

First, the model/prototype comparison shown on the Introduction (Section 1) clearly illustrates, that although the spreading angles of the two jets are very similar, the prototype jet entrains air across its free surface whereas the model does not. (Later in this section we will discuss the conditions necessary for the commencement of free surface aeration) Thus the most obvious effect is that prototype jets may appear white whereas model jets may not.

Second, the mean pressures experienced on a plunge pool base must be reduced with the introduction of air bubbles. If we consider the hypothetical case where air bubbles are completely and uniformly distributed though the plunging jet, then the resulting mixture might be approximated to a pseudo-fluid with density $(1-\alpha)\rho_w$, where α is the air void fraction. Thus the max. possible impact pressure for this pseudo fluid would be

$$\Delta p_{max} \simeq (1-\alpha)\rho \tfrac{1}{2} u_1^2$$

i.e. for an air concentration of 50% the max. pressure would be reduced by 50% and so forth.

It is technically possible for air concentrations of 70%, giving $\Delta p_{max} \simeq 0.3 (\tfrac{1}{2}\rho u_1^2)$

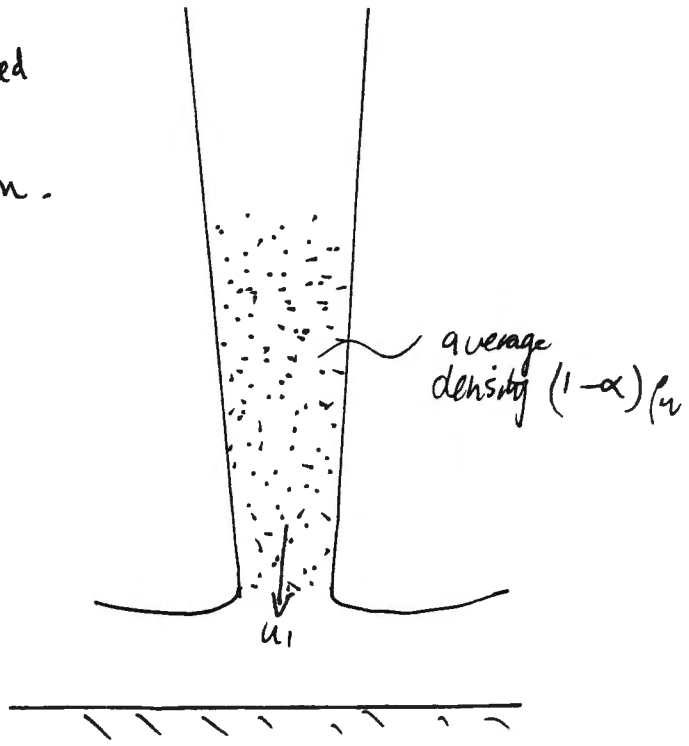

Third, the influence of air bubbles in a plunge pool, will provide a cushion or sponge effect, so that cavitation events in the most intense region of shearing vortices should be greatly curtailed if not eliminated. This mechanism would be analagous to air slots in tunnel spillways.

To illustrate these points more effectively, let us compare a model and prototype situation as shown on the sketch overleaf, and let us make the following assumptions

(1) both model and prototype have equal turbulence intensities, and equal outer and inner angles of jet spread (δ_1 and δ_2)

(2) The outer core of the prototype jet is saturated with air bubbles ($\alpha = 0.5 \rightarrow 0.7$), whereas the outer core of model jet contains no air bubbles.

(3) At the plunge point both model and prototype entrain air bubbles of approximately equal diameter and hence, bubble rise velocity in the plunge pool approx equal ($u_{br} \sim 0.25$ m/s)

(4) There is a linear decay in air concentration with plunge pool depth. This is based on the premise that centre-line jet velocities in the plunge pool decay linearly.

(5) In an unconfined pool some bubbles will descend until $u \sim 0.25$ m/s this being the maximum penetration depth of the air bubbles and the point of zero air concentration. The air concentration profile thus decreases linearly from maximum at the free surface to zero at the point $u = 0.25$ m/s

(6) The pressure on the plunge pool floor thus is $\frac{1}{2} \rho u^2 (1 - \alpha)$ where α is the average air concentration at that point

(7) Assume the initial air concentration is the same in model + prototype on entry to the plunge pool ($\alpha = 0.6$, say)

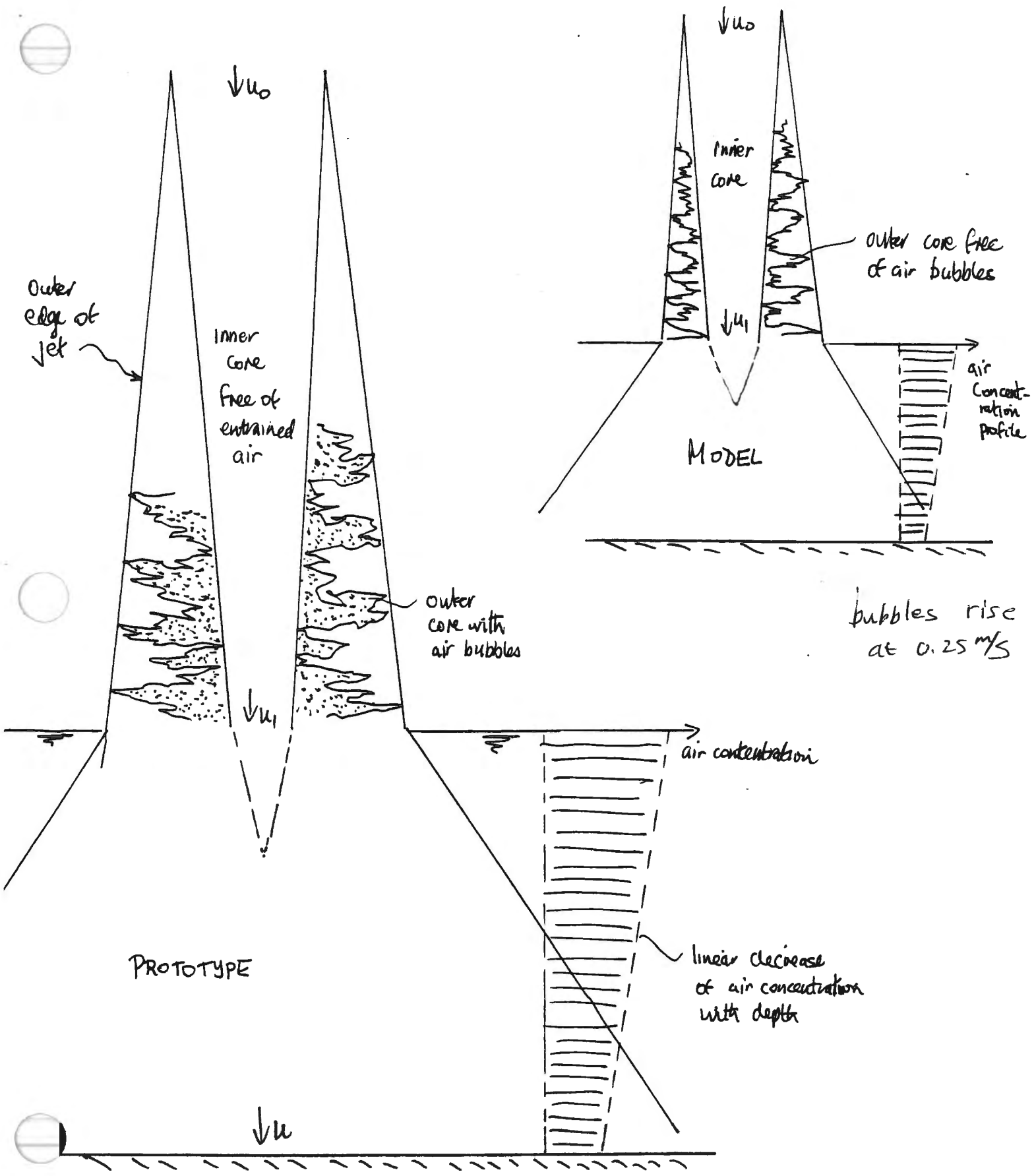
u_o
Outer edge of jet
Inner core free of entrained air
Outer core with air bubbles
u_1
air concentration
Linear decrease of air concentration with depth
u
PROTOTYPE
u_o
Inner core
Outer core free of air bubbles
u_1
air Concentration profile
MODEL
bubbles rise at 0.25 m/s

Using model / prototype data for Morrow Point.

u_1 prototype = 48 m/s

Q_p = 283 m^3/s

shear layer spread 1/4

max air bubble penetration

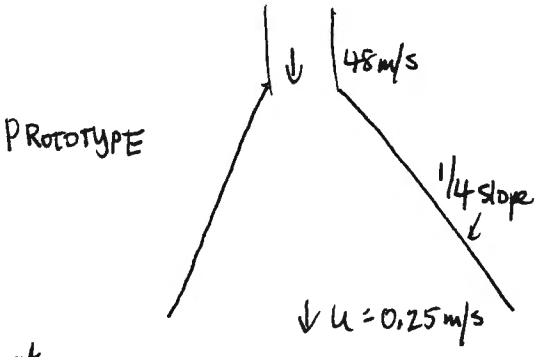

Area at u = 0.25 m/s → $A = \frac{283}{0.25} = 1133\ m^2$

$d = 38\ m$

Vertical distance = 70m = max penetration

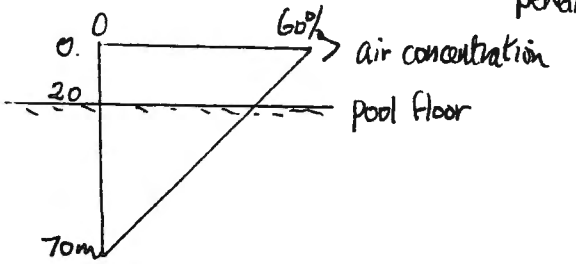

Pool Floor $\alpha = 43\%$

$P = 0.57\ (\frac{1}{2}\rho u^2)$

PROTOTYPE

u_{model} = 9.8 m/s

$Q_{model} \sim 0.1\ m^3/s$

shear layer spread 1/4

max air bubble penetration

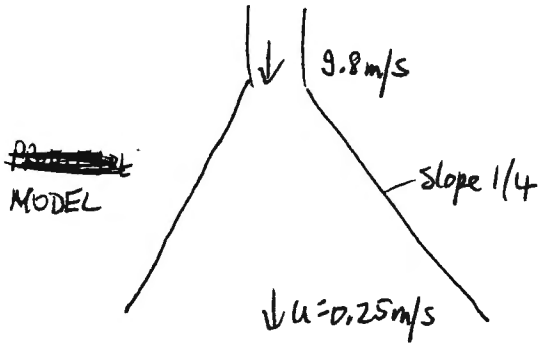

Area at u = 0.25 m/s → $A = 0.1/0.25 = 0.4\ m^2$

$d = 0.71\ m$

Vertical distance = 1.2m = max penetration

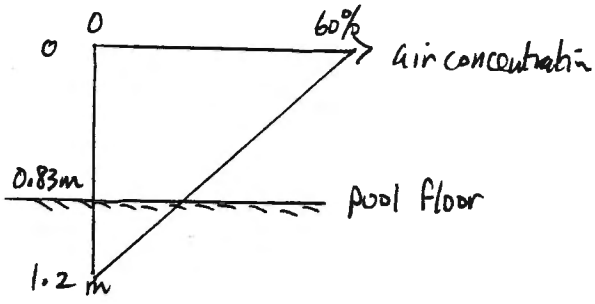

Pool Floor $\alpha = 18\%$

$P = 0.82\ (\frac{1}{2}\rho u^2)$

MODEL

As an order of magnitude the mean prototype pressures at Morrow Point plunge pool will be 70% of predicted pressures from model. This is a measure of air entrainment influence.

Pressure fluctuations in plunge pools

So far in our discussions we have considered only mean pressures likely to be acting in plunge pool basins. A plot of pressure with time is more likely to look like

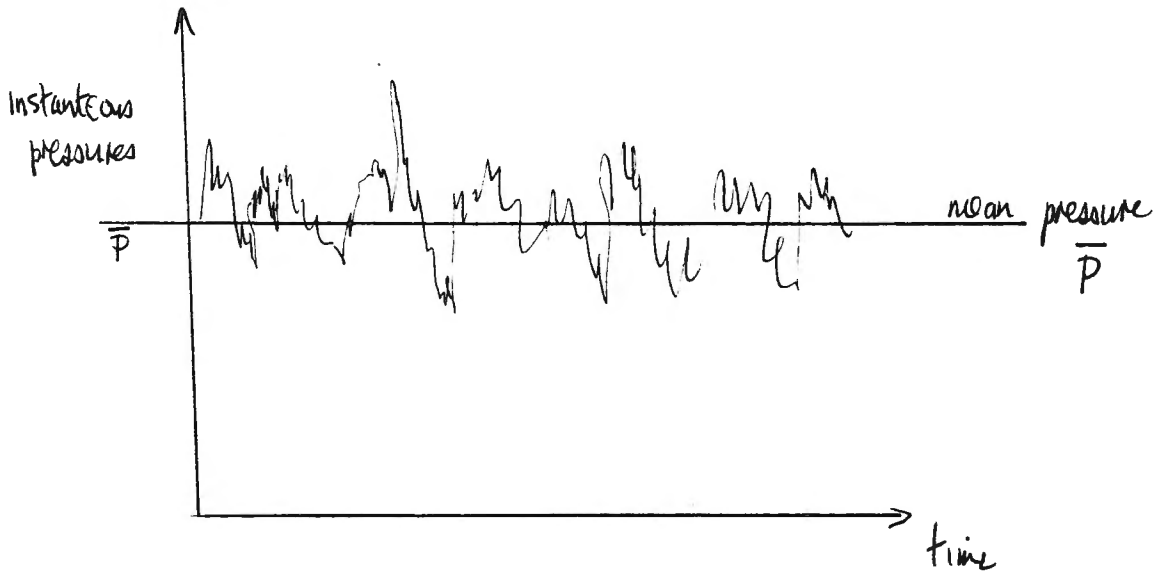

What magnitude are the peak pressures likely to be above the mean? Should a plunge pool basin be designed for instantaneous peak pressures if their period of existence is very small? These questions may be answered more fully from model studies and also application of the $K-\varepsilon$ model, or simply by consulting with Hank Falvey!

My own thoughts are probably over simplified and go as follows,

① In a plunge pool shear layer it has been shown that the half angle of spread is approx. equal to the mean turbulence intensity

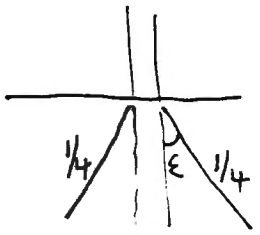

or $\varepsilon \sim 1/4 \sim \dfrac{\sqrt{\overline{u'^2}}}{u}$

(2) Pressure in the spreading jet $= \frac{1}{2}\rho u^2$

and turbulent pressure RMS value $\sqrt{\overline{p'^2}} = \frac{1}{2}\rho\left(\sqrt{\overline{u'^2}}\right)^2$

$$\therefore \frac{\sqrt{\overline{p'^2}}}{\bar{p}} = \frac{\frac{1}{2}\rho\left(\sqrt{\overline{u'^2}}\right)^2}{\frac{1}{2}\rho u^2} = \left(\frac{u'}{u}\right)^2_{RMS} = \left(\frac{1}{4}\right)^2 = \frac{1}{16}$$

(3) Now according to Gaussian probability turbulence

$$\left(u'/u\right)_{peak} \sim 3\left(\frac{u'}{u}\right)_{RMS}$$

$$\therefore \left(u'/u\right)^2_{peak} = 9\left(\frac{u'}{u}\right)^2_{RMS} = 9/16 = 0.56 = \left(\bar{P}'/\bar{P}\right)_{peak}$$

In other words peak fluctuating pressures $p' \sim 0.56\,\bar{P}$

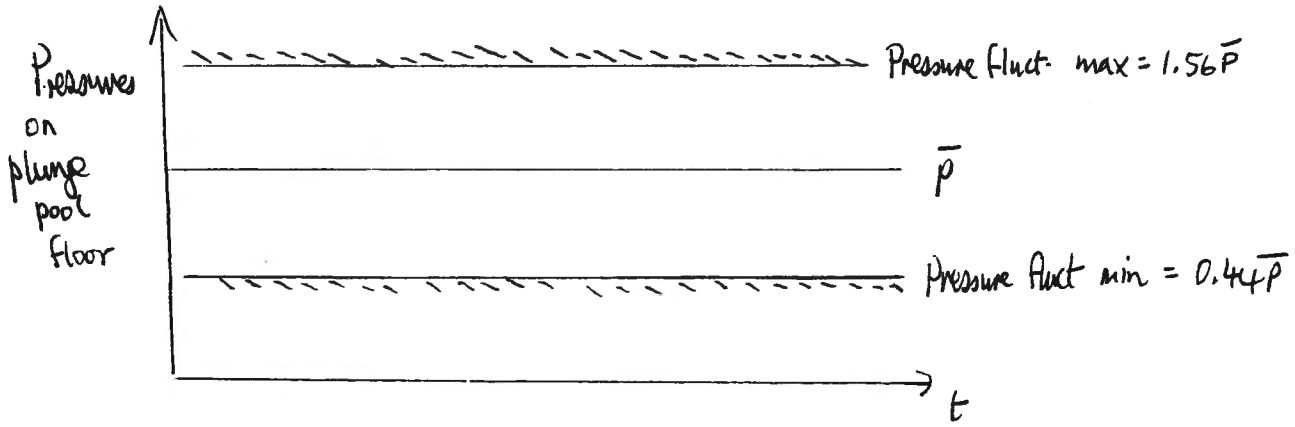

Thus for morrow Point model $\bar{P} \sim 120$ ft $\therefore P_{max} \sim 187$ ft
P_{max} is more likely to occur at higher Reynolds Number flows

The only other question now is if this type of plunging jet is likely to cavitate. Certainly submerged jets with no air entrainment can cavitate at high velocity when the cavitation index is small. According to Hank Falvey, the most likely mode of cavitation is that generated in the intense vortex cores close to the plunge pool surface. Cavitation bubbles may then be transported downstream by the vortex cores and cause damage on the solid boundary. In my view this is unlikely in deeper plunge pools with air concentrations typically 40–70%

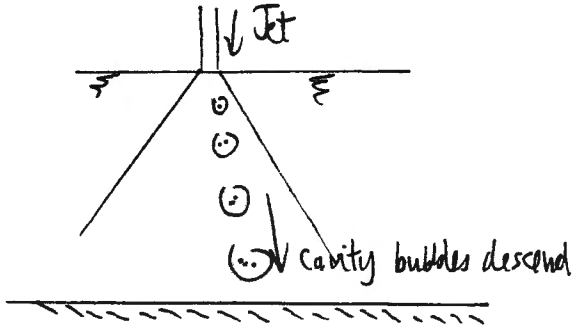

However, shallow plunge pools with the plunge pool depth, less than the zone of flow establishment, this phenomenon may indeed produce cavitation pressures at the solid boundary, much greater than $p'/\bar{p} = 0.56$. Also for shallow pools $\bar{p} \sim \frac{1}{2}\rho u_1^{*2}$ or the mean pressure head can be as high as the reservoir head. Thus p'(peak) can be as high as 1.56 × reservoir head, or if cavitation occurs p' peak > 1.56 × reservoir head

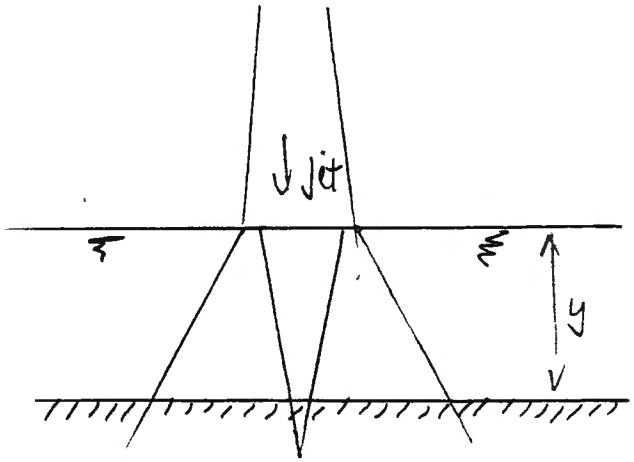

$y < y_c$

Cavitation possible at boundary

Lesson Ensure a deep plunge pool

Summary—to calculate pressures on a plunge pool floor

(1) The maximum average pressure on a plunge pool floor $\bar{P} \sim \frac{1}{2}\rho_w u^2 (1-\alpha)$

(2) The maximum instantaneous pressure $\sim 1.56\bar{P} = \frac{1}{2}\rho u^2 (1.56)(1-\alpha)$

where u is the centre line velocity at the plunge pool floor and α is the average air concentration at that point

(a) to calculate u, assume the inner core of the jet on entering the pool contracts at $1/4 \rightarrow 1/5$ i.e.

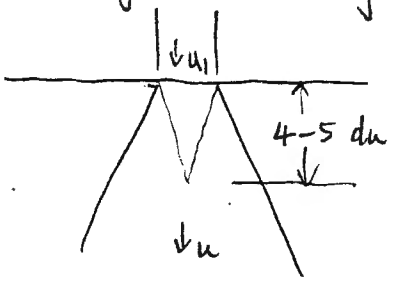

calculate u_1 for the jet accelerating under gravity

$\therefore$ when $y < 4 \rightarrow 5\, d_u$, $u = u_1$

when $y > 4 \rightarrow 5\, d_u$, $u = 4 \rightarrow 5\, u_1 \left(\frac{d_u}{4 \cdot y}\right)$

(d_u is simply calculated from $Q/u_1 = \pi/4\, d_u^2$)

(b) to calculate α, assume α at plunge pool surface $\sim 50-70\%$

Calculate penetration depth of bubbles until $u = 0.25$ m/s for unconfined pool

assume linear decay of α with depth for an unconfined pool

$\therefore$ Calculate value of α at plunge pool floor

$$\therefore \frac{\bar{P}}{\frac{1}{2}\rho u_1^2} = 16 \rightarrow 25 \left(\frac{d_u}{y}\right)^2 (1-\alpha) = \frac{\bar{P}}{(H+L)}$$

For Monroe Point $\frac{\bar{P}}{(H+L)} = 0.33 \rightarrow 0.5\,(1-\alpha)$

where $\alpha \sim 18\%$ model

$\alpha = 43\%$ prototype

SECTION 3 — A TANGENT — INCEPTION CONDITIONS FOR FREE SURFACE

The criterion for inception of free surface aeration in open channel flows has been elusive. Some theories have been presented (see Kobus and Rao) all of which have had limited success. One thing we are sure of, is that free surface aeration is encouraged by high turbulence levels. This is evident in open channel spillways where the criterion is essentially free surface aeration where the turbulent boundary layer comes to the free surface. (This in fact also needs to be accompanied with a high mean velocity)

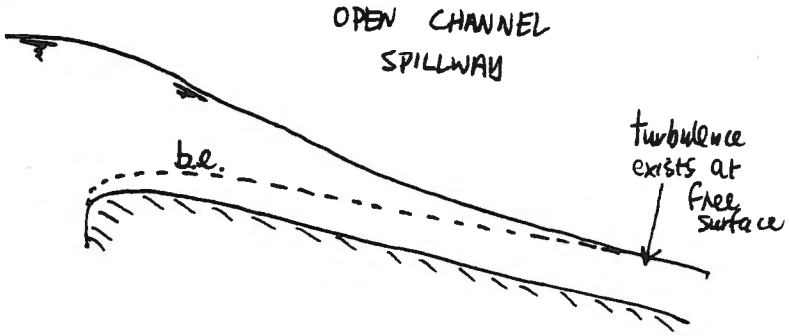

The same principle is in evidence for air slots. These appear to act as a turbulence generator, which has the ability to transfer turbulence from the underside of the jet to the upper surface even though the boundary layer is not fully developed.

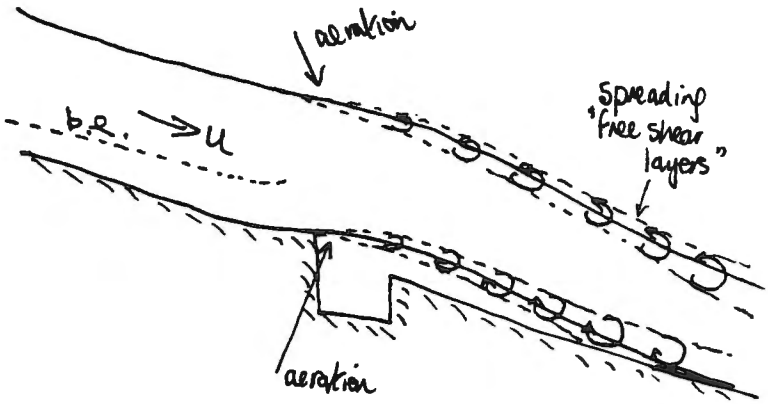

AIR SLOT

The boundary layer is in fact completely disrupted and the equivalent of free shear layers develop on both sides of the jet. These decay is intensity in the downstream direction as the turbulence is essentially artificially generated. In larger models the free shear layers will have the capacity to cause free surface aeration if the following conditions are met

(a) the turbulent energy is sufficient to overcome surface tension pressures

(b) the turbulent energy in the shear layer vortices is sufficient to trap and transport air bubbles i.e. for small scale models, small vortices may be formed where turbulent energy is dissipated by viscosity. This is a function of Reynolds Number (Re) or eddy length/jet dimension l'/d

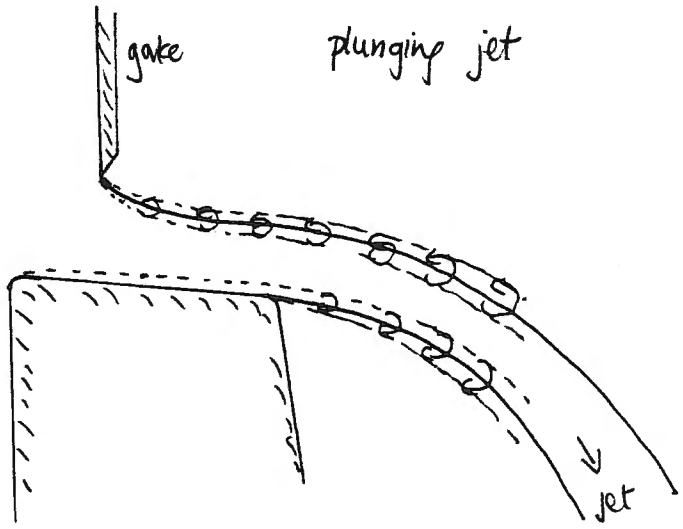

Thus aeration in an air slot is analogous to a plunging jet exiting from an orifice or sliding gate arrangement eg. Morrow point. The gate and the underside concrete base will stimulate the growth of boundary layers on both surfaces of the jet. As well, the gate may act to some degree as a turbulence generator, and thus for this type of jet, the b.l. will always be at the free surfaces of the jet and thus aeration is possible (if conditions (a) and (b) are met) right from the exit to the atmosphere.

The question presents itself, can we predict the onset of free surface aeration for plunging jets? Consider first a dimensional analysis using the method of synthesis

$$f(u, \mu, \sigma, g, \rho, u', \ell', d) = 0$$

where fluid properties μ, σ, ρ are all significant, gravity (g) is included because at least at the upper surface of the jet, aeration may occur by the mechanism of falling water ~~g~~ droplets. The parameter u' is equal to $\sqrt{\overline{u'^2}}$ the RMS of fluctuating velocities and ℓ' is the characteristic eddy length responsible for the onset of aeration.

It will be postulated later that the turbulent energy in the characteristic eddy length reach a certain value, rather than the mean turbulent energy reaching a certain value, to cause aeration.

Using synthesis we obtain

$$f\left(\underbrace{\frac{u^2}{g}, \frac{\nu}{u}, \frac{\sigma}{\rho u^2}, \frac{\nu^{2/3}}{g^{1/3}}, \frac{\nu^2\rho}{\sigma}, \left(\frac{\sigma}{\rho g}\right)^{\frac{1}{2}}, \frac{u'^2}{g}, \frac{\nu}{u'}, \frac{\sigma}{\rho u'^2}}_{\text{Choose 4 from}}, l', d\right) = 0$$

$$f\left(\frac{u^2}{g}, \frac{\nu}{u}, \left(\frac{\sigma}{\rho g}\right)^{\frac{1}{2}}, \frac{\sigma}{\rho u'^2}, l', d\right) = 0$$

$\div d$

$$f\left(\frac{u^2}{gd}, \frac{ud}{\nu}, \frac{\left(\sigma/\rho g\right)^{\frac{1}{2}}}{d}, \frac{\rho u'^2 d}{\sigma}, \frac{l'}{d}\right) = 0$$

where u' is the RMS turbulent velocity at the point of inception

$$\frac{\rho u'^2 d}{\sigma} = f\left(Fr^2, Re, \frac{l_\sigma}{d}, \frac{l'}{d}\right)$$

where l_σ is the capillary length $= \left(\sigma/\rho g\right)^{\frac{1}{2}} = 2.7\,mm$ for air and water.
and l' is the eddy length responsible for aeration.

$\frac{\rho u'^2 d}{\sigma}$ can be sub divided into $\left(\frac{u'}{u}\right)^2 \frac{\rho u^2 d}{\sigma} = \left(\frac{u'}{u}\right)^2 We$

Thus the turbulence intensity to cause free surface aeration

$$(u'/u)^2 = f\left(Fr, We, Re, l_\sigma/d, l'/d\right)$$

Consider then a jet exiting from an orifice or sliding gate, where turbulence exists at least close to the jet surface. Assume initially that the Reynolds number is high, viscosity is not a problem at eddy lengths required to entrain air

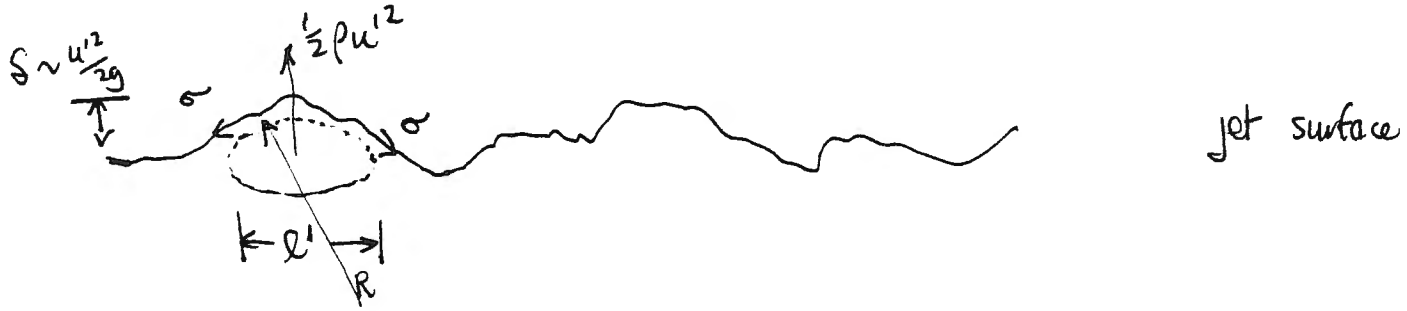

→ jet flow (mean velocity u)

The important parameters here are

(a) outward turbulent pressure = $\frac{1}{2}\rho u'^2$

(b) restraining surface tension pressure $\sim 2\sigma/R$

(c) amplitude of disturbance $\sim \delta \sim u'^2/2g$ (Julian Hunt)

(d) wavelength of disturbance $\propto \ell'$ the eddy length (This is related to the frequency n of surface disturbances by wavelength $\Lambda \propto \ell' = u/n$ Thus the term $\ell'/d \propto u/nd$ = 1/Strouhal Number)

Our first criterion of aeration is surface tension overcome

$$\frac{1}{2}\rho u'^2 > 2\sigma/R \qquad \text{or} \qquad u' > \left(\frac{4\sigma}{\rho R}\right)^{\frac{1}{2}}$$

$$R = 4\sigma/\rho u'^2$$

It is clear from photographs that small velocity jets with small turbulence intensities do in fact produce large values of R, with no free surface aeration

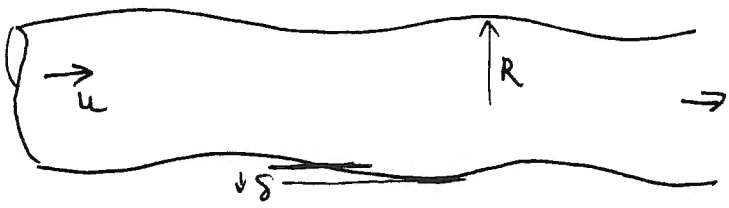

In this case $R \gg \delta$

As we increase velocity, diameter, Re, Turbulence etc, the character of the free surface changes substantially as smaller and smaller eddies have increasing energy levels so that the surface of the jet becomes, and aeration may be possible

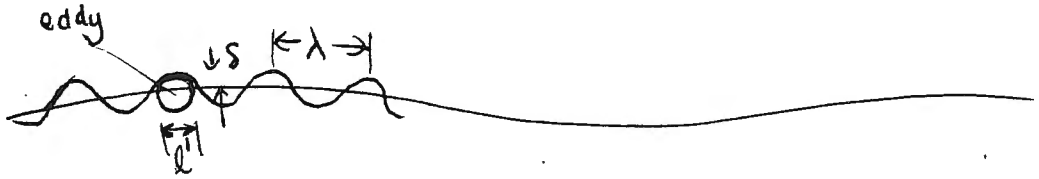

So that $R \sim \delta \sim l'/2 \sim \lambda/4 \sim \frac{u}{4n}$ where n = frequency, u = av. velocity

Now $R \sim 4\sigma/\rho u'^2$ where u' is turbulent velocity in this small eddy

$\delta \sim u'^2/2g$

Thus $4\sigma/\rho u'^2 \sim u_1'^2/2g \sim l'/2$

$u'^4 \sim 8\sigma g/\rho$ or $u' \sim 0.25 \Rightarrow 0.3$ m/s

Thus as a first order approximation of free surface aeration $u' = \sqrt{\overline{u}^2} = 0.25 - 0.3$

Thus $\left(\frac{u'}{u}\right) u = 0.25 - 0.3$

or the velocity required to produce aeration $u = \frac{0.25 \Rightarrow 0.3}{(Tu)}$

Thus for open channel 

the average turbulence intensity at the free surface ~ 5% giving $u = 0.25 \to 0.3 / 1/20 = 5 \to 6$ m/s for aeration

For an air slot, the turbulence generated may be of the order 10%, giving
$u = 0.25 \to 0.3 / 1/10 = 2.5 \to 3$ m/s for aeration

Even for plunge point shear layer where turbulence is as high as 25–30%, then $u = 1$ m/s 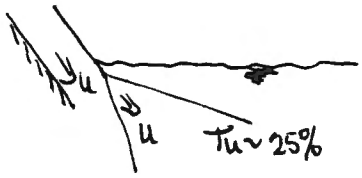

The next question then becomes; is the criterion of $u' \sim 0.25 \to 0.3$ m/s true for all model scales, Reynolds Numbers, etc. <u>The answer is no</u>. What has been presented is simply an average turbulent energy level for high Reynolds Number flows in order to achieve aeration.

To develope this idea further we should again look at our tentative relationship

$$\frac{\sigma}{\rho u'^2} \sim \frac{u'^2}{2g} \sim \ell'/2$$

where ℓ' is the eddy length
$u' \sim 0.25 - 0.3$ m/s

Substituting $u' \sim 0.25 - 0.3$ m/s we obtain a characteristic eddy length of 6 – 9 mm for inception of air entrainment

However, aeration may commence due to peak values of u' rather than mean values, and in Gaussian distribution of turbulence $(u')_{peak} = 3\, u'_{mean}$

Thus $\left(\frac{4\sigma}{\rho u'^2}\right)_{peak} \sim \left(\frac{4\sigma}{9\rho u'^2}\right)_{mean} = \frac{\ell'}{2}$

or the characteristic eddy lengths could be as low as 1 mm

Thus we might speculate that for free surface aeration, eddy lengths in the region $1 \rightarrow 9$ mm should contain sufficient energy, $u' \sim 0.25 \rightarrow 0.3$ m/s In order words we are dealing with an absolute value of turbulent energy at absolute values of eddy length. Incidentally, the required eddy lengths are of the same order as measured air bubble diameters. It follows therefore that peak turbulent fluctuations will produce the smallest bubbles diameters and mean turbulent fluctuations will produce the mean bubble sizes 3-5mm diameter. Therefore bubble sizes are generally smaller than eddy lengths, $d_b \sim \ell'/2$.

If we were now in a position to carry out a spectrum analysis revealing the distribution of turbulent energy within the various eddy lengths (or frequencies), and we compared a prototype flow structure with that of a reasonable sized model and a very small model, the picture would look something like that sketched overleaf

The graph is plotted in absolute terms with the turbulent energy $\underset{\sim}{u'^2}$ against the absolute eddy length. The following points can be made

(1) The prototype flow (large Reynolds Number) will entrain air as $u' > 0.3$ m/s when $\ell' = 1-9$ mm. i.e. the smaller eddies still contain adequate energy and viscous effects do not have sufficient dampening

(2) The large model (curve B) will still entrain air although at large bubble diameters

(3) The smaller model (curve C) will not entrain any air as turbulent energy is dampened in eddies of length $1-9$ mm.

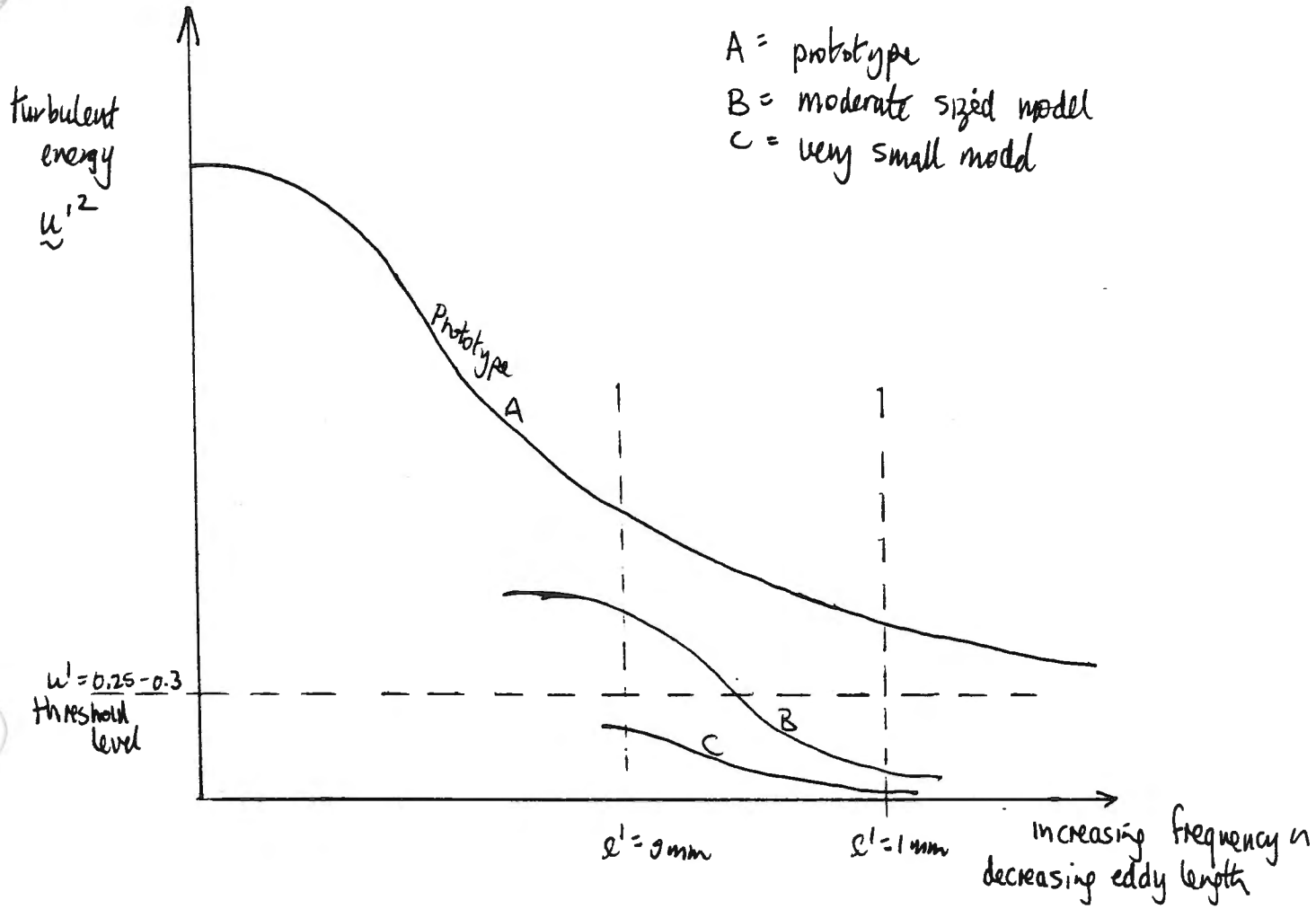
A = prototype
B = moderate sized model
C = very small model
turbulent energy
$\underset{\sim}{u'^2}$
Prototype
A
B
C
$u' = 0.25 - 0.3$
threshold level
$\ell' = 9\,mm$
$\ell' = 1\,mm$
increasing frequency or decreasing eddy length

Experimental apparatus and initial data SECTION 4

Apparatus

It was originally intended to investigate the behaviour of impinging jets spreading through the atmosphere, and a downstream plunge pool using the existing facility with maximum head around 3 m. This tank in fact burst at an early stage and recourse was made to a simpler model designed to produce high velocity, high Reynolds Number jets, but sacrificed somewhat on turbulence control.

The model is illustrated on slides at the lecture and also sketched overleaf in plan view. Flow from the high head pump ($Q_{max} = 6\ ft^3/s$ $H_{max} \sim 600\ ft$) passes through a Venturi meter for flow measurement and later transfers from a 6" diameter high pressure pipeline to an 8" diameter high pressure pipeline. The exit end of the model consists of a 1" thick brass orifice plate constructed in two orifice diameters, 50mm and 100mm. Jets velocities up to 30 m/s were produced and a steel deflector plate was designed to deflect the high velocity jet back to the pump sump. (See slides)

The purpose of this model was <u>not</u> to investigate jets spreading in plunge pools and the resultant pressures, but rather a more simplified study on the behaviour of jets in the atmosphere, including, spreading, free surface aeration, etc, etc. Thus the original tank burst precluded half the proposed area of study, but it was still considered a worthwhile Venture in view of the short time period available.

It was decided to vary the jet velocity 3 - 30 m/s, the jet diameter 50 - 100 mm, the jet turbulence level (if possible), and to investigate jet parameters along the length of the jet, L. The Laser Doppler Anemometer was used to record point velocities and axial turbulence intensities, the probability

Plan View of Model

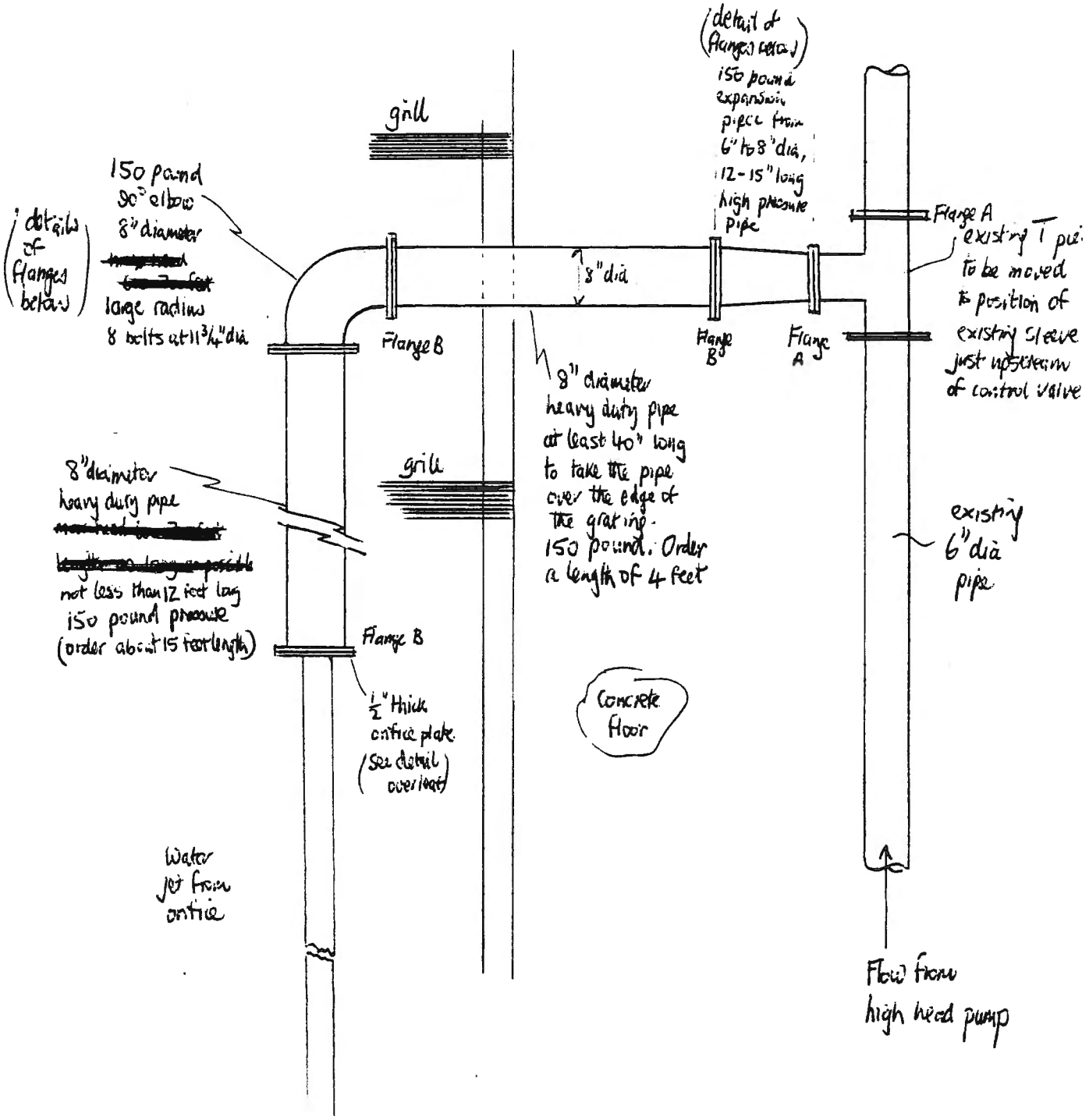

* Flange A 6" dia pipe, 8 bolts, slip on welding flange, 150 pound, 9 1/2" bolt diameter

* Flange B 8" dia pipe, 8 bolts, slip on welding flange, 150 pound, 11 3/4" bolt diameter

Need a minimum of 2 Flange A and 4 Flange B

Side elevation Jet Deflector

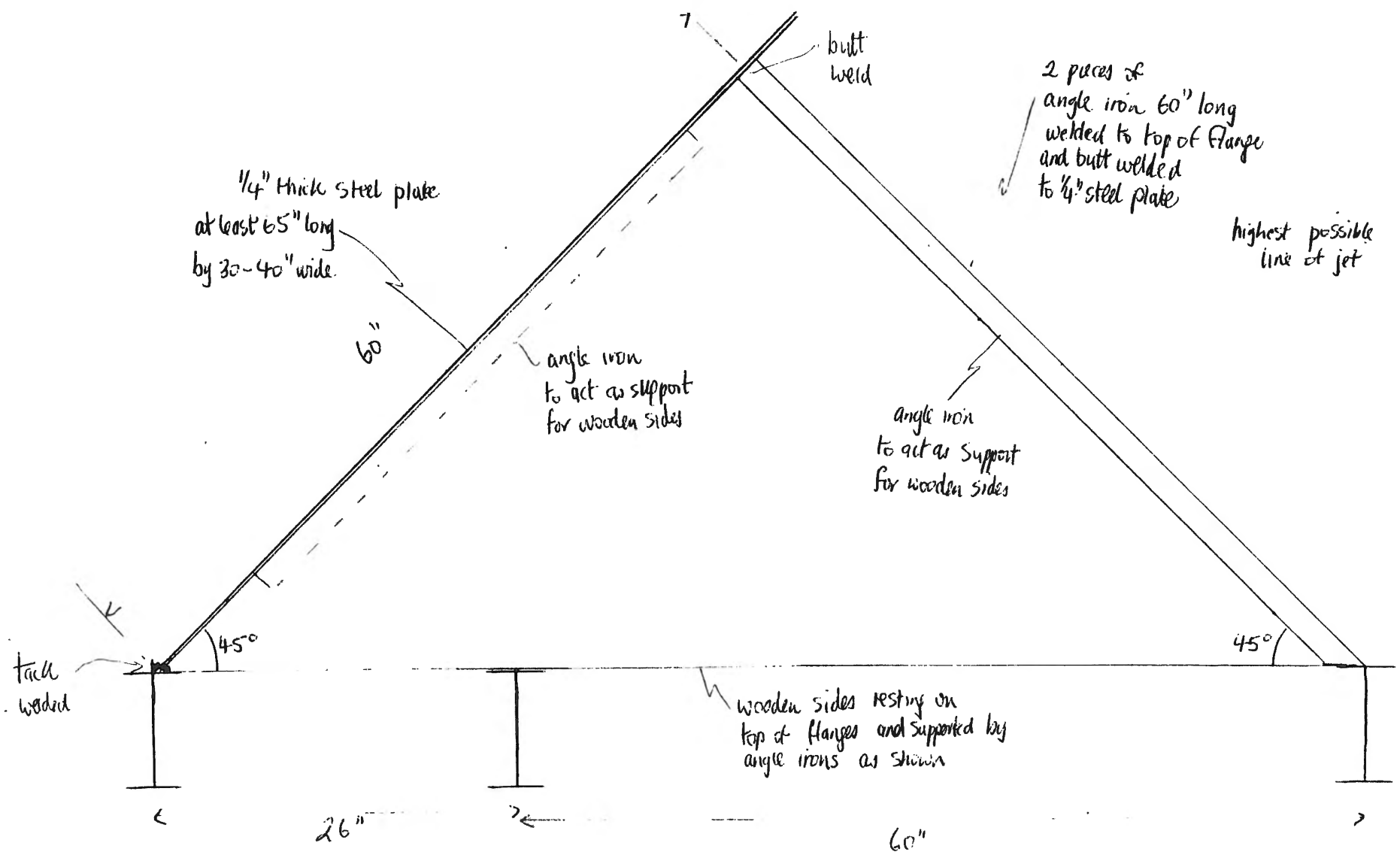

probe was used to determine the nature of the edge of the jet, and high speed photography to capture details of jet spread not apparent to the naked eye.

Initial tests revealed that the jet contained excessive turbulent bursts probably emanating from the elbow upstream of the orifice, the T-piece and the high head pump. It became apparent that satisfactory measurements would require a swirl inhibitor and flow straightener just downstream of the 90° elbow. This was designed (a tube bundle, ½" dia tubes) and installed over the past few days.

Photography

A series of high speed photographs of the 100mm and 50mm jet were taken by Wayne Lambert using stroboscopic light. These will be illustrated in the form of slides at the lecture, but some black+white prints are also included overleaf for interest. The prints overleaf all pertain to the highly turbulent flow case before the introduction of the flow straightner.

The questions which might be answered from these photographs were

(1) the influence of increasing the jet velocity?
(2) the influence of increased distance L from the orifice plate?
(3) the influence of varying the jet diameter?
(4) the influence of varying turbulence intensity?
(5) the incepting point of free surface aeration? velocity?
(6) the variation in jet surface roughness and air entrainment on the upper jet surface as opposed to the lower surface?
(7) the conditions under which fine spray developed off the edge of the jet.

The two pages of photographs overleaf for the 100 mm jet show the influence of both increasing velocity and increasing distance out from the orifice plate

(a) increasing jet velocity has a dramatic effect on the texture of the jet surface. – At $u = 3.3$ m/s → smooth undulating surface, small δ, large R
– At $u = 5$ m/s → surface begins to be disrupted, distinct undulations appear, no air entrainment, larger δ, smaller R
– At $u = 11.8$ m/s ⇒ extensive air entrainment, surface increasingly undulated, larger δ, smaller R, greater frequency of undulations entrainment appears to occur equally at upper and lower surfaces of jet
– At $u = 17.7$ m/s ⇒ greater surface disruption, first signs of jet surface disturbed by aerodynamic forces, first signs of fine spray off the edge of the jet, greater aeration etc
– A $u = 20 - 30$ m/s the process becomes even further disrupted

Thus it appears that an increase in velocity encourages more energetic eddies at the smaller eddy lengths (say < 10 mm) leading to higher frequency disturbances, greater amplitude of disturbances, smaller wavelengths, more air entrainment and spray.

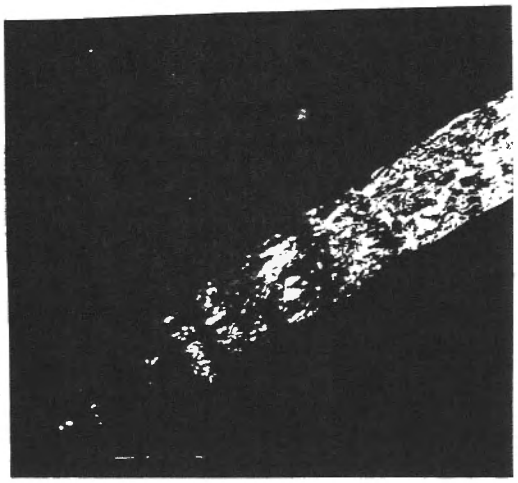

d_o = 100mm, L = 22"-37", u_{vc} = 3.3 m/s

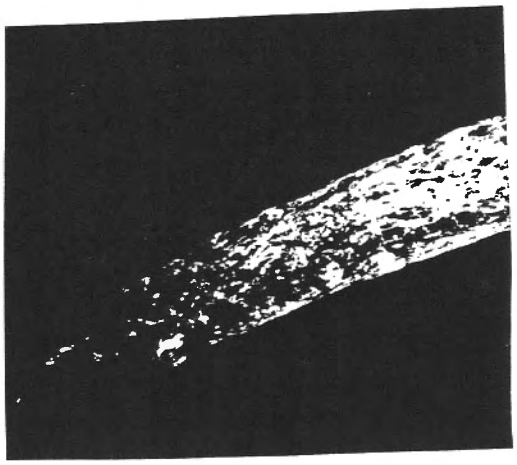

d_o = 100mm, L = 9"-23", u_{vc} = 3.3 m/s

d_o = 100mm, L = 22-37", u_{vc} = 5 m/s

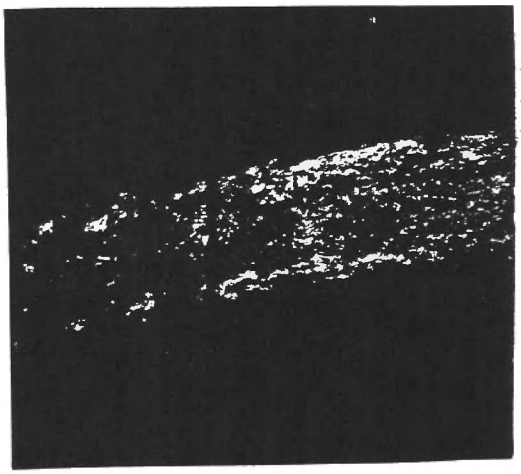

d_o = 100mm, L = 9"-23" u_{vc} = 5 m/s

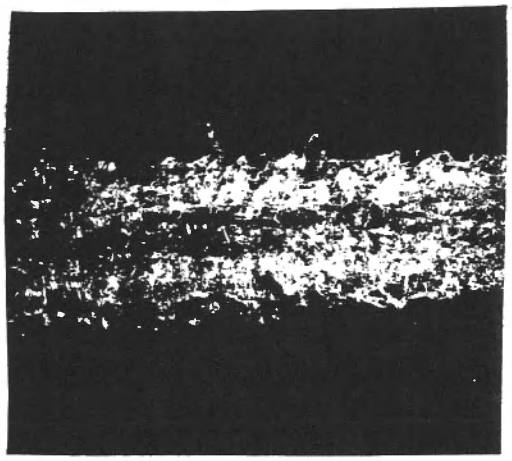

d_o = 100mm, L = 22-37", u_{vc} = 11.8 m/s

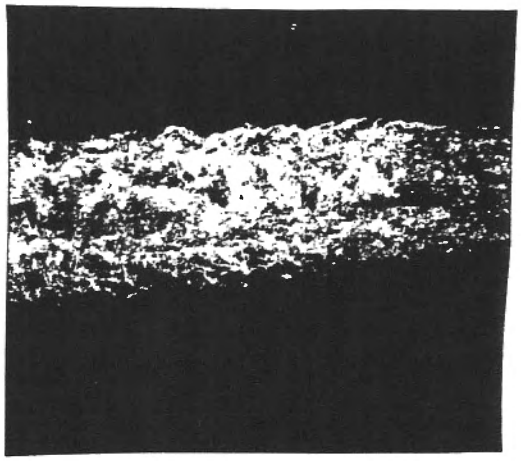

d_o = 100mm, L = 9"-23", u_{vc} = 11.8 m/s

d_o = 100 mm, L = 22-37" U_{VC} = 17.7 m/s

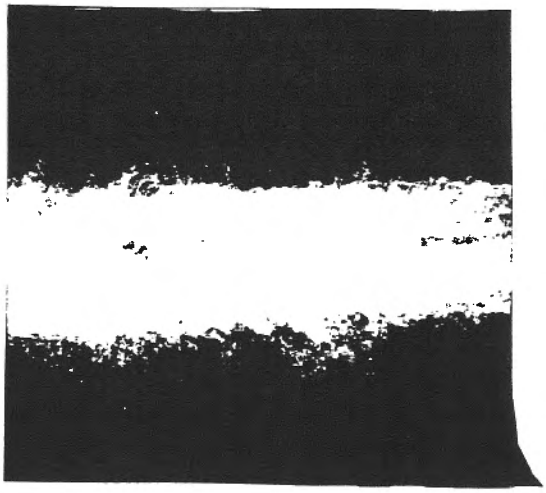

d_o = 100mm, L = 9-23", U_{VC} = 17.7 m/s

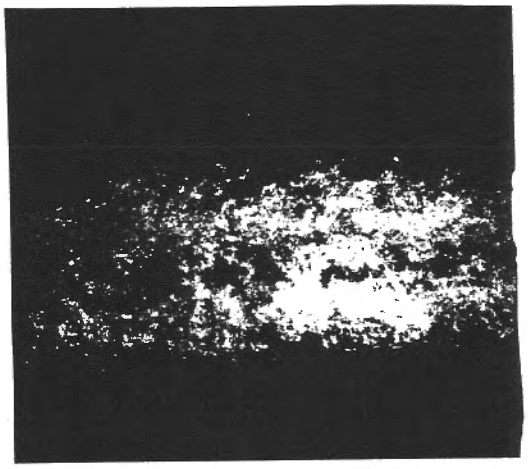

d_o = 100 mm, L = 22-37", U_{VC} = 23.7 m/s

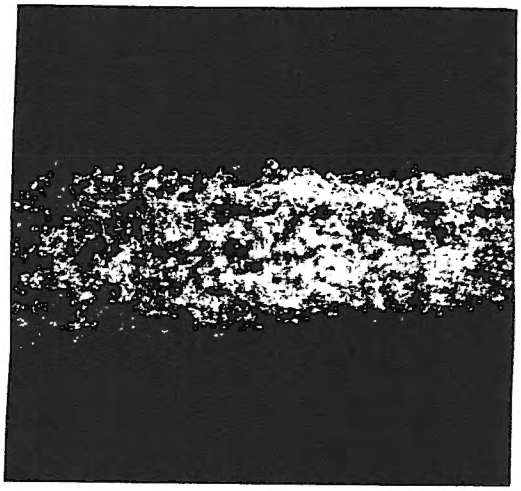

d_o = 100mm, L = 9-23", U_{VC} = 23.7 m/s

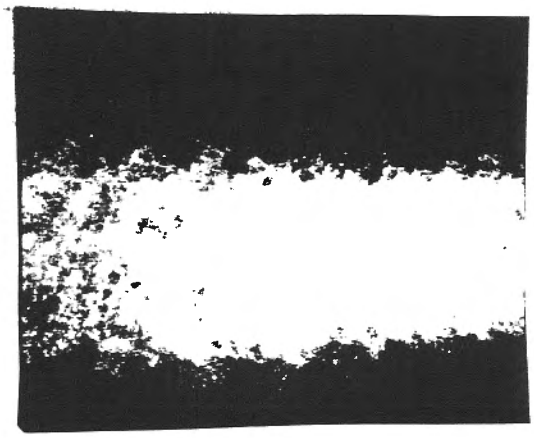

d_o = 100mm, L = 22-37", U_{VC} = 29.6 m/s

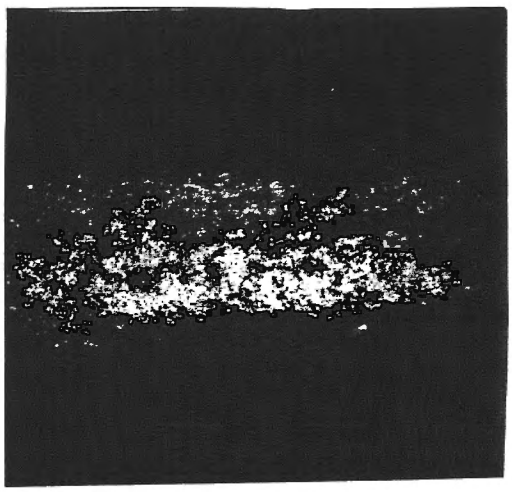

d_o = 100mm, L = 9-23", U_{VC} = 29.6 m/s

(b) the effect of increasing distance along the axis of the jet from the orifice plate is also evident from the previous 2 pages of photographs and also from the Polaroid picture shown overleaf for the 100mm jet at $Q = 0.14 m^3/s$.

- the jet surface appears more disrupted as we move downstream.
- the jet continues to spread laterally, initial measurements showing an almost linear spread in the downstream direction. These photographs are taken over a total distance of $L/d_{vc} \sim 12$ or $(L/d_0 \sim 9)$
- this process is true for all the jets EXCEPT for jet velocity $u = 3.3 m/s$

The possible reasons for this have already been described in the theory sections. The characteristic of a free shear layer is that turbulence intensity decreases in the downstream direction, implying for the jets shown that surface disturbances would not continue to increase in intensity indefinitely. It is apparent from the photographs that initial turbulence intensity might be responsible for the initial spreading angle which appears to be maintained in the downstream direction. That is, at the origin just downstream of the orifice the two components of velocity are,

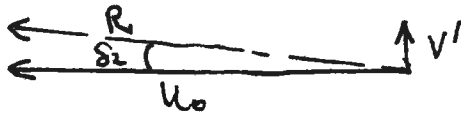

R = Resultant outer spread

For the case of isotropic turbulence $V' = u'$ and hence $\delta_2 \sim u'/u_0$
Generally $V' < u'$, hence it is likely $\delta_2 < u'/u_0$

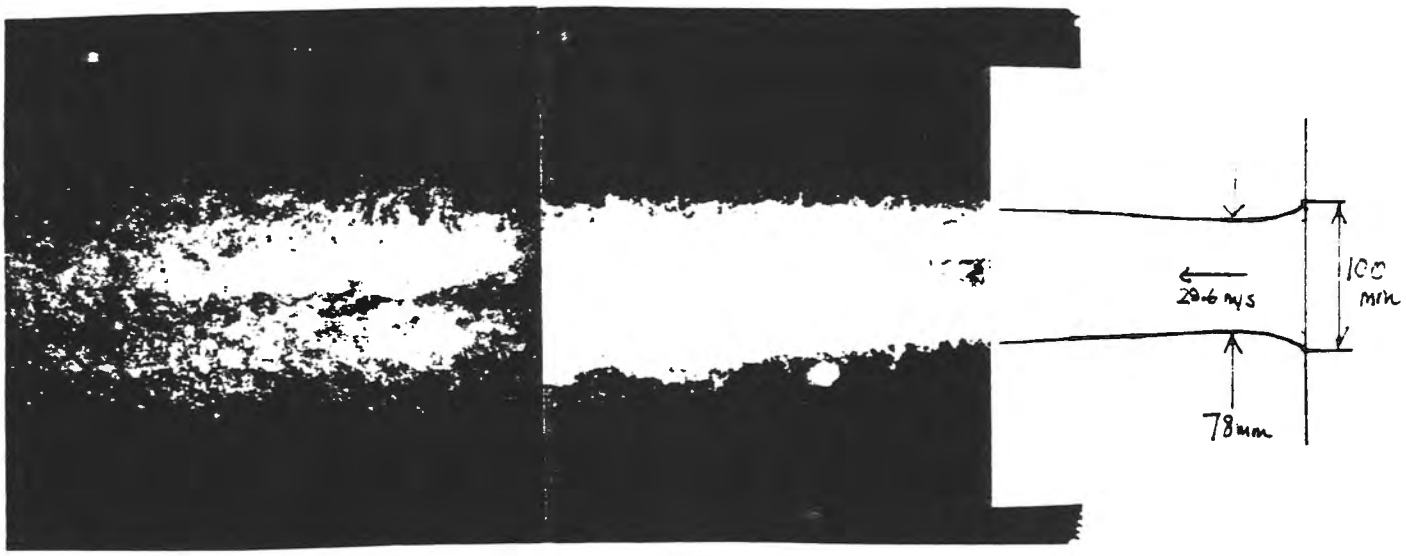

POLAROID PICTURE INDICATING LINEAR JET SPREAD WITH DISTANCE

$Q = 5\ ft^3/s\ (0.14 m^3/s)$, $d_o = 100mm$, $d_{VC} = 78mm$, $u_{VC} = 29.6\ m/s$

HALF ANGLE OF SPREAD $\simeq 4.5\%$, LENGTH SHOWN IS 36-37" from ORIFICE PLATE EXTENSIVE AIR ENTRAINMENT AND FINE SPRAY

(c) the effect of decreasing the jet diameter from 100mm down to 50mm is shown (in the slides) and also some photographs overleaf. (P45) These photographs should be compared visually with those on Pages 38+39 for the 100mm jet.

The photographs clearly show much smaller surface disturbances for the smaller jet at equal velocity to the larger jet.

If the amplitude of disturbances $\delta \propto u'^2 = \left(\frac{u'}{u}\right)^2 u^2$ then for equal velocity and turbulence intensity, the value of δ should be the same in each case. We can conclude that (u'/u) is smaller in the 50mm jet.

Therefore we ask, does (u'/u) decrease as the jet diameter or Reynolds Number decreases. The answer must be yes. As Re decreases the smaller eddies have less turbulent energy due to dissipation of viscosity. Smaller jets have smaller eddies!

$d_o = 50mm$

$U_{vc} = 3.3$ m/s

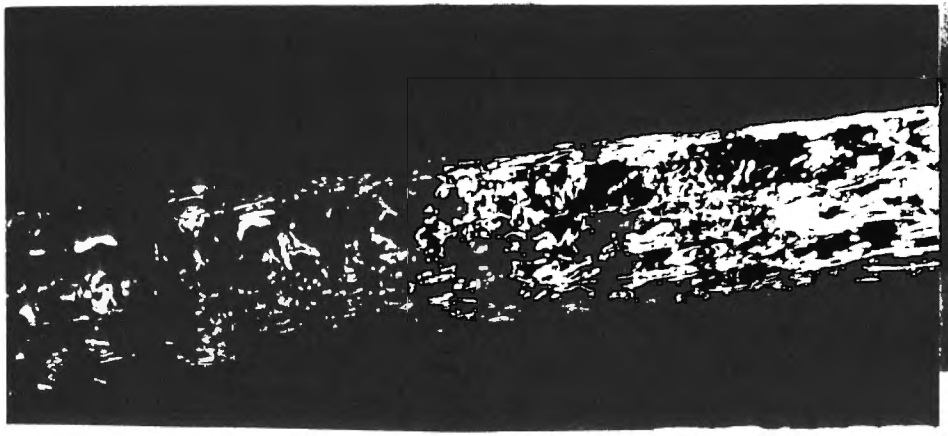

$d_o = 50mm$, $U_{vc} = 5$ m/s

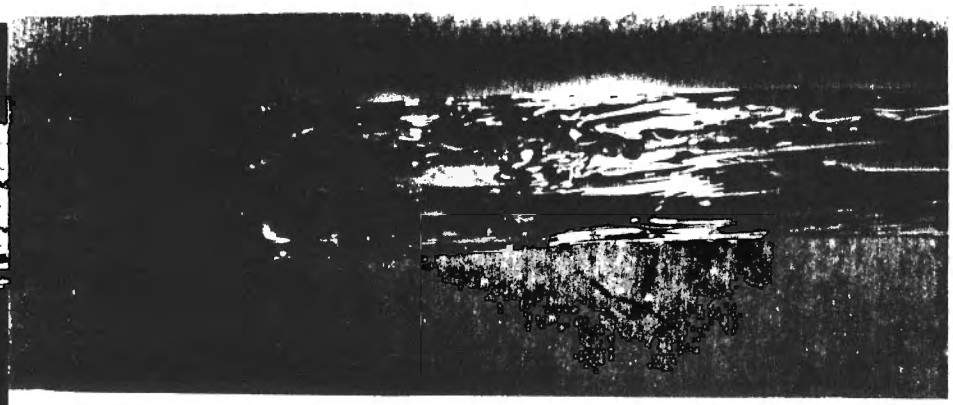

$d_o = 50mm$, $U_{vc} = 5$ m/s

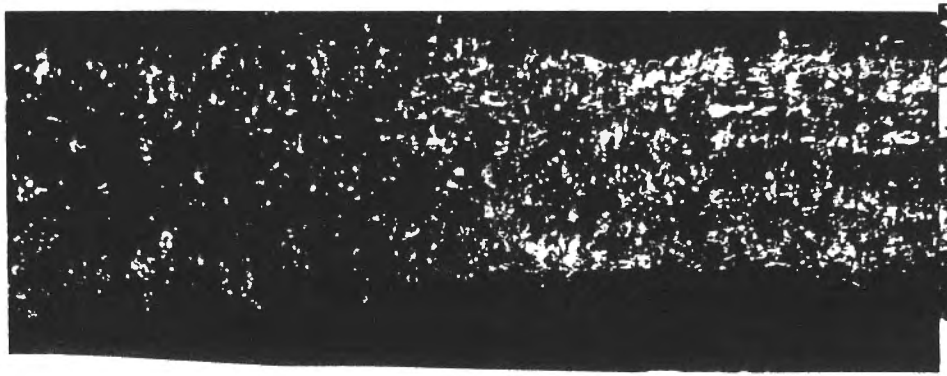

$d_o = 50mm$, $U_{vc} = 18$ m/s

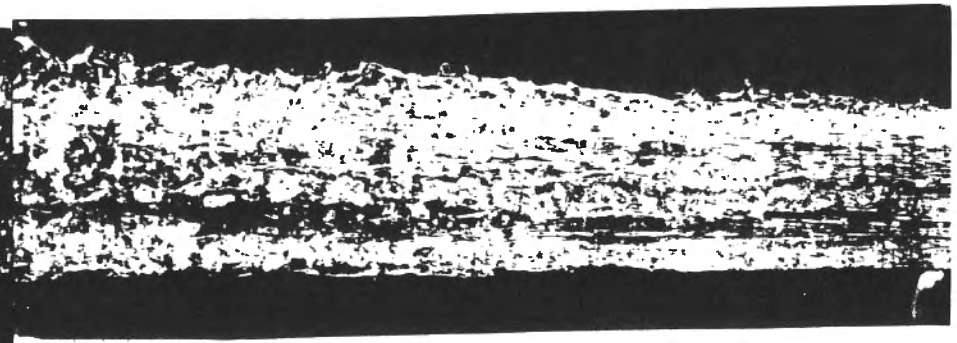

$d_o = 50mm$, $U_{vc} = 18$ m/s

Spreading of the outer edge of the jet

The author has carried out measurements of the half spreading angle of the 100mm and 50mm jets at velocities up to 30 m/s. These values are shown overleaf, for both jets, with each point averaged over a series of 4-6 photographs (Page 45)

(1) 100mm jet has a higher spreading angle than the 50mm jet with max. values around 4½%.

(2) Jet spreading angles tend towards a constant value at higher velocities, Reynolds Numbers? or Weber Numbers?

(3) Smaller velocity jets indicate a zero or negative spreading angle (this has already been discussed under theory section) even though moderate turbulence exists at the orifice exit. This is related to the balance between turbulent energy and surface tension

The question now is the relationship between turbulence and spreading angle

Before we discuss this, prototype spreading angles at Morrow Point have been measured by the author from photographs provided by Tom Rhone. These are shown on Page 46. These results represent an almost constant value of u_o ($\sim$ 9 m/s) but large Reynolds Numbers ($>5 \times 10^6$). The half angle of spread is greater than the model circular jets but not substantially so, indicating the angle of spread may be much more related to u'/u_o rather than Reynolds or Weber Number. The average spreading angle is approx 6% indicating an initial turbulence intensity $V'/u_o \sim 6\%$ or $u'/u_o \geq 6\%$

It is clear also that the jet spreading angle is also a function of the jet aspect ratio b/d, probably related to the number of secondary circulation cells formed in the jet core.

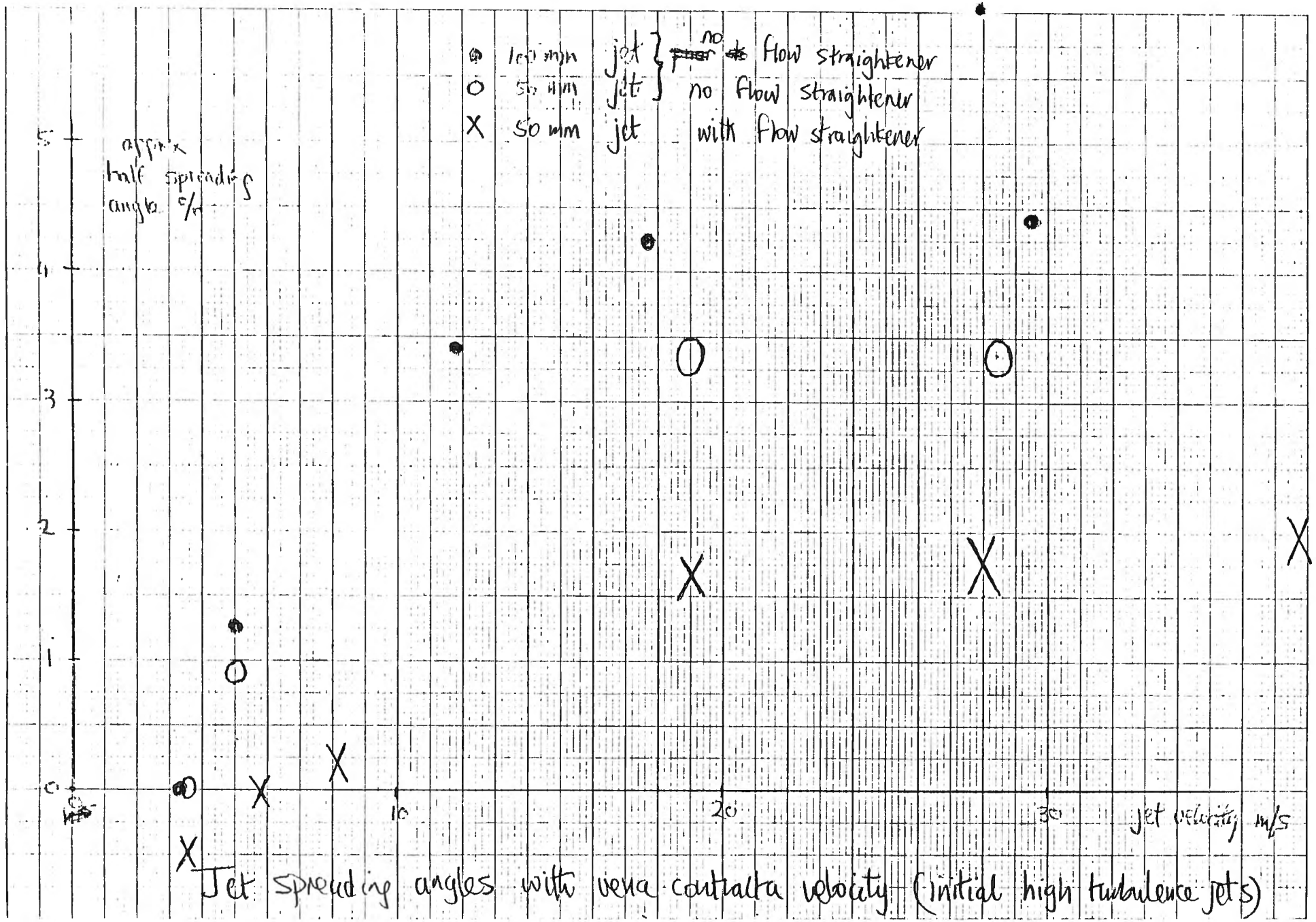

Jet spreading angles with vena contracta velocity (initial high turbulence jets)

MORROW POINT DAM — APPROX HALF ANGLE OF SPREAD OF PLUNGING JETS

OUTLET VELOCITY APPROX. CONSTANT 9 → 9.6 m/s

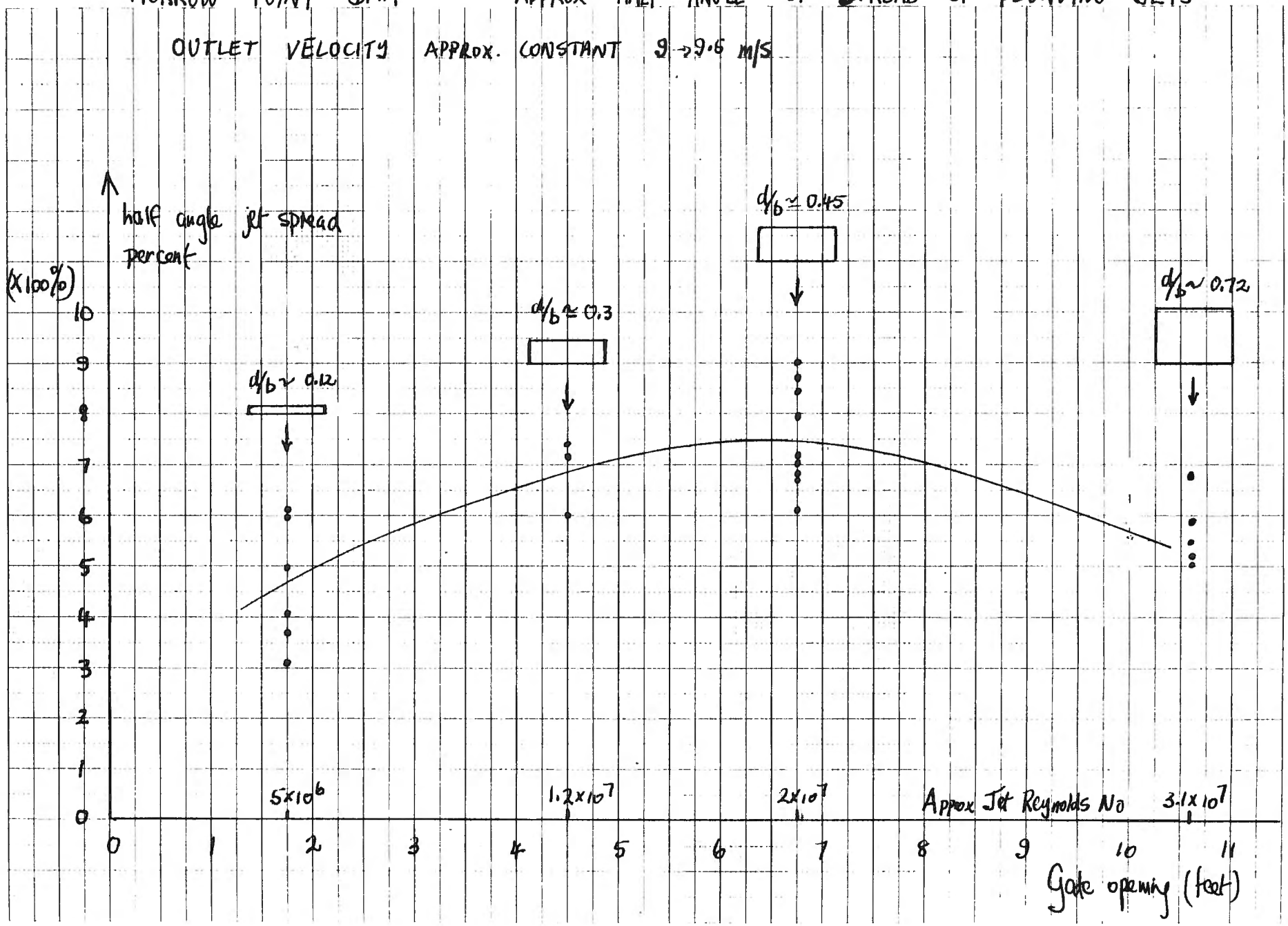

Initial turbulence intensity measurements

An attempt was made to measure axial relative turbulence intensity in the jet just downstream of the orifice plate. Two problems were encountered

(1) Picking up excessive noise off the rough cured edge of the jet This was overcome by placing a flat perspex plate just touching one edge of the jet (see slide) thus permitting a reduction in surface noise and the ability to measure turbulence levels

(2) Flow from the orifice appear to contain excessive bursts of turbulence from the upstream pipe system and pump. This was at least partly overcome by the introduction of a flow straightener device.

Turbulence measurements on the 50mm jet are shown on Page 49 before the introduction of the flow straightener device. The value of u'/u_0 increases with jet velocity and Reynolds Number levelling off in this case around 8%. This corresponds to a half angle of spread of 4%, indicating maybe $v' \sim \frac{1}{2}u'$.

The phenomenon can be investigated further in the jet tests proper, but it is interesting to relate ~~Fig~~ Page 49 to Page 45, indicating a close link between jet spreading angle and u'/u_0

9/5/55 30 mm diameter Vena Contracta
50 mm diameter orifice, radial direction, 14.5mm from edge of jet

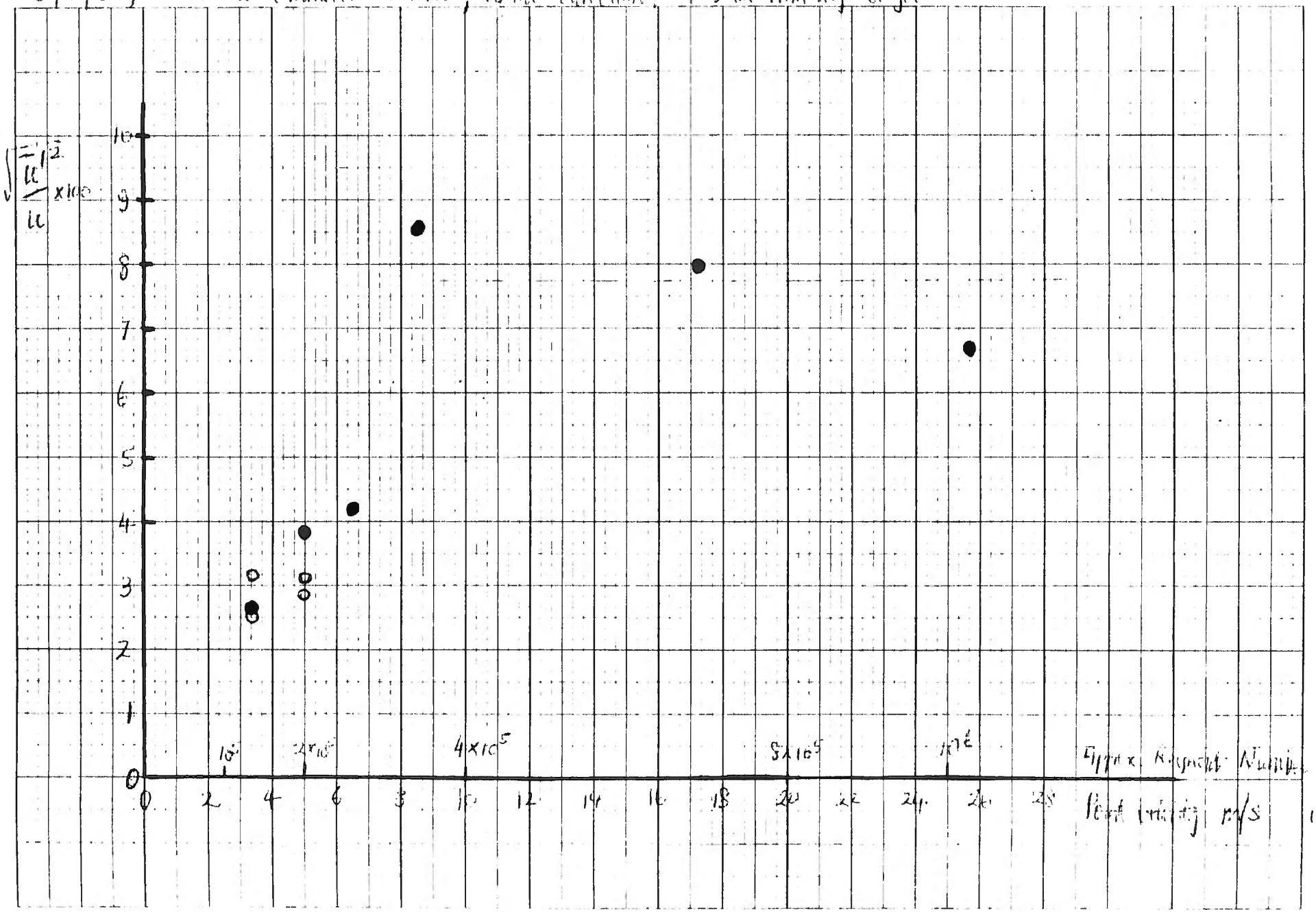

Recommendations for future research on impinging jets

The original purpose of this research visit was to make recommendations for future progress on the impinging jet program. The author has attempted in the earlier sections of this discussion document to obtain an understanding of the phenomenon first, so that more relevant recommendations may be advanced

Point (1) It is possible using a straight forward piece of apparatus to carry out two investigations simultaneously. (a) mean pressures and fluctuating pressures on a plunge pool floor for a wide range of upstream parameters and (b) investigations into the inception of free surface aeration for plunging jets which would have implications for scaling of aeration in other areas such as air slots, etc

Point (2) A thorough investigation on plunge pool basin pressures can be carried out by varying the following parameters

U_o	jet velocity at exit to atmosphere
u'	jet turbulence intensity at exit to atmosphere
d_o	jet dimension at exit to atmosphere
L	jet plunge length through the atmosphere
y	plunge pool depth
α	angle of jet nozzle to horizontal
χ	shape of jet nozzle circular, rectangular, square, etc.

My first recommendation is that (at least initially) α and χ be ommitted as variables and the jet be kept <u>circular</u> and plunging <u>vertically</u>

As an order of magnitude the minimum acceptable number of variations of the remaining five parameters is three i.e. three jet velocities, three turbulence levels, etc, giving a total minimum number of test runs of $(3)^5 = 243$. It may be preferable to test more than three jet velocities and plunge pool depths.

(3) Excluding the shape of the exit nozzle and the nozzle angle to the horizontal, the independent parameters become,

$$f(u_o \; u' \; d_o \; L \; y \; \rho \; g \; \mu \; \sigma \; l') = 0$$

and the total number of possibilities are

$$\left(u_o^2/g \,,\, \frac{\nu}{u_o} \,,\, \frac{\sigma}{\rho u_o^2} \,,\, \frac{\nu^{4/3}}{g^{1/2}} \,,\, \frac{\nu^2 \rho}{\sigma} \,,\, (\sigma/\rho g)^{1/2} \,,\, \frac{u'^2}{g} \,,\, \frac{\nu}{u'} \,,\, \frac{\sigma}{\rho u'^2} \,,\, d_o \,,\, L \,,\, y \,,\, l'\right) = 0$$

giving

$$f\left(\frac{u_o^2}{g d_o} \,,\, \frac{\nu}{u_o d_o} \,,\, \frac{\sigma}{\rho u_o^2 d_o} \,,\, \frac{u'^2}{g d_o} \,,\, \frac{L}{d_o} \,,\, y/d_o \,,\, l'/d_o\right) = 0$$

— Now $u'^2/gd = (u'/u_o)^2 \; u_o^2/gd_o$ and as u_o^2/gd_o is already included this reduces to $(u'/u_o)^2$

— Also the eddy length l' may be difficult to measure and hence the spectrum analyser may be used for frequency variation. i.e. $l' \propto u_o/n$ or $l'/d \propto u_o/nd$ = Strouhal Number

The final array of non-dimensional Numbers becomes,

$$f(Fr_o \,,\, Re_o \,,\, We_o \,,\, Str_o \,,\, u'/u_o \,,\, L/d_o \,,\, y/d_o) = 0$$

Systematic variation of these non-dimensional numbers will fully describe jet behaviour in the atmosphere, spreading of outer edge of the jet contraction of the inner core, degree of free surface aeration in the jet, jet spreading in the plunge pool, aeration in the plunge pool, pressures and turbulence intensities in the plunge pool, etc. The main constraint is of course Reynolds Number, and Weber Number to a lesser degree. The other variables not included in the analysis above are (a) more than one jet plunging into the pool and (b) the plunge pool plan dimensions. These parameters are not very significant in this type of fundamental study, but of course would be investigated for a specific design case.

Let us consider the variation in independent parameters in turn

(4) Mean velocity at the exit nozzle

It would be desirable to vary jet velocity up to at least 20 m/s. Free surface aeration will occur around 5–10 m/s, spray will come off the edge of the jet 10–20 m/s, and 20 m/s is a reasonable prototype velocity range. For the case of orifice outlets, the best idea is to design the orifice opening for velocities of 20 m/s and subsequent velocities at the vena contracta are approx $20/0.61 = 32$ m/s. It is advisable also to investigate around five jet velocities, say 2 m/s, 5 m/s, 10 m/s, 15 m/s, 20 m/s.

(5) Variation of turbulence u' and eddy lengths at the nozzle exit

This is probably the most crucial aspect of this study – TURBULENCE CONTROL. The first requirement in turbulence control is the production of minimal turbulence in the upstream system. Using the high head pump, T-pieces, valves, elbows etc, turbulence production has been shown to be extensive

and requires to be eliminated as much as possible before reaching the outlet nozzle. The most effective method of achieving this is the insertion of a tube bundle downstream of the ~~last~~ final turbulence producing element (elbow) and before the outlet nozzle.

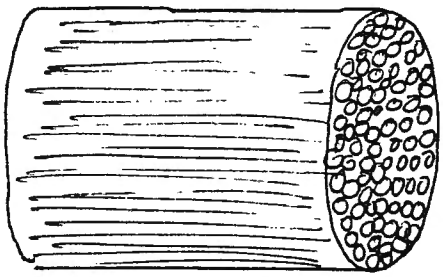

tube bundle

Important here to use small diameter thin walled tubes. I recommend 1/4" diameter tubes carefully packed throughout the pipe diameter. With L/d of 50, this device ought to be at least 12" long

The purpose of this device is to reduce of eliminate swirl and pump pulses and will produce very fine scale turbulence at its downstream end $\ell' \sim 1/8"$ which will decay substantially before reaching nozzle outlet, giving a relative turbulence intensity around 1-2%.

The next stage in turbulence control concerns the variation of turbulence intensity and eddy lengths at the nozzle exit. It would be advisable to test initial turbulence intensities from 1% → 10%. This can be achieved (I think!) by changing the nozzle design and by introducing coarse and fine grids. For lowest possible turbulence intensities it is important to have accelerating flow at the nozzle which can be achieved with nozzles 1 and 2 (overleaf)

Larger turbulence intensities can be generated using an orifice with wire mesh. Variation in wire mesh sizes will have the dual effect of increasing turbulence and reducing initial eddy lengths. Variation in eddy lengths will alter the initial frequency (n)

Trial and error will determine the optimum nozzles to be used to vary turbulence intensity up to 10%. A minimum of three nozzle designs should be used in this process

Nozzle ①

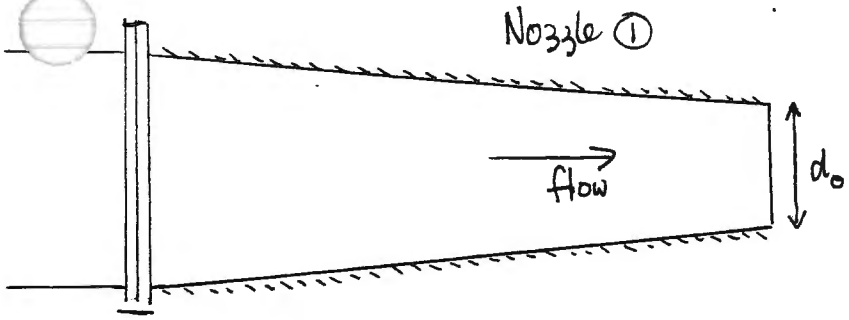

$\frac{u'}{u} \sim 1 \to 2\%$

Nozzle ②

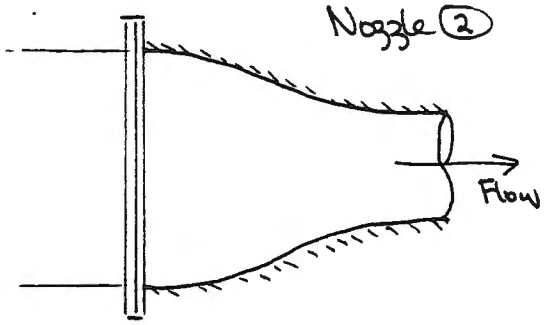

See tests at Iowa St. U.

$\frac{u'}{u} \sim 1-3\%$

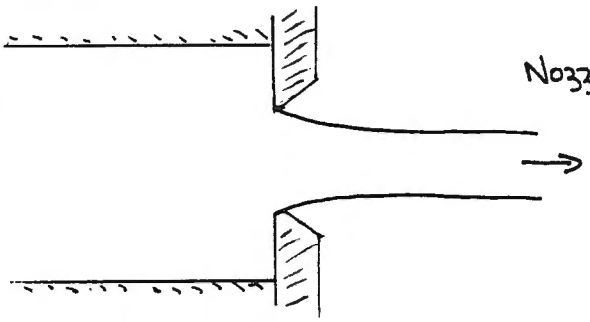

Nozzle ③ orifice plate

$\frac{u'}{u} \sim 2-5\%$

Nozzle ④

Orifice plate with fine grid + wide spacings

$u'/u \sim 3-8\%$

Nozzle ⑤

Orifice plate with coarse grid and small spacings

$u'/u = 5-10\%$

(6) Variation in jet diameter at exit to atmosphere (d_o)

The key here is the larger the jet diameter the better. The restraints of using larger jet diameters are three fold, (a) Upper limit of discharge from high head pump = 6 ft^3/s and hence large diameters restrict the outlet velocity. (b) large values of d_o restrict the higher ratio's of L/d_o, and y/d_o. The benefits of a larger d_o values are increased Reynolds Number, Weber Number, and above all, much smaller ratios of l'/d_o. A minimum of three jet diameters are required for proper analysis of results, and a suitable range of diameters is 30mm → 150mm. A 150mm jet will produce velocities up to 10 m/s which is slightly restrictive, so I suggest initially tests at 25mm, 50mm and 100mm diameter, with possibly a special test to look at some aspects of a 150mm ϕ jet.

(7) The jet plunge length (L) from the nozzle exit to the plunge pool water surface should also be as large as possible, with the obvious restraints of vertical space in the laboratory. Morrow Point dam has a minimum L/d_o of 20-25, although I would recommend L/d_o values as high as 100 → 200, this being the traditional break-up region. Thus, a plunge length of 5m would give for 25mm jet, $L/d_o \sim 200$, and the 100mm jet, $L/d_o \sim 50$ which is adequate. I suggest a range of L/d_o values ranging from around 5 to 200. This could best be organised by having the down pipe flanged in about 1m lengths as shown. The nozzles and orifices could be attached to the end of each section in turn, giving $L/d_o = 5 \rightarrow 200$

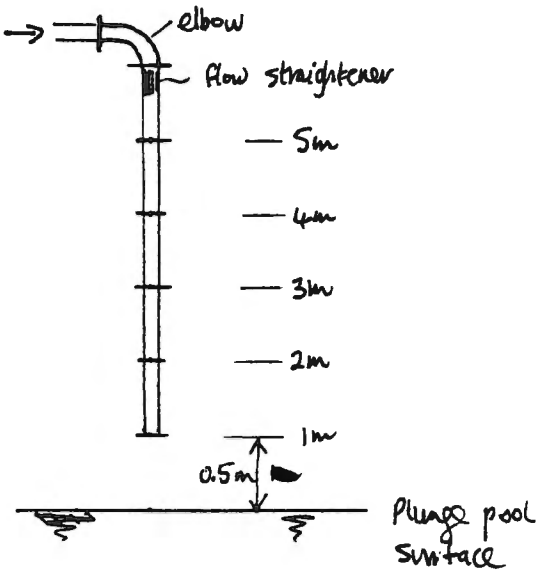

(8) Variation in plunge pool depth

A proper comprehensive study of jet spreading in plunge pools should provide for y/d_o at least 40-50. For the 100mm jet this would require 4-5m plunge pool depth. The ideal solution therefore is to have the jet plunging into the pump sump, having the positive advantages of a steady top water level, a depth of around 3m, and adequate space for jet spreading in the pool. The jet will spread around 1/4 giving a minimum base plate diameter of 1.5m, or 2m diameter for insurance. The main disadvantage of this system would be inability to take visual measurements of pool behaviour such as using lasers, etc, photographs.

The idea therefore would be to keep the plunge pool water level constant but to vary the level of the base plate for pressure measurements. This may not be a simple operation (see opposite) as the base plate may have to withstand high forces ½ → 1 tonne and therefore may be required to be constructed in aluminium or steel. Also due to jets spreading both in the atmosphere (1/20) and in the pool (1/4), the plate would really need to be 2 → 3 m square.

Again at least three values of y/d_o should be tested for each jet. Say, on the plunge pool floor, about ½ way up the pump sump, and somewhere close to the water surface. That is, to incorporate pressure measurements both inside and outside the zone of flow establishment

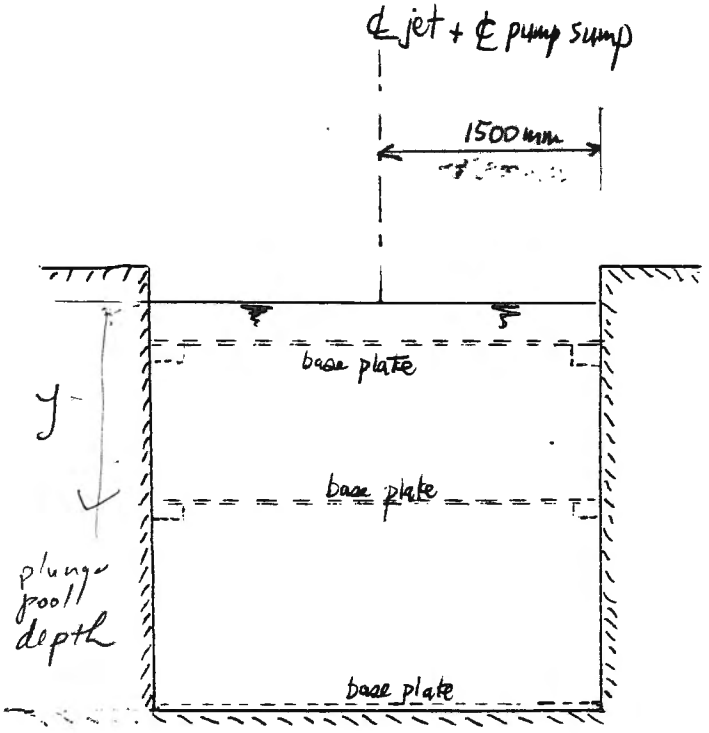

Pump Sump

Probably better having the base plate spanning across the 3m wide sump. Need to incorporate facility to raise and lower the base plate.

(9) Total number of test runs is approximately

5 velocities X 3 (at least) turbulence levels x 3 nozzle diameters
x 3-4 plunge lengths x 3 pool depths $\simeq$ 400 test runs

This represents a substantial effort of research, as each of the 400 test runs will require extensive data recording and photographic evidence.

(10) DATA REQUIRED FOR EACH TEST RUN

Each of the 400 test runs may require extensive data recording

(1) Photographic evidence - It may not be necessary to take photographs of every single jet, but certainly the influence of jet velocity, jet diameter, plunge length, and varying turbulence intensity should be incoporated into four series of photographs

(2) Point velocity measurements of the plunging jet. It is important to obtain point velocities and a velocity traverse across the jet at least close to the nozzle. This may be done using the perspex side strip (as already described) with the laser doppler system. I feel it is also advisable to attempt point velocity measurements in the jet core some distance down stream of the nozzle in an attempt to determine core development as the jet plunges through the atmosphere. These measurements further downstream from the nozzle, may also be taken with the laser using an extended perspex strip, or alternatively a specially designed pitot-static tube in the solid jet core Pitot-static tube measurements require great care in preventing air bubbles lodging close to the tip of the tube, producing spurious velocity reading My feeling is that despite local scepticisms on the quality of the laser data, this will produce a more reliable data using the extended

perspex strip idea. Extended core velocity measurements do not require to be taken for every single test run, but certainly over a range of parameters U_o, L, do, u'/u_o, etc, to give an idea of inner core contraction above that due to gravity.

(3) Relative turbulence intensity measurements in the plunging jet. Again using the laser doppler system with extended perspex strip along one side of the plunging jet. Axial relative intensities are the easiest to measure but the most relevant measurements are of the RMS value of the radial component of turbulence intensity. (determining lateral spreading of jet)

(4) Probability probe measurements in the plunging jet. In a sense this is complementary to velocity and turbulence measurements and does not require to be carried out for every single test run. The aim would be
(I) to obtain probability measurements of the jet edge + core to assist in a math model of a plunging jet
(II) to confirm or otherwise the inner core contraction measurements already inferred from point velocity measurements
(III) to confirm or otherwise, the outer jet spread already inferred from photography

(5) All this data on the plunging jet (for 400 test runs) can then be used to produce a reliable math model, empirical correlations, evidence of the onset of aeration, spray formation, indicators of the influence of turbulence intensity, Reynolds Number, etc, etc

(6) Plunge pool measurements. This is something which to date I have not given as much thought as the plunging jet, but is just as important

(I) Pressure transducer measurements on the base plate. This should be done for each of the 400 test runs using static pressure probes and dynamic (instantaneous) (Hank Falvey is the man to see about this!) We are dealing with symetrical jets impinging on the plate and hence the number of pressure transducers can be greatly reduced. That is, if we knew the exact position of the centre line of the jet 3 or 4 transducers would suffice

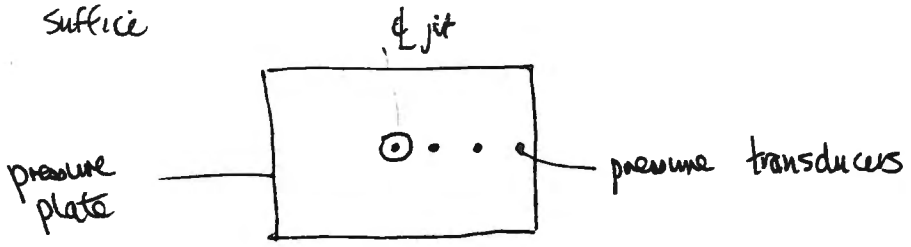

In practice a few more should be placed close to the jet centre line position to pick up any eccentricity at impact.

(II) The real problem here with plunge pool measurements is that the same kind of data, (point velocities, turbulence intensity, inner and outer spreading angles) are required as per the jet plunging through the atmosphere The laser cannot be used because the pump sump is being used and air concentration is too high anyway. Pitot static tube measurements are invalid because of air concentration, & and photography is also out.

This is an area which needs to be discussed in some detail as jet spreading in the pool is one of the most significant parameters under investigation.

Side Elevation of experimental apparatus

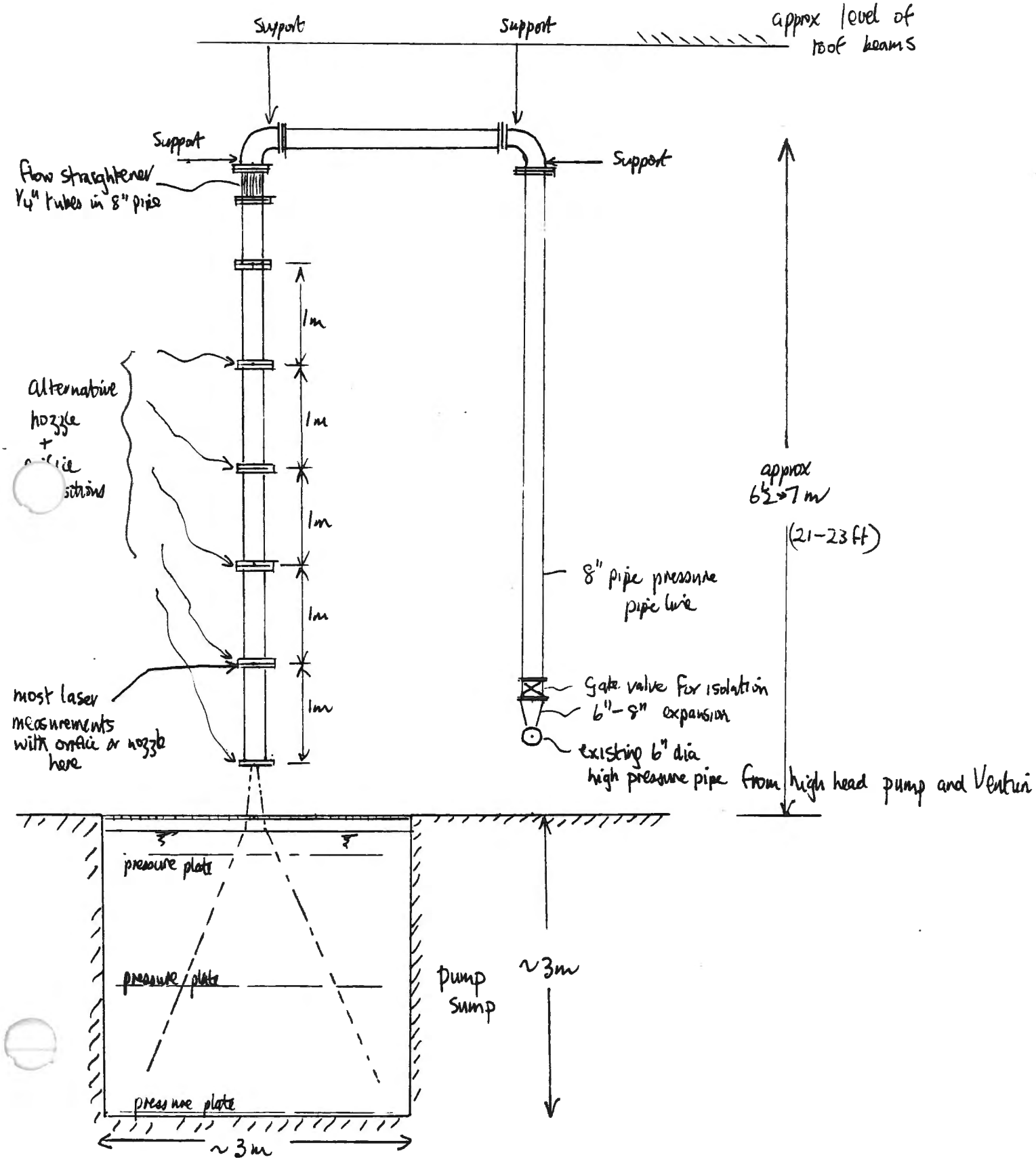

References Associated with Sections 2 and 3 on Bubbly Flows

1. AHMED, A. A. "The Process of Aeration in Closed Conduit Hydraulic Structures." Ph. D. thesis at University of Glasgow, June 1984

2. AHMED, A. A., ERVINE, D. A. and McKEOGH, E. J. The Process of Aeration in Cosed Conduit Hydraulic Structures. Proc. Symp. of Scale Effects in Modelling Hydraulic Structures, Paper 4.13, Esslingen, Germany, September1984.

3. ALBERTSON, M. L., et al. Diffusion of Submerged Jets. Proc. ASCE pp. 1571-1596, December 1948.

4. ANDERSON, S. H. Model Studies of Storm-sewer Drop Shafts. Dept. of Public Works, City of St. Paul, University of Minnesota, St. Anthony Falls Hydraulic Lab., Tech. Paper 35, Series B, December 1961.

5. AUTON, T. R., et al. Entrapment and Transport of Bubbles by Transient Large Eddies in Multi-phase Turbulent Shear Flows. Int. Conf. on Phy. Mod. of Multi-phase Flow, Coventry, England, pp. 169-184, April 1983.

6. AVERY, S. and NOVAK, P. Oxygen Uptake in Hydraulic Jumps and at Overfalls. Proc. XVI Congress I.A.H.R., Paper C38, 329-337, 1975.

7. AVERY, S. and NOVAK, P. Modelling of Oxygen Transfer from Air Entrained by Solid Jets Entering a Free Water Recipient. Proc. I.A.H.R., 17th Congress, Baden-Baden, August 1977.

8. AVERY, S. and NOVAK, P. Oxygen Transfer at Hydraulic Structures, Hyd. Div., A.S.C.E., November 1978

9. BIN, A. K. Air Entrainment by Plunging Liquid Jets. Sym. on Scale Effects in Modelling Hydraulic Structures. Paper 5.5, Esslingen, Germany, September 1984.

10. BONNECAZE, W. E. and GRESKOVICH, E. J. Hold up and Pressure Drop for Two-phase Slug Flow in Inclined Pipelines. AICHE Journal, Vol. 17, No. 5, 1109-1113, September 1971.

11. CAMPBELL, F. B. and GUYTON, B. Air Demand in Gated Outlet Works. I.A.H.R., Minnesota, Int. Hyd. Convention, 529-533, 1953.

12. CASTELEYN, J.A., VAN GROEN, P. and KOLKMAN, P. A. Air Entrainment in Siphons: Results of Tests in Two Scale Models and an Attempt at Extrapolation. 17th Congress of the I.A.H.R., Baden-Baden, 15-19, November 1977.

13. COLGATE, D. Hydraulic Model Studies of the Flow Characteristics and Air Entrainment in the Check Towers of the Main Aqueduct, Canadian River Project, Texas. Hydraulic Laboratory Report HYD-555, Bureau of Reclamation, Denver, Colorado, June 1966.

14. COLLINE, R. The Effect of a Containing Cylindrical Boundary on the Velocity of a Large Gas Bubble in a Liquid. J. Fluid Mech., Vol. 28, Part 1, pp. 97-112, 1967.

15. COMOLET, R. On the Movement of a Gas Bubble in a Liquid. LaHouille Blanche, No. 1, pp. 31-42, 1979.

16. CUMMING, I. W. The Impact of Falling Liquids with Liquid Surfaces. Ph. D. thesis. Loughborough University, U. K., 1975.

17. CURTET, P. R. and DJONIN, E.T.K. Study of a Vertical Downward Mixed Water and Air Flow: Flow and Concentration Conditions. LaHouille Blanche, pp. 531-550, May 1967.

18. DAVIES, R. M. and TAYLOR, G. I. The Mechanics of Large Bubbles Rising Through Extended Liquids and Through Liquids in Tubes. Proc. Royal Society of Engineering, London A 200, 1950.

19. DAWSON, F. M. and KALINSKE, A. A. Report on Hydraulics and Pneumatics of Plumbing Drainage Systems. Bulletin 10, University of Iowa City, Iowa, 1937.

20. ERVINE, D. A. and ELSAWY, E. M. Some Scale Effects in Modelling Air-Regulated Siphon Spillways. Proc. of Symp. on Design and Operation of Siphon Spillways, Paper B2, B.H.R.A., May 1975.

21. ERVICE, D. A. The Design and Modelling of Air-regulated Siphon Spillways. Proc. I.C.E., Part 2, Vol. 61, pp. 383-400, June 1976.

22. ERVINE, D. A. and ELSAWY, E. M. The Effect of a Falling Nappe on River Aeration. Proc. XVIth Congress I.A.H.R., Paper C45, Sao Paulo, Brazil, July 1975.

23. ERVINE, D. A., McKEOGH, E. J. and ELSAWY, E. M. Effect of Turbulence Intensity on the Rate of Air Entrainment by Plunging Water Jets. Proc. I.C.E., Part 2, Vol. 69, pp. 425-445, June 1980.

24. ERVINE, D. A. and KOLKMAN, P. A. Air Entrainment and Transport in Closed Conduit Hydraulic Structures, Int. Report S330, Delft Hy. Lab., August 1980.

25. ERVINE, D. A. and AHMED, A. A. Scaling Relationship for Two Dimensional Vertical Dropshaft. Proc. B.H.R.A. Conf. on Hyd-Struct. Paper E1, Coventry, U. K., September 1982.

26. FALVEY, H. T. Air-water Mixtures, Engineering Monograph No. 41, U. S. Department of the Interior, Water and Power Resources Services, December 1980.

27. FALVEY, H. T. Predicting Cavitation in Tunnel Spillways. J. of Water Power and Dam Construction, pp. 13-15, August 1982.

28. GOLDRING, B. T. The Use of Small-scale Siphon Models. Proc. Instn. Civ. Engrs., Part 2, pp 929-942, December 1979.

29. GOLDRING, B. T. et al. Level Surges in the Circulating Water Downshaft of Large Generating Station. Third International Conf. on Pressure Surges, Canterbury, England, Paper F2, pp-279-300, March 1980.

30. GOLDRING, B. T. A Comparison of Air Entrainment Theories Using Siphon Priming Calculations. Memorandum, C.E.G.B. LM/Eng/444, August 1980.

31. GOLDRING, B. T. Air Voids at Dropshaft-tunnel Bends. Hyd. Div., ASCE, Vol. 109, No. 2, February 1983.

32. GOLDRING, B. T. Model and Prototype Tests on a Low Head Siphon Symp. on Scale Effects in Modelling Hydraulic Structures, Paper 5.9, Esslingen, Germany, September 1984.

33. GOLDRING, B. T. Private Communication "Blowbacks in Downward Sloping Pipes," February 1985.

34. HABERMAN, W. L. and MORTON, R. K. An Experimental Study of Bubbles Moving in Liquids. Proc. ASCE, Vol. 80, pp 379-427, 1954.

35. HACK, H. P. Air Entrainment in Dropshaft with Anular Flow by Turbulent Diffusion. Proc. I.A.H.R., 17th Congress, Baden-Baden, 15-19, August 1977.

36. HAINDL, K. Zone Length of Air Emulsion in Water Downstream of the Ring Jump in Pipes. Proc. I.A.AH.R., Japan, Kgoto, 1969.

37. HAINDL, K. and SOTORNIK, V. Quantity of Air Drawn into a Conduit by the Hydraulic Jump and its Measurement by Gamma-Radiation. Proc. of VII Congress of I.A.H.R., Lisbon, Vol. 2, 1957.

38. HAINDL, K. and RAMESOVA, L. Modelling of Zones of Natural Desaeration. Proc. of I.A.H.R., 17th Congress, Baden-Baden, August 1977.

39. HALL, L. S. Model-prototype Conformity. Trans. ASCE, Vol. 109, pp 150-154, 1944.

40. HALL, L. S. Entrainment of Air in Flowing Water. "Open Channel Flow" Symposium, Trans. ASCE, Vol. 108, pp. 1394-1434, 1943.

41. HARSHBARGER, E. D. et al. "Discussion", Air Entrainment in High Head Gated Conduits. Proc. of Hyd. Div. ASCE, December 1977.

42. HENDERSON, J. B. et al. Entrainment by Plunging Jets. Butterworths London, 1970, Sec. 2. (86-100) Chemeca '70. 1970 Melbourne, Australia.

43. HUNT, J.C.R. Turbulent Structure and Turbulent Diffusion Near Gas Liquid Interfaces. Gas Tansfer at Water Surfaces, pp. 67-82, D. Reidel Publishing Company, 1984.

44. JAIN, A. et al. Vortex Formation at Vertical Pipe Intakes, Jour. of Hyd. Div. ASCE, Hy. 10, Vol. 104, pp. 1429-1445, October 1978.

45. JEVDJEVICH, V. Entrainment of Air in Flowing Water and Technical Problems Connected with it. Proc. I.A.H.R., pp. 439-454, 1953.

46. KALINSKE, A. A. and ROBERTSON, J. M. (1943). Closed Conduit Flow. (Symposium). Entrainment of Air in Flowing Water. Transactions, ASCE, Vol. 108, pp 1435-1447.

47. KALINSKE, A. A. Hydraulics of Vertical Drain and Overlfow Pipes. Bulletin No. 26, University of Iowa, pp. 26-40, December 1941.

48. KALINSKI, A. A. and BLISS, P. H. Removal of Air from Pipelines by Flowing Water. ASCE, Civil Engineering, Vol. 13, No. 10, October 1943.

49. KENN. M. J. An Experimental Study of the Control of Siphonic Water Flow by Atmospheric Air. Journal I.W.E. 11, 3, p. 225, May 1957.

50. KENN, M. J. Further Studies Concerning the Air Control of Siphonic Water Flow. Journ. I.W.E. 19, 3, p. 231. June 1965.

51. KENN, M. J. A Pocket Froude Model. Journ. I.W.E., July 1965.

52. KENN. M. J. and zanker, K. J. Aspects of Similarity for Air Entraining Water Flows. Nature, Vol. 213, (No. 5071), January 1967.

53. KENN, M. J. Dynamical Similarity for Flow Systems in Which Inertia Effects are Small. Journ. I.W.E., Vol. 23, pp. 251-253, June 1969.

54. KENN, M. J. et al. Vibration of Bolarque Dam. Symposium Germany, I.A.H.R., University of Karlsruhe, 1979, pp. 508-511, September 3-6, 1979.

55. KENN, M. J. and GARRIOD, A. D. Cavitation Damage and the Tarbela Tunnel Collapse of 1974. Proc. Instn. Civ. Engrs., Part 1, 70, pp. 65-89, February 1981.

56. KOBUS, H. and RAO, L. Characteristics of Self-aerated Flows. Ench Schmidt Verlay, Berlin and Bicleteld, 1975.

57. KOBUS, H. and WESTRICH, B. An Example of Combined Discharge Control and Aeration Structure. XX Congress, IAHR, Paper S.3.7, Vol. VII, Moscow, September 1983.

58. KOBUS, H. Local Air Entrainment and Detrainment. Symp. on Scale Effects in Modelling Hydraulic Structures. Paper 4.10, Esslingen, Germany, September 1984.

59. KUMAGAI, M. IMAI, H. Gas Entrainment Characteristics of an Impinging Water Jet. Kagaku Kogaku Roubunshi 8 (1982) 1, 1-6.

60. LEUTHEUSSER, H. J. et al. Water Quality Enhancement Through Hydraulic Aeration. 15th Congress I.A.H.R., Vol. 2, B22, August 1973.

61. LAUSHEY, L. M. and MAVIS, F. T. Air Entrainment by Water Flowing Down Vertical Shafts. 5th Congress I.A.H.R., Minneapolis, 1953.

62. LIN, J. L. and DONNELLY, G. D. Gas Bubble Entrainment by Plunging Laminar Liquid Jets. Journ. A.I.Ch.E., Vol. 12, No. 3, p. 563, May 1966.

63. MANLEY, G. D. and MARKLAND, E. A Partial Siphon of Compact Design. Symposium on Design and Operation of Siphons and Siphon Spillways, B.H.R.A., London, May 13th-14th, 1975.

64. Modern Developments.

65. MURKOFSKY, M. and KOBUS, H. On the Study f Artificial Reoxygenation. Proc. I.A.H.R., 17th Congress, Baden-Baden, Paper A58, pp. 459-466, August 1977.

66. McKEOGH, E. J. and ELSAWY, E. M. (1977). Self-aeration by Plunging Jet. VIth Canadian Congress of Applied Mechanics Proc., pp. 591, Vancouver.

67. McKEOGH, E. J. A Study of Air Entrainment Using Plunging Jets. Ph. D. Thesis, The Queen's University of Belfact, October 1978.

68. McKEOGH, E. J. and ERVINE, D. A. Air Entrainment Rate and Diffusion Pattern of Plunging Liquid Jets. Jour. Chem. Sci., Vol. 36, pp. 1161-1172, June 1981.

69. OYAHA, Y. et al. Air Entrainment Phenomena by Jets. Rept. Sci. Research Inst. (Japan), 29, 344, 1954.

70. PETERKA, A. J. Morning Glory Shaft Spillways Performance Tests on Prototype and Model. Trans. ASCE, Vol. 121, Paper 2802, 1956.

71. PETERKA, A. J. The Effect of Entrained Air on Cavitaion Pitting. Proc. I.A.H.R. 5th Congress, Minnesota, USA, pp. 507-518, 1955.

72. PLOVER,COVE. Water Supply Scheme. Hydraulics Research Station, Report EX264, 1965.

73. QUICK, M.C. The Annular Hydraulic Jump. Civil Eng. and Public Works Review, p. 1176, 1961.

74. RAJARATNAM, N. An Experimental Study of the Air Entrainment Characteristics of Hydraulic Jump. The Instn. of Engrs. (India), Vol. 42, No. 7, March 1962.

75. RENNER, J. Air Entrainment in surface rollers. Symposium on the Design and Operation of Siphons and Siphon Spillways. BHRA, London, 1975.

76. ROGALA, R. Aeration d'une Lame Deversaute XX Congress IAHR, Paper S.3.5, Volume VII, Moscow, Septembe 1983.

77. SAILER, R. E. San Diego Aqueduct, Civil Engineering, Vol. 25, No. 5 May 1955.

78. SHARMA, H. R. Air Entrainment in High Head Gated Conduits. Proc. ASCE, Hyd Div., Paper No. 12523, HY 11, pp. 1629-1646, November 1976.

79. SENE, K. J. Aspects of Bubbly Two-phase Flow, Ph.D. thesis, Trinity College, Cambridge, U.K., December 1984.

80 THOMAS, N. H. (with Goldring and Mawer) Level Surges in Circulating Water Downshaft of Large Generating Stations, Third Int. Conf. on Pressure Surges (BHRA), Canterbury, U.K., 1980.

81. THOMAS, N. H. Unpublished M.S. Department Applied Mech. and Theoretical Physics, Cambridge Univ., U.K., 1978. (Submitted privately to B. T. Goldring. CERL Leatherhead, Surrey.)

82. THOMAS, N. H. Air Demand Distortion in Hydraulic Models: Experimental Evidence of Bi-model Structure in Air Entraining Flows and A Scaling Analysis of Detrainment with Special Applications to Siphon Priming. Int. Conf. on the Hyd. Mod. of Civ. Eng. Struc. B.H.R.A., Paper E5, Coventry, England, pp. 253-272, September 1982.

83. THOMAS, N. H. et al. Entrapment and Transport of Bubbles by Transient Large Eddies in Multi-phase Turbulent Shear Flows. Int. Conf. on the Phy. Mod. of Multi-phase Flow, Coventry, England, pp. 169-184, April 1983.

84. THORN, M.F.C. Modelling the Air Demand of Vertical Dropshafts. Proc. I.A.H.R., Baden-Baden, 1977.

85. TOWNSON, J. M. Oscillations in a Cooling Water Outfall System. Proc. Instn. Civ. Engrs., Part 2, 59, pp. 837-847, December 1975.

86. U.S. CORPS OF ENGINEERS. Air Demand at Regulated Outlet Works, Hydraulic Design Criteria, Chart 050-1.

87. VAN DE SANDE, E. and SMITH, J. M. Surface Entrainment of Air by High Water Jets. Jour. Chem. Eng. Sci., Vol. 28, pp. 1161-1168, 1973.

88. VAN DE SANDE, E. and SMITH, J. M. Mass Transfer from Plunging Water Jets. The Chemical Engineering Journal, pp. 225-233, 1976.

89. VAN DE DONK, J.A.C. Water Aeration With Plunging Jets. Ph. D. thesis Technische Hogeschool, Delft, 1981.

90. VIGANDER, S. Bubbles, Drops, and Friction on the Judgement Scale. Sump. on Scale Effects in Modelling Hydraulic Structures. Paper 5.1 Esslingen, Germany, September 1984.

91. VIPARELLI, M. Air and Water Currents in Vertical Shafts. La Houille Blanche, No. 6, pp. 857-869, December 1961.

92. WALLIS, G. B. One-dimensional Two-phase Flow. McGraw-Hill, 1969.

93. WHILLOCK, A. F. and THORN, M.F.C. Air Entrainment in Dropshafts. C.I.R.I.A. Tech. Note 48, April 1973.

94. WHITE, E. T. and BEARDMORE, R. H. The Velocity of Rise and Single Cylindrical Air Bubbles Through Liquids Contained in Vertical Tubes. Jour. Chem. Eng. Sci., Vol. 17, pp. 351-361, 1962.

95. WHITTINGTON, R. B. and ALI, H. M. Siphons: Some Scale Effects in Model. Proc. A.S.C.E., Hy. 1, Jan. 1972.

96. WHITTINGTON, R. B. and ALI, K.H.M. Discussion on "Siphons: Some Scale Effects in Models," Proc. Hyd. Div. ASCE, Hy. 6, pp. 982-988, June 1973.

97. WIJEYESEKERA, D. S. Air Entrainment in Vertical Shafts. Ph.D. thesis, Edinburgh University, 1969.

98. WIJEYESEKERA, D. S. Air Entrainment in Vertical Shafts. Water Power, pp. 220-223, June 1974.

99. WISNER, P. E. On the Role of the Froude Criterion in the Study of Air entrainment by High Velocity Flows. 11th Congress, I.A.H.R., Leningrad, Paper 1.15, 1965.

100. WISNER, P. E. et al. Removal of Air from Water Lines by Hydraulic Means. Proc. Hyd. Div. ASCE, Paper 11142, pp. 243-257, Feb. 1975.

101. ZUKOSKI, E. E. Influence of Viscosity, Surface Tension, and Inclination Angle on Motion of Long Bubbles in Closed Tubes. J. Fluid Mech, Vol. 25, Part 4, pp. 821-837, 1966.

102. AGRAWAL, S.S., GREGORY, G. A., and GOVIER, G. W. (1973) On "An Analysis of Horizontal Stratified Two-phase Flow in Pipes." The Canadian Journal of Chemical Engineering, Vol. 51, pp. 280-286.

103. AHMED, A.A., ERVINE, D. A., and McKEOGH, E. J. (1984) on "The Process of Aeration in Closed Conduit Hydraulic Structures." Symposium on Scale Effects in Modelling Hydraulic Structures. Esslingen, September 1984.

104. AMPHLETT, M. B., (1976) on "Air Entraining Vortices at a Horizontal Intake," Report No. OD7 of Water Resources and Irrigation.

105. ANDERSON, S. H., (1961) on "Model Studies of Storm Sewer Dropshafts." St. Anthony Falls Hydraulic Laboratory. University of Minnesota, Technical Paper No. 35, Series B.

106. BABB, A. F., SCHNEIDER, J. P., and THOMPSON, K. (1973) on "Air Flow in Combined Intake and Shaft Spillway," ASCE, Journal of Hydraulics Division, Vol. 99, No. Hy 7, pp. 1097-1108.

107. BACOPOULOUS, T. (1984) on "The Motion of Air Cavities in Large Water-Filled Conduits." Thesis Submitted for the Degree of Doctor of Philosophy. University of Strathclyde, Glasgow, July 1984.

108. BALL, J. W. (1976) on "Cavitation From Surface Irregularities in High Velocity," ASCE, Journal of Hydraulics Division, Vol. 102, No. Hy 9, pp. 1283-1297.

109. BENJAMIN, T. B., (1968) on "Gravity Currents and Related Phenomena," J. Fluid Mechanics, Vol. 31, Part 2, pp. 209-248.

110. BONNECAZE, R. H., ERSKINE, W., Jr., and GRESKOVICH, E. J. (1971) on "Holdup and Pressure Drop for Two-phase Slug Flow in Inclined Pipelines." A.I.Ch.E, Journal, Vol. 17, No. 5, pp. 1109-1113.

111. BRADLEY, J. N. on "Prototype Behaviour," Trans. ASCE, Vol. 121, 1956.

112. BRETHERTON, F. P., (1961) on "The Motion of Long Bubbles in Tubes." J. Fluid Mechanics, Vol. 10, pp. 166-188.

113. BROOK, H. N. and BLACKMER, W. H. on "Vortex Energy Dissipator for San Diego Ocean Outfall Laboratory Investigations." Final Report to Holmes and Narver Montgomery, Los Angeles, California, December 1962.

114. BROWN, R.A.S. (1965) on "The Mechanics of Large Gas Bubbles in Tubes." The Canadian Journal of Chemical Engineering, pp. 217-223.

115. BROWN, R.A.S. and GOVIER, G. W. (1965) on "The Mechanics of Large Gas Bubbles in Tubes." The Canadian Journal of Chemical Engineering, pp. 224-230.

116. COLGATE, D., (1966) on "Hydraulic Model Studies of Flow Characteristics and Air Entrainment in the Check Towers of the Main Aqueduct, Canadian River Project, Texas," Report No. Hyd. 555, Denver, Colorado.

117. COLLINS, R. (1967) on "The Effect of a Containing Cylindrical Boundary on the Velocity of a Large Gas Bubble in a Liquid." J. Fluid Mechanics. Vol 28, Part 1, pp. 97-112.

118. COLLINS, R., MORAES, F.F.D., DAVIDSON, J. F. and HARRISON, D. (1978) on "The Motion of a Large Gas Bubble Rising Through Liquid Flowing in a Tube." J. Fluid Mechanics, Vol. 89, Part 3, pp. 497-514.

119. DAVIES, R. M. and TAYLOR, G. I. (1950) on "The Mechanics of Large Bubbles Rising Through Extended Liquids and Through Liquids in Tubes." Proc. Roy. Soc. (London), Vol. 200, Ser. A., pp. 375-390.

120. DUKLER, A. E. and BERGELIN, O. P. (1952) on "Characteristics of Flow in Falling Liquid Films.: Chemical Engineering Progress, Vol. 48, No. 11, pp. 557-563.

121. DUMITRESCU, D. T., (1943) Z. Angew Meth. Mech., Vol. 23, No. 3, p. 139.

122. EDMUNDS, R. C. (1979) on "Air Binding in Pipes," Journal A.W.W.A., May, p. 272-277.

123. ERVINE, D. A. and HIMMO, S. (1984) on "Modelling the Behaviour of Air Pockets in Closed Conduit Hydraulic Systems." Symp. on Scale Effects in Modelling Hydrualic Structures, Paper 4.15, Esslingen, September 1984.

124. FALVEY, H. T., (1982) on "Predicting Cavitation in Tunnel Spillways," Water Power and Dam Construction, pp. 13-15.

125. GANDENBERGER, W., 1957, Uber die Wirtschaftliche und Betriebssichere Gestaltung von Fernwasserleitungen, R. Oldenbourg Verlag, Munich, Germany.

126. GARDNER, G. C. and CROW, I. G. (1970) on "The Motion of Large Bubbles in Horizontal Channels." J. Fluid Mechanics, Vol. 43, Part 2, pp. 241-255.

127. GARDNER, G. C. and ADEBIGI, G. A. (1974) on "The Liquid Film Left Behind by a Large Bubble in a Sloping Channel." Chemical Engineering Science, Vol. 29, pp. 461-473.

128. GOLDRING, B. T. (1979) on "The Use of Small-Scale Siphon Models." Proc. Instn. Civ. Eng., Part 2, Vol. 67, pp. 929-942.

129. GOLDRING, B. T., MAWER, W. T., and THOMAS, N., (1980) on "Level Surges in the Circulating Water Downshaft of Large Generating Stations." Third International Conference on Pressure Surges, pp. 279-299.

130. GOLDRING, B. T. on "Air Voids at Dropshaft-tunnel Bends." Hyd. Div., ASCE, Vol. 109, No. 2, February 1983.

131. GOLDRING, B. T., on "Modeling and Prototype Tests on a Low Head Siphon," Symp. on Scale Effects in Modelling Hydraulic Structures, Paper 5.9, Esslingen, Germany, September 1984.

132. GOLDRING, B. T. "Private Communication "Blowbacks in Downward Sloping Pipes," February 1985.

133. GOLDSMITH, J. L. and MASON, S. G. (1962) on "The Movement of Single Large Bubbles in Closed Vertical Tubes." J. Fluid Mech., Vol. 14, pp. 42-58.

134. GOSLINE, J. E., (1935) on "Experiments on the Vertical Flow of Gas-Liquid Mixtures in Glass Pipes."

135. GOVIER, G. W. and SHORT, W. L. (1958) on "The Upward Vertical Flow of Air-Water Mixtures," The Canadian Journal of Chemical Engineering, pp. 195-202.

136. GREGORY, G. A. (1974) on "Comments on the Prediction of Liquid Holdup for Gas-Liquid Flow in Inclined Pipes." The Canadian Journal of Chemical Engineering, Vol. 52, pp. 463-467.

137. GREGORY, G. A., (1975) on "Comparison of Methods for Prediction of Liquid Holdup for Upward Gas Liquid Flow in Inclined Pipes." The Canadian Journal of Chemical Engineering, Vol. 53, pp. 384-388.

138. GRESKOVICH, E. J. (1969) on "True Gas Content for Horizontal Gas Liquid Flow." Ind. Eng. Chem Fundamental. Vol. 8, No. 3, pp. 591-593.

139. GRESKOVICH, E. J. and SHRIER, A. L. (1971) on "Pressure Drop and Holdup in Horizontal Slug Flow." A. I. Ch. E. Journal Vol. 17, No. 5, pp. 1214-1219.

140. GRESKOVICH, E. J. and SHRIER, A. L. (1972) on "Slug Frequency in Horizontal Gas-Liquid Slug Flow." Ind. Eng. Chem. Process Des. Develop, Vol. 11, No. 2, pp. 317-320.

141. GRESKOVICH, E. J. (1973) on "Prediction of Gas Liquid Holdup for Inclined Flows." A. I. Ch. E. Journal, Vol. 19, No. 5, pp. 1060-1061.

142. GRESKOVICH, E. J. and COOPER, W. T. (1975) on "Correlation and Prediction of Gas-Liquid Holdups in Inclined Upflows." A.I.Ch.E. Journal, Vol. 21, No. 6, pp. 1189-1192.

143. GRIFFITH, P., and WALLIS, G. B., Massachusetts Institute of Technology Technical Report No. 15, NONR 1959, 39, 1841.

144. GRIFFITH, P. and WALLIS, G. B., (1961) on "Two Phase Slug Flow," Journal of Heat Transfer, Trans. ASME, Series C., Vol. 83, pp. 307-320.

145. GUTTI, S. R. (1968) on "Behaviour of Small Gas Bubbles in Accelerated Liquid." ASCE, Journal of Hydraulic Division, Vol. 94, No. Hy 4, pp. 1073-1082.

146. GUTTI, S. R., (1971) on "Movement of Small Gas Bubbles in Smoothly Decelerating Liquids, ASCE, Journal of Hydraulics Division, Vol. 97, No. Hy 7, pp. 1117-1128.

147. HABERMAN, W. L. and MORTON, R. K. (1956) on "An Experimental Study of Bubbles Moving in Liquids." Trans. Am. Soc. Civ. Eng., Vol. 121 pp. 227-250.

148. HAINDLE, K. "Zone Lengths of Air Emulsion in Water Downstream of the Ring Jump in Pipes." 13th Congress of the International Association for Hydraulic Research, August 31 - September 5, Vol. 2, pp. 9-18 Kyoto, Japan, 1969.

149. HALL, L.S. "Model-Prototype Conformity." Trans. ASCE, Vol. 109, 1944, pp. 150-154.

150. HARMATHY, T. Z. (1960) on "Velocity of Large Drops and Bubbles in Midia of Infinite or Restricted Extent." A.I.Ch.E. Journal, Vol. 6, No. 2, pp. 281-288.

151. HEAD, C. R. (1975) on "Low Head Air Regulated Siphons." ASCE, Journal of Hydraulic Division, Vol. 101, No. HY3, pp. 329-345.

152. HIMMS, S. "The Behaviour of Air Pockets in an Upward Sloping Pipe With Moving Water Conditions." Int. Report 2, Dept. Civil Engineering, University of Glasgow, April 1985.

153. HIMMO, S. "The Behaviour of Air Voids at a Dropshaft-tunnel Junction." Int. Report 3, Department of Civil Engineering, University of Glasgow, May 1985.

154. KALINSKE, A. A. and BLISS, P H. (1943) on "Removal of Air form Pipe Lines by Flowing Water." ASCE, Vol. 13, No. 10, pp. 480-482.

155. KALINSKE, A. A. and ROBERTSON, J. M. (1943) on "Closed Conduit Flow." Transactions, ASCE, Vol. 108, pp. 1435-1516.

156. KAO, T. W. (1977) on "Density Currents and Their Applications," Journal of Hydraulics Division, ASCE, Vol. 103, HY 5, pp. 543-555.

157. KARMAN, T.V. (1940) on "The Engineer Grapples with Nonlinear Problems,' Bull. Am. Math. Soc., Vol. 46, pp. 615-683.

158. KENT, J. C. "The Entrainment of Air by Water Flowing Through Circular Conduits with Downgrade Slopes." Thesis presented to the Unviersity of California at Berkeley, California, in 1952 in partial fulfilment of the requirements for the degree of Doctor of Philosophy.

159. LAIRD, A.D.K. and CHISHOLM, D. (1956) on "Pressure and Forces along Cylindrical Bubbles in a Vertical Tube." Industrial and Engineering Chemistry, Vol. 48, No. 8, pp. 1361-1364.

160. LARA, C. D. Degayage Natural dans les pints incline relient les a ductions secondaires aux galeries en charge, Proceedings of the 6th General Meeting, International Association for Hydraulic Research, The Hague, Netherlands, 1955 (in France).

161. MARTIN, C. S., "Characteristics of an Air-Water Mixture in a Vertical Shaft." Proc. Hyd. Div. Specialty Conference, Am. Soc. Civ. Eng., Bozeman, Mont., August 15-17, pp. 323-334 (1973).

162. MARTIN, C.S., (1976) on "Vertically Downward Two-phase Slug Flow," Journal of Fluids Engineering, Trans ASME, Vol. 98, Series 1, No. 4, pp. 715-721.

163. MECHLER, W. A., (1966) on "Factors Influencing Flow in Large Conduits," Translation of the work done by Gandenberger, Journal of Hydraulics Division ASCE, Vol. 92, HY4, pp. 203-218.

164. MECHLER, W. A., (1976) on "Discussion on Removal of Air from Water Lines by Hydraulic Means." Journal of Hydraulics Division, ASCE, Vol. 102, HY3, pp. 420-421.

165. MILLER, D.S. "Model Studies of Kalan Power Station Outlets and Dropshaft. B.H.R.A., RR 1350, May 1976.

166. MOISSIS, R. and GRIFFITH, P., (1962) on "Entrance Effects in a Two-phase Slug Flow." Journal of Heat Transfer, Trans. ASME, Series C., Vol. 1, pp. 29-39.

167. MUSALLI, Y. G., (1978) on "Size Determination of Partly Full Conduits." ASCE, Journal of Hydraulic Division, Vol. 104, No. HY7, pp. 959-974.

168. NGUYEN, V. T. and SPEDDING, P. L., (1977) on "Hold Up in Two-phase Gas-Liquid Flow - I." Chemical Engineering Science, Vol. 32, pp. 1003-1014.

169. NGUYEN, V. T. and SPEDDING, P.L. (1977) on "Holdup in Two-Phase Gas-Liquid Flow - II." Chemical Engineering Science, Vol. 32, pp. 1015-1021.

170. NICKLIN, D. J., WILKES, J. O. and DAVIDSON, J. F. (1962) on "Two Phase Flow in Vertical Tubes." Trans. Instn. Chem. Engrs. Vol. 40, pp. 61-68.

171. PETERKA, A. J., (1954) on "Performance Tests on Prototype and Model." Transactions, Proceedings, Separate No. 488, pp. 385-409.

172. QUINTELA, A. C., (1980) on "Flow Aeration to Prevent Cavitation Erosion," Water Power and Dam Construction, pp. 17-22.

173. RESCH, F. J., LEUTHEUSSER, J. J. and ALEMU SOLOMON, (1974) on "Bubbly Tow-Phase Flow in Hydraulic Jump." Journal of Hydraulics Division ASCE, Vol. 100, HY1, pp. 137-149.

174. RICHARDS, R. T. (1957) on "Air Binding in Large Pipelines Flowing Under Vacuum." Journal of the Hydraulic Division, ASCE, Vol. 83, No. HY6, pp. 1454-(1-10).

175. RUNGE, D. E., and WALLIS, G. B., AEC Rept. NYO - 3114 - 8, (EURAEC - 1416), 1965.

176. SAILER, R. E., (1955) on "Air Entrainment in Siphon Barrels," Civil Engineering, Vol. 25, No. 5, pp.268-271.

177. SALIH, M. A., (1979) on "Air Bubbles in a Convectively Accelerated Water Flow," Journal of Hydraulic Research, 17, No. 4, pp. 315-327.

178. SHARMA, H. R., (1976) on "Air Entrainment in High Head Gated Conduits," ASCE, Journal of Hydraulics Division, Vol. 102, No. HY11, pp. 1629-1646.

179. SINGH, G. and GRIFFITH, P., (1970) on "Determination of the Pressure Drop Optimum Pipe Size for a Two-Phase Slug Flow in an Inclined Pipe." Journal of Enginering for Industry, Trans ASME, Vol. 92, pp. 717-726.

180. SPEDDING, P. L. and NGUYEN, V. T. (1978) on "Bubble Rise and Liquid Content in Horizontal and Inclined Tubes," Chemical Engineering Science, Vol. 33, pp. 987-994.

181. TAITEL, Y. and DUKLER, A. E., (1976) on "A Model for Predicting Flow Regime Transitions in Horizontal and Near Horizontal Gas-Liquid Flow." Journal of A.I. Ch.E, Vol. 22, No. 1, pp. 47-55.

182. TAKELI, S. and MAXWELL, W.H.C., (1981) on "Hot Film Response and Digital Analysis in Bubbly Flows," ASCE, Journal of Hydraulics Division, Vol. 108, No. HY2, pp. 267-272.

183. THOMAS, N. H. (with Goldring and Mawer) "Level Surges in Circulating Water Downshaft of Large Generating Stations. Third Int. Conf. on Pressure Surges (BHRA) Canterbury, U. K. 1980

184. THOMAS, N. H. "Air Demand Distortion in Hydraulic Models: Experimental Evidence of Bi-model Structure in Air Entraining Flows and A Scaling Analysis of Detrainment with Special Applications to Siphon Priming." Int. Conf. on Hyd Mod. of Civ. Eng. Struc., B.H.R.A. Paper E5, Coventry, England, September 1982, pp. 253-272.

185. THOMAS, W. J. and PORTALSKI, S., (1958) on "Counter-Current Flow in Wetted Wall Columns." Industrial and Engineering Chemistry, Vol. 50, No. 7, pp. 1081-1088.

186. TOWNSON, J. M., (1975) on "Oscillations in a Cooling Water Outfall System," Proc. Instn, Civ. Engrs., Part 2, Vol. 59, pp. 837-847.

187. TULLIS, J. P. and MARSCHNER, B. W., (1986) on "Review of Cavitation Research on Valves,' ASCE, Journal of Hydraulics Division, Vol. 94, No. HY1, pp. 1-16.

188. TULLIS, J. P., (1981) on "Modelling Cavitation for Closed Conduit Flow: ASCE, Journal of Hydraulics Division, Vol. 107, No. HY11, pp. 1335-1349.

189. TUNG, K. W. and PARLANGE, J. Y. (1976) on "Note on the Motion of Long Bubbles in Closed Tubes - Influence of Surface Tension." Acta Mechanica, Vol. 24, pp. 313-317.

190. U. S. Bureau of Reclamation Report (1980) on "Air-Water Mixtures," Engineering Monograph No. 41, U. S. Dept. of Interior, Water and Power Resources Service.

191. VERONESE, A., (1937) on "Sul Motto Delle Bolle d'Aria Nelle Condotte d'Acqua" (in Italian), Estrato dal Fasciacolo X, Vol.XIV, Ottobre, P. XV.

192. WALLIS, G. B., General Electric Company, Schenectady, N. Y., Rept. 62GL130, 1962.

193. WALLIS, G. B., "One-dimensional Two-Phase Flow," McGraw-Hill, 1969.

194. WALLIS, G. B., CROWLEY, C. J. and HAGI, Y., (1977) on "Conditions for a Pipe to Run Full When Discharging Liquid into a Space Filled with Gas." Journal of Fluids Engineering, ASME, Vol. 99, pp. 405-413.

195. WALLIS, G. B. (1982) on "Review - Theoretical Models of Gas-Liquid Flows." ASME, Journal of Fluids Engineering, Vol. 104, pp. 279-283.

196. WHILLOCK, A. F., and THORN, M. F. C., (1973) on "Air Entrainment in Dropshafts."

197. WHITE, E. T. AND BEARDMORE, R. H. (1962) on "The Velocity of Rise of Single Cylindrical Air Bubbles Through Liquids Contained in Vertical Tubes." Chemical Engineering Science, Vo. 17, pp. 351-361.

198. WIJNYAARDEN, L. V. (1968) on "On the Equations of Motion for Mixtures of Liquid and Gas Bubbles." J. Fluid Mechanics., Vol. 33, Part 3, pp. 465-474.

199. WILKINSON, D.L. (1982) on "Motion of Air Cavities in Long Horizontal Ducts," J. Fluid Mechanics, Vol. 118, pp. 109-122.

200. WISNER, P. E., MOHSEN, F. M. and KOUWEN, N. (1975) on "Removal of Air From Water Lines by Hydraulic Means." Journal of the Hydraulic Division, ASCE, Vol. 101, No. HY2, pp. 234-257.

201. ZUBER, N. and FINDLAY, J. A., (1965) on "Average Volumetric Concentration in Two Phase Flow Systems," ASME, Journal of Heat Transfer, pp. 453-468.

202. ZUKOSKI, E.E., (1966) on "Influence of Viscosity, Surface Tension and Inclination Angle on Motion of Long Bubbles in Closed Tubes." J. Fluid Mechanics, Vol. 25, Part 4, pp. 821-837.